# MODELLING GROUNDWATER CONTAMINATION IN THE ATLANTIS AQUIFER

By JF Botha, JP Verwey, J Buys, G Tredoux <
JW Moodie & M Hodgkiss

WRC Report No 175/1/90

# MODELLING GROUNDWATER CONTAMINATION IN THE ATLANTIS AQUIFER

**Contributors**

**J.F. Botha[1), J.P. Verwey[1), J. Buys[1), G. Tredoux[2),**
**J.W. Moodie[3) and M. Hodgkiss[3)**
1) Institute for Groundwater Studies, University of the Orange Free State
2) Division of Water Technology of the CSIR
3) Department of Medical Virology, University of Cape Town

**Report to The Water Research Commission on the project :**
**"Modelling of Groundwater Quality in the Atlantis Aquifer"**

**Edited by**

**J.F. Botha**

**WRC Report No 175/1/90** **ISBN 0 947447 90 3**

**Bloemfontein** **August 1990**

# ACKNOWLEDGEMENTS

The research in this report emanated from a project funded by the Water Research Commission, in conjunction with the Department of Water Affairs, the Division of Water Technology of the CSIR and the Western Cape Regional Services Council, entitled:

"Modelling of Groundwater Quality in the Atlantis Aquifer".

The Steering Committee responsible for the project, whose contributions to the project are hereby gratefully acknowledged, consisted of the following persons:

| | |
|---|---|
| Dr P.J.T. Roberts[1] | Water Research Commission (Chairman) |
| Mr P.W. Weideman | Water Research Commission (Secretary) |
| Mr J.R. Vegter | Department of Water Affairs |
| Mr A.H. Smit | Department of Water Affairs |
| Dr G. Tredoux | Division of Water Technology, CSIR |
| Mr S.J.J. Geldenhuys | Steffen, Robertson and Kirsten |
| Prof H.J. Potgieter | University of the Orange Free State |
| Prof J.F. Botha | University of the Orange Free State |
| Prof F.D.I. Hodgson | University of the Orange Free State |
| Mr J. A. Clark | Western Cape Regional Services Council |

[1] Mr H.M. du Plessis took over the chairmanship after Dr Roberts resigned from the Commission.

This project was only possible through the co-operation of many individuals and other institutions. The authors would, therefore, like to take this opportunity to express their sincere thanks to the following additional institutions and people, without whose help the investigation could not have been carried out:

**Department of Agriculture and Water Supply**, in particular Drs P. Marais and W.A.G. Kotze, the Director and Head of the Soil Physics Section of the Fruit and Food Technology Institute at Stellenbosch, respectively, for the high quality work in determining the soil moisture retention curves of the Atlantis sands.

**The Computing Centre for Water Research** at the University of Natal for their contribution in obtaining climatological data.

**The Universities of the Orange Free State and Cape Town** for the facilities provided in conducting this research.

**The Laboratory of the DWT in Bellville**, particularly Messrs. Louw and Pascall, for their high quality work in analysing the multitude of chemical samples.

**The Institute for Groundwater Studies**, in particular the Director, Prof F.D.I. Hodgson, for his assistance and encouragement during the investigation and Mss M. Botha and C. le Roux, for their contribution in the editing and production of this report.

# TABLE OF CONTENTS

## PART 1

## VIROLOGICAL, CHEMICAL AND HYDROGEOLOGICAL INVESTIGATIONS AT ATLANTIS

### Chapter 1 Introduction

### Chapter 2 Site Description

### Chapter 3 Virological Studies at Atlantis

### Chapter 4 Groundwater Quality in the Atlantis Aquifer

Chapter 5 Identification of the Hydraulic Parameters

Chapter 6 Horizontal Flow Models

## Chapter 7 Modelling Unsaturated Flow and Mass Transport

## PART 2

## PRINCIPLES OF MASS TRANSPORT IN POROUS MEDIA

## Chapter 8 Physical Properties of Fluids

## Chapter 9 Physical Properties of a Porous Medium

## Chapter 10 Darcy's Law

## Chapter 11 The Equation of Fluid Motion

## Chapter 12 Two-dimensional Flow in Non-deformable Porous Media

## Chapter 13 Contamination of Groundwater

## Chapter 14 Summary and Recommendations

## Appendices

# EXECUTIVE SUMMARY

## 1 GENERAL

All living organisms produce by-products, which are of little economic value, and have to be disposed of. To dispose of this waste requires a method that is cheap and least repulsive to the public. Few people believed that serious consequences could ensue, even if the method being used was ultimately found to be inadequate. Land disposal has thus, from times immemorial, been used as a natural method for waste disposal.

One of the primary pathways for the migration of waste is the water cycle. Although it has been known for a long time that surface water is very susceptible to contamination, it took disasters like Love Canal to show that groundwater may present an even bigger danger. The most obvious way to ensure that groundwater does not become polluted, would be to monitor it continuously. However, this can be a very time-consuming and expensive exercise. Moreover, such a monitoring system yields only passive information, that is it can only tell if and when an aquifer becomes polluted, but not how to prevent a further spreading of the contamination, or to clean up an already contaminated aquifer. To combat groundwater pollution, scientists, therefore, more and more supplement the traditional monitoring system with a more indirect method – *conceptual models.*

The most far-reaching step ever taken in the history of science, was the introduction of what may be called the *principle of decomposition.* According to this principle, any physical phenomena (i.e. phenomena associated with *matter*) can be decomposed into a set of basic interactions, which could be measured in terms of numbers. Since numbers form the basis of all mathematics, the question arises whether it is not possible to combine the human reasoning power with well-planned observations, and describe natural phenomena in abstract *mathematical terms*, or to use more modern terminology, in terms of a *conceptual model.*

The basic premise behind conceptualization, which is rather simple, is to decompose the phenomenon into smaller *quantifiable* interactions, also referred to as *observables.* Once this has been done, it is quite natural to try and relate observables for the same phenomenon, or even observables from different phenomena, with one another. The latter objective is usually accomplished by the introduction of a set of well-defined and measurable *relational parameters* (the universal constant of gravitation, for example). With this in mind, the method of conceptualization can be expressed more precisely in symbolical form as

$$\mathbf{L}u(\mathbf{p}, \mathbf{v}) = f, \tag{1}$$

where **L** is the *relational operator*, which relates the observable u to a set of other observables (**v**) through the *relational parameters* (**p**) and *functional* f. The successful application of a conceptual model thus hinges on the possibility to determine, not only the relational operator and functional, but also the parameters **p**.

The most important property of Equation (1) is that it contains the relational parameters implicitly. These parameters must, therefore, be known at all the relevant points in space and time, before Equation (1) can be applied in practice. The success of a conceptual model thus hinges on the ability of the user to define these parameters uniquely over all space and time of interest. This is a rather severe restriction on the practical application of Equation (1), particularly in the case of environmental phenomena. Fortunately for the environmental sciences, there are often historical data available on a specific phenomenon, which can be *fitted* to a conceptual model. Once this has been done, the model can be used to evaluate the sufficiency of the data and to plan and collect new data, which will enhance the overall performance of the fitted model.

Many of the interactions responsible for environmental phenomena are, unfortunately, so complex that they cannot be explained fully in terms of well-known physical processes, at least at this moment in time. The fitting of a conceptual model to a natural asset, such as a groundwater resource, should thus not be construed as a one-time, but rather as a continuous process, which is best performed by the management of the resource.

Because of the complexity of groundwater phenomena, it is generally not possible to fit a conceptual model without the use of a computer, except for a few very simple cases (e.g. the Theiss equation). In fact, general groundwater models only became viable with the introduction of large-scale computers around 1970. The fitting of a conceptual model is thus usually conducted in three stages.

The first stage consists of translating the conceptual model, related to that specific phenomenon, into computer terms. In practice, this means that one has to write a computer program for the conceptual model (in one or other high level computer language). Once this has been done, the computer program can be used to *simulate* the behaviour of the actual phenomenon, using part of the available historical (or new) data. Since it is not possible to supply the program with all the information on the conceptual parameters, at least in groundwater phenomena, the first simulation usually differs considerably from the actual behaviour of the real world phenomenon. To get a better insight into the behaviour of the phenomenon, the unknown conceptual parameters are varied, using whatever information is available, until the simulated results agree with the observations. This second stage of the modelling process, is generally referred to as *the calibration* of the model. The third and final stage of the modelling process is reached, when the simulated results and observations agree within some prescribed bounds. In this stage, also known as *the verification* of the model, the calibrated model is used to predict the behaviour of the phenomenon, for that part of the historical data not used in the calibration phase. Only if the simulated results and observations agree, again within the prescribed bounds. can the model be considered as satisfactory. If this is not the case, stage two has to repeated, this time using a larger set of the historical data.

## 2 PURPOSE OF THE PRESENT PROJECT

As stated in the original contract, the main objective of the present study was to gain information on the mechanisms which are responsible for the pollution of groundwater. This information is not only needed for combatting the problem, but more importantly to prevent it. Such knowledge may, in future, also be helpful in cleaning up polluted aquifers.

Groundwater pollution is a rather complicated phenomenon. It would thus not be possible to cover all aspects of the phenomenon in a limited investigation. The present investigation was, therefore, limited to the following aspects:

(a) An investigation of the physical and chemical mechanisms which control the pollution of groundwater.
(b) The development of a model, based on the information gathered in (a), which can be applied to other contaminated aquifers, with small or no adjustments.
(c) Application and refinement of the model developed in (b) in the light of information gained from the study of sea-water intrusion and artificial recharge in the Atlantis aquifer, with the view to increase the yield of the aquifer.

At the time of submitting the proposal for the project to the Water Research Commission, the term model, as used in (b) above, was internationally interpreted as the computer program to implement the conceptual model. Since that time, the terminology has been somewhat modified. A model is nowadays considered to consist of the computer program and its related input data, which simulates a given phenomenon accurately, over a sufficient period of time. The term model in (c) should be interpreted in this way.

The choice of the Atlantis aquifer for this study was based on the knowledge that the aquifer was already subjected to some minor pollution, due to the intentional recharge of the aquifer by purified sewerage and storm-water run-off. The aquifer would thus seem to present an ideal basis for the evaluation of the developed computer programme. Of course, it can be argued that, since the Atlantis aquifer is basically a phreatic aquifer, the use of this aquifer may disqualify the model for use with other South African aquifers, particularly the confined aquifers present in the Karoo sediments. However, the modelling of groundwater pollution usually requires two different models – one for the flow of groundwater and the other for the transport of dissolved solids. Since the latter model does not depend on the aquifer explicitly, the original objective could be fulfilled by the development of suitable programs for confined (semi-confined) aquifers.

The Division of Water Technology (DWT) has been carrying out an extensive investigation into artificial groundwater recharge and related aspects of water quality at Atlantis, for the Western Cape Regional Services Council, since 1983. This meant that the DWT already had considerable experience with pollution in the aquifer and the necessary infrastructure for the chemical analyses required for the investigation. Because of their interest in establishing a groundwater pollution model, as an aid to the management of the Atlantis aquifer, they accepted a proposal from the Institute to participate in this investigation. The basic objectives on their part, as specified in a contract negotiated between the Institute for Groundwater Studies and the CSIR, were:

(a) Gathering of data for the proposed model.
(b) Detailed stratigraphic investigations of water quality in the aquifer.
(c) To monitor variations in water quality due to the artificial recharge of the aquifer.
(d) Co-operation with the Institute in planning the water quality model.
(e) Assistance in conducting dispersion tests, where necessary.

Six months after the present project started, the WRC granted a sub contract to the Department of Medical Virology at the University of Cape Town to investigate the behaviour of viruses in a continuous liquid phase, rather than a percolate. The main objectives of this investigation were as follows:

(a) To investigate and document the occurrence or absence of human pathogenic viruses in groundwater of the Atlantis aquifer.
(b) To develop a model of the soil conditions pertaining to Atlantis to allow simulation of the effects of saturation by influx water, winter rainfall and intermittent drying.
(c) To investigate the survival and migration patterns of enteric viruses, such as

Poliomyelitis virus (Leon strain), under simulated conditions, using the laboratory model.

Although there are cases where aquifers have been polluted by contaminated water being discharged directly into them, contamination by percolating rain water is more common. Since aquifers are very often separated from the soil surface by an unsaturated zone, a true model of groundwater pollution should really be based on the conceptual model for full three-dimensional saturated and unsaturated flow. However, such a model can only be applied successfully, if more information on the relational parameters is available than what is at present economically feasible. Groundwater pollution studies are, consequently at present, mainly investigated with the help of three two-dimensional models – a combined saturated-unsaturated flow model for the vertical motion of water, a horizontal saturated flow model and a mass transport model. This philosophy was also adopted in the present investigation.

## 3 RESULTS AND CONCLUSIONS

### 3.1 Mechanisms Responsible for the Pollution of Groundwater

There is no doubt that the success with which a conceptual model can be applied in modelling a given phenomenon, depends ultimately on the developer's ability to understand and interpret the physical basis of the conceptual model. This information is available in a few highly mathematical text books, e.g. Bear (1972, 1979), with little or no attention to the physics involved. Previous experience in teaching postgraduate courses on groundwater modelling, locally and overseas, has indicated that students have difficulty in using these texts to develop a physically sound model for their specific applications. To comply with the basic purpose of the present project, Part 2 of the present report is devoted to a dicussion of the physics of groundwater motion and contaminant transport, which hopefully is more understandable to future (and present) groundwater modellers. Some parts of this work are new and the rest are a new interpretation of accepted results.

### 3.2 Virological Studies (Chapter 3)

The virological studies conducted at Atlantis indicated that the aquifer is not contaminated with enteric viruses. The worst situation would relate to saturated conditions, low pH and non-adsorbed viruses.

Survival studies at room temperature (survival would be longer in the dark, cool aquifer) indicate that live virus could be carried in the liquid phase of the aquifer with little retardation for possibly 60 days. However, the studies did not yield unambiguous results. Integration of the information into a mathematical model seems to be the only feasible alternative to determine a safety factor, as far as virus migration in the aquifer is concerned.

### 3.3 Groundwater Quality (Chapter 4)

Although there existed a number of monotoring points in the aquifer at the start of the investigation in 1986, an analysis of their spacing and the available data on groundwater quality suggested that the number of monitoring points had to be increased, in order to obtain a better understanding of pollution in the aquifer, especially around the infiltration pan. A number of additional well-points were, therefore, installed around the pan, with funds available under the present contract, while the network of observational boreholes, in the rest of the aquifer, was also extended with boreholes drilled by the Department of Water Affairs. This exercise contributed significantly to a better understanding of the groundwater movement and accompanying quality aspects.

The water-levels observed around the infiltration pan indicated that the main flow direction of the water is in a south-southwesterly direction. It is also possible that the aquifer can be replenished in an easterly direction, if the water level in the pan is sufficiently high. However, the presence of surface flow, especially on the southern side of the basin, complicates the interpretation considrably.

Hydrochemical stratification is an accomplished fact and the replenished water is found mainly in the upper layers of the aquifer. An analysis of the chemical composition of the groundwater in the vicinity of the recharge basin indicated that specific constituents are subject to divergent processes which need further study. This behaviour of the contaminants complicated the development of a suitable model for the Atlantis aquifer considerably.

### 3.4 Parameter Identification (Chapter 5)

The most difficult part in the development of a model for a groundwater phenomenon, is to derive suitable boundary and initial conditions and the conceptual parameters required by the model. The conceptual parameters involved with the phenomena for which computer programs were developed, or used in this investigation, include:

(a) transmissivity and storage coefficient of a confined aquifer,
(b) transmissivity and effective porosity of an unconfined aquifer,
(c) soil moisture retention curve for unsaturated flow,
(d) hydraulic conductivity of the unsaturated zone and

(e) the dispersivities for mass transport.

The transmissivity, storage coefficient and effective porosity can be determined from drawdowns observed in an aquifer during controlled pumping tests and/or a particle size analysis (see Section 4.5). In the present investigation, attention was directed to the cross-borehole packer tests, unsaturated flow parameters and dispersivities.

The need for cross-borehole packer tests arose from an earlier investigation, which indicated that there is a possibility of sea-water intrusion into the aquifer through the Malmesbury Formation, which bounds the Atlantis aquifer on the coast. These tests showed that the Malmesbury Formation is highly fractured up to a depth of 30 m below sea-level and that sea-water intrusion presents a real threat to the aquifer.

The unsaturated parameters for the aquifer were determined by the Soil Section of the Institute of Fruit and Food Technology, while the soil moisture measurements were conducted by the DWT. The unsaturated parameters and soil moisture measurements fitted very nicely.

A major disappointment experienced during the investigation, was the failure to determine dispersivities for the Atlantis aquifer, notwithstanding numerous attempts. This failure, which can be ascribed to the divergent processes observed in the transport of dissolved solids in the aquifer, is rather unfortunate, for it meant that one of the objectives of the study, the development of a mass transport model for the aquifer, had to be abandoned.

### 3.5 Horizontal Flow Models (Chapter 6)

Computer programs for saturated flow were in the past developed with the assumption that the boundaries of aquifers can be considered as impermeable. This is certainly not true for many of the South African aquifers. A new computer program was, therefore, developed for confined and semi-confined aquifers with general boundary conditions. Extensive numerical tests were conducted to verify the mathematical and numerical correctness of the program. However, its application under actual field conditions will have to wait until suitable field data are available.

Unconfined or phreatic flow has in the past often been modelled with computer programs based on the conceptual model for confined flow. In order to evaluate the correctness of this approach, a completely new program, using the Boussinesq equation as the basic conceptual model, was developed. This program was used to develop a preliminary model for groundwater flow in the Atlantis aquifer with excellent results.

### 3.6 Modelling Unsaturated Flow and Mass Transport (Chapter 7)

An earlier, but similar investigation as the one reported on here, showed that the computer programs available at the Institute for modelling saturated/unsaturated flow, used numerical approximations that tend to be unstable or do not satisfy the law of mass conservation. New computer programs had, therefore, to be developed for that particular investigation. These programs were used to establish preliminary saturated/unsaturated flow and mass transport models for the area around the infiltration pan at Atlantis.

A rather unexpected result obtained from the investigation of mass transport around the infiltration pan, is the large effect that the Darcy velocity have on the transport of conservative and non-conservative tracers. This difference in behaviour should be taken as a warning not to compare the behaviour of different types of tracers with one another.

## 4 RECOMMENDATIONS FOR FUTURE RESEARCH

### 4.1 The Atlantis Aquifer

Although the present investigation has shown that the Atlantis aquifer is not seriously polluted at present, the fact remains that it is situated in an industrial area and could, therefore, easily be contaminated by accidental spills and/or wrong management decisions. Two areas that would definitely require more attention, if the pollution of the aquifer is to be avoided, are: (a) the determination of more precise dispersivity values and (b) a more detailed investigation of sea-water intrusion, particularly in the Silwerstroom area.

### 4.2 Surface Pollution Sources and Waste Disposal Sites

The experience gained in this investigation of the Atlantis aquifer, suggested that the following precautions should be taken when investigating surface pollution sources and waste disposal sites:

(a) Observations should be conducted at a higher frequency than is usual for saturated flow.

(b) Observations on the different variables, such as water levels, concentrations and soil moisture contents should be limited to strategic periods of time, such as rainfall and flood events, and carried out simultaneously, rather than scattered over long periods of time. The latter procedure can be followed between these strategic periods of time.

(c) Observations should not be limited to the immediate surrounding area of a surface pollution source, but extended to areas immediately below the source.

(d) Piezometric water levels in the aquifer containing a surface pollution source, should be measured over as large an area as possible. However, observations on the other variables could be limited to detailed studies in profile at a few strategically placed observation sites.

(e) The highly non-linear nature of unsaturated flow and mass transport makes it impossible to predict the spread of pollution from a surface source situated in the unsaturated zone of the earth's surface *a priori*, even by someone with considerable practical experience. This ignorance can be avoided, if the observations on a waste disposal site, as prescribed by law or otherwise, are supplemented with a saturated/unsaturated flow and mass transport model. In view of this, it is recommended that suitable models should be developed for all existing and future major waste disposal sites, if such a model does not exist already, along the lines suggested above.

# LIST OF FIGURES

## Chapter 2 Site Description

## Chapter 3 Virological Studies at Atlantis

## Chapter 4 Groundwater Quality in the Atlantis Aquifer

## Chapter 5 Identification of the Hydraulic Parameters

## Chapter 6 Horizontal Flow Models

### Chapter 7 Modelling Unsaturated Flow and Mass Transport

### Chapter 8 Physical Properties of Fluids

### Chapter 9 Physical Properties of a Porous Medium

## Chapter 10 Darcy's Law

## Chapter 11 The Equation of Fluid Motion

## Chapter 12 Two-dimensional Flow in Non-deformable Porous Media

## Chapter 13 Contamination of Groundwater

## Appendices

# LIST OF TABLES

### Chapter 3 Virological Studies at Atlantis

### Chapter 4 Groundwater Quality in the Atlantis Aquifer

### Chapter 5 Identification of the Hydraulic Parameters

### Chapter 6 Horizontal Flow Models

### Chapter 7 Modelling Unsaturated Flow and Mass Transport

### Chapter 9 Physical Properties of a Porous Medium

### Chapter 11 The Equation of Fluid Motion

## Appendices

# LIST OF SYMBOLS USED

## 1 Latin Symbols

a, b = Coefficients in the calibration curve of a gamma ray density meter

b(x) = Height of impervious bottom of an phreatic aquifer (relative to a suitable reference datum, e.g. mean sea level) [L]

C = Mass fraction concentration of a dissolved solid, or [M.M$^{-1}$]
Moisture capacity of a porous medium [L$^{-1}$]

c = Volumetric concentration of a dissolved solid [M.L$^{-3}$]

$C_u$ = Hasen's effective grain-size coefficient [1]

$\underline{\mathbf{D}}_h$, $\underline{\mathbf{D}}$ = Hydrodynamic dispersion tensor (coefficient) [L$^2$.T$^{-1}$]

$D_{ij}$ = The ij-th component of the dispersion tensor [L$^2$.T$^{-1}$]

$D_m$ = Molecular diffusion coefficient in a free fluid [L$^2$.T$^{-1}$]

$\underline{\mathbf{D}}_m$ = Molecular diffusion tensor in a porous medium [L$^2$.T$^{-1}$]

d = Distance between packers in cross-borehole packer tests [L]

$d_{10}$ = Hasen's effective grain size [%]

$d_m$ = Mass percentage of material that passes a given sieve [%]

$E(\tau)$ = Error associated with the Lagrange interpolation polynomial

$E[\bullet]$ = Symbolic expectation operator

**F** = An applied force [N]

f = Forcing function

$f(\mathbf{x},t)$ = Strength of a source (+) or sink (–) [T$^{-1}$]

G = Count rate of the gamma ray density meter [T$^{-1}$]

g = Acceleration of gravity [L.T$^{-2}$]

$h(\mathbf{x},t)$ = Piezometric water level, or pressure head [L]

$\mathbf{J}(\mathbf{x},t)$ = Mass flux per unit area [M.L$^{-2}$.T$^{-1}$]

K = Scalar hydraulic conductivity [L.T$^{-1}$]

$\underline{\mathbf{K}}(\mathbf{x},t)$ = Hydraulic conductivity tensor of a porous medium [L.T$^{-1}$]

$k(\mathbf{x},t)$ = Scalar permeability [L]

$\underline{\mathbf{k}}(\mathbf{x},t)$ = Permeability tensor of a porous medium [L]

$K_d^*$ = Mass distribution coefficient (= $\rho K_d$) [1]

$K_d$ = Volumetric distribution coefficient [L$^3$.M$^{-1}$]

$K_d(\mathbf{n})$ = Directional hydraulic conductivity [L.T$^{-1}$]

$K_{ij}$ = The ij-th component of the hydraulic conductivity tensor [L.T$^{-1}$]

$K_n$ = Hydraulic conductivity in direction of the Darcy velocity [L.T$^{-1}$]

**L** = Symbolic relational operator

$L(\mathbf{x})$ = Thickness of the aquifer at point **x** [L]

$l_k(t)$ = Lagrange interpolation polynomial
$m$ = Total mass of fluid and solids in a volume of porous material [M]
$M$, $m$ = Mass of a body [M]
$m_a$ = Mass of solid absorbed on a volume of porous matrix [M]
$m_b$ = Total mass of solids in a volume $v_b$ of porous material ($=m_a + m_m$) [M]
$m_f$ = Mass of fluid in a volume porous material [M]
$m_m$ = Mass of the porous matrix [M]
$m_s$ = Mass of solids dissolved in a volume of porous material [M]
$N$ = Count rate of a neutron moisture meter [$T^{-1}$]
$\mathbf{n}$ = Unit Cartesian vector normal to a surface
$n$, $m$ = Characteristic constants in Van Genuchten's retention curve
$p$ = Fluid pressure [Pa]
$\mathbf{p}$ = Set of relational parameters connecting two or more observables
$p_o$, $p_i$ = Outer and inner forces acting on a plane [Pa]
$p_c$ = Capillary pressure of a fluid [Pa]
$\mathbf{P}_\zeta$ = $\{\mathbf{x}',\zeta,t\}$, reduced value plane in the coordinates $(\mathbf{x}',t)$
$Q(\mathbf{x},t)$ = Rate of injection (+) or withdrawal (–) from a borehole [$L^3.T^{-1}$]
$\mathbf{q}(\mathbf{x},t)$ = Darcy velocity of a fluid in a porous medium [$L.T^{-1}$]
$q(\mathbf{x},t)$ = Magnitude of the Darcy velocity $\mathbf{q}(\mathbf{x},t)$ [$L.T^{-1}$]
$\mathbf{q}^*$ = Generalized microscopic Darcy velocity [$L.T^{-1}$]
$\overline{\mathbf{q}}^*$ = Mean value of the generalized microscopic Darcy velocity [$L.T^{-1}$]
$\mathbf{q}_0$ = Deviation of $\mathbf{q}^*$ from $\overline{\mathbf{q}}^*$ [$L.T^{-1}$]
$r$ = Magnitude of the radius vector [L]
$\mathbf{r}$ = Radius vector from one point in space to another [L]
$R(\mathbf{x},t)$ = Rate of an areal source (e.g. rainfall) [L.T-1]
$r_1$, $r_2$ = Radii of curvature [L]
$r_{max}$ = Maximum radius of a pore [L]
$r_{min}$ = Minimum radius of a pore [L]
$S$ = $\{\mathbf{x},t\}$, the space-time continuum [L, T]
$s$ = Fraction of dissolved solids partaking in a chemical reaction [$M.M^{-1}$]
$S_0(\mathbf{x})$ = Specific storativity of an aquifer [$L^{-1}$]
$S(\mathbf{x},t)$ = $S_0(\mathbf{x})L(\mathbf{x})$, storage coefficient of an aquifer [1]
$S_d$ = Retained water saturation of drainage of an unconfined aquifer [1]
$S_w$ = Water saturation [1]
$S_y(\mathbf{x},t)$ = Specific yield of an unconfined aquifer [1]
$T$ = Magnitude of transmissivity tensor, or [$L^2.T^{-1}$]
Temperature [°C or °K]
$\underline{\mathbf{T}}$ = Tortuosity tensor of a porous medium [1]

$t$ = Time [T]
$\underline{\mathbf{T}}(\mathbf{x})$ = $\underline{\mathbf{K}}(\mathbf{x})L(\mathbf{x})$ , transmissivity tensor $[L^2.T^{-1}]$
$u$ = A single observable quantity
$u(z)$ = Velocity of fluid motion in the xz-plane $[L.T^{-1}]$
$V$ = Volume $[L^3]$
$\mathbf{v}$ = Set of observables
$v(r)$ = Velocity of a fluid in the direction of r $[L.T^{-1}]$
$\mathbf{v}(\mathbf{x},t)$ = Seepage velocity of a fluid in a porous medium $[L.T^{-1}]$
$v(\mathbf{x},t)$ = Magnitude of the seepage velocity $[L.T^{-1}]$
$\mathbf{v}_m(\mathbf{x},t)$ = Velocity of a porous matrix relative to a fixed coordinate system $[L.T^{-1}]$
$\mathbf{v}_r(\mathbf{x},t)$ = Seepage velocity of a fluid relative to a porous medium $[L.T^{-1}]$
$V_b$ = Bulk volume of a porous material $[L^3]$
$V_s$ = Volume of solids in the volume $V_b$ of a porous material $[L^3]$
$\mathbf{x}$ = Cartesian coordinates of a point in space (x,y,z) [L]
$x^i$ = Cartesian components of the position vector **r** [L]
$z$ = Reference datum (usually in vertical direction) [L]

## 2 Greek Symbols

$a$ = Characteristic constant in Van Genuchten's retention curve, or $[L^{-1}]$
Compressibility coefficient of a porous medium $[T^2.M^{-1}.L^{-1}]$
$\alpha(r)$ = Scheidegger's pore-size distribution [1]
$\alpha, \beta, \gamma, \delta$ = Coefficients in calibration curve of a neutron moisture meter
$\alpha_L$ = Longitudinal dispersivity [L]
$\alpha_T$ = Transverse dispersivity [L]
$\beta$ = Isothermal compressibility of a fluid $[T^2.M^{-1}.L^{-1}]$
$\gamma$ = The universal constant of gravitation $[L^3.M^{-1}.T^{-2}]$
$\delta(x)$ = Dirac delta function $[L^{-1}]$
$\varepsilon$ = Volumatric porosity of a porous medium $[L^3.L^{-3}]$
$\varepsilon_a$ = Areal porosity of a porous medium $[L^2.L^{-2}]$
$\phi(\mathbf{x},t)$ = Piezometric head (also known as Hubert's potential) [L]
$\lambda$ = Radioactive decay constant $[T^{-1}]$
$\lambda, \psi_b$ = Characteristic coefficients in Brooks and Corey retention curve [1, L]
$\Theta$ = Reduced moisture content of a porous medium [1]
$\theta$ = Angle, or [Radians]
Volumetric soil moisture content $[L^3.L^{-3}]$
$\theta_d$ = Water contents retained by a draining unconfined aquifer $[L^3.L^{-3}]$
$\theta_e$ = Effective porosity of an unconfined aquifer $[L^3.L^{-3}]$

$\theta_r$ = Irreducible or residual water content of a porous medium $[L^3.L^{-3}]$

$\theta_s$ = Saturated moisture contents of a porous medium $[L^3.L^{-3}]$

$\rho$ = Density of water, or solute $[M.L^{-3}]$

$\rho_b$ = Bulk density of a soil $[M.L^{-3}]$

$\rho_f$ = Density of a fluid $[M.L^{-3}]$

$\rho_s$ = Density of the solid skeleton of a porous medium $[M.L^{-3}]$

$\rho_w$ = Wet density of a soil $[M.L^{-3}]$

$\sigma$ = Surface tension of a fluid $[M.L^{-1}.T^{-2}]$

$\sigma_e$ = Effective solid matrix stress of Terzaghi $[M.L^{-1}.T^{-2}]$

$\tau_x$ = Shearing stress in the direction of fluid motion $[M.T^{-2}]$

$\psi$ = Soil matric pressure $[Pa, L]$

$\mu$ = Absolute or dynamic viscosity of a fluid $[M.L^{-1}.T^{-1}]$

$\nabla$ = Gradient operator in two or three spatial dimensions $[L^{-1}]$

$\nabla'$ = Gradient operator in two spatial dimensions only $[L^{-1}]$

# CHAPTER 1

# INTRODUCTION

## 1.1 GENERAL

All living organisms produce by-products, which are of little economic value, and have to be disposed of. To dispose of this waste, requires a method that is cheap and least repulsive to the public. Few people believed that serious consequences could ensue, even if the method being used was ultimately found to be inadequate. Land disposal has thus, from times immemorial, been used by man as a natural method for the disposal wastes.

Before the advent of the industrial and particularly the present technological age, the volumes of waste were small and consisted mostly of natural substances. The land could thus easily absorb the waste without any apparent detrimental consequence to the human race. What people did not realize, is that the earth's surface has only a finite capacity to absorb waste. With the ever-increasing population of the world and large volumes of waste produced by industry, the situation has now been reached that, in many parts of the world, the earth cannot absorb all the waste produced any longer. Moreover, many of the wastes produced nowadays, are of an artificial origin and foreign to the natural environment. Therefore, instead of being decomposed, land contact tends to 'harden' the waste. Large quantities of waste, previously thought to have been disposed of safely, can thus re-emerge in the biosphere, with detrimental consequences for all living organisms.

One of the primary pathways for the migration of waste is the water cycle. Although it has been known for a long time that surface water is very susceptible to contamination, it took disasters like Love Canal [Princeton Water Resources Program (1984)] to show that groundwater may present an even bigger danger. The main reasons for this state of affairs can be briefly summarized as follows.

(i) All groundwater, with the possible exception of connate water, originates from precipitation which infiltrates the earth's surface. Any water that percolates through a waste disposal site, will dissolve some of the waste to form contaminants which can be transported from the site to larger regions of the soil zone and, too often, to an underlying aquifer.

(ii) Since most contaminants cannot be seen in water and groundwater is, with the exception of springs, not visible, it is difficult to detect the contamination of groundwater, without a suitable monitoring system.

(iii) While most people would agree that surface water can transport dissolved solids over large distances, few seem to realize that groundwater is always subjected to the natural groundwater gradient and thus in a state of motion. Groundwater can thus also transport dissolved solids over large distances

(iv) Groundwater generally moves very slowly. Contamination of the source may thus not be detected until years after land disposal of the waste has begun. (In the case of Love Canal, it took almost fifty years for the detrimental effect of the waste to be noticed.)

(v) Groundwater flows naturally towards any surface stream, river, lake or ocean, in its immediate vicinity. Such a surface source, can thus be polluted by groundwater, even if it is effectively screened from pollution by surface sources, without being detected.

It is thus of the utmost importance that the pollution of groundwater should be prevented, as far as possible.

The most obvious way to check on the pollution of an aquifer, would be to monitor it continuously. However, this can be a very time-consuming and expensive exercise. Moreover, such a monitoring system yields only passive information, in the sense that it can only be used to detect if and when an aquifer becomes polluted, but not how to prevent or contain the pollution, or clean up an already contaminated aquifer. Experience has shown that the latter two objectives can only be achieved through a better understanding of the physical and chemical behaviour of the pollutant. The earth's subsurface is unfortunately so heterogeneous that it is impossible to conduct meaningful experiments of this nature in the field. There is, however, a simpler, albeit indirect approach – supplementing the traditional monitoring system with a *conceptual model.*

The use of conceptual models, unfortunately, still tends to be a bone of contention in many groundwater circles, particularly when applied to groundwater pollution. One reason for this state of affairs is the rather complex numerical methods required to implement the conceptual model for groundwater pollution in practice. However, there is another and often more fundamental reason – a lack of knowledge on the limitations and interpretation of the conceptual model.

One aspect often not appreciated by scientists using conceptual models, is that a conceptual model is nothing more than an interpretation of how man perceives the physical phenomena through his senses. Since man's intellect is not infallible, a conceptual model may not always be successful in explaining the observed behaviour of a natural phenomenon.

However, the conceptual models available today, are quite complex and able to describe natural phenomena accurately. One should, therefore, not reject a model merely because it does not satisfy some pre-conceived and unsubstantiated ideas of an investigator. The best way to prevent these malpractices, is through a better knowledge of the basic philosophy behind a conceptual model. It may thus be worthwhile to review the nature of a conceptual model, before proceeding with a discussion of the modelling of groundwater pollution.

## 1.2 THE NATURE OF A CONCEPTUAL MODEL

The most far-reaching step ever taken in the history of science, was the introduction of what may be called the *principle of decomposition.* According to this principle, a physical phenomenon (i.e. a phenomenon associated with *matter*) can be decomposed into a set of basic interactions, which can be *measured,* or in other words expressed in terms of *numbers.* Since numbers form the basis of all mathematics, the question arises if it is not possible to combine the human reasoning power with well-planned observations, and describe natural phenomena in abstract *mathematical terms* or, to use more modern terminology, in terms of *a conceptual model.* Building on the foundations laid by the eminent British scientist, Sir Isaac Newton, in the seventeenth century, this procedure has become so entrenched in the exact sciences, that it is almost impossible to think of one where the procedure is not applied in one form or another.

To illustrate the basic idea behind the conceptualization of natural phenomena, consider the classical example of the motion of planets. The fact that the planets seem to follow very precise periodic orbits around the sun, puzzled astronomers and ordinary people from the days of ancient Egypt and Babylon. Although various attempts were made to explain this behaviour, an acceptable solution was not provided until the work of Newton in the seventeenth century.

In his attempt to solve this problem, Newton observed that all bodies released near the earth's surface always fall towards the surface. A detailed study of this, and other related phenomena, revealed two important clues to him. The first is that the position of a body in motion can only be changed if acted on by an external agent, what he called *force.* By measuring the masses and displacements of bodies subjected to different forces, Newton deduced that all bodies in motion must satisfy his *second law of motion,* commonly expressed in mathematical terms

$$\mathbf{F}^{\dagger} = m \frac{d^2\mathbf{r}}{dt^2}, \qquad (1.1)$$

---

† Symbols in bold denote vectors

where F is the force applied to the body with mass m, r (magnitude r) the radius vector from the body to a conveniently chosen point of origin and t the time. According to this interpretation, all bodies falling to the earth must experience some kind of force. After some further experimentation and deductions, Newton concluded that two bodies will always attract each other with a force, proportional to the product of their masses and the inverse of the square of the distance between them. This relation, better known as Newton's law of universal gravitation, says that the sun (mass M) and planet (mass m) will always attract each other with a force

$$\mathbf{F} = \frac{\gamma M m}{r^3}\mathbf{r}, \tag{1.2}$$

where $\gamma$ is the universal constant of gravitation. By substituting Equation (1.1) into Equation (1.2), it is easy to see that the position of a planet, with respect to the sun, must satisfy the differential equation

$$\frac{d^2\mathbf{r}}{dt^2} = \frac{\gamma M}{r^3}\mathbf{r}.$$

As is well-known, the solution of this equation is an ellipse, fixed in space, with the sun at one of its focus points, in complete agreement with all known observations.

The success of Newton, and his followers, in explaining the motion of heavenly bodies, suggests that the decomposition principle may be equally useful in other situations as well. That this is indeed the case, is well-documented in the history of science, particularly in those situations where the phenomena can be reproduced accurately under laboratory conditions. This allows the scientist to study specific details of the phenomenon one at a time, thereby, reducing the complexity of the conceptualization considerably. However, the situation changes drastically when the scientist is confronted with phenomena related to one of the what may be called *environmental sciences*. While many of these phenomena can still be studied under idealized laboratory conditions, the environment on earth is so diverse, that the straightforward application of laboratory results becomes meaningless. The success with which a conceptual model can be applied in the environmental sciences, thus depends ultimately on a clear understanding of the nature of these models.

## 1.3 CONCEPTUAL MODELS IN THE ENVIRONMENTAL SCIENCES

As discussed above, the basic premise for conceptualization in the exact sciences is that a phenomenon can be decomposed into smaller *quantifiable* interactions. Following the jargon of quantum mechanics, these properties will, henceforth, be referred to as *observables*. Once this has been done, it is quite natural to try and relate observables for the same phenomenon, or even observables from different phenomena, with one another. The latter objective is usually accomplished by the introduction of a set of well-defined and measurable *relational parameters* (the universal constant of gravitation for example). With this in mind, the method of conceptualization can be expressed more precisely in symbolical form as

$$\mathbf{L}u(\mathbf{p},v) = f, \qquad (1.3)$$

where **L** is the *relational operator*, which relates the observable u to a set of other observables (v) through the *relational parameters* (**p**) and *functional* f, also known as the *forcing function*. The successful application of a conceptual model thus hinges on the possibility to determine, not only the relational operator and functional, but also the parameters **p**. As will be shown later on, it is not an easy task to establish that a given phenomena does indeed satisfy the conceptual relation given in Equation (1.3). The discussion to follow will, therefore, be applicable only to phenomena for which Equation (1.3) is known to exist.

The most important property of Equation (1.3) is that it contains the relational parameters implicitly. These parameters must, therefore, be known at all the relevant points in space and time, before Equation (1.3) can be applied in practice. The success of a conceptual model thus hinges on the ability of the user to define these parameters uniquely over all space and time of interest. This is a rather severe restriction on the practical application of Equation (1.3), particularly in those situations where the conceptual relation is represented by a differential equation with its non-denumerable number of points in space and time.

One of the main reasons for the success of conceptual models in the exact sciences, was that the relational parameters are often simple constants (as, for instance, in the case of planetary motions), or that they can be controlled experimentally. This is, unfortunately, not true in environmental phenomena. The parameters encountered in these phenomena, are often so variable that it is unrealistic to try and determine them in full, or indeed replace them with a few laboratory determined values. Environmental scientists had, therefore, to turn to other strategies in order to apply conceptual models.

A most obvious strategy to use, would be to reduce the number of points at which the relational parameters are required, in space and time, to as few as possible. In the environmental sciences, many of the models are based on differential equations for which no analytical solutions are known. The application of these models thus usually requires the use of a numerical method. Since the majority of numerical methods, available for the solution of differential equations, are all based on the discretization of its domain of definition, it would seem that a reduction in the number of parameters can be achieved automatically.

However, to guarantee accuracy, the discretization cannot be too coarse. In fact, the information required on relational parameters for ecological models, may be so extensive, that they have to be determined indirectly.

The variable u in Equation (1.3) is often much better known in environmental sciences than the parameters **p**. A satisfactory solution to the parameter problem could thus be obtained quite simply by selecting a suitable set of u values and invert Equation (1.3). As is known [see eg. Meyer (1975)], this method can be quite successful, however, not if Equation (1.3) is represented by a differential equation. In this case, the inverse of Equation (1.3) has an infinite number of solutions.

Another way to circumvent the parameter difficulty, applicable whenever sufficient historical data are available, is to measure the parameters at as many points in space and time as possible and then interpolate them to the discretization points where their values are required. Interpolation is, unfortunately, only an approximate procedure. A solution of Equation (1.3) based on these interpolated parameters, may thus not represent observations accurately. In an effort to ensure that their models do indeed represent the observed phenomenon as accurately as possible, environmental scientists turned to what may be called the *fitting* of a conceptual model.

Although not absolutely necessary, the fitting of a conceptual model is usually divided into two phases. In phase one, also known as the *calibration phase*, the model is run with a set of interpolated parameters and the results compared with a subset of the historically observed u-values. If the model predictions agree with the historical information, the interpolated parameters are provisionally accepted as representative of the phenomenon, otherwise the parameters are modified and the procedure repeated. The second (*verification*) phase starts after the calibration phase has been completed successfully. The aim here is to see how closely the model can predict historical u-values not used in the calibration phase. A fitting is considered successful, if the model prediction represents the historical u-values within prescribed tolerances over a suitable period of time. Otherwise, the set of u-values, used for the calibration phase, is enlarged and the procedure repeated.

## 1.4 OBJECTIVES OF THE STUDY

There is an increased awareness of groundwater pollution in the Republic of South Africa. This can be seen, amongst others, in the regulations regarding the licensing of waste disposal sites which were published in terms of the different environmental acts. However, it is generally recognized that observations on groundwater pollution cannot be adequately interpreted without relating them to the physical properties and behaviour of the aquifer. To achieve this, it is essential that the information collected by monitoring the pollution should not only be utilised in an empirical way, but be evaluated by means of a groundwater quality model. This philosophy formed the basis of the contract between the WRC and the Institute for Groundwater Studies (IGS) of the University of the Orange Free State for the development of a suite of computer programs with which groundwater pollution, in both primary and secondary aquifers, could be modelled. The three-year contract commenced on 1985–07–01, but was later extended, until the end of 1988, to accommodate a sub-project, by the Department of Medical Microbiology at the University of Cape Town, on the longevity of bacteria and viruses in groundwater.

The first idea originally was to select a suite of computer programmes from the collection of programmes available commercially and/or among the international community of groundwater modellers and evaluate them with data obtained from a typical South African aquifer. To evaluate computer programmes of this nature, can be costly and time consuming. Much can, therefore, be gained by using an aquifer(s) with well-documented properties, or one for which this information can be obtained as cheaply as possible. After looking carefully at a number of South African aquifers, it was decided to select the Atlantis aquifer near Cape Town for the present investigation.

The main reasons for choosing the Atlantis aquifer for this investigation can be briefly summarized as follows:

(a) The aquifer, which serves as the sole water-supply source for the Atlantis township, has been studied for many years by the Division of Water Technology (DWT) of the CSIR through its Bellville Office, and a vast amount of information has been amassed under operational conditions.

(b) The aquifer is already polluted, due to intentional recharge by purified sewage and storm water run-off, [Müller and Botha (1986), Tredoux (1984)].

(c) The Division of Water Technology (DWT), formerly the National Institute for Water Research of the CSIR, has been carrying out an extensive investigation into artificial recharge and related aspects of water quality in the vicinity of Atlantis, at the request of the Western Cape Regional Services Council. Their willingness to cooperate in this venture was, therefore, much appreciated, as it meant that the Institute could rely on the experience of the DWT to supply the necessary data and guidance in determining the relevant relational parameters. This would give the Institute more time to evaluate and/or develop the necessary computer programmes. Once this has been achieved, both groups could combine to develop a pollution model for the Atlantis aquifer.

A disadvantage of the Atlantis aquifer, as a reference for the development of the proposed suite of computer programs, is that the aquifer is phreatic. It can, therefore, be argued that computer programmes evaluated with data from this aquifer need not be applicable to other South African aquifers, particularly the confined aquifers present in Karroo sediments. While this argument is true as far as the flow of groundwater is concerned, the conceptual model for mass transport does not depend on the type of aquifer. To fulfil the original objective, the suite of programmes used for Atlantis was supplemented with a program for flow in confined and semi-confined aquifers.

Although there are cases where aquifers have been polluted by discharging contaminated water directly into an aquifer, the more usual source of contamination is the percolation of rain water. Since aquifers are mostly separated from the soil surface by an unsaturated zone, the correct procedure would be to use a three-dimensional conceptual model that takes both saturated and unsaturated flow into account. However, such a model usually requires more information on the relational parameters, than can be supplied with present technology. At present, groundwater pollution is, therefore, mainly investigated with the help of a mass transport model and either a combined saturated/unsaturated vertical flow model (when interest is centred on the source of contamination), or a saturated horizontal flow model (when the extent and movement of contamination is required). This philosophy was also adopted in the present investigation.

A detailed investigation of the computer programs, available at the Institute for the modelling of saturated/unsaturated flow and mass transport, for a related project, revealed that the numerical approximations used in them, are unstable and do not satisfy the law of mass conservation. A new suite of computer programs had, therefore, to be developed for that project. These programs will also be used in the present investigation.

## 1.5 OUTLINE OF THE PRESENT STUDY

There is substantial evidence that the success of modelling an environmental phenomenon depends ultimately on: (a) the developer's knowledge of the physical processes which governs the phenomenon and (b) the quality and quantity of historical information available for the phenomenon.

Although there are a number of books available, which describe the principles of groundwater phenomena, the authors tend to approach the subject from the pure mathematical [Bear (1972), (1979)], or the application [McWhorter and Sunada (1977)] point of view, with little attention to the physics and chemistry governing the phenomenon. Because a modeller can only develop a successful model, if he fully understands the physics of the phenomenon to be modelled, it was thought worthwhile to include a rather complete description of the physics of flow in a porous medium in this report. This approach may cause difficulties for those who are merely interested in the results and not the development of a model. The present report has, therefore, been divided into two parts.

Part 1 starts in Chapter 2 with a discussion of the Atlantis aquifer and the observational network used in this investigation. This is followed by a discussion of the work done by the Department of Medical Microbiology on the longevity of certain bacteria and viruses in the groundwater at Atlantis in Chapter 3. The quality of groundwater, at the time of the investigations reported here, is discussed in the report of the DWT in Chapter 4.

One of the most difficult requirements to meet in constructing a model for subsurface flow is the determination of the conceptual parameters. The various parameters needed to model mass transport in subsurface flow, and methods that can be used to determine them, are described in Chapter 5.

An unresolved problem, carried over from the earlier work of Müller and Botha (1986), is the extent to which the Malmesbury Formation may influence sea-water intrusion into the aquifer. Because of its relation to the hydraulic conductivity, this problem is also discussed in Chapter 5, where it is shown that the Malmesbury Formation is highly permeable.

Two-dimensional unconfined (phreatic) flow is often modelled with a model of confined flow for which the transmissivity is allowed to vary as a function of time. However, as is shown in Chapter 12, the two types of flow differ considerably from the physical point of view. The conceptual model adopted for this purpose, and some results obtained with it for the Atlantis aquifer, are discussed in Chapter 6, together with the program for modelling horizontal flow in a semi-confined aquifer.

Unsaturated flow is probably the most difficult and exciting groundwater related phenomenon to model conceptually. Because of the difficulties experienced with existing models, it was necessary to develop a completely new model. Although the development of this model falls outside the scope of the present investigation, its application in conjunction with the mass transport to the pollution around the infiltration pan at Atlantis, is discussed in Chapter 7.

Part 2 of the report starts with a discussion of the basic properties of fluids in Chapter 8 and a porous medium in Chapter 9. This information is used as the basis for a discussion of the most basic component of the conceptual model for groundwater flow – Darcy's Law – in Chapter 10.

The general conceptual model for groundwater flow, discussed in Chapter 11, forms the basis for the discussion of the more specialized conceptual models for confined, unconfined and combined saturated and unsaturated flow in Chapter 12.

The physical basis, customarily used to derive a conceptual model for mass transport, is at present in doubt. Although the problem is receiving considerable attention on an international scale, it will take time before a more physically acceptable conceptual model, will emerge. The computer program used for mass transport in this investigation, is therefore still based on the classical principles, discussed in Chapter 13.

# PART 1

# VIROLOGICAL, CHEMICAL AND HYDROGEOLOGICAL INVESTIGATIONS AT ATLANTIS

# CHAPTER 2

# SITE DESCRIPTION

## 2.1 INTRODUCTION

The Atlantis aquifer is situated on the west coast of the Cape Province, more or less 50 km north of Cape Town, and covers an area of approximately 250 $km^2$ (see Figure 2-1). The aquifer is the sole source of water for the Atlantis township and its associated industries, which are located more or less in the centre of the aquifer. The Koeberg nuclear power station is on the southern part of the aquifer.

The physiography of the aquifer and its environment have been described in detail by Müller and Botha (1986) to which the reader is referred for further information. The climate of the area is Mediterranean, with mean maximum and minimum temperatures of 23,2°C and 11,8°C, respectively. The mean annual rainfall varies across the aquifer from 416 mm, as measured at Melkbosstrand, to the 369 mm measured at Mamre (see Figure 2-1). About 65% of the rainfall events occur during the winter months, May to September.

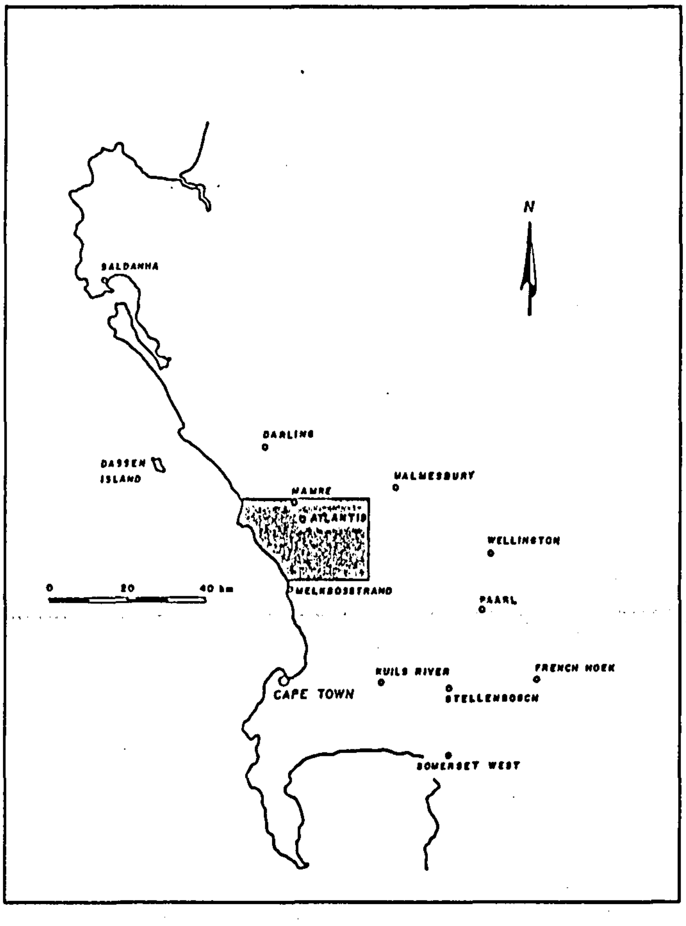

Figure 2-1 Locality map of the study area

## 2.2 GEOLOGY

The geology of the Atlantis area can be divided chronologically into three main units (see also Figure 2–2):

(a) The Malmesbury Group.
(b) Intrusive granite of the Darling Pluton.
(c) Cenozoic sediments.

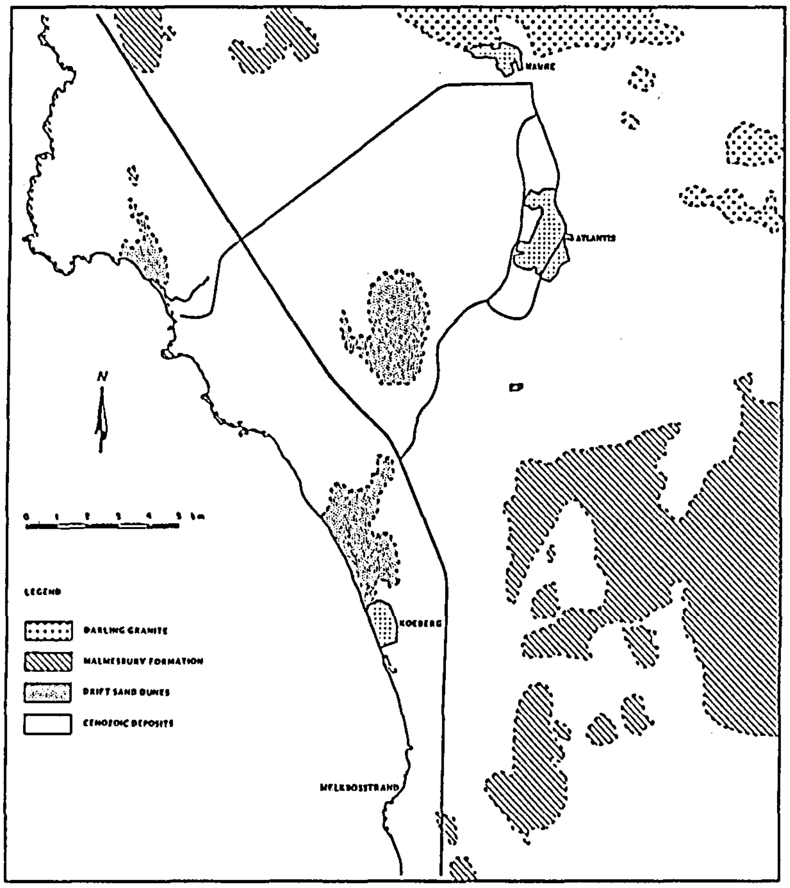

Figure 2-2 Geological map of the Atlantis area, after Müller and Botha (1986)

Although the cenozoic sediments comprise the main water-bearing unit, the other geological units form an integral part of the aquifer, to the extent that they define physical boundaries for the aquifer (the Malmesbury Group and intrusive granite).

In their previous investigation of the aquifer, Müller and Botha (1986) hinted at the possibility that the Malmesbury Group may, at least in some places, be highly fractured and contain considerable volumes of water. This possibility is rather disturbing, since the Malmesbury Group is the main boundary between the cenozoic deposits and the sea (see Figure 2–2). If this is true, any large-scale withdrawal of water from the aquifer may cause the intrusion of sea-water.

## 2.3 PRESENT MANAGEMENT PRACTICES

At the present moment, withdrawal of water from the Atlantis aquifer is restricted to two areas – the Witzand and Silwerstroom production fields (see Figure 2–3). The volume of water withdrawn varies considerably from summer to winter and even from year to year, depending on the climatic factors.

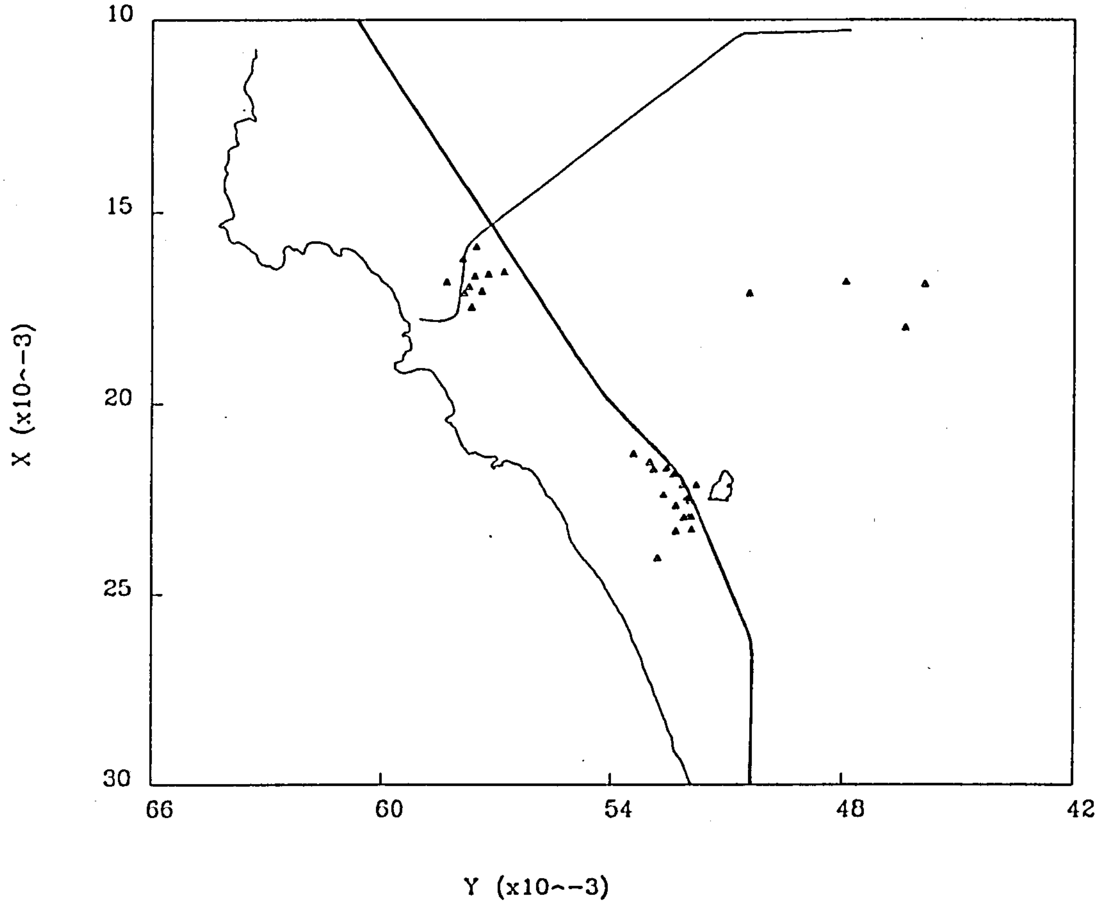

**Figure 2-3** Location of the production fields (at Silwerstroom and Witzand) and the infiltration pan (Pan 7) at Atlantis

In the original white paper on the Atlantis project, it was proposed to mine the aquifer, before water would be supplied to the area from the Berg River. In an effort to ensure that the aquifer could supply in the demand until the surface water scheme was implemented, the then Divisional Council of the Cape, who was responsible for the development of the area, decided to recharge the aquifer with storm and purified sewage water from the township and industrial area. For this purpose, the storm water is collected through a series of ponds, before it is mixed with the purified sewage water and discharged into the infiltration pond, Pan 7 in Figure 2–3.

## 2.4 MONITORING NETWORK AROUND THE RECHARGE BASIN

### 2.4.1 Groundwater Level and Quality Network

Although the infiltration pan has been in operation from the beginning of the operations at Atlantis, no attention was paid to its actual influence on groundwater levels and quality. No observation points existed in the vicinity of the artificial recharge basin, when the DWT became involved with the water-supply scheme at Atlantis in 1983.

The first boreholes in this area were drilled in the second half of 1983 on their request. In July 1985, when the groundwater quality project started, the observation network consisted of 17 piezometers and four boreholes. A further 17 piezometers were installed in 1986, with the assistance of the Directorate of Geohydrology of the Department of Water Affairs. In a number of instances, the installation of piezometers failed, due to the presence of clay layers or calcrete. For this reason, a private drilling contractor was employed for extending the monitoring network at the beginning of 1987, as part of the present project. Together with the piezometers which were installed by the Directorate of Geohydrology, the total number of observation points finally reached 60.

For all the observation points installed during 1986 and 1987, a drilling mud (Revert) was used. After completion of the holes, the drilling mud was flushed from the holes by means of fresh water. The larger part of the remaining drilling mud was subsequently removed by developing the holes with compressed air. At the northern side of the basin, clay deposits were found which complicated drilling. In that area, drilling usually ended at a depth of nine to 10 m in a thick clay layer. Eventually, a borehole of approximately 20 m deep was drilled just inside the basin itself (No. 54, on Figure 2–4). Although the borehole is situated within the 60 contour line, the water seldom reaches that point. The clay layer at that point is less than a metre thick and the borehole also ends in argillaceous sediments. The monitoring point network as it existed towards the end of February 1987, is shown in Figure 2–4. In the vicinity of borehole G33110, piezometer numbers 36 to 40 were installed, at a distance of 10 m apart around the borehole, for the experimental determination of dispersion in the aquifer.

At most of the observation points, a pair of piezometers was installed. The purpose was to monitor the two subsections of the Bredasdorp Formation, namely the Witzand and Springfontyn Members, separately. Small differences exist in the piezometric heads which could lead to contamination of the overlying or underlying formations, should one piezometer be used to monitor both horizons.

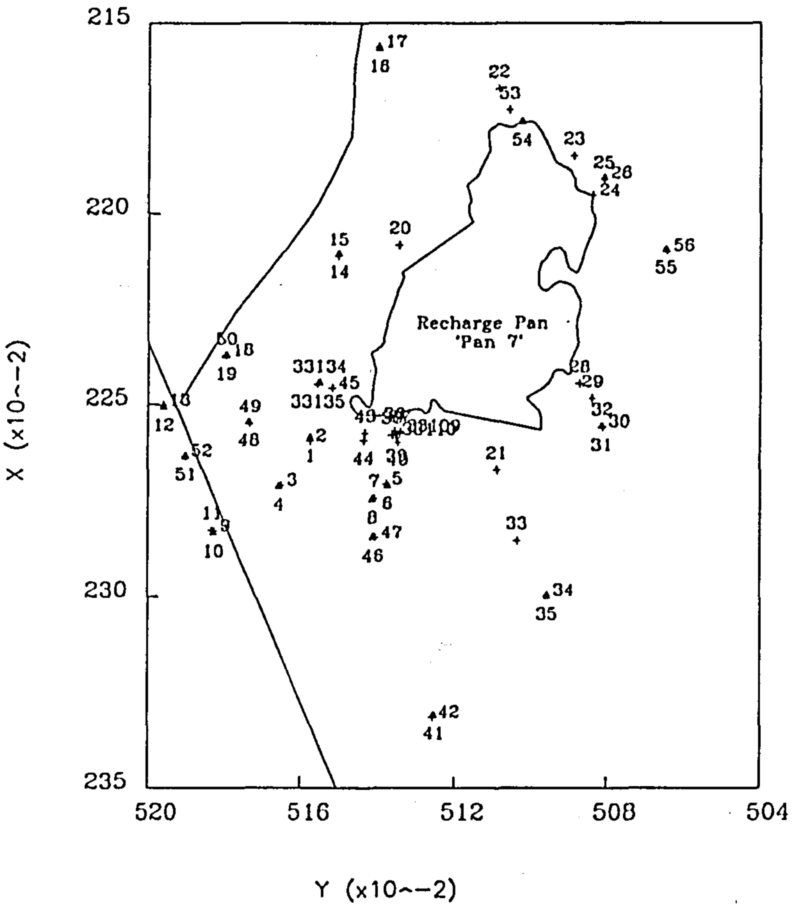

Figure 2–4 Positions of the observation points around the infiltration pond at Atlantis (Δ shallow, + deep)

The extension of the observation network around the basin was carried out at the lowest cost possible. This methods utilised, therefore, precluded the gathering of detailed information about the deposits themselves. This lack of knowledge on the deposits is rather unfortunate, especially on the northern side of the basin where relatively impermeable layers occur and the groundwater movement could be impaired considerably. Moreover, it appears that the sand itself is also clayey, which could seriously restrict groundwater movement. It would, therefore, be ideal if the clay content of the sand and the thickness of clay layers, in this area, could be determined at some time in the future.

### 2.4.2 Soil Moisture Tubes

Initially, it was intended that the 10 aluminium tubes for neutron soil moisture measurements would be installed by the drilling contractor. However, the contractor could not drill without drilling mud, and in view of the size of the holes and the creation of cavities during drilling with a rotary drill, it was decided to install the aluminium tubes by hand. For this purpose, the DWT obtained a 50 mm diameter auger which was slightly modified and then successfully used to auger holes to the groundwater level in which the aluminium tubes fitted tightly. The installation took place at the end of the dry season at a stage when the groundwater level was at its lowest. The lower end of the tubes was sealed with rubber stoppers. The location of the aluminium tubes is shown in Figure 2–5.

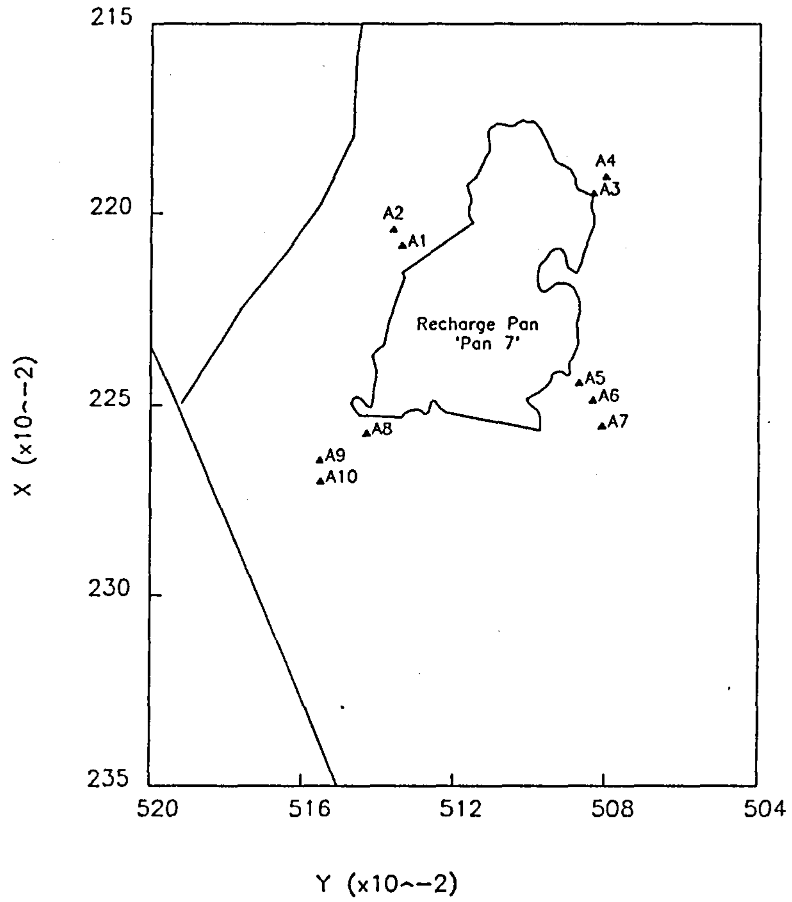

**Figure 2–5** Positions of the neutron observation holes around the infiltration pond at Atlantis

Based on the experience gained in this and other related investigations, it can be said that the number of neutron tubes installed was too small. One should really install a cluster of tubes at a specific observation point, rather than single tubes as used here, if the hetereogeneities in natural soils are to be accounted for.

# CHAPTER 3

# VIROLOGICAL STUDIES AT ATLANTIS

## 3.1 MOTIVATION

Studies already in progress at the Institute for Groundwater Studies, as well as the chemical analyses and bacteriology performed by the NIWR (Bellville), lacked information on virus pollution. The danger, therefore, exists that the aquifer would be a potential source of epidemic or sporadic disease, should the percolated groundwater become contaminated with viruses. Such diseases include hepatitis, gastro-enteritis, poliomyelitis and encephalitis.

Existing models in the literature were felt not to be appropriate for an aquifer which is observed to be saturated in winter and unique in soil composition. Moreover, the behaviour of viruses in a continuous liquid phase, rather than a percolate, was not known. It was, therefore, decided to evaluate the potential for migration, both vertically and horizontally, of human pathogenic enteric viruses in conjunction with the ongoing investigation of chemical pollution of the aquifer.

## 3.2 HUMAN PATHOGENIC VIRUSES IN ATLANTIS WATER

### 3.2.1 Inflow

Storm-water samples from the inflow to Pan 7 were examined for viral content on three occasions. Coliphages and faecal coliforms were present in all three samples. Coxsackie B1 and reovirus III were recovered from one, coxsackie virus B6 and reovirus III from another and coxsackie B4 from the third.

Reovirus and an enterovirus have been isolated from a sample from Pan 6 which also contained coliphages.

### 3.2.2 Borehole Samples

Eight boreholes in the vicinity of Pan 7 were assayed for virus. Water from borehole 33110 and 33135 was contaminated with faecal coliforms. No virus was isolated from any of the borehole waters (see Appendix A and Table 3–1). A sample of water from borehole 33443, near the secondary infiltration ponds, showed no detectable virus or coliphage contamination (Table 3–1).

**Table 3–1** Faecal coliforms, coliphages and viruses observed in water samples from boreholes near the secondary infiltration ponds at Atlantis

| Code | Date | Borehole | Faecal Coliforms (per 100 ml) | Coliphages. per (100 ml) | Viral Isolation | Titre |
|---|---|---|---|---|---|---|
| A1/87 | 1987–09–03 | G30966 | <2,0 | <2,0 | none | |
| A2/87 | 1987–10–03 | G33110 | $1,0x10^{3}$ | <2,0 | none | |
| A3/87 | 1987–17–03 | G33135 | $1,0x10^{2}$ | <2,0 | none | |
| A4/87 | 1987–23–03 | G33109 | <2,0 | <2,0 | none | |
| A5/87 | 1987–30–03 | G33134 | <2,0 | <2,0 | none | |
| A6/87 | 1987–08–04 | G33110 | 2,0 | <2,0 | none | |
| A7/87 | 1987–21–04 | G33135 | <2,0 | <2,0 | none | |
| A8/87 | 1987–27–04 | Pan 7 Inlet | 80,0 | $8,0x10^{2}$ | Coxsackievirus B1 | 20,0 |
| | | | | | Reovirus III | 20,0 |
| A9/87 | 1987–05–05 | Pan 7 Inlet | $1,0x10^{2}$ | $1,3x10^{4}$ | Coxsackievirus B6 | 20,0 |
| | | | | | Reovirus III | 200,0 |
| A10/87 | 1987–11–05 | Pan 7 Inlet | 60,0 | $2,0x10^{2}$ | Coxsackievirus B4 | 20,0 |
| A1/88 | 1988–23–08 | Pan 6 Inlet | <2,0 | $1,3x10^{2}$ | Enterovirus | 100,0 |
| | | | | | Reovirus | 50,0 |
| A2/88 | 1988–25–08 | G33443 | <2,0 | <2,0 | none | |

## 3.3 HUMAN PATHOGENIC VIRUSES IN THE ATLANTIS SOIL

In order to evaluate the virus adsorption capacity of sand at Atlantis, perspex columns were set up in the laboratory. Initially, columns of 480 mm x 55 mm were packed with sand from Pan 1. Three millilitres poliovirus Vaccine Type I was absorbed into the column and eluted with distilled water at a rate of 2 ml.min$^{-1}$, or 3,38 m.d$^{-1}$. All the viruses were recovered in the eluate. The experiment was repeated with coxsackie B6 virus. This virus did not absorb to the sand either.

Samples of sand were taken from the secondary infiltration ponds (1) and (2) for further study. A large column of 600 mm x 92 mm was filled with sand from the upper soil layer of infiltration pond (1) and a column of 480 mm x 55 mm with sand from a depth of 700 mm in the pond.

Poliovirus Vaccine type I was layered onto the upper soil column, absorbed into the sand, and eluted with storm water. The filtrate from this column was sampled for viral titration and subsequently passed through the deeper sand column. The experiment was repeated with coxsackie B6 virus. Columns of sand from the secondary infiltration pond (2) were treated in a similar manner.

All the viruses were recovered in the filtrate from all columns, although the poliovirus was eluted at a slower rate than the coxsackie virus.

## 3.4 SURVIVAL AND MIGRATION PATTERNS

### 3.4.1 Survival Times

In order to study the survival of enteric viruses in conditions similar to the Atlantis environment, water samples from Pan 7 were seeded with a vaccine strain (Sabin) of poliovirus, a coxsackie virus (B6), reovirus type III and a rotavirus. Volumes of tap water, distilled water and unbuffered physiological saline were seeded with the same viruses for comparison.

The suspensions have been left on the bench for more than six months during which time the ambient temperature reached 30°C on hot summer days and dropped as low as 4°C on winter nights. The content of virus was titrated at weekly intervals for 26 weeks. The results of these titrations are depicted in Figures 3–1 to 3–2.

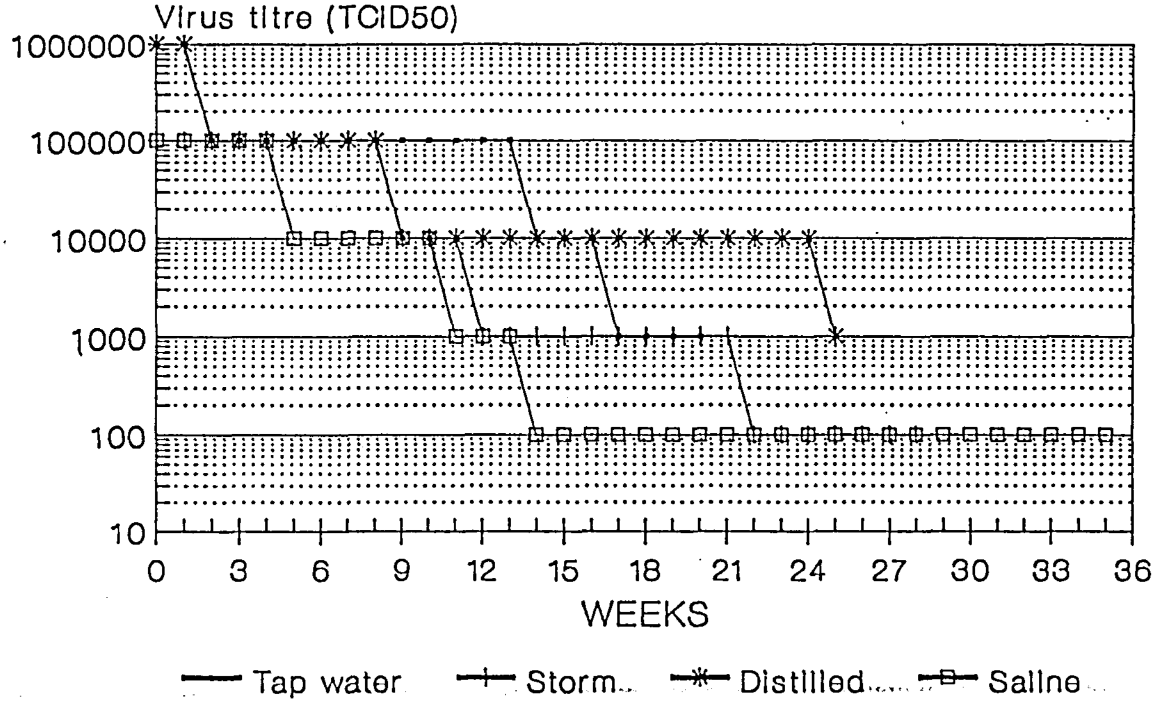

**Figure 3–1** Survival time of the coxsackie virus (B6) in different types of water

The titre of all the viruses diminished some thousandfold during the six-month period. The attrition rate of poliovirus was similar in all media. Coxsackie B6 survived best in distilled and least well in saline water, while the poliovirus survived best in saline and storm water.

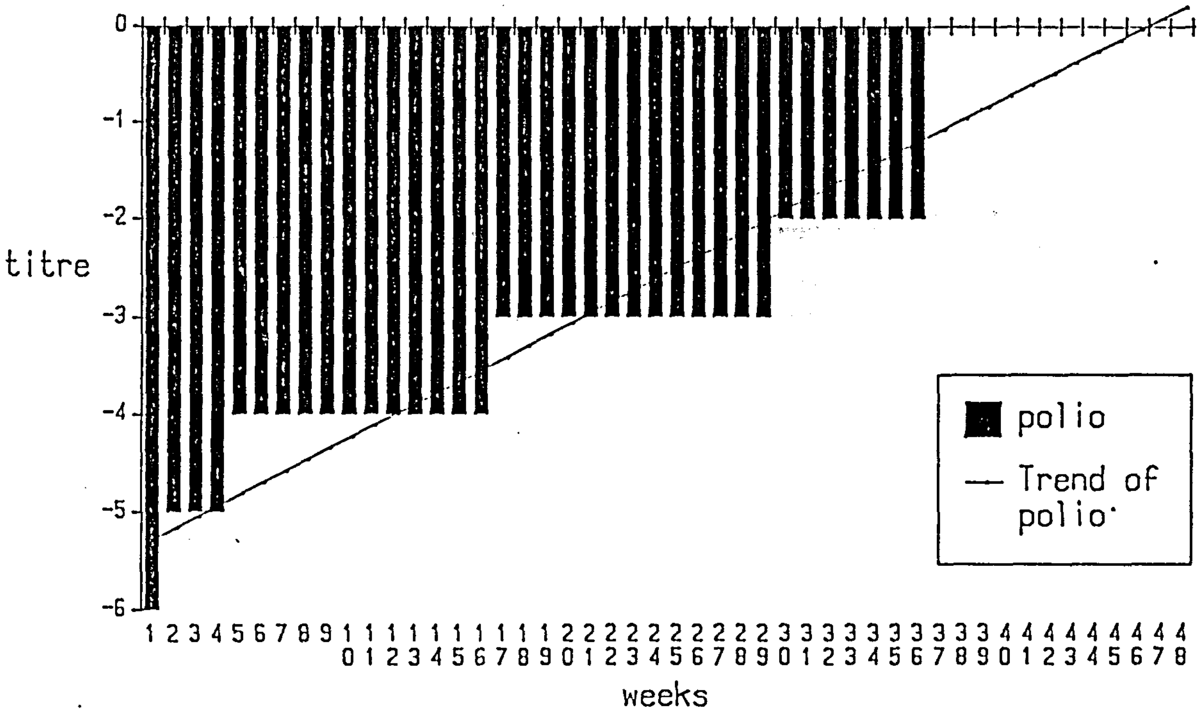

Figure 3–2 Survival time of the poliovirus in in different types of water

Fluctuations in titre, particularly that of reovirus, reflect the variability of various batches of cells used for assay rather than a true change in the amount of virus.

Of the different media, tap water maintained rotavirus best and coxsackie virus least. In distilled water, reovirus survived longer than other viruses. Saline water maintained reo and rotaviruses longer than polio and coxsackie viruses. In water from Pan 7, the survival rate of reo and rotavirus was the highest and poliovirus and coxsackie virus the least. Reovirus appeared to maintain infectivity longer than other viruses tested.

Reovirus is frequently isolated from effluent derived water samples in South Africa and it may be that the virus survives for longer periods and is more tolerant of differing water conditions than other enteric viruses, notwithstanding the large number of viral particles present in the excreta of most animals, birds and insects.

### 3.4.2 Virus Adsorption Studies

Equal samples of sand (1 gm) from 700 cm below the surface of secondary infiltration pond 1, were mixed with varying dilutions of virus over a two-hour period. The sand was removed by centrifugation and the supernatant fluids were titrated and compared with control dilutions to estimate the amount of virus adsorbed by the sand.

The pH of the distiled water used to dilute the virus was adjusted to pH levels of 4,0; 7,0 and 9,5.

*Coxsackie B6*

This virus was isolated from inlet water to Pan 7. A linear relationship with increasing amounts of virus was observed between adsorbed and free virus to a constant mass of Atlantis sand, for all three pH levels used (see Figure 3–3). The slopes of these curves describe the adsorption capacity of the sand.

*Reovirus*

Reovirus type III isolated from water on the Cape Flats adsorbed well at pH 4,0; 7,0 and 9,5 (see Figure 3–4).

*Poliovirus*

A linear relationship was observed for varying concentrations of poliovirus and adsorption to Atlantis sand. This strain (Sabin type I) adsorbs well at pH 4,0; 7,0 and 9,5 (see Figure 3–5).

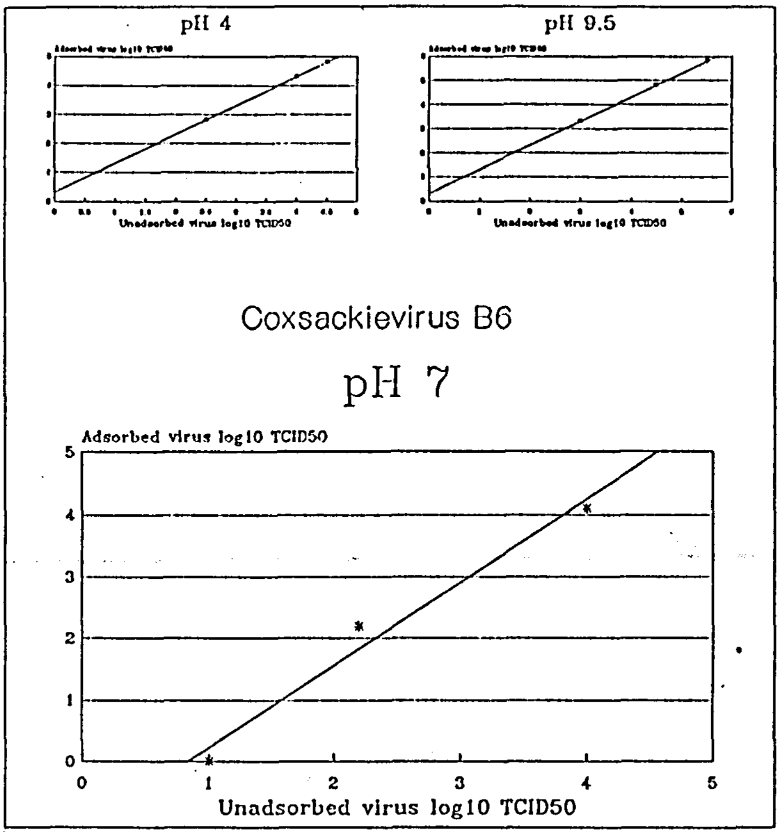

Figure 3–3 Adsorption properties of the Coxsackie B6 virus to the Atlantis sands

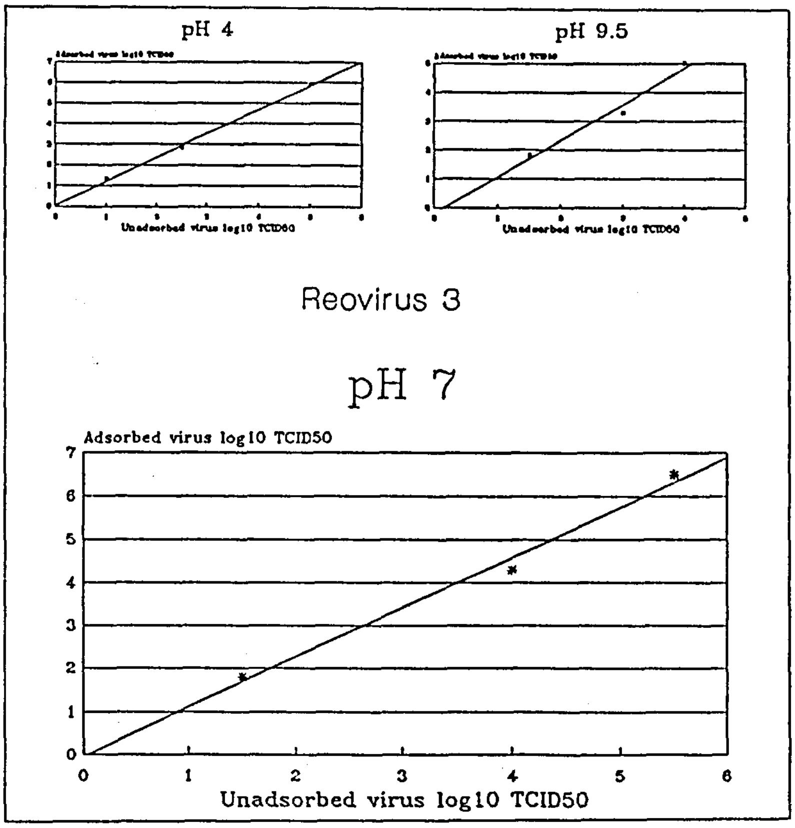

Figure 3–4 Adsorption properties of the Reovirus to the Atlantis sands

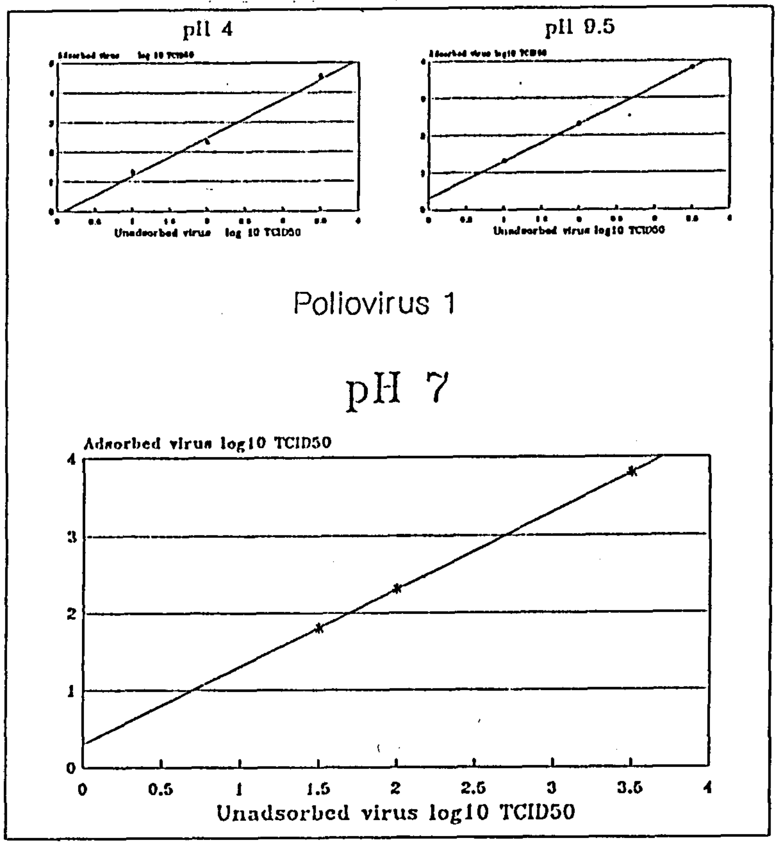

Figure 3–5 Adsorption properties of the Poliovirus 1 to the Atlantis sands

## 3.5 CONCLUSIONS

Enteric viruses were demonstrated in the inflow water to both Pans 6 and 7. The viruses isolated were human in origin and all potentially pathogenic to man. No viruses were recovered from borehole water below the injection pans.

Virus survival studies in water indicate an extinction interval of more than 36 weeks at ambient room temperature. At present, the study has been in operation for 38 weeks and all inoculated water still contains live virus.

Several laboratory column models, using both distilled (rain) and storm water, were developed to try and simulate conditions in the aquifer. Unfortunately, these models were less sensitive to adsorption/elution studies than was visualized. In fact, no adsorption could be detected, using these models.

An additional study was introduced to provide information for determining migration patterns. These kinetic adsorption experiments were extremely sensitive and showed that adsorption to the Atlantis sand differed with virus strain and with pH. The linear relationships observed in the adsorption of viruses to the sand, not only validate the experimental data, but could simplify the modelling of virus migration in the aquifer considerably.

The variability in adsorption of viruses is noted elsewhere in the international literature and can be ascribed to minor alteration in the protein coat of the virus which affects its charge density. Viruses of the same family or even of the same species may differ in this characteristic.

In conclusion, it can be said that the aquifer is not contaminated with enteric viruses. The worst situation would relate to saturated conditions, low pH and non-adsorbed viruses. Survival studies at room temperature (survival would be longer in the dark, cool aquifer) indicate that live virus could be carried in the liquid phase of the aquifer with little retardation for possibly 60 days. Integration of the information into a mathematical model, seems to be the only feasible alternative to determine a safety factor, as far as virus migration in the aquifer is concerned.

# CHAPTER 4

# GROUNDWATER QUALITY IN THE ATLANTIS AQUIFER

## 4.1 INTRODUCTION

The successful translation of a conceptual model to a computer code depends largely on the quality of the information available for at least one real world example of the phenomenon in question. The aquifer serving as a water-supply source for Atlantis has been studied for many years and a vast amount of information has been amassed under operational conditions. The artificial recharge of the aquifer with storm water, and earlier on also with treated effluents, provided the opportunity for studying and modelling the transport of chemical impurities in the groundwater. Thus, it was decided to use this primary aquifer for the initial development of a computer code that could form the basis for modelling contaminant transport in South African Aquifers.

Analysis of the information, available in 1986, proved that extension of the network of monitoring points was necessary. Consequently, more intensive observations were carried out in 1987 and 1988. These included water-level and soil moisture measurements. The increase in field observations and particularly the analytical work required a significantly larger financial input by the Division of Water Technology.

## 4.2 COLLECTION OF DATA

### 4.2.1 Soil Moisture Measurements

Some difficulties were experienced in obtaining continuous sets of soil moisture measurements, because the neutron moisture meter had to be shared with another project of the Institute. This was rather unfortunate, because it became impossible to measure soil moisture contents and water levels simultaneously, or to follow the water contents continuously after a rainfall event. The final result was that only 13 sets of soil moisture measurements could be carried out, during the period from August 1987 to October 1988, at the dates shown in Table 4–1.

**Table 4–1** Dates at which neutron soil moisture readings were taken around the infiltration pan at Atlantis

| | | | | |
|---|---|---|---|---|
| 1987–08–06 | 1987–08–20 | 1987–09–10 | 1987–10–14 | 1987–11–05 |
| 1988–01–13 | 1988–04–21 | 1988–07–28 | 1988–08–15 | 1988–09–05 |
| 1988–09–29 | 1988–10–14 | 1988–10–21 | | |

### 4.2.2 Water-level Measurements

The DWT was responsible for measuring water levels in the vicinity of the artificial groundwater recharge basin. The frequency of measurement of water levels varied from once a week to once a month, depending on the location of that particular observation point with respect to the artificial recharge basin. Although water-level measurements were carried out over the whole period, the full programme only came into operation at the beginning of 1987, after completion of the network of monitoring points.

### 4.2.3 Groundwater Sampling

The main task of the DWT was the gathering of detailed information on the groundwater chemistry in the aquifer. The additional observation points installed at the beginning of 1987 were of special importance, both for the determination of the groundwater level and obtaining additional hydrochemical information. Taking the size of the recharge basin (28,3 ha when full) into account, it is evident that 60 monitoring points (which should monitor two horizons) are hardly sufficient for thorough monitoring. The longer monitoring is continued, the more accurate the groundwater system can be defined. At the beginning of 1987, a new intensive sampling programme was implemented which incorporated all the new sampling points. Again, sampling frequency varied according to the distance from the recharge basin to the observation point.

### 4.2.4 Operation of the Artificial Groundwater Recharge Basin

The operation of the recharge basin constitutes a part of the management programme for the Atlantis aquifer and, strictly speaking, does not form part of the present project. Nevertheless, decisions which are taken with respect to recharge operations have a direct effect on the quality of the water recharged to the aquifer. For this reason, some details are given below.

The most important aspect is that the recharge of purified waste water was discontinued in November, 1986. The main reason was that the industrial component of the purified effluents increased. The risk of the presence of non-degradable organic compounds and the increasing salinity rendered them unsuitable for unrestricted re-use. Once the domestic and industrial waste water treatment is fully separated, the recharge of maturation pond effluent from domestic origin, will be reconsidered. Since November 1987, the base flow in the storm-water system is also diverted from the recharge basin during the summer months. The main consideration in this case was the high salinity of the water, especially that originating from the industrial area.

## 4.3 LITERATURE STUDY

### 4.3.1 General

A limited literature study was carried out to determine to what extent the physical-chemical interaction between the chemical components in the recharge water and the aquifer material had previously been investigated. Information was also sought on the possible determination of dispersion by means of chemical observations.

### 4.3.2 Physical-chemical Interactions

From the literature, it is evident that the reactions of inorganic components in the water with the aquifer material are relatively well-known [Garrels and Christ (1965), Hem (1970), Krauskopf (1967) and Matthess (1973)]. Certain ions, such as chloride, do not enter into any reactions which are worth mentioning and are transported advectively by the water. Cations, such as potassium, are subject to ion exchange or adsorption in the presence of clay minerals. Anions, such as dissolved phosphate, also occur, especially in calcareous aquifer material, such as those found at Atlantis. Other reactions, influencing the concentration of chemical constituents, are oxidation and reduction. Under saturated conditions, as present at Atlantis, anoxic (and possibly anaerobic) conditions occur readily. Conversion of compounds to other oxidation states, can, therefore, readily take place. In the case of nitrogen compounds, oxidation of ammonia to nitrate readily occurs, often followed by nitrate reduction. Nitrate reduction is brought about by denitrifying bacteria under anoxic conditions. In the underlying horizons, sulphate reduction even occurs. A pollution model for the Atlantis aquifer will, therefore, have to make provision for all these chemical processes.

Most of the organic compounds occurring in effluents, storm water and other sources, create a considerably larger problem [Piet and Zoeteman (1980)]. According to the literature, the adsorption of hydrophobic compounds is generally adequately described by the Freundlich isotherm and the distribution coefficients of the compounds [Roy and Griffin (1985)]. For this purpose, it is necessary to determine the organic carbon content of the soil or deposits. It is also stated that the relationship is not necessarily valid for deposits with little carbon, for instance in the case of sandy aquifers. Nevertheless, the Langelier and Freundlich isotherm is widely applied and is considered suitable to describe the exchange process with respect to heterogeneous material such as soil and sediments [Kinniburgh (1986)]. In general, the upper one and a half metre of sand at Atlantis are rich in organic material, the exception being the area with unvegetated dunes. There, the organic content of the sand is considerably lower.

Most of the organic compounds present in the effluents are biodegradable to form simpler compounds such as carbon dioxide and water. However, a non-degradable fraction remains and these persistent compounds create a problem, because they will eventually appear in the water withdrawn from the aquifer. Their persistence does not only depend on the chemistry, but also on the nature of the particular ecosystem. It is described as follows by Zoeteman *et al.* (1980):

> *'The persistence of an aquatic pollutant is the capability of the chemical in the aquatic system considered to resist a reduction of the original concentration in the water phase after a certain period of time, while undergoing a variety of physical, chemical and biological processes.'*

There is a difference in the persistence of chemicals in the surface zone as compared to groundwater. In groundwater, most organic compounds are more persistent, even a hundred times more persistent, when particular compounds are compared from a river and from groundwater [Zoeteman *et al.* (1980)].

For the purposes of the groundwater quality model, it is impossible to make provision for all organic compounds (even those that have already been identified). It would, therefore, be advisable to select a number of the EPA priority pollutants for modelling purposes.

The required degree of complexity of the eventual groundwater quality model which would make provision for all changes in quality during the movement of pollutants through the unsaturated and saturated zone, cannot be determined exactly at this stage. The literature study has shown that various approaches have been followed. For successful simulation of all the chemical processes taking place in the aquifer, it might even be necessary to develop a multiphase model [see e.g. Abriola and Pinder (1985(a) and (b))]. This refers to a detailed section in the immediate vicinity of the recharge basin or pollution source where most of the chemical reactions are expected to take place.

### 4.3.3 Dispersion

Dispersion coefficients can be determined for the aquifer in the vicinity of the recharge basin by means of chemical tracers (pollutants) which are present in the recharged water. At the Koeberg Nuclear Power Station, not far from Atlantis, dispersion coefficients were determined by means of radioactive tracers [Meyer *et al.* (1981)]. This method can also be utilised with non-radioactive tracers, provided breakthrough curves can be determined for the tracers involved. It has, however, become evident that initially the monitoring points were not sampled regularly enough over a sufficiently long period for this purpose. The frequency of monitoring was, therefore, increased in an attempt to obtain the necessary information. In the case of the experiment at Koeberg, the observations were carried out over distances of only two and four metres, while the observation points at Atlantis are at least 10 m apart.

### 4.3.4 Hydrochemical Stratification

Hydrochemical stratification has been described in the literature on a number of occasions [Barker *et al.* (1987) and Ronen *et al.* (1987(a))]. Particularly in the coastal aquifer in Israel, large variations in the chemical composition of groundwater with depth, were observed *in situ* [Ronen *et al.* (1987(a))]. A special groundwater sampler was designed which could sample a five metre water column in a borehole at depth intervals of 30 mm, so as to be able to observe differences in the groundwater composition with depth [Ronen *et al.* (1987(b))]. Molz and Widdowson (1988) modelled these detailed variations in concentrations with depth and came to the conclusion that such concentration gradients can only occur when the transverse dispersivity in the vertical direction amounts to at least one mm. Their model provides for the simulation of chemical and microbiological activity in the aquifer.

## 4.4 DISCUSSION OF THE GROUNDWATER LEVELS

Since the beginning of 1987, groundwater levels were measured regularly at each of the 16 monitoring points which comprised the extended network. In 1987, considerable variations were observed in the water levels. In 1988, when the rainfall was significantly lower, a much smaller variation in water levels was observed. For the period from March to September 1987, contour maps of the water-level configuration were compiled at two-monthly intervals (see Figure 4–1). Only one contour map was compiled for 1988 (see Figure 4–2).

In Figure 4–3, the water levels in the recharge basin are compared with the variations in groundwater levels at monitoring points on the western and north-eastern side of the basin, while Figure 4–4 shows the ‘secondary basins’ which occur around the recharge basin when the water level rises.

The contours in Figure 4–1 clearly shows that the groundwater level has a general gradient in a west-south-westerly direction. The steep gradient in the immediate vicinity of the recharge basin is clearly discernible. In March 1987, the situation is depicted where the water level in the artificial recharge basin reaches a minimum of 57,15 m above sea level. An irregularity in the water-level distribution is clearly noticeable at the 53 m contour line in the vicinity of boreholes G33134 and G33135 [see Figure 4–1(a)].

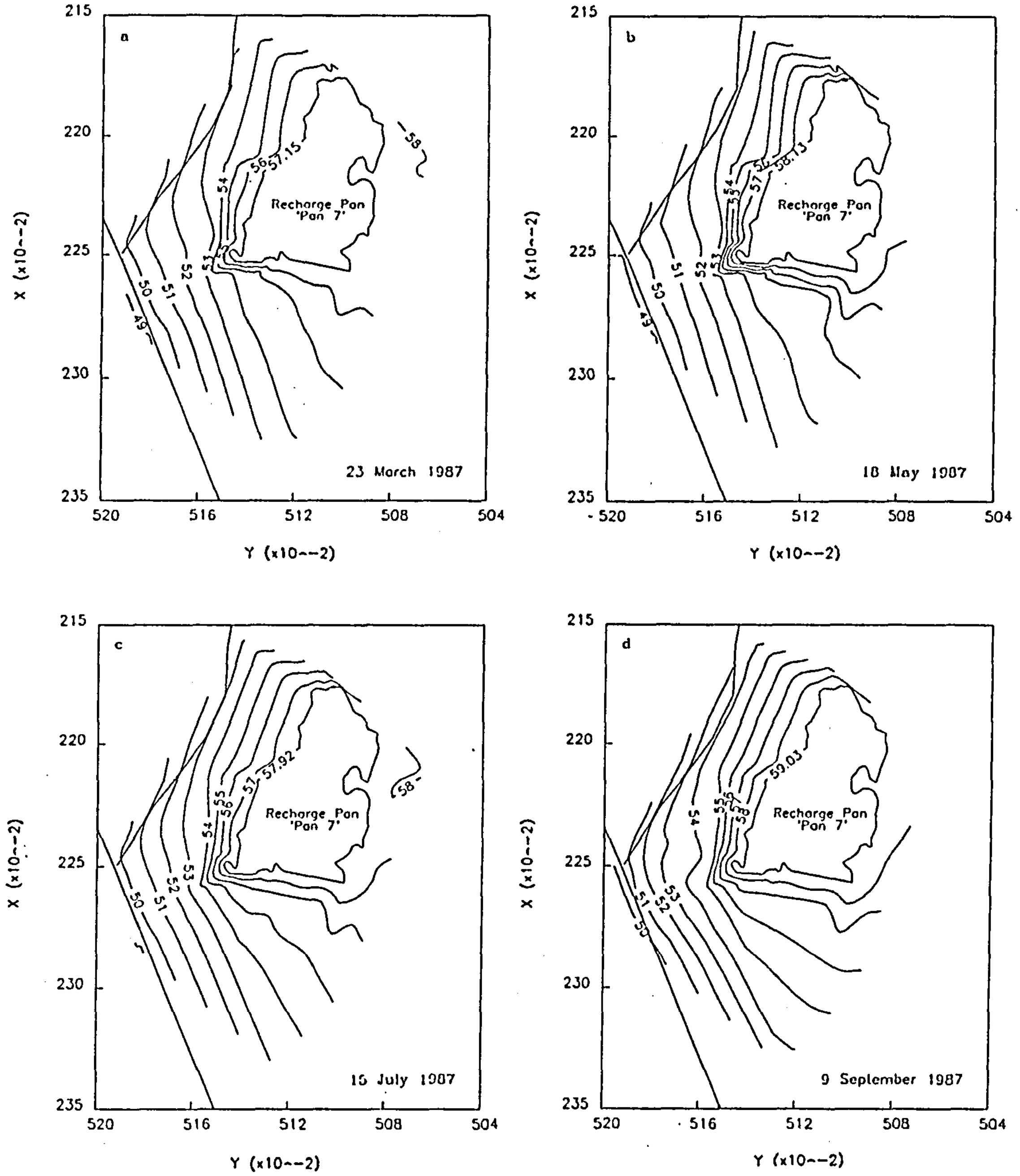

**Figure 4–1** Contours of the groundwater-levels in the vicinity of the infiltration pond at Atlantis on a few selected dates

From the contour map for 18 May 1987 [Figure 4–1(b)], it is evident that despite the one metre rise of the water level in the recharge basin, only those contours in the immediate vicinity of the basin are affected. The 56 and 57 m contours are situated further from the basin. The 55 m contour on the western side of the basin also moved somewhat further westwards, i.e. further from the basin. At the northern and southern end of the basin, even the 55 m contour line is still situated closer to the basin than in March. All the other contour lines from 49 to 54 m show a drop in the water level from March to May. In the middle of July, the water level in the recharge basin was still only 58 m above sea level. At that stage, all the water levels over the whole of the area up to and including the 49 m contour in the west, showed an increase [see Figure 4–1(c)]. The natural groundwater level at the north-eastern end of the basin, however, remained at approximately 58 m above sea level. In July, the first 'secondary basins' formed in depressions south of the recharge basin [see Figure 4–4(a)]. From the figure, it is evident that there was an increase in the water-level gradient in the western and south-western side of the recharge basin.

By September 1987, the water level in the recharge basin was at 59 m above sea level, which is a metre higher than in July. In the north-western part of the area, the water level was at the same height as in March 1987, i.e. 53 m above sea level. To the west of the West Coast Road, the water level was, however, a metre higher than in March [see Figure 4–1(d)]. At the north-eastern end of the basin, the groundwater level in the immediate vicinity of the basin was eventually higher than the natural groundwater level, which meant that recharge from the basin also took place in this direction. At that stage, groundwater appeared in nearly all the depressions on the southern and eastern end of the basin [see Figure 4–4(b)]. The significance of this phenomenon is that the 'secondary basins' at the southern end of the recharge basin became so large that 'short circuiting' of the aquifer took place along the surface. This meant that the water could move along the surface over a distance of several hundred metres instead of through the aquifer. This phenomenon could have important implications with respect to the water quality, should large quantities of water move into the production field in this way without adequate retention time in the aquifer itself. This would also have to be taken into account in the development of the mass transport model.

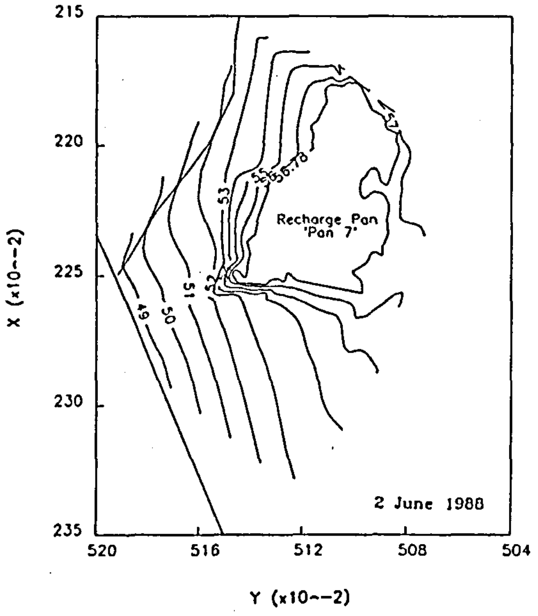

**Figure 4–2** Contours of the groundwater levels in the vicinity of the infiltration pond at Atlantis on 1988–06–02

On the 2nd June 1988, the basin was still relatively empty and the groundwater level had reached its lowest level in several years (see Figure 4–2). The water level in the vicinity of the production well field (to the west of the West Coast Road) had dropped to 48 m, which was approximately a metre lower than in 1987. This was due to three reasons, namely all the treated waste water was diverted to the Donkergat River, the base flow in the stormwater system was diverted to the Donkergat River during summer and finally, the rainfall was lower in 1988 compared to 1987. The limited influence of the basin during 1988 is clearly evident from the water-level configuration. In 1988, very few secondary basins had formed.

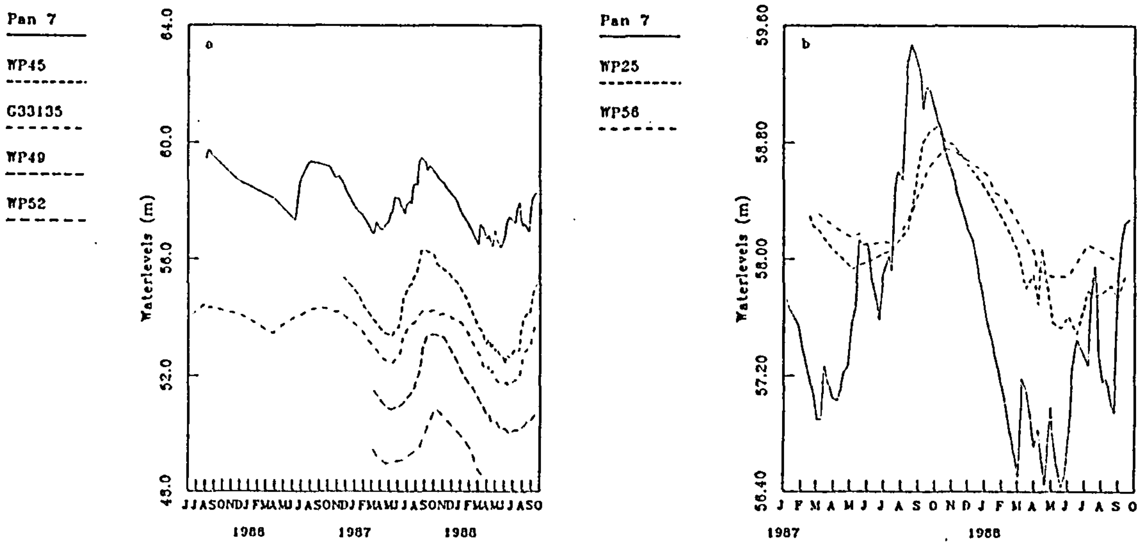

Figure 4–3 Variations in the water-levels at sites west (a) and north-east (b) of the infiltration pan

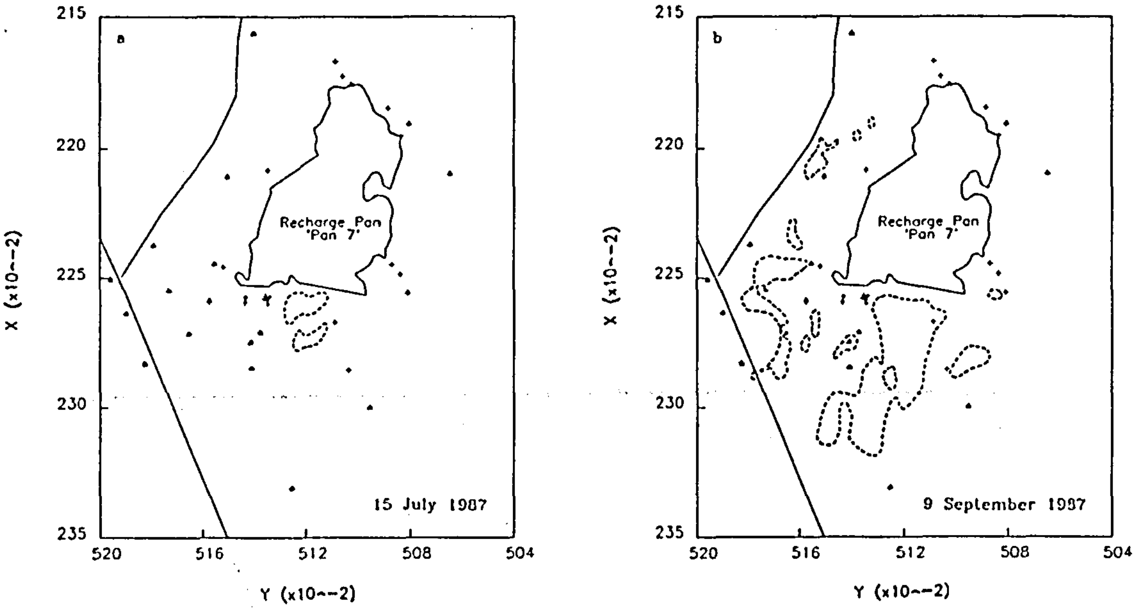

Figure 4–4 Positions of secondary ponds that developed around the main infiltration pond at Atlantis, due to a rise in the groundwater level

During the 1987 rainy season, a considerable amount of run-off was produced and the recharge basin reached a maximum level of 59,5 m in August [see Figure 4–3(a)]. This is equivalent to a content of approximately 450 000 m$^3$. Subsequently, the water level decreased rapidly. The main reason for this was that since November 1987, the storm-water base flow was diverted from the basin due to its salinity.

In Figure 4–3(a), the groundwater level is shown for a number of observation points to the west-south-west of the basin. Comparison of the curves for these points during the second half of 1987 shows that from the time that basin No. 7 reached its maximum water level during mid August 1987, it took approximately 45 days before the furthest monitoring point (approximately 500 m from the basin) reached its maximum. Apart from the expected lag in response of the groundwater level at the various monitoring points further from the basin, the absolute value of the variation varies from point to point. The approximate rise observed from the lowest point reached, in the first half of 1987, up to the peak in the second half of 1987, and the subsequent decrease up to the middle of 1988, is indicated in Table 4-2 for a few of the observation points.

**Table 4–2** Approximate rises and the subsequent decreases in a few observation points from the first half of 1987 to the middle of 1988

| Observation Point | Increase (m) | Decrease (m) |
|---|---|---|
| Basin No. 7 | 2,8 | 3,1 |
| WP45 | 3,0 | 4,0 |
| G33135 | 1,9 | 2,8 |
| WP49 | 2,8 | 3,5 |
| WP52 | 1,9 | 2,9 |

These values show that the variations at the monitoring points are related to the rise and fall of the water table in the basin itself, but that the local maxima and minima vary from point to point. The variations in the local maxima and minima can probably be ascribed to variations in the permeability of the deposits from point to point; 'short-circuiting' along the surface where the groundwater level rises above ground level; the proximity of the recharge basin and production well field and the rate of recharge from basin No. 7. The importance of each of these factors varies from point to point and, in addition, the recharge rate depends on the height of the water level in basin No. 7. The water level in the basin is not directly related to the volume of water in the basin, but nevertheless it would seem that the recharge rate decreases rapidly when the water level drops below 57 m. This is evident from the fact that the piezometric level at the closest monitoring point, i.e. WP45, continues to drop even when the water level in the basin begins to stabilise. The effect of the short-circuiting along the surface can best be noticed at borehole G33135, where the water runs along the surface past the borehole when the basin is relatively full. Most of this water soaks away before it reaches observation point WP49. This is clearly reflected in the larger water-level variations at this monitoring point in comparison to borehole G33135. Observation point WP52 is situated close to the production well field and the influence of the groundwater withdrawal is considerably greater at that point. At this point, the seasonal increase and decrease in withdrawal rate will also have an effect.

To the north-east of the basin, i.e. updip with respect to the water-level gradient, the reaction of the groundwater table to a rise or drop of the water level in the basin differs totally from that on the western side [see Figure 4–3(b)]. Although the observation points WP25 and WP56 are only 100 and 250 m respectively from the basin, the change in water level is only one and 0,7 m respectively. At these points, the lag is also considerably larger than at points situated at a comparable distance to the west of the basin. This can be ascribed, at least partially, to the higher clay content and lower permeability of the deposits at the northern and north-eastern side of the basin.

## 4.5 DISCUSSION OF THE GROUNDWATER CHEMISTRY

### 4.5.1 General

The main task of the Division of Water Technology was to collect detailed information on the groundwater chemistry in the aquifer, study the reaction between the components of the recharge water, the aquifer material and the natural groundwater and also other chemical reactions taking place in the aquifer. The new monitoring points were of special interest for determining the groundwater levels, but the hydrochemical information gained from these was just as important. Early in 1987, a regular and intensive sampling programme was put into operation for all monitoring points around the recharge basin. This yielded a mass of information of which only the most important aspects are mentioned. Considerable attention was devoted to hydrochemical stratification and some of the results are described below. As could be expected, the chemical composition of the water varies with time. Graphs showing the extent of these variations for a number of parameters at four observations holes are described below.

### 4.5.2 Hydrochemical Stratification

In the vicinity of the artificial groundwater recharge basin, the aquifer consists essentially of two members of the Bredasdorp Formation, namely Witzand and Springfontyn. The overlying Witzand Member is calcareous and also contains calcrete lenses, while the underlying Springfontyn Member consists of relatively pure silica sand. A degree of hydrochemical stratification was observed during an earlier investigation of the natural groundwater quality. As artificial groundwater recharge has now been practised for many years in this area, most of the natural groundwater in the overlying Witzand deposits would have been replaced, except possibly at the north-eastern side of the basin. In contrast, inspection of the chemical data for the underlying Springfontyn Member shows that this water consists essentially of natural groundwater. This is characterised, for example, by the extremely low potassium concentration and the small variations with time. For these reasons, no attempt was made to compile potassium contour maps for the Springfontyn Member.

To illustrate the differences in water quality in the two members, chloride contours for the groundwater in the upper and lower horizons are shown for various dates (see Figures 4–5 and 4–6). The dates chosen for these contour maps are 13 May 1987 and 1 September 1987. As indicated above, the groundwater levels had not shown any reaction to the increased flow of storm water to the recharge basin in May 1987. By September, however, the groundwater levels had risen substantially.

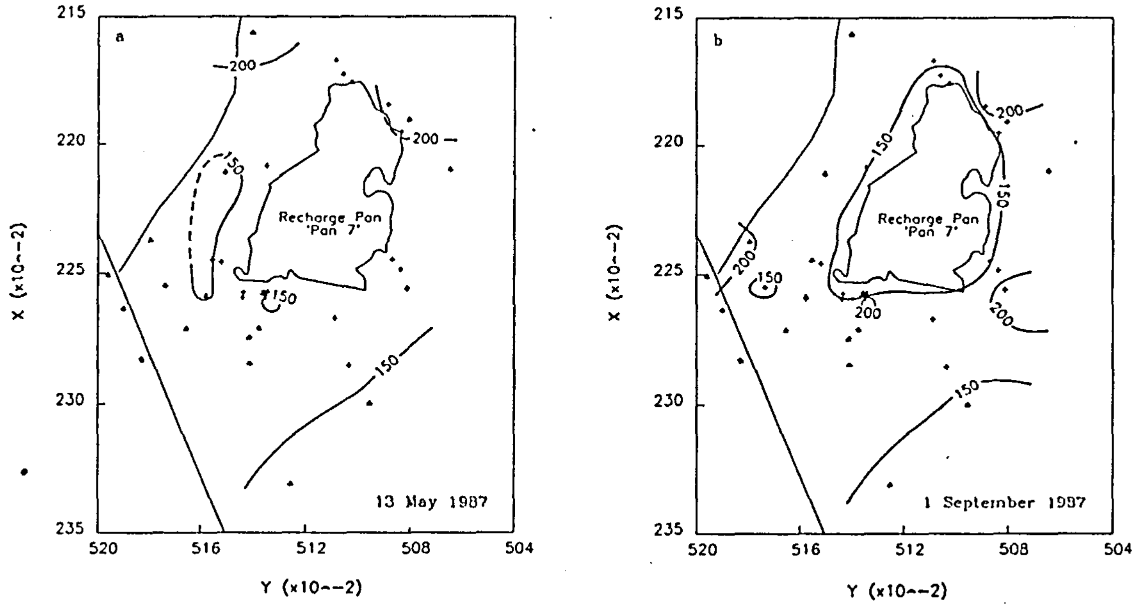

Figure 4–5 Chloride concentrations in the upper (Witzand) member in the vicinity of the infiltration pond at Atlantis.

The contour map for the upper horizon (Witzand) for May 1987, shows chloride concentrations above 200 mg/L to the north and especially to the north-east of the basin. It is expected that this represents the chlorinity of the natural groundwater in that area. In the larger part of the area, the concentration is between 150 and 200 mg/L. Very few exceptions are noticeable. To the west of the basin and in a small area south of the basin, as well as in the extreme south-east, concentrations below 150 mg/L are found (see Figure 4-7). At the beginning of September 1987, when the increased water level in the recharge basin and the associated increase in groundwater recharge had influenced the whole of the area, a change in the chlorinity of the water in the upper horizon was clearly evident. Except for one point to the north-east of the basin, the chlorinity in the immediate vicinity of the basin had dropped below 150 mg/L. It would seem that the water with the chlorinity below 150 mg/L, which was situated immediately to the west of the recharge basin in May, had moved further west in September and was largely situated in an area in which it could not be detected by monitoring points. Only at one point (WP49) was such water noticeable in September. Similarly, water with a chlorinity above 200 mg/L, appeared at WP18 and WP19 in September. It is presumed that during May, this water was situated in an area further eastwards, which was not covered by monitoring points. These observations are supported by the graph showing the chlorinity against time for borehole G33135 in Figure 4–11(b).

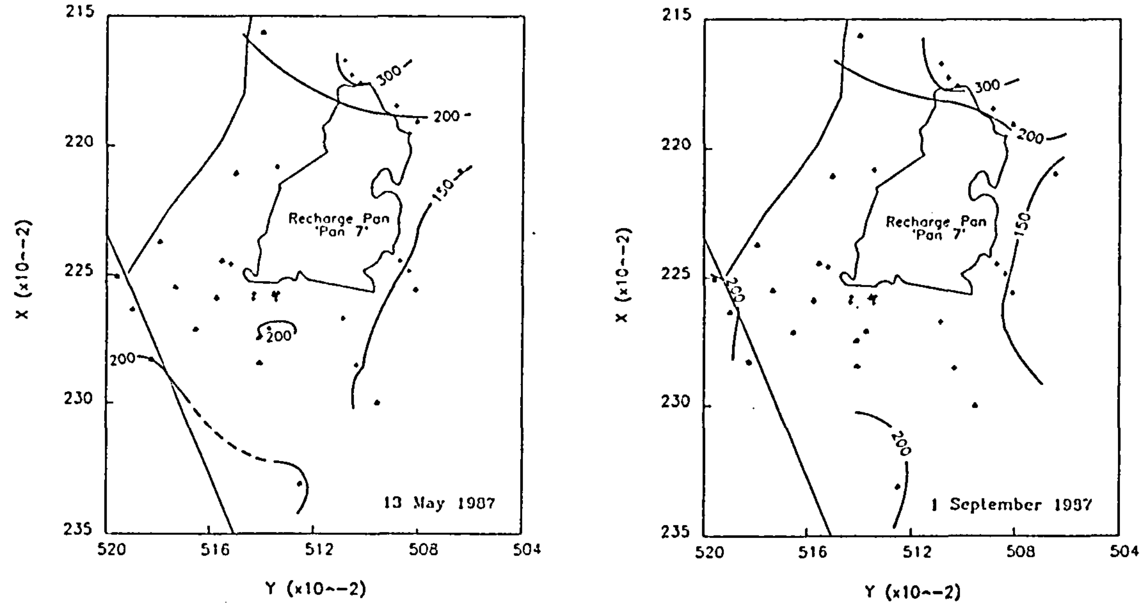

Figure 4–6 Chloride concentrations in the lower (Springfontyn) member in the vicinity of the infiltration pond at Atlantis

In the underlying horizon (Springfontyn Member), little change is noticeable from May to September (see Figure 4–6). The only definite changes occurred to the west of the West Coast Road in the vicinity of the production well field. In this area, variations in the chemical quality in the lower horizon (Springfontyn) do occur. Problems were experienced with some of the well points at certain stages, due to the fact that the water levels were drawn down considerably due to the proximity of the well field. The construction of these well points only allows sampling by suction from the surface.

### 4.5.3 Chemical Composition of the Water in the Recharge Basin

In Figure 4–7, the water-level variations in the recharge basin are shown together with three water quality variables. These graphs give an overview of the quality of the recharged water over the three years from 1986 to 1988.

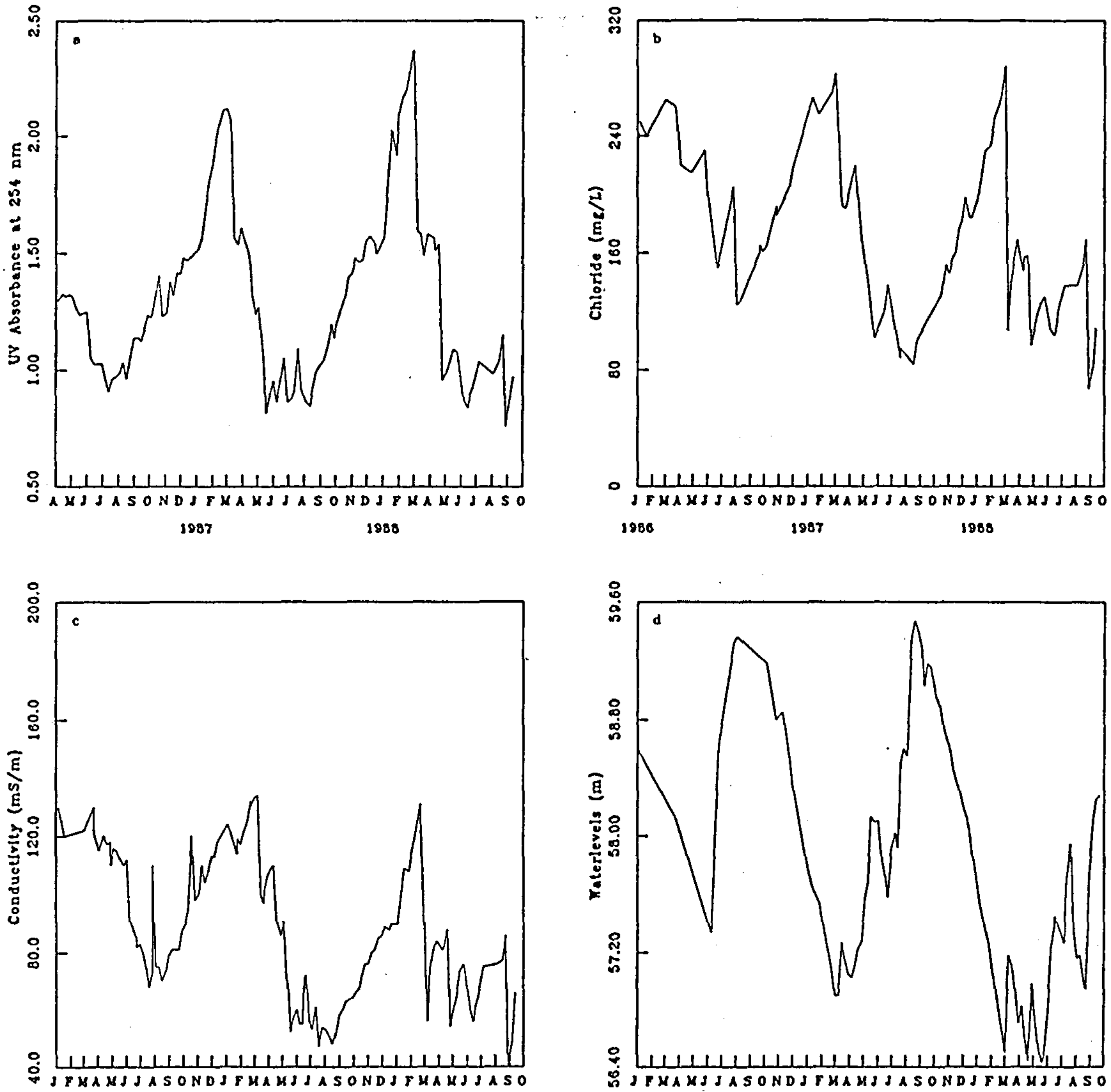

Figure 4–7 Variations in the level and chemical composition of water in the infiltration pond at Atlantis

It is evident from the graphs that the quality of the water is inversely related to the water level and thus also to the volume of the water in the basin. Although the volume of the water in the basin is not directly related to the water level, the latter gives a good indication of the quantity of water in the basin at any given time. In general, the quality of the water improves when the quantity increases, while the quality deteriorates when the volume decreases. The water-level graph also shows that the quantity of water contained in the basin in August 1988, was only a small fraction of the quantity in August 1987. Despite the low rainfall in 1988 and the small volume in the basin, the quality of the water in 1988 is comparable or even better than in the previous years. This is particularly the case in the dry summer months. However, the improvement is less than expected and after investigation, it was found that the incorrect installation of diversion sluices at one of the storm-water detention basins, caused highly saline storm-water run-off, from the noxious industrial area of Atlantis, to enter the recharge basin. The situation was rectified in August 1988. In general, any inflow of storm-water run-off causes an improvement in the quality of the water in the basin.

The ultraviolet absorbance at 254 mm gives an indication of the dissolved organic content of the water. Turbidity or algae in the water does not influence the UV absorbance. Should die-off algae occur, various organic decomposition products will appear in the water which can be detected by an increase in the UV absorbance. The graphs in Figure 4–7 indicate that in January 1987, and again in January 1988, the UV absorbance increased faster than the other chemical components. This phenomenon is ascribed to an algal bloom followed by die-off of the algae.

### 4.5.4 Electrical Conductivity

In the paragraphs below, the variations in chemical quality at two pairs of observation boreholes, namely G33110 (shallow) and G33109 (deep), as well as at G33135 (shallow) and G33134 (deep) are discussed, together with those for a number of other observation points. The electrical conductivity (which serves to give an indication of the total salinity) at the four observation boreholes is shown in Figure 4–8. The largest variations occur at the shallow borehole closest to the basin (G33110). Each year from 1985 to 1987, the electrical conductivity (salinity) reaches its maximum in the middle of the winter. The dilution by winter rainfall run-off causes a drastic reduction in the salinity of the water. The adjacent borehole monitoring the underlying Springfontyn Member, only shows a slight variation in salinity which is apparently seasonally related. The salinity at the shallow borehole further to the west of the basin (G33135) also shows a degree of variation, but the amplitude of the variations is considerably smaller. Again, it is evident that the variation in the salinity in the overlying Witzand Member has little influence on the underlying Springfontyn Member.

From the graph showing electrical conductivity at borehole G33110 [see Figure 4–8(a)], it can be seen that the maximum value in July 1987, was considerably lower than the maximum for the year before. This is ascribed to the diversion of the relatively saline maturation pond effluent since November 1986. From October 1987 to July 1988, the salinity was continually lower than the year before. Again, the deeper lying horizon (Springfontyn) shows little variation.

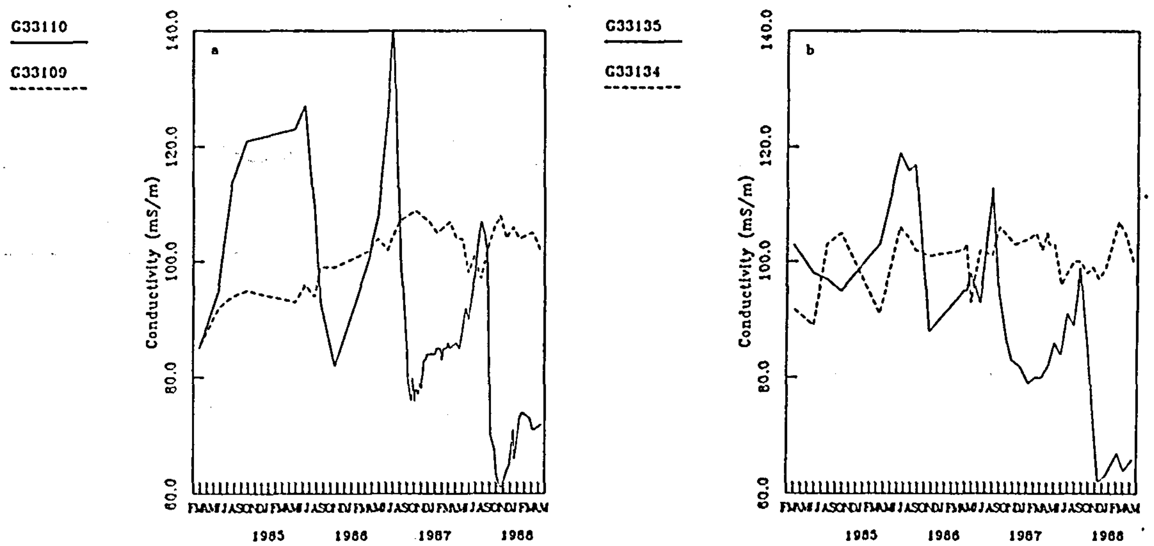

Figure 4–8 Variations in electrical conductivity (mS.m$^{-1}$) at the indicated boreholes

In Figure 4–9, the conductivity at two pairs of well points to the west and south-west of the basin is shown. The shallow well points monitoring the Witzand Member again show seasonal variations, while in the deeper lying Springfontyn Member, the variation is much smaller. The somewhat more pronounced variations observed at well point, WP1, could be due to the construction of these earlier well points. They were bidim-wrapped and provided with a partial gravel pack and this could affect the actual depth being monitored.

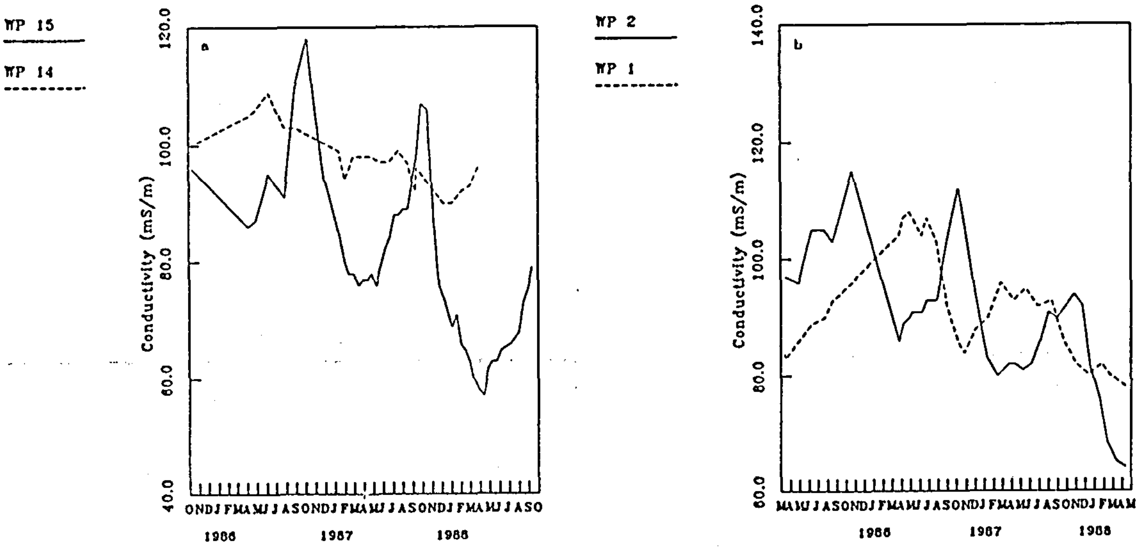

Figure 4–9 Variations in electrical conductivity (mS.m$^{-1}$) at the indicated well points

The electrical conductivity of the groundwater at WP52 and WP51 is shown in Figure 4-10(a). These observation points are situated approximately 500 m from the recharge basin close to the Witzand production well field. In this case, both the shallow and deep well points show variations which are ascribed to the proximity of the production well field, where the water-level gradient increases and vertical movement of the water is enhanced. As the period of the variations is shorter than a year, it could mean that the variations occurring as a result of a change in the abstraction rate of the groundwater, are superimposed on the seasonal variations which are observed in the vicinity of the recharge basin.

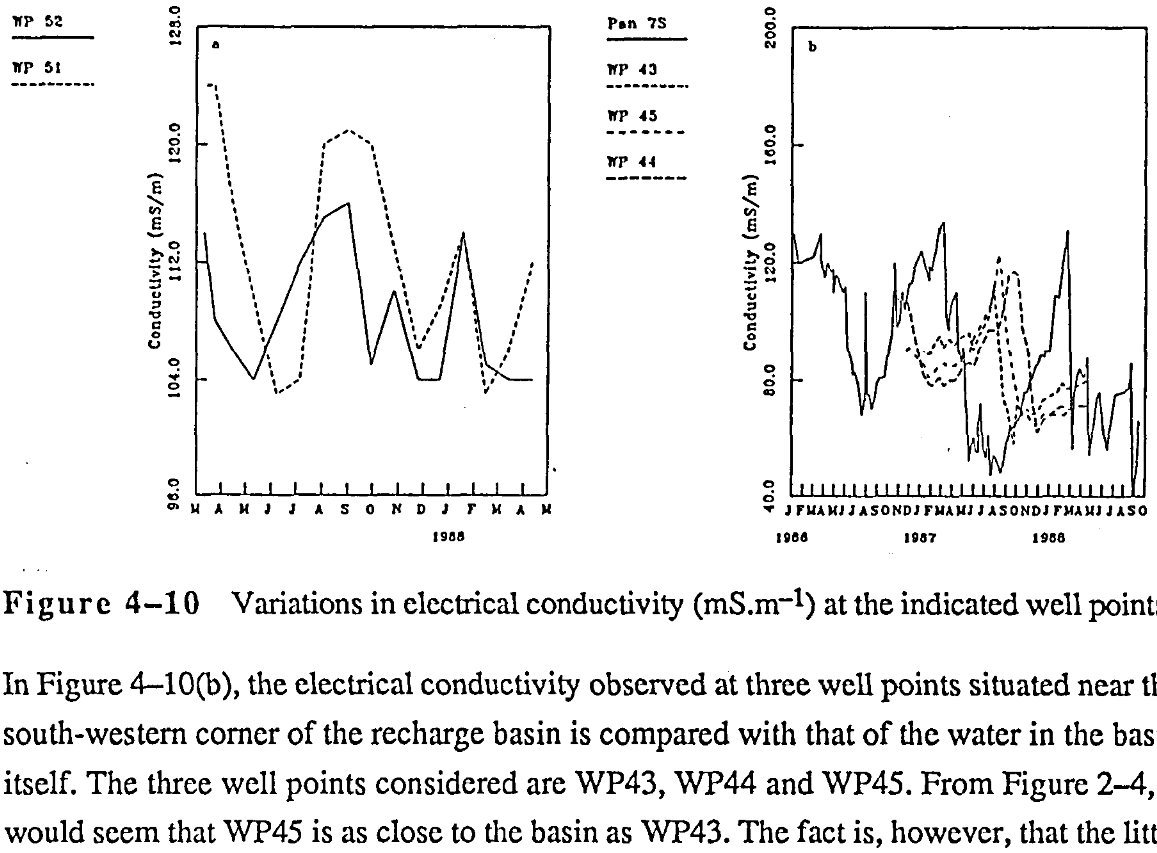

**Figure 4–10** Variations in electrical conductivity ($mS.m^{-1}$) at the indicated well points

In Figure 4–10(b), the electrical conductivity observed at three well points situated near the south-western corner of the recharge basin is compared with that of the water in the basin itself. The three well points considered are WP43, WP44 and WP45. From Figure 2–4, it would seem that WP45 is as close to the basin as WP43. The fact is, however, that the little sub-basin which extends from the main basin towards WP45, only has water when the main basin is virtually full. Therefore, WP45 is, in actual fact, considerably further from the basin than well point WP43. Nevertheless, the lag at WP45 is only four months compared to the three and a half months at WP43. Furthermore, the lag is considerably more at WP44, which is situated approximately 20 m further than WP43 from the basin. The reason for these differences becomes apparent when the water-table configuration in Figure 4-3 is considered. These figures show that the flow direction of the water changes as the basin fills. The same argument holds for the considerable lag observed for the 1988 salinity peak in the basin to appear at these well points. In 1988, the water in the basin was largely restricted to the centre of the basin. For this reason, the recharged water had to move significantly further through the sand deposits before reaching the monitoring points.

### 4.5.5 Chlorinity

The chlorinity recorded at four monitoring boreholes (G33110, G33109, G33135 and G33134) is shown in Figure 4–11. In general, the pattern of variation in chlorinity agrees with that of the electrical conductivity, although the peaks are not as conspicuous, partly because of the lower frequency of chloride analysis. In the case of the two boreholes closest to the basin, namely G33110 and G33109, it would seem as if the chlorinity of the water follows an inverse trend in the upper and lower horizons. In the underlying Springfontyn Member, the variations are smaller and the chloride concentration higher.

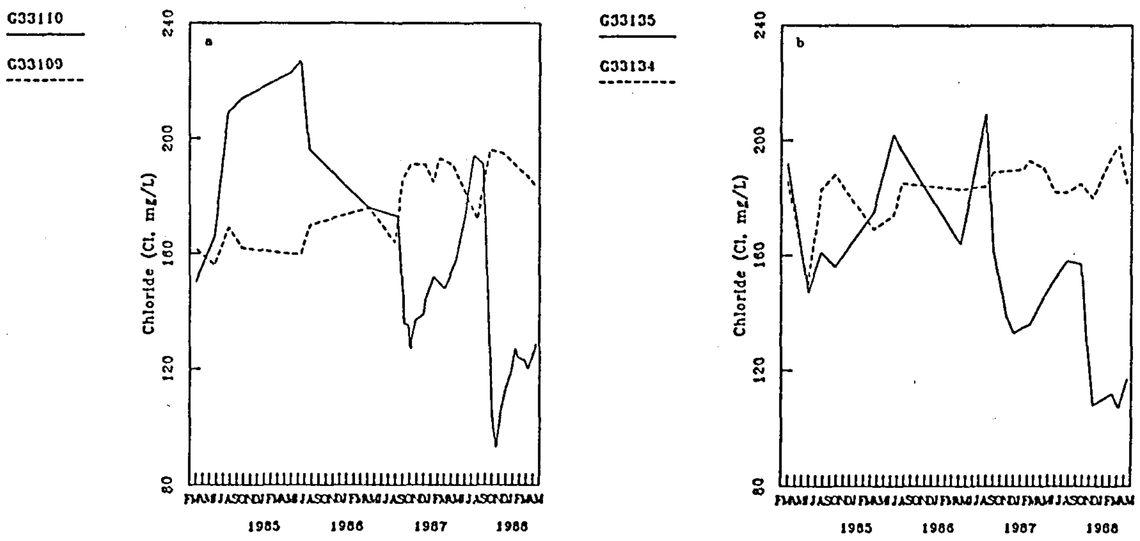

Figure 4–11 Variations in the chloride concentrations at the indicated boreholes

In Figure 4–12, the chlorinity observed at well points to the west and north-west of the basin is shown. Well points WP20 and WP15 both monitor the Witzand Member (upper horizon) and consequently the curves for these monitoring points follow a similar pattern as those for the basin. WP15 is located further from the basin than WP20 and consequently shows a greater lag. The fact that the maxima at the well points (especially those in 1987) are lower than those of the basin itself, indicates that dispersion takes place. Calculation of dispersion on the basis of these results proved to be more difficult than expected.

Well points WP17 and WP16 [see Figure 4–12(b)] are both of the older type and problems are experienced from time to time to obtain water samples. The problems are compounded when the water level drops. Again, seasonal variations are observed in the upper layers of the deposits on the north-western side of the basin. The chlorinity in the Springfontyn Member (deeper horizon) remains relatively constant and is somewhat higher than that observed at the more southerly well points, which also monitor the Springfontyn Member. It is evident that the artificial groundwater recharge does not have a direct influence on the deeper horizon in this area.

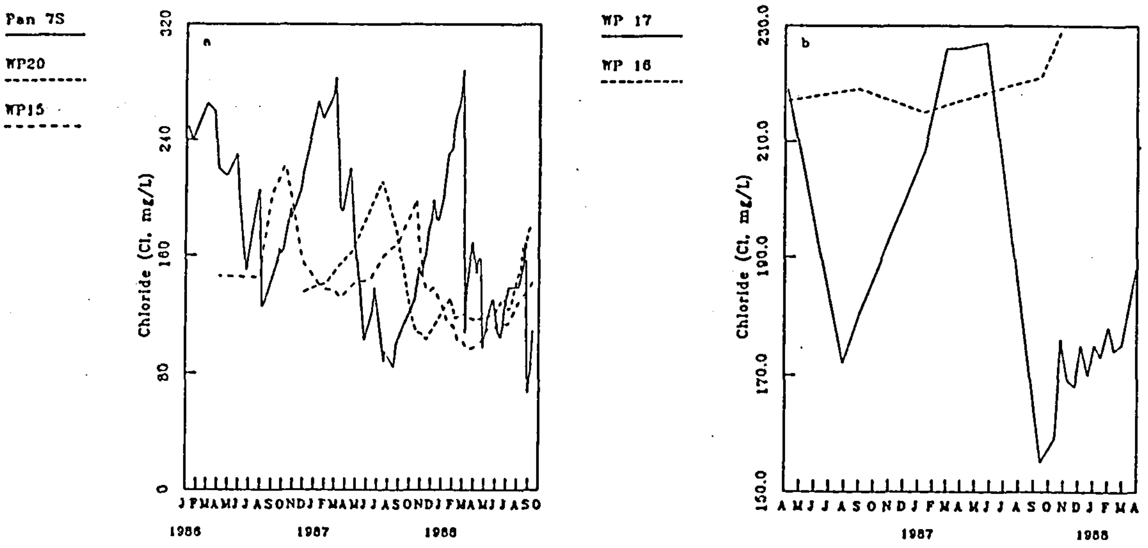

Figure 4–12 Variations in the chloride concentration at the indicated observation holes

## 4.5.6 Potassium

The potassium concentration recorded at the four monitoring boreholes is shown in Figure 4–13. Figure 4–13(a) also shows the potassium concentration at a point along the southern edge of the recharge basin.

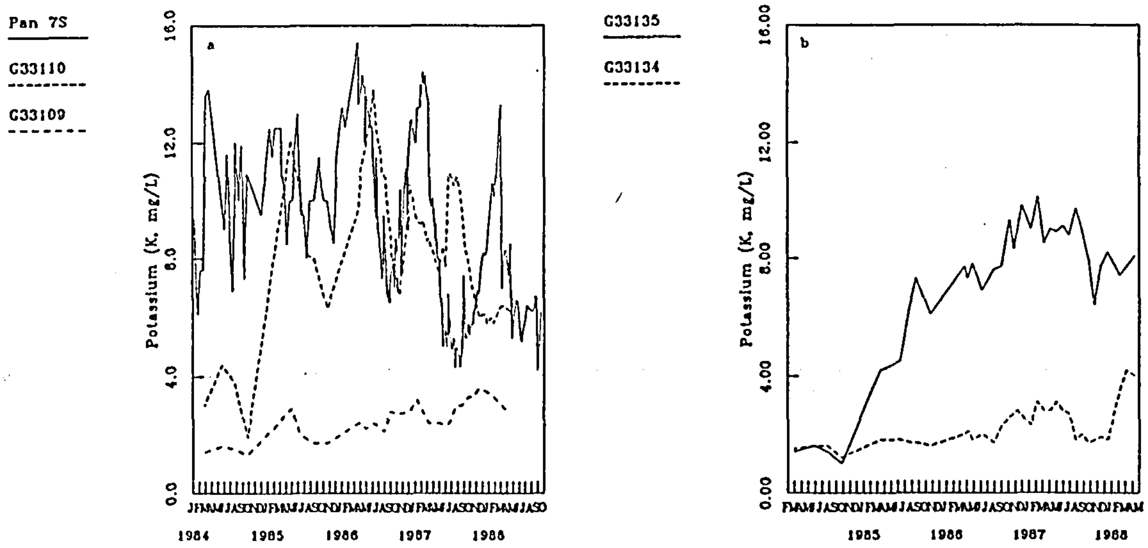

Figure 4–13 Variation of the K-concentration in Pan 7 and the adjoining boreholes G33109, G33110, G33134 and G33135 at Atlantis

These graphs indicate (especially in 1986) that the maximum peaks in the potassium concentration at borehole G33110 have a time lag of approximately two and a half months compared to the peak in the recharge basin. The curve for borehole G33109 which represents the underlying Springfontyn Member, shows no definite peaks, but a gradual increase in the potassium concentration over the first four years, with a levelling off in 1988. At the two boreholes furthest from the basin (G33135 and G33134), the annual cycle is not clearly visible. It is evident that the potassium concentration in the lower horizon (represented by G33134) is still lower, but doubled in 1988, compared to the second half of 1987. Considering the 1988 data, it would seem that it is gradually becoming possible to identify the cycle with a period of one year. It is possible that the lag, with respect to the water quality changes in the overlying deposits, could amount to 18 months [see Figure 4–13(b)].

### 4.5.7 UV Absorbance

The ultraviolet absorbance at 254 mm is used as a summary variable or index to give an indication of the organic pollution in the water. Again, the upper horizon (Witzand Member), represented by boreholes G33110 and G33135, indicates a considerably larger variation than the deeper horizon (see Figure 4–14).

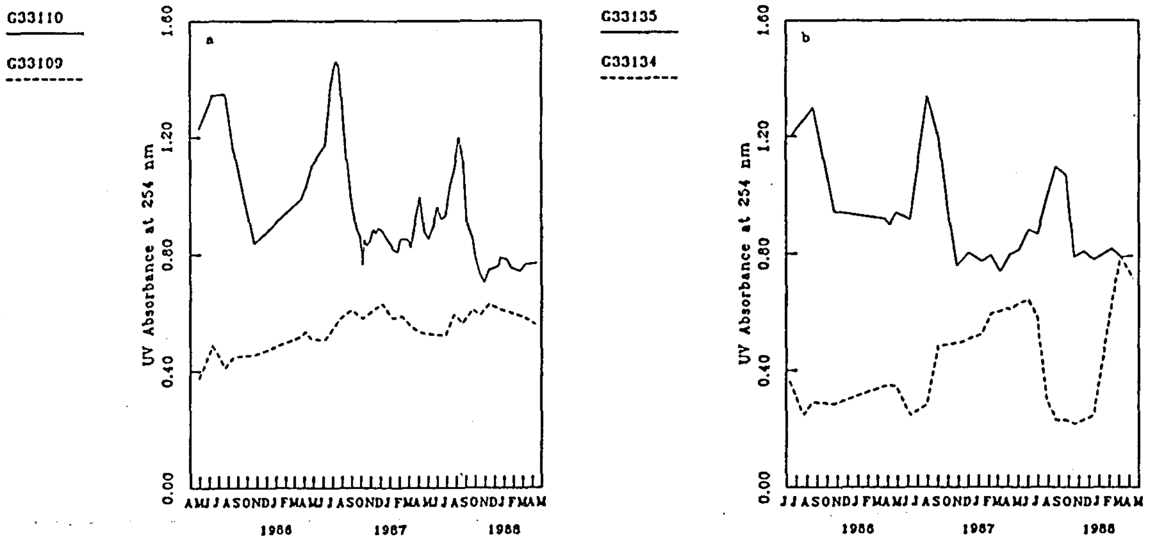

Figure 4–14 Variations in the ultra-violet absorbance (at 254 nm) at the indicated observation holes

It is evident that there is a gradual increase in the organic content of the water in the deeper horizon (Springfontyn Member) until the end of 1987. Subsequently, the concentration levelled off. In the case of borehole G33134 (deeper horizon), the increase is accompanied by relatively large seasonal variations. Again, it is possible that the seasonal pattern at borehole G33134 has a lag of approximately 18 months with respect to that observed at borehole G33135. This would agree with the observations with respect to the potassium concentrations at these boreholes.

In Figure 4–15, the variation in ultraviolet absorbance in the artificial recharge basin is compared with that in the nearest observation boreholes. These graphs indicate that the maxima observed at the basin occur at the observation holes after a delay of six to seven months. Considering the fact that the UV absorbance only refers to dissolved compounds, the reduction in the concentration of organic compounds from the basin to the boreholes is remarkable. It is suggested that the larger part of the decrease occurs in the immediate vicinity of the basin and possibly in the upper soil layers. This is supported by the fact that the decrease further away from the basin is considerably smaller and can possibly be ascribed to dispersion and diffusion.

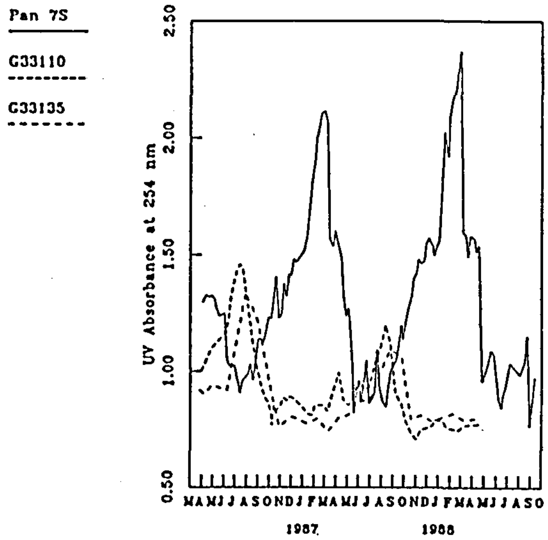

**Figure 4–15** Variations in the ultra-violet absorbance (at 254 nm) at the indicated positions

## 4.6 GENERAL DISCUSSION

Considering the objectives of the present project and those of the management programme for the artificial recharge of the Atlantis aquifer, these are seen to be somewhat contradictory in a certain sense. Towards the end of 1985 and early 1986, a re-evaluation of the impact of artificial groundwater recharge on the groundwater quality in the aquifer took place. At that time information had been collected for several seasons, on the artificial recharge practice and groundwater qualities, to allow a preliminary long term estimate of the impact that the artificial recharge may have on the groundwater quality in the area of the recharge pond. These studies indicated that the quality of groundwater in the Witzand production well field could deteriorate considerably in the immediate future, if action was not taken immediately. The management decisions, with respect to the artificial recharge of the groundwater, taken at that time led to immediate changes in the groundwater quality. However, the operation of the existing recharge basin still does not comply with the requirements for maximum improvement in water quality. Further changes in the management of recharge can, therefore, be expected. The final aim is to reach a stage where the pollution load in the recharge water is too small to have a significant detrimental effect on the groundwater quality. Although the transport of chemical compounds can still be modelled at that stage, it would in effect not represent a pollution situation any more.

A second problem with respect to the development of a model for the recharge basin at Atlantis, is the continuous hydraulic connection maintained between the water in the recharge basin and the groundwater itself. This means that at no stage does an unsaturated zone exist. The unsaturated zone is considered essential for the decomposition of pollutants and other chemical interactions removing pollutants from solution. At this stage, it seems unlikely that this aspect could be fully elucidated at Atlantis.

Despite the problems mentioned above, a chemical transport model remains an essential management tool for proper utilization and protection of the aquifer.

The diverse reactions with respect to the various constituents clearly indicate the complexity of the situation in the aquifer. As a first approach, the electrical conductivity, the chloride concentration, the potassium concentration and the UV absorbance (at 254 mm) of the groundwater were investigated. The electrical conductivity gives an indication of the total salinity of the water and, therefore, gives a general indication of the quality of the water. The chloride concentration serves as a reference level for the evaluation of physical-chemical processes which affect the concentration of the other ions. Potassium can serve as an example of a cation undergoing ion exchange and, therefore, not transported advectively. The UV absorbance serves as an index related to the presence of organic compounds in solution. Presently, dissolved organic carbon determinations are also carried out on a regular basis.

## 4.7 CONCLUSIONS

Certain general conclusions can be made, as the intensive data collection over the past years has contributed to a better understanding of the groundwater movement and accompanying quality aspects:

- The new well points have filled important voids in the monitoring network. Gaps still exist with regard to the monitoring of natural groundwater on the eastern side of the basin, as well as in the deeper deposits and the region of the production well field.
- Techniques which would enable the installation of monitoring points and the sampling of aquifer material in problem areas, should be investigated.

- It is evident from the water-level data that the main flow direction of the water is in a south-southwesterly direction. It is possible that if the water level in the basin rises sufficiently high, the aquifer can even be replenished in an easterly direction. However, surface flow, especially on the southern side of the basin, complicates the interpretation.
- Hydrochemical stratification is an accomplished fact and the replenished water is found mainly in the upper layers of the aquifer. Closer investigation is necessary in the region of the production well field.
- An analysis of the chemical composition of the groundwater in the vicinity of the recharge basin indicates that specific constituents are subject to divergent processes which need further study.
- The groundwater quality in the vicinity of the recharge basin started improving in 1987. This was as a result of the suspension of recharge of maturation pond effluent in November 1986, and the good winter rainfall in 1987.

# CHAPTER 5

# IDENTIFICATION OF THE HYDRAULIC PARAMETERS

## 5.1 GENERAL

A differential equation can only be solved if suitable boundary and initial conditions are prescribed and all the conceptual parameters known. However, as discussed in Chapter 1, the latter procedure (often referred to as the problem of *parameter identification*) is not a simple task and depends in the first place on the problem at hand.

The conceptual parameters involved with the phenomena for which computer programs were developed, or used in this investigation include:

(a) transmissivity and storage coefficient of a confined aquifer,
(b) transmissivity and effective porosity of an unconfined aquifer,
(c) soil moisture retention curve for unsaturated flow,
(d) hydraulic conductivity of the unsaturated zone and
(e) the dispersivities for mass transport.

The transmissivity, storage coefficient and effective porosity can be determined from drawdowns observed in an aquifer during controlled pump tests [Kruseman and De Ridder (1976)] and/or a particle size analysis [Van der Merwe (1983)]. As these methods are quite well-known, the rest of this discussion will be restricted to the cross-borehole packer tests, unsaturated flow parameters and dispersivities.

## 5.2 CROSS-BOREHOLE PACKER TESTS

### 5.2.1 General

Since there is a vast difference between the physics of porous and fracture flow, it will be necessary to know the prevalent type of flow in an aquifer, before a model of the particular groundwater phenomenon can be developed. A detailed study of the available literature on the subject revealed that there is only one method, known today, that can provide an answer to this question – *the cross-borehole packer test*, originally developed by Hsieh *et al.* (1983). Very little is known at present of the nature of flow in the more common Karoo sediments of the Republic of South Africa. It will, therefore, be necessary to conduct these tests on a more regular basis, especially if any of the methods for modelling contaminant transport developed here, are to be applied in studies of Karoo aquifers. However, as cross-borehole packer tests are a very recent development, it will be necessary to evaluate them in more detail, before they are applied in actual field investigations.

A perfect opportunity to evaluate the cross-borehole packer test arose in the present investigation at Atlantis, where the possible intrusion of sea-water can only occur through fractures, or porous domains, in the Malmesbury Formation. Application of cross-borehole packer tests at Atlantis could thus serve two purposes at once: (a) an opportunity to evaluate the test and (b) to clarify the possible intrusion of sea-water in the aquifer.

Müller and Botha (1986) identified two small areas along the coast where the sand deposits continue below sea-level and sea-water intrusion could readily take place. The site for conducting the cross-packer tests was therefore chosen in one of these areas (see Figure 5–1). The positions of the three test holes, drilled by the Department of Water Affairs, are also presented in the figure. The geological profiles of the boreholes, obtained from the Department, are summarized in Table 5–1.

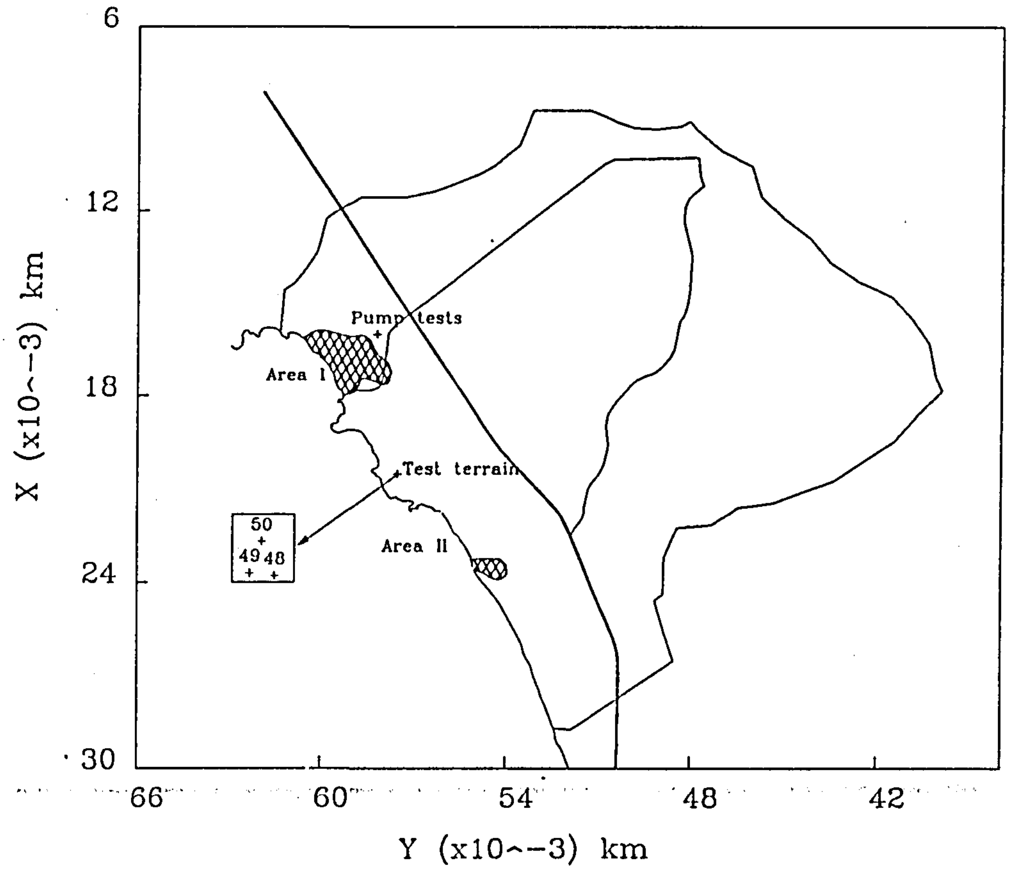

**Figure 5–1** Location of the two areas where sand deposits continue below sea-level in the Atlantis aquifer [Müller and Botha (1986)] and the positions of the three test boreholes, (G33448, G33449, G33450), used to evaluate the cross-borehole packer test and the possible intrusion of sea-water into the aquifer

**Table 5-1** Geological profiles of the test boreholes drilled in the Malmesbury Formation and used for the cross-borehole packer tests in Atlantis

| Depth (m) | Formation type |
|---|---|
| 0 – 19 | Unconsolidated sand deposits |
| 19 – 34 | Weathered Malmesbury |
| 36 – 81 | Malmesbury Formation |

### 5.2.2 Description of the Cross-borehole Packer Test

The basic idea behind the method is very simple. Two sections of adjacent boreholes are sealed off by pneumatic packers (see Figure 5-2). Water is then injected into the sealed section in one of the boreholes. If the two sections are connected through one or more fractures, or if the aquifer is fully porous, the pressure in the sealed section of the other borehole will also increase as a function of time.

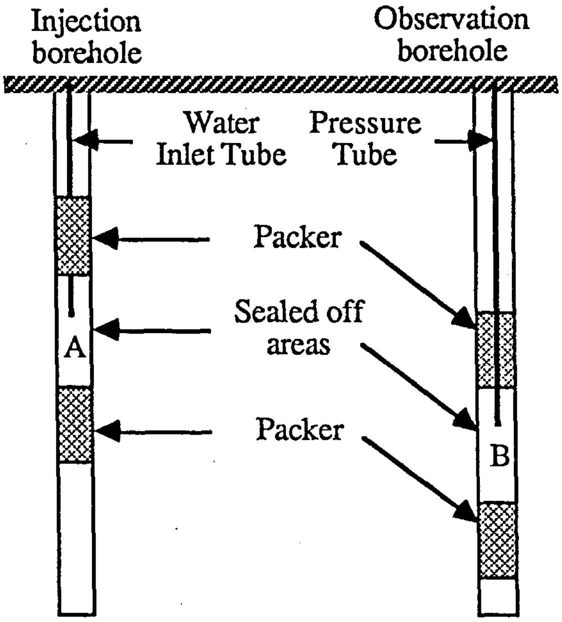

**Figure 5-2** Graphical representation of the packer set-up used in cross-borehole packer tests

If the connections between the injection and observation boreholes sustain porous flow, the pressure distribution in the observation borehole must satisfy the saturated flow equation for a porous medium [see Equation (12.5)],

$$S_0 D_t h(x,t) = \nabla \bullet [\underline{K}(x) d \nabla h(x,t)] + Q, \tag{5.1}$$

where Q is the rate at which water is injected into the pumping hole and d the distance between the packers. Assuming that the initial and boundary conditions of the aquifer can be represented by the equations,

$$h(x,t) = h_0 \quad (t = 0) \quad \text{and} \quad h(x,t) = h_0 \quad (t > 0,\ x \rightarrow \infty),$$

respectively, it can be shown [Hsieh *et al.* (1983)] that the pressure increase observed in the observation borehole must satisfy the equation

$$\Delta h = \frac{Q}{4\pi\sqrt{G}} \operatorname{erfc}\left(\frac{S_0 G}{4Dt}\right)^{1/2}, \tag{5.2}$$

where

$$\mathrm{erfc}(u) = \frac{2}{\sqrt{\pi}} \int_u^{\infty} \exp(-s^2)ds = 1 - \mathrm{erf}(u)$$

is the well-known complementary error function and the parameters D and G are functions of $K_{ij}$, the ij-th component of the hydraulic conductivity tensor $\underline{\mathbf{K}}$ and the cartesian components, $x^i$, of the position vector **R** (see Figure 5–3). To be more specific

$$D = K_{11}K_{22}K_{33} + 2K_{12}K_{23}K_{13} - K_{11}(K_{23})^2 - K_{22}(K_{13})^2 - K_{33}(K_{12})^2 \tag{5.3}$$

$$G = (x^1)^2A_{11} + (x^2)^2A_{22} + (x^3)^2A_{33} + 2x^1x^2A_{12} + 2x^2x^3A_{23} + 2x^1x^3A_{13}$$

where A is the symmetric adjoint matrix of $\underline{\mathbf{K}}$ with elements:

$$A_{11} = K_{22}K_{33} - K_{23}^2;\ A_{22} = K_{11}K_{33} - K_{13}^2;\ A_{33} = K_{11}K_{22} - K_{12}^2 \tag{5.4}$$

$$A_{12} = K_{13}K_{23} - K_{12}K_{33},\ A_{23} = K_{12}K_{13} - K_{23}K_{11},$$

$$A_{13} = K_{12}K_{23} - K_{13}K_{22}.$$

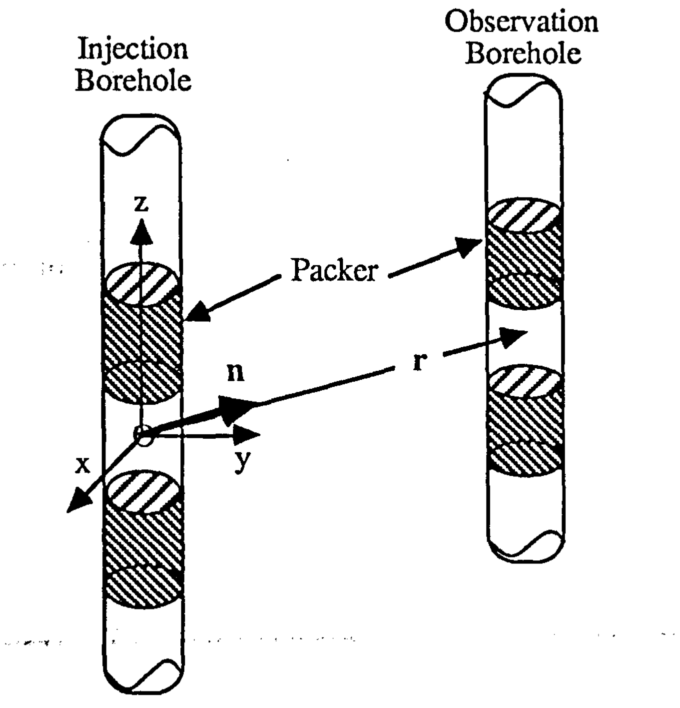

**Figure 5–3** Definition of the distance vector **r** and unit vector **n** in three dimensions

It thus follows that if Equation (5.2) is not satisfied by the observed pressure increase, *the flow cannot be described as porous flow, but must be a form of fractured flow.*

The analysis of the cross-borehole packer tests can be simplified considerably by introducing the *directional hydraulic conductivity* [Hsieh *et al.* (1983)]. To define this quantity, consider the unit vector **n**, defined in Figure 5–3. The position vector **r**, with components $\{x^1, x^2, x^3\}$, can then be rewritten as

$$\mathbf{r} = \mathbf{n}r,$$

and the quantity G in Equation (5.3) as

$$G = r^2(n^TAn) = r^2D(n^TK^{-1}n) = \frac{r^2D}{K_d(n)}. \qquad (5.5)$$

where $K_d(n)$ is the directional hydraulic conductivity. With this notation, Equation (5.2) can also be expressed as

$$\Delta h = \alpha \text{ erfc}\left(\frac{\beta}{\sqrt{t}}\right) \qquad (5.6)$$

with

$$\alpha = \frac{K_d(n)}{D} \text{ and } \beta = \frac{S_0}{K_d(n)}.$$

By measuring $\Delta h$ as a function of the time, for at least two time steps, Equation (5.6) can be used to determine the two unknown quotients $\alpha$ and $\beta$. If these measurements are available for six or more observation points $\mathbf{r}_i$ in a given aquifer, the quantity G in Equation (5.3), expressed through Equation (5.5) as

$$(x_i^1)^2A_{11} + (x_i^2)^2A_{22} + (x_i^3)^2A_{33} + 2x_i^1x_i^2A_{12} + 2x_i^2x_i^3A_{23} + 2x_i^1x_i^3A_{13} = \frac{r_i^2D}{K_d(n_i)} \qquad (5.7)$$

can be used to solve first for A and then through Equation (5.4) for the components of $\underline{K}$. However, to ensure that the system of linear equations, defined by Equation (5.7), does not become ill-conditioned, the observations must be conducted in such a fashion that: (a) not more than two observation boreholes lie in a straight line, (b) not more than three observations are in the same plane and (c) the observation boreholes do not lie on the axes of the co-ordinate system being used.

In practice, it is advantageous to measure $\Delta h$ at as many points in time as possible, for a specific $\mathbf{r}_i$, and then compute $\alpha$ and $\beta$ from a linear least squares fit of the data to Equation (5.6).

### 5.2.3 Description of the Apparatus

The apparatus used at Atlantis was developed by the Institute, in collaboration with the electronics workshop of the Department of Physics. Its basic components consisted of:

(a) packers to seal off sections in the boreholes,
(b) a pump system to inject water into the sealed-off areas of the injection hole,
(c) differential pressure transducers to monitor the water-levels,
(d) an electronic monitoring system, comprising of a Commodore 64 computer and peripheral equipment, to collect and store the data,
(e) a water tight container for the electronic components and

(f) levers and winches to handle the packers, cables and pipes.

The apparatus is represented schematically in Figure 5–4.

The advantage of using differential pressure transducers is that they can be adjusted easily to suit a specific need. For example, the expected pressure increase above the packers and in the sealed observation area is small. More sensitive transducers can therefore be used in these low pressure areas. However, pressures in the sealed injection area can be high. (In the case of the present investigation, pressures of 300 kPa (≈ 30 m water) and more were observed, depending on the water-level and depth at which observations were carried out).

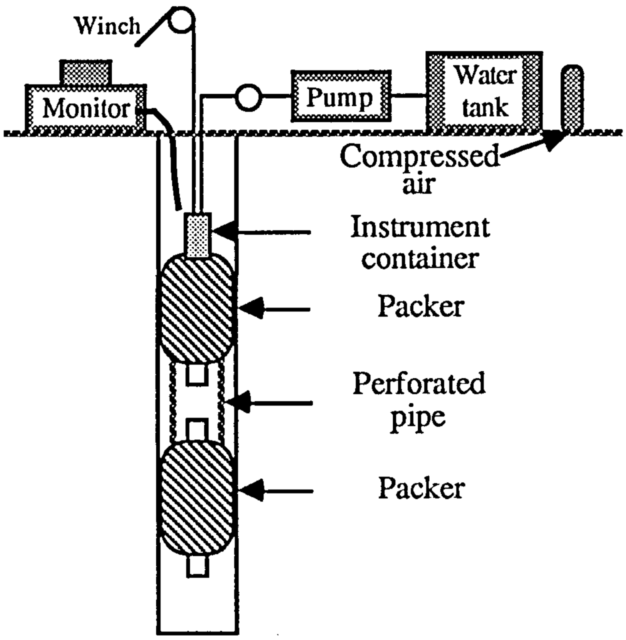

**Figure 5–4** Schematic representation of the cross-borehole packer apparatus

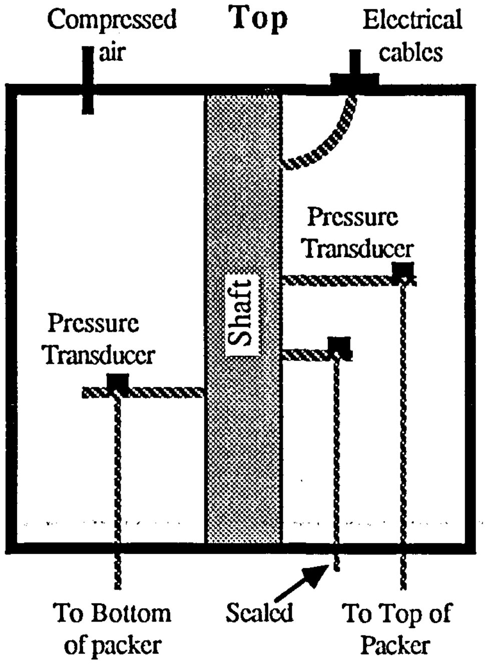

**Figure 5–5** Schematic presentation of the stainless steel container used to house the pressure transducers

The transducers were built into stainless steel containers, shown schematically in Figure 5–5. These containers were then fixed to the top of each packer combination. Each container had a diameter of 100 mm and a length of 300 mm. The removable top and bottom of the containers were bolted to the body of the container and sealed with o-rings. Water was supplied to the sealed-off area in the injection hole through a 25 mm pipe, which passed through the centre of the stainless steel container. A detailed description of the erection and usage of the apparatus can be found in Verwey (1987).

### 5.2.4 Application of Cross-borehole Packer Tests at Atlantis

The cross-borehole method was applied in Atlantis on the boreholes shown in Figure 5–1. Although only three boreholes were used, a sufficient number of tests were done by alternating the places of injection and observation between the three boreholes.

As can be seen from the geological profiles of the boreholes in Table 5–1, the geology is firm enough to conduct the cross-borehole tests from 37 m down to 81 m. The injection borehole was subsequently sealed at 5 m intervals and readings taken in the observation hole with the sealed-off area at the same depth, and 5 m above and below the sealed-off area in the injection borehole.

A problem often encountered with packer tests, is to know whether the packers seal properly. In a cross-packer test, this problem is eliminated completely, because any leakage – whether it originates from water leaking past packers, or through the geological formation – will be registered as a pressure increase by the transducers above and below the packers.

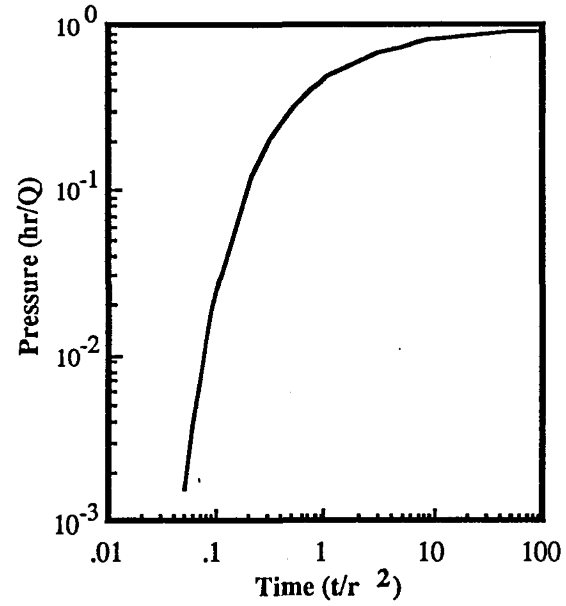

**Figure 5–6** Graph of $\Delta hr/Q$ as a function of the time variable $t/r^2$

As noticed above, the fundamental principle of a cross-borehole packer test, is the assumption that the observed pressure increase will satisfy Equation (5.1). A convenient way to determine whether this is true for a specific test, is to draw a graph of $\Delta hr/Q$ against $t/r^2$, such as the one in Figure 5–6. If the data fit the curve, the flow can be readily taken as porous flow, otherwise it must be considered as fractured flow and dealt with in an appropriate manner. If the pressure in the observation hole remains constant, throughout the test, the formation dividing the injection and observation borehole must be considered as fully impermeable. Examples of the first two types of pressure curves are given in Figure 5–7.

### 5.2.5 Discussion of the Results

In the final analysis of the data obtained during the present investigation, attention was paid mainly to those tests which match the theoretical constraints. They were grouped together at three depths, 37 – 48 m, 43 m and 44 – 48 m, all measured from ground level. Values of $K_d(n)/D$ and $S_0/K_d(n)$ were determined from Equation (5.6), for each depth and test performed, by the method of linear least squares, and values of A from Equation (5.7).

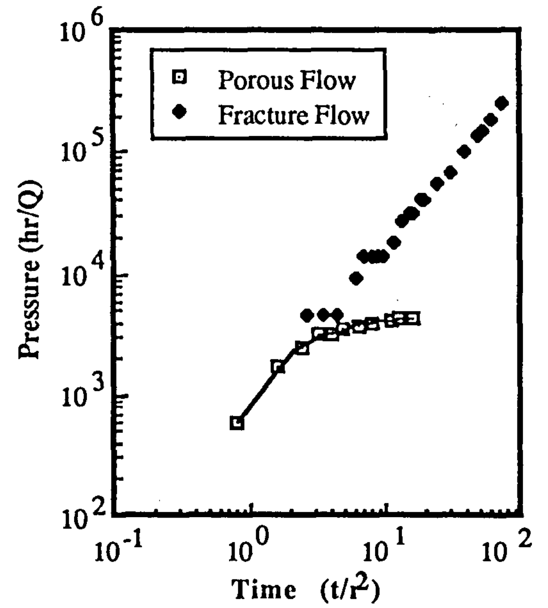

**Figure 5–7** Examples of the observed pressure increases for porous and fractured flow

As noticed above, six values of $K_d(n)/D$ and $S_0/K_d(n)$ had to be known, for Equation (5.7) to yield a unique A. Since more than six values were available at the depths considered here, the components of A were determined by multiple regression analysis.

With A known, the components of the hydraulic conductivity tensor, $K_{ij}$ can be computed from Equations (5.3) and (5.4). The three principle directions and values of $\underline{K}(x)$ can then be determined from a diagonalization of the hydraulic conductivity tensor. Magnitudes of the principle hydraulic conductivities and principal directions, expressed in terms of their direction cosines, are given in Tables 5–2 and 5–3. Figure 5–8 represents an attempt to display them in relation to the coastline.

**Table 5–2** Components of the hydraulic conductivity tensor and specific storage in the Malmesbury Formation at Atlantis

| Depth (m) | Components of the Hydraulic Conductivity tensor (m/s) | | | Specific storativity $S_0$ ($m^{-1}$) |
|---|---|---|---|---|
| 37–48 | $1{,}53.10^{-6}$ | $2{,}83.10^{-6}$ | $1{,}38.10^{-5}$ | $5{,}1.10^{-7}$ |
| 43 | $2{,}04.10^{-6}$ | $4{,}34.10^{-6}$ | $9{,}89.10^{-6}$ | $7{,}0.10^{-7}$ |
| 44–58 | $8{,}86.10^{-7}$ | $2{,}08.10^{-6}$ | $1{,}36.10^{-5}$ | $1{,}1.10^{-5}$ |

The specific storativity can be computed directly from Equation (5–3) and the known values of $K_d(n)/D$ and $S_0/K_d(n)$. The results for the three depth zones considered here, are presented in Table 5–2. A more detailed discussion of these computations can be found in Appendix B.

It is interesting to note that, for depths from 35 to 50 m, the biggest principle component of the hydraulic conductivity is in a vertical direction [see Figures 5–8(a) and (b)], and that its horizontal component is perpendicular to the coastline. Since these depths are already from 5 to 20 m below sea-level, there is a real danger of sea-water intrusion into the Atlantis aquifer through the Malmesbury Formation, should the fresh-water levels in the vicinity of the coastline be lowered extensively for production purposes.

**Table 5–3** Direction cosines of the principle axes of the hydraulic conductivity tensor in the Malmesbury Formation at Atlantis

| Depth (m) | Direction cosines | | |
|---|---|---|---|
| | $K_{xx}$ | $K_{yy}$ | $K_{zz}$ |
| 37–48 | –0.807 | 0,573 | 0,144 |
| | –0.547 | –0,817 | 0,184 |
| | 0,223 | 0,670 | 0,972 |
| 43 | –0,883 | 0,349 | 0,313 |
| | –0,340 | –0,937 | 0,084 |
| | 0,322 | –0,033 | 0,946 |
| 44–58 | 0,459 | 0,816 | 0,350 |
| | –0,136 | 0,454 | –0,880 |
| | –0,878 | 0,357 | 0,320 |

Pressure changes were registered in very few of the tests, conducted at depths larger than 50 m. The Malmesbury Formation is thus considerably less fractured here than at the shallower depths. Since the principle component of $\underline{K}$ is here, moreover, parallel to the coast [see Figure 5–8(c)], sea-water intrusion should not be a problem at these depths.

The main conclusion to be reached from the results of the present investigation (see Tables 5–2 and 5–3 and Figure 5–8) is that the Malmesbury Formation is so fractured at the test site, that it must be considered as an anisotropic porous medium, at least to depths equivalent at the bottom of the sand deposits. After that, the degree of fracturing steadily decreases with depth.

It is interesting to note that the prevailing conditions at the injection hole of a cross-packer test are exactly the same as those of a normal double-packer test. Results from the cross-packer tests were, consequently, also analysed with the double-packer theory and presented in Table 5–4.

In 1986, the Directorate Geohydrology conducted a constant rate pumping test on borehole G33457 to determine the hydraulic properties of the Malmesbury Formation. The values obtained for the transmissivity and storativity from these tests are $6{,}0.10^{-3}$ m$^2$/d and $7{,}0.10^{-4}$, respectively. The average thickness of the Malmesbury formation in this area is approximately 60 m, as shown by the geological profiles of both the pumped and observation boreholes supplied to the Institute by the Directorate. As shown by the results in Table 5–4, the hydraulic conductivity and specific storativity derived from this test, compare favourably with those obtained from both the cross- and double-packer methods.

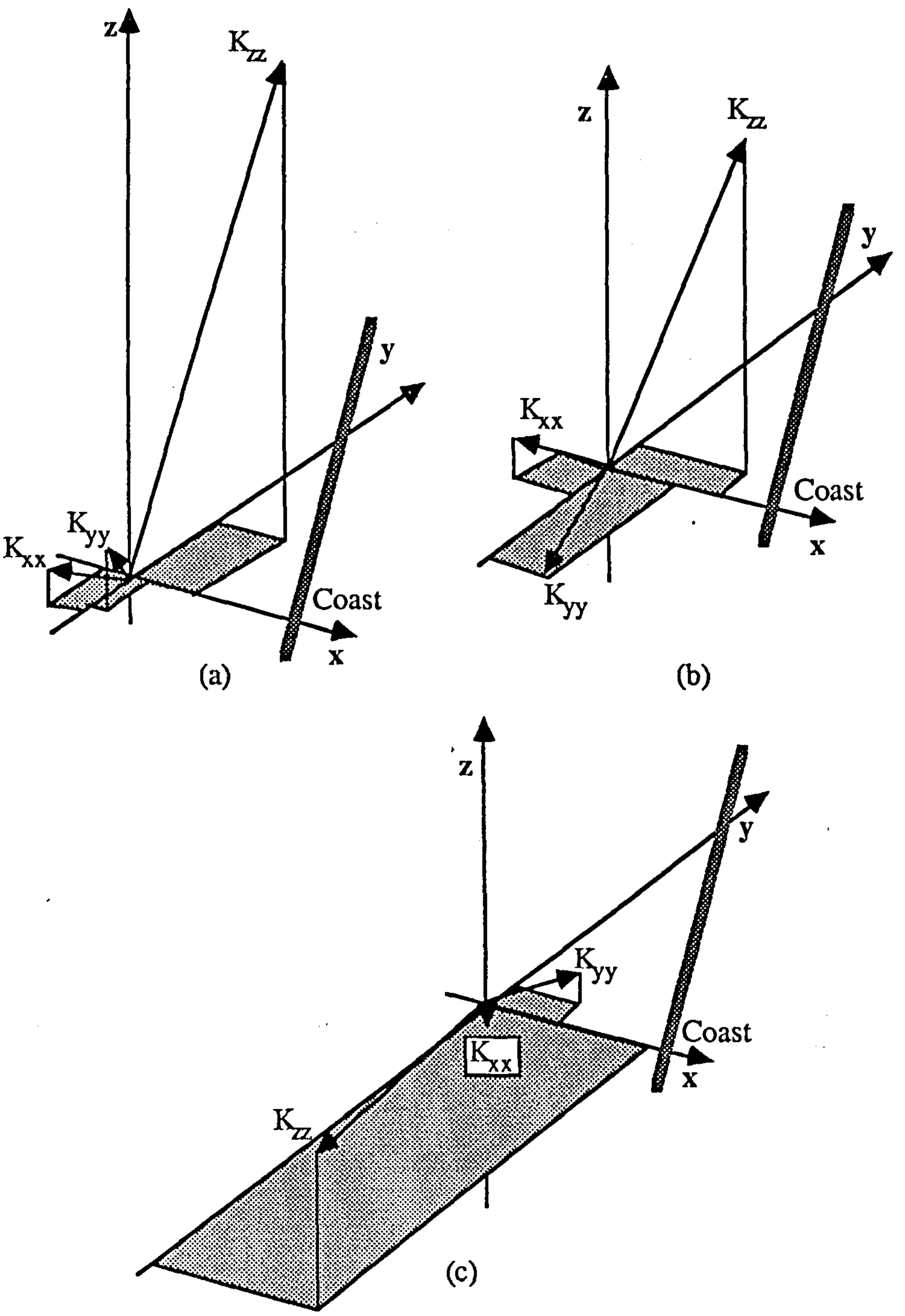

Figure 5–8 Graphical representation of the main components of the hydraulic conductivity, as observed at depths of (a) 43 m, (b) 37 – 48 m and (c) 44–58 m in the Malmesbury Formation at Atlantis

In order to present an efficient management model for the Atlantis aquifer, the cross-borehole tests should be conducted at a few more places. Attention should also be given to the development of a more detailed sea-water intrusion model than the one used by Botha and Müller (1986). This model should include the effect of the infiltration of water with a poor quality (such as purified industrial sewerage) to prevent sea-water intrusion into a coastal aquifer.

**Table 5–4** Values of the hydraulic conductivity and storativity of the Malmesbury Formation at Atlantis, as determined from cross-packer, double-packer and an ordinary pump test

| | Cross-packer Test | Double-Packer Test | Pump Test |
|---|---|---|---|
| K ($m.s^{-1}$) | $4{,}0 \times 10^{-5}$ | $8{,}7 \times 10^{-5}$ | $9{,}9 \times 10^{-5}$ |
| $S_0$ ($m^{-1}$) | $4{,}0 \times 10^{-6}$ | – | $1{,}2 \times 10^{-5}$ |

## 5.3 UNSATURATED FLOW PARAMETERS

### 5.3.1 General

At first sight, it would seem as if the unsaturated flow equation contains only one conceptual parameter – the unsaturated hydraulic conductivity – until it is realized that Equation (12.12) can only be solved if the functional relation between the soil moisture content and matric head is available. The soil moisture retention curve is thus, without any doubt, the most important conceptual parameter in modelling unsaturated flow. This importance is further underlined by the fact that it is difficult to determine the unsaturated hydraulic conductivity in the field, with the result that a modeller has to rely on semi-empirical relations based on the retention curve [e.g. Equation (9.36)] for its determination. The quality of the moisture retention curves used in modelling unsaturated flow is thus of critical importance. Care should, therefore, be exercised to ensure that the experimental retention curves used, in modelling unsaturated flow, are as accurate as possible.

As shown in Section 9.5, the moisture retention curve is always a multi-valued relation of the soil moisture contents and matric heads. While this may not be difficult to overcome experimentally, it does present some difficulties from the modelling point of view. For example, it is not just enough to track the status of all nodes in the computer program used for modelling unsaturated flow, but the program must also be able to decide on what branch of the retention curve a particular node falls [Scott *et al.* (1983)]. A computer program which accounts for the hysteretic nature of the retention curve, is thus considerably more complicated than one in which it is neglected. The question thus arises if the effect of the hysteresis on the solution of Equation (12.12) is of such an extent that it is really necessary to account for it in a computer program? With this in mind, Scott *et al.* (1983) compared the results obtained from laboratory studies of unsaturated flow in columns with those obtained from one-dimensional finite difference models of the columns. Taken at face value, their results would seem to indicate that the hysteretic nature of the retention curve has to be taken into account, if the model is to yield meaningful results. However, there are other considerations that have also to be taken into account.

Unsaturated flow is actually a two-phase flow phenomena – water and air. The argument could, therefore, be advanced that models which take only the water phase into account, are already in considerable error. Morel-Seytoux and Vauclin (1983), again comparing laboratory results with that obtained from a one-dimensional model, came to the conclusion that this is indeed the case. A true conceptual model of unsaturated flow should thus take both phenomena into account.

The previous interpretation is obviously physically correct. Nevertheless, it is rather strange that in both the papers referred to above, the discrepancy between the observed and computed results is not ascribed to the hysteretic nature of the retention curve and the two-phase nature of the phenomenon simultaneously, but only to one at a time. This suggests that the real cause of the discrepancy may actually be in restricting the flow to one dimension only (in both the laboratory and conceptual models). This conjecture can, unfortunately, not be proved beyond any doubt with the resources available at the Institute. However, the Institute has, at its disposal, results from experiments on porous flow channels conducted by the Department of Water Affairs of Namibia, which do not agree with one-dimensional two phase, or hysteretic flow models, but with a non-hysteretic two-dimensional one phase flow model. The freedom of flow allowed for in an unsaturated model may thus be of more importance than either air or hysteretic effects. Taken at face value, these observations would seem to suggest that a non-hysteretic two-dimensional one-phase model may be sufficient for most practical purposes, especially in the absence of detailed observations. The present investigation has, consequently, been restricted to two-dimensional one-phase flow.

### 5.3.2 Moisture Retention Curves for the Sands at Atlantis

The moisture retention curves for the sands at Atlantis were determined by the Soil Physics Section of the Fruit and Food Technology Institute at Stellenbosch. For this purpose, a number of soil samples were taken at different depths from the vicinity of the neutron tubes installed around Pan 7 at Atlantis (see Figure 2–5). The experimental results were analysed at the Institute and fitted to the Van Genuchten approximation [Equation (9.15)] with results listed in Table 5–5. The excellent fits obtained between the observed data and the theoretical approximation are demonstrated by the graph for the sand at a depth of 0,2 m at observation hole A1 in Figure 5–9.

The fact that the sands in the vicinity of Pan 7 (up to a depth of approximately 20 m) belong to Witzand member of the Bredasdorp Formation is reflected by the uniformity of the Van Genuchten parameters in Table 5–5. It is difficult to explain the deviation of the parameters for observation holes A3, A4 and (to a lesser extent) A5 from the rest. One possibility, supported by results obtained at Vaalputs, is that the sand in this area contains lenses of calcrete. However, this does not distract from the fact that one has here probably one of the best sets of moisture retention curves for any soil type in South Africa.

**Table 5–5** Parameters of Van Genuchten's analytic soil moisture retention curve for the sand in the vicinity of Pan 7 at Atlantis

| Position | Depth (m) | $\alpha$ | n | $\theta_r(x10^2)$ | $\theta_s(x10^1)$ |
|---|---|---|---|---|---|
| A1 | 0,2 | 3,958 | 2,366 | 3,207 | 3,778 |
| | 0,6 | 5,388 | 2,315 | 1,365 | 3,928 |
| | 1,8 | 4,132 | 2,320 | 1,486 | 3,858 |
| A2 | 0,7 | 4,607 | 2,349 | 1,362 | 4,010 |
| | 1,6 | 5,535 | 2,249 | 1,948 | 3,989 |
| | 2,3 | 4,838 | 2,427 | 1,096 | 3,627 |
| A3 | 0,7 | 3,308 | 1,256 | 0,000 | 0,798 |
| | 1,7 | 0,672 | 1,819 | 3,706 | 3,115 |
| | 2,3 | 4,058 | 1,455 | 0,000 | 2,682 |
| A4 | 0,8 | 2,038 | 1,529 | 3,293 | 1,212 |
| | 1,3 | 1,233 | 5,489 | 3,970 | 1,431 |
| | 1,8 | 1,239 | 5,648 | 2,528 | 1,084 |
| | 2,6 | 1,273 | 1,590 | 0,518 | 0,556 |
| A5 | 0,7 | 0,584 | 2,194 | 2,586 | 3,374 |
| | 1,5 | 0,995 | 1,700 | 2,428 | 2,475 |
| | 2,3 | 0,879 | 1,994 | 2,025 | 2,997 |
| A6 | 0,7 | 4,702 | 2,699 | 2,294 | 3,409 |
| | 1,8 | 4,419 | 3,066 | 1,565 | 3,415 |
| | 2,3 | 4,526 | 2,899 | 1,311 | 3,662 |
| A7 | 0,8 | 3,881 | 2,916 | 2,198 | 3,602 |
| | 1,3 | 4,201 | 2,675 | 1,406 | 3,152 |
| | 2,3 | 4,740 | 2,800 | 1,731 | 3,450 |
| A8 | 0,8 | 3,948 | 2,973 | 2,808 | 3,906 |
| | 1,7 | 4,378 | 2,976 | 1,897 | 3,722 |
| | 2,3 | 4,488 | 2,718 | 2,917 | 3,697 |
| A9 | 0,5 | 4,347 | 2,512 | 1,462 | 3,758 |
| | 1,5 | 4,096 | 2,569 | 1,264 | 3,586 |
| | 2,8 | 4,919 | 2,496 | 0,904 | 3,491 |
| A10 | 0,6 | 3,962 | 2,769 | 4,578 | 3,997 |
| | 1,6 | 4,151 | 2,781 | 3,600 | 3,827 |
| | 2,3 | 3,605 | 2,644 | 2,898 | 3,940 |

### 5.3.3 Saturated Hydraulic Conductivity

Values of the saturated hydraulic conductivities, or more precisely the quantity ($k\rho/\mu$), were also determined by the Section of Soil Science of the Research Institute for Fruit and Food Technology. These values are given in Table 5–6, together with the sand analysis, for the same positions at which the moisture retention curves were determined.

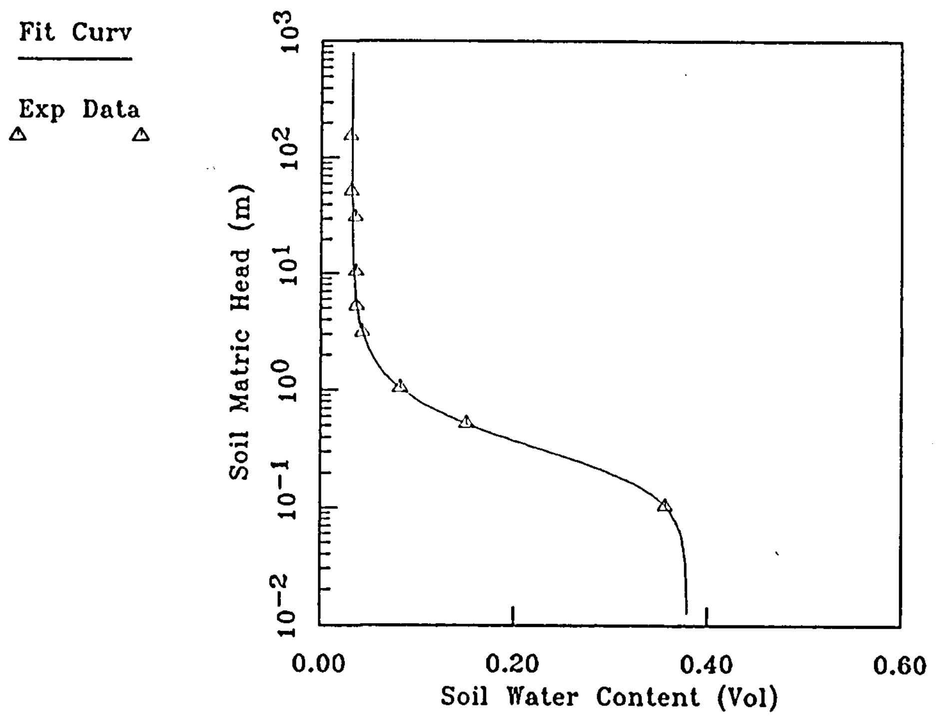

**Figure 5–9** Example of the Van Genuchten approximation to the observed moisture retention curve for the sands at Atlantis

## 5.4 HYDRODYNAMIC DISPERSION COEFFICIENT

The hydrodynamic dispersion coefficient, $\underline{D}$, or alternatively the longitudinal and transverse dispersivities, $\alpha_L$ and $\alpha_T$ (see Equation 13.19), is probably the most difficult conceptual parameters to measure in practice. The reason for this is that there is no method available to measure it directly at present. The majority of values available in the literature have consequently been determined indirectly – by comparing data obtained from laboratory experiments or tracer tests in the field, with analytical solutions for idealized forms of the general equation. One method often applied for this purpose is to fit the solution of the one-dimensional hydrodynamic dispersion equation to experimentally observed breakthrough curves of a conservative tracer.

To illustrate the previous procedure, consider the situation where a slug of conservative tracer is injected into a fluid, which flows at a constant velocity in the x-direction through a uniform column of porous material. Under these conditions, the hydrodynamic dispersion coefficient simplifies to $\underline{D}_h = \alpha_L u$, if molecular diffusion is neglected, and the hydrodynamic dispersion equation, Equation (13.27), to

$$D_t c = \alpha_L u D_x^2 c - u D_x c \qquad (5.8).$$

**Table 5-6** Sand analyses and saturated hydraulic conductivities (in $m.s^{-1} \times 10^5$) for the sand in the vicinity of Pan 7 at Atlantis

| Position | Depth (m) | Clay | Silt | Sand |  |  | Hydraulic Conductivity |
|---|---|---|---|---|---|---|---|
|  |  |  |  | Fine | Medium | Coarse |  |
| A1 | 0,2 | 1,7 | 1,4 | 24,0 | 71,1 | 1,8 | 1,87 |
|  | 0,6 | 1,5 | 0,1 | 21,5 | 74,9 | 2,0 | 1,96 |
|  | 1,8 | 1,8 | 0,6 | 24,8 | 72,3 | 0,5 | 1,95 |
| A2 | 0,7 | 0,9 | 0,7 | 23,9 | 74,1 | 0,4 | 2,01 |
|  | 1,6 | 2,2 | 0,9 | 17,5 | 77,5 | 1,9 | 1,80 |
|  | 2,3 | 1,1 | 0,7 | 13,7 | 83,1 | 1,4 | 1,89 |
| A3 | 0,7 | 1,0 | 0,6 | 16,2 | 66,1 | 16,1 | 1,81 |
|  | 1,7 | 1,2 | 0,8 | 19,8 | 68,1 | 10,1 | 1,87 |
|  | 2,3 | 1,1 | 0,8 | 11,1 | 64,4 | 22,6 | 1,86 |
| A4 | 0,8 | 1,5 | 1,1 | 19,5 | 67,9 | 10,0 | 1,79 |
|  | 1,3 | 1,7 | 0,9 | 19,2 | 68,7 | 9,5 | 1,85 |
|  | 1,8 | 1,5 | 0,7 | 14,5 | 80,5 | 2,8 | 1,86 |
| A5 | 0,7 | 1,3 | 1,1 | 23,5 | 69,9 | 3,2 | 1,94 |
|  | 1,5 | 0,7 | 0,4 | 16,6 | 62,4 | 19,9 | 1,89 |
|  | 2,3 | 1,1 | 0,5 | 18,3 | 71,0 | 9,1 | 1,88 |
| A6 | 0,7 | 1,1 | 0,5 | 22,5 | 63,1 | 12,8 | 1,88 |
|  | 1,8 | 0,7 | 0,7 | 16,9 | 73,6 | 8,1 | 1,85 |
|  | 2,3 | 1,5 | 0,6 | 23,3 | 70,1 | 4,5 | 1,86 |
| A7 | 0,8 | 1,0 | 0,8 | 37,2 | 49,7 | 11,3 | 1,77 |
|  | 1,3 | 0,6 | 0,2 | 33,9 | 50,4 | 14,9 | 1,83 |
|  | 2,3 | 1,5 | 0,3 | 38,3 | 56,4 | 13,5 | 1,93 |
| A8 | 0,8 | 1,7 | 0,4 | 22,5 | 72,3 | 3,1 | 1,88 |
|  | 1,7 | 1,4 | 0,2 | 17,3 | 74,0 | 7,1 | 1,86 |
|  | 2,3 | 1,2 | 0,4 | 15,3 | 80,8 | 2,3 | 1,91 |
| A9 | 0,5 | 1,2 | 0,9 | 17,0 | 75,2 | 5,7 | 1,88 |
|  | 1,5 | 1,2 | 0.4 | 17,8 | 77,0 | 3,6 | 1,86 |
|  | 2,8 | 1,2 | 0,4 | 13,8 | 80,1 | 3,5 | 1,88 |
| A10 | 0,6 | 1,6 | 1,0 | 17,6 | 76,0 | 3,8 | 1,90 |
|  | 1,6 | 2,4 | 0,7 | 17,0 | 76,5 | 3,4 | 1,78 |
|  | 2,3 | 1,8 | 0,8 | 47,3 | 49,2 | 0,9 | 1,85 |

If the material and fluid are initially free of the tracer, the appropriate initial and boundary conditions are

$$c(x,0) = \frac{m}{\varepsilon}\delta(x) \text{ and } c(\pm\infty,t) = 0 \ \forall \ t, \qquad (5.9)$$

where m = the mass of tracer contained in the slug, ε the porosity of the medium and δ(x) the Dirac delta function. The solution of Equation (5.8), subject to Equation (5.9), is [see e.g. Bear (1972)]

$$c(x,t) = \frac{m}{2\varepsilon\sqrt{\alpha u t}} \exp\left[-\frac{(x-ut)^2}{4\alpha t}\right]. \qquad (5.10)$$

Thus, if u is known and c(x,t) measured at different positions in space and time, $\alpha_L$ can be determined by using a least squares, or graphical, approximation to fit the observed concentrations to Equation (5.10).

Although there are more realistic solutions available for Equation (13.27) [Sauty (1980)], they also require more elaborate experimental and fitting techniques, in order to determine the dispersivities. Moreover, as can be seen by comparing the graphs of the potassium concentrations in Figure 4–13 with Equation (5.10), the concentrations observed under 'natural' conditions may not satisfy an analytical solution at all. The fitting of observed concentrations to an analytical solution, can thus be a very frustrating experience, as an attempt to fit the data in Figure 4–13 to Equation (5.10) will show. It may thus be necessary to devise special observations, such as the tracer technique [Meyer *et al.* (1981)], if the dispersivities of a particular aquifer are to be determined by fitting observed concentrations to an analytical solution of the hydrodynamic dispersion equation.

Since no special observations were available for the Atlantis aquifer, another technique had to be used in order to obtain some estimate of the dispersivities. For this purpose, a suitable hydraulic conductivity value was selected from those given in Müller and Botha (1986) and a mean porosity determined for the observation point A9 (see Figure 2–5), from those given in Table 5–5. By using this information, and the triangular element technique, described in Appendix 3, an approximate horizontal flow velocity was calculated for well point WP49. With this information and the times at which the maximum and minimum peak concentrations occur in Figure 4–13, the longitudinal dispersivity was calculated from Equation (5.10) as $\alpha_L \approx 4{,}0\ m^2.d^{-1}$. Unfortunately, this method does not yield any information on the transverse dispersivity. However, since it is generally accepted that $\alpha_L \approx 10 - 20$ times $\alpha_T$ [Sauty (1980)], $\alpha_T$ was simply set equal to $0{,}4\ m^2.d^{-1}$.

# CHAPTER 6

# HORIZONTAL FLOW MODELS

## 6.1 INTRODUCTION

As can be seen from the discussion in Chapter 12, there is a considerable difference between the equation describing flow in a horizontally confined aquifer and that describing flow in a phreatic aquifer. It was thus necessary to develop two different computer programs, in order to ensure that the majority of South African aquifers will be covered.

There are other computer programs available at the Institute for use with confined aquifers [Van Tonder (1987), Pinder (1974)], but the boundary conditions allowed for in them are very restrictive. The simplest approach would be to just modify the boundary conditions in these programs. However, the programs were originally developed for mainframe computers and use somewhat outdated numerical methods. It was, therefore, decided to develop the programs from scratch and make them more user-friendly, for greater ease of use on micro computers.

The model developed for a phreatic aquifer is, as far as could be ascertained, the first model of its kind where the position of the water table is taken into account.

## 6.2 MODELLING A CONFINED AQUIFER

### 6.2.1 General

The basic conceptual model, which governs the flow of water in a confined aquifer, is descibed mathematically by the two-dimensional parabolic partial differential equation (see Section 12.2.1)

$$SD_t h(x,t) = \nabla \bullet [\underline{T}(x) \nabla h(x,t)] + R(x,t) + Q(x,t)\delta(x - x_0) \qquad (6.1)$$

where

$h(x,t)$ = piezometric water level $[L]$
$\underline{T}(x)$ = $\underline{K}(x)L(x)$, the transmissivity tensor $[L^2.T^{-1}]$
$\underline{K}(x)$ = the hydraulic conductivity tensor at x $[L.T^{-1}]$
$S$ = $S_0(x)L(x)$, the storage coefficient $[L^{-1}]$
$S_0$ = the storativity of the aquifer $[1]$
$L(x)$ = thickness of the aquifer at x $[L]$
$R(x,t)$ = areal sources (for example rainfall) $[L.T-1]$
$Q(x,t)$ = the yield of sources (+) or sinks (-) $[L^3.T^{-1}]$

and $\nabla$ the usual two-dimensional gradient operator.

Equation (6.1) can only be solved if suitable initial and boundary conditions are prescribed on a suitable domain, $\Omega$ and its boundary $\partial\Omega$, respectively. The initial condition is quite simple and needs only to describe the water levels at a specific point in time, usually equated with the time $t = 0$. It can, therefore, be represented mathematically by the equation

$$h(x,0) = h_0(x). \tag{6.2}$$

The boundary conditions allowed with a parabolic equation, like Equation (6.1), can be either one of two types: *Dirichlet* and *Neumann* conditions. Dirichlet conditions are used when the behaviour of the solution of the differential equation on the boundary $\partial\Omega$ is known, while Neumann conditions are used when there is a known flux across $\partial\Omega$. Two typical examples of these conditions in groundwater flow are: (a) the boundary between the sea and a coastal aquifer (Dirichlet), and (b) where an aquifer is bisected by a semi-permeable vertical dyke (Neumann).

Boundary conditions can be functions of the spatial coordinates and the time. The correct way to specify Dirichlet and Neumann conditions for Equation (6.1) is through equations of the form

$$\begin{gathered} h(x,t) = f(x,t) \\ q_n = \mathbf{T}(x)\nabla h(x,t)\bullet \mathbf{n} \end{gathered} \tag{6.3}$$

where $\mathbf{n}$ is the *outward directed* unit vector normal to the boundary $\partial\Omega$ and $q_n$ the flux normal to $\partial\Omega$. This fact has usually been neglected in earlier programs, as demonstrated by the programs at present available at the Institute, which allow only time-independent Dirichlet conditions [$f(x,t) \equiv f(x)$] and zero flux ($q_n = 0$) Neumann conditions. The application of these programs are thus very restrictive, as Van Rensburg (1985) experienced in his model of the Grootfontein Compartment.

Time-dependent Dirichlet boundary conditions can be easily implemented in a computer program. All that need be done is to make provision for the conditions to be read in at the times required. Time-dependent and, in fact, even time-independent Neumann conditions are of a completely different nature [Botha and Pinder (1983), Huyakorn and Pinder (1983)]. Because it is easier to incorporate time-dependent Neumann boundary conditions in a finite element approximation than in a finite difference approximation of a differential equation [Botha and Pinder (1983)], the present program is based on a finite element approximation of Equation (6.1).

Since the basic algorithms needed in the finite element approximation of Equation (6.1), is well-documented in the references sited above, they will not be discussed here. A brief discussion can, however, be found in Appendix C, where the computer program for a confined aquifer GCON is described in greater detail.

The major difference, apart from boundary conditions, between the program GCON and other available programs, is the inclusion of higher order Lagrange and Serendip elements (up to order 3). Although Botha and Bakkes (1981) have shown that not much can be gained by using elements of order greater than one when point sources or sinks are present in an aquifer, waste disposal sites are often situated in aquifers with no-production boreholes. In such cases, it may be advantageous to use a coarse mesh without loss in accuracy.

### 6.2.2 Testing of the Program

To ensure that the program is, as far as possible, error free, use was made of a hypothetical square aquifer with constant thickness and zero flux Neumann conditions. The reason for this choice is that the analytical solution of such an aquifer can be calculated by the method of images [Walton (1970)], thereby yielding an excellent standard with which to compare the approximate finite element solution.

The aquifer used in testing the present program consisted of an area of 1 200 x 1 200 $m^2$, with a thickness of 10 m, with a constant transmissivity $T = 10^{-2}$ ($m^2.s^{-1}$) and storage coefficient $S = 10^{-3}$. Three boreholes were placed in the hypothetical aquifer, in order to simulate the development of a flow model for a true aquifer as closely as possible. A ‘production’ borehole with a yield of 0,05 $m^3.s^{-1}$ was placed at x = (400, 800) and two ‘observation’ boreholes at distances of 400 and $400\sqrt{2}$ m from it (see Figure 6–1).

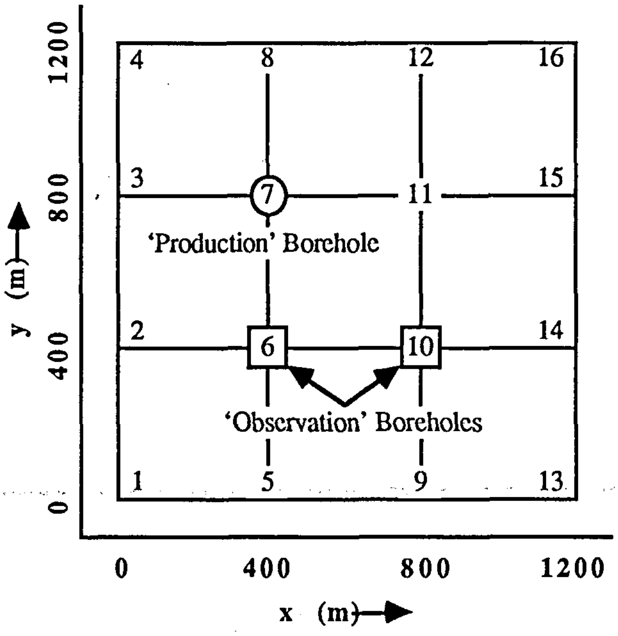

**Figure 6–1** Example of a finite element mesh used to establish the numerical accuracy of the program developed for a confined aquifer

The convergence rate of numerical approximations, used in the program, was investigated by computing the solution of the hypothetical aquifer on a sequence of meshes, starting with the coarse mesh in Figure 6–1 and then doubling the number of nodes of the subsequent mesh. The positions of the production and observation boreholes were, however, kept fixed. The rapid convergence of the absolute errors in the water levels at the two 'observation' boreholes (see Figure 6–2), can be considered as an indication that there are no algorithmic or numerical errors in the program.

## 6.3 THE PHREATIC AQUIFER

### 6.3.1 General

As discussed in Section 11.3.3, a phreatic aquifer should be regarded as the saturated part of a saturated/unsaturated flow problem, unless one is willing to track the position of the water table. This is, unfortunately, not an easy task when the differential equation is solved numerically. The majority of available programs avoid this *moving boundary* in phreatic aquifers by taking the transmissivity as the product of the hydraulic conductivity and the saturated thickness of the aquifer at the previous time step [Pinder (1974)].

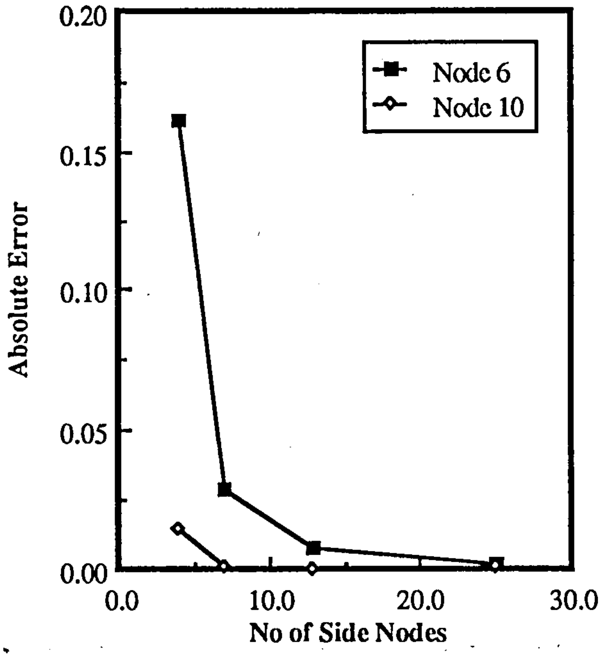

Figure 6–2 Convergence of the solution for the hypothetical confined aquifer at the 'observation' boreholes (nodes 6 and 10 in Figure 6–1) as a function of the number of nodes in the mesh

Another conceptual model for a phreatic aquifer that has been available for quite sometime in the literature, is the Boussinesq equation [see Equation (12.15)]. This equation is still not fully compatible with the physics of phreatic flow, but it does account for the moving boundary without the need to trace it explicitly. However, this is achieved at the cost that one now has to solve a non-linear differential equation. Although this is a much more tractable numerical exercise than tracking a moving boundary, a non-linear equation can only be solved iteratively. The fact that iterative methods can be very time-consuming, is probably the main reason why Boussinesq's equation has not been used in the past to model phreatic flow. Since time is not a serious restriction with the present generation of micro computers and there is very little information in the existing literature on the accuracy of the variable transmissivity approach, it was decided to base the present program on the generalized Boussinesq's equation

$$\nabla\bullet[\underline{\mathbf{K}}(x)(h(x,t)-b(x))\nabla h(x,t)]+Q(x,t)=\theta_e\,D_t\,h(x,t), \qquad (6.4)$$

where

$b(x)$ = height of the impervious bottom measured relatively to a suitable reference datum (usually mean sea level)
$\theta_e(x)$ = the specific yield of the aquifer

and the rest of the symbols have the same meaning as in Equation (6.1). The initial and boundary conditions are again those given in Equations (6.2) and (6.3).

### 6.3.2 Numerical Approximation of the Boussinesq Equation

Although Equation (6.4) could be approximated directly with the Galerkin finite element method, such an approach would yield a system of non-linear equations in the variable h, which can only be solved with the slow converging Picard iteration method [Botha and Pinder (1983)]. To avoid this, it was decided to derive a faster converging Newton type method.

It is known [Botha and Pinder (1983)] that any function $h(x,t)$ can be approximated over the interval $[t_{n+1}, t_n]$ through a linear Lagrange interpolation polynomial, $l_k(t)$, in the form

$$h(x,t)=\sum_{k=n}^{n+1} l_k(t)h(x,t_k)+E(\tau), \qquad (6.5)$$

where $h(x,t_n)$ is the exact value of $h(x,t)$ at the time $t_k$ and $E(\tau)$ the associated interpolation error. If $E(\tau)$ and $h(x,t_k)$ were known, then Equation (6.5) could be used to obtain an exact solution of Equation (6.4). Unfortunately, this is not the case and one has to be satisfied with the approximation

$$h(x,t)\approx\sum_{k=n}^{n+1} l_k(t)h^k(x), \qquad (6.6)$$

where $h^k(x)$ denotes an approximation to $h(x,t_k)$. Substitution of this approximation in Equation (6.4) yields a non-linear elliptic differential equation, which when collocated at the time $t_k = t_n+1$, can be expressed in the form

$$\theta_e[h^{n+1}(x)-h^n(x)]=\Delta t[\nabla\bullet\underline{\mathbf{K}}\{h^{n+1}(x)-b\}\nabla h^{n+1}(x)+Q(x,t_{n+1})] \qquad (6.7)$$

Let $h^{n+1,m}(x)$ denotes the iterative solution of Equation (6.7) after the m-th iteration step at the time level n+1. The next iterate may then be expressed in the form

$$h^{n+1,m+1}(x) = h^{n+1,m}(x) + \delta h^{n+1,m}(x) \qquad (6.8)$$

where $\delta h^{n+1,m}(x)$ denotes the correction to $h^{n+1,m}(x)$. Substitution of this equation into Equation (6.7) yields, after some rearrangement of terms, the equation

$$\begin{aligned}\theta_c(x)[h^{n+1,m}(x) + \delta h^{n+1,m}(x) - h^n(x)] &= \Delta t\nabla\bullet[\underline{K}\{h^{n+1,m}(x) - b(x)\}\nabla h^{n+1,m}(x)]\\ &+ \Delta t\nabla\bullet[\underline{K}\{h^{n+1,m}(x) - b(x)\}\delta h^{n+1,m}(x)]\\ &+ \Delta t\nabla\bullet[\underline{K}\delta h^{n+1,m}(x)\nabla\{h^{n+1,m}(x) + \delta h^{n+1,m}(x)\}] + \Delta t\ Q(x,t_{n+1}). \qquad (6.9)\end{aligned}$$

The second last term on the right-hand side of (6.9) contains the hopefully small unknown error term $\delta h^{n+1,m}$ as a factor and will, therefore, be neglected. With this assumption, Equation (6.9) can be rewritten in the form

$$\begin{aligned}&\theta_c(x)\delta h^{n+1,m}(x) - \Delta t\nabla\bullet[\underline{K}(x)\{h^{n+1,m}(x) - b(x)\}\nabla\delta h^{n+1,m}(x)]\\ &= \Delta t\nabla\bullet[\underline{K}(x)\{h^{n+1,m}(x) - b(x)\}\nabla h^{n+1,m}(x)] - \theta_c(x)[h^{n+1,m}(x) - h^n(x)]\\ &\quad + \Delta t\ Q(x,t_{n+1}) \qquad (6.10)\end{aligned}$$

Application of Galerkin's method to Equation (6.10) yields, after application of the finite element approximations

$$h^{n+1,m}(x) = \sum_{j=1}^{N} h_j^{n+1,m}\phi_j(x) \text{ and } b(x) \approx \hat{b}(x) = \sum_{j=1}^{N} b_k\phi_k(x),$$

and Green's theorem, the set of N linear equations (i = 1, ..., N)

$$\begin{aligned}&\int_{\partial\Omega}\Big[\theta_c(x)\delta^{n+1,m}(x)\phi_i(x) + \Delta t\ \underline{K}(x)\{h^{n+1,m}(x) - \hat{b}(x)\}\nabla\delta^{n+1,m}(x)\nabla\phi_i(x)\Big]d\Omega\\ &= -\Delta t\int_{\partial\Omega}\underline{K}(x)[h^{n+1,m}(x) - \hat{b}(x)]\nabla h^{n+1,m}(x)\nabla\phi_i(x)d\Omega\\ &\quad - \int_{\partial\Omega}\Big[\theta_c(x)\{h^{n+1,m}(x) - h^n(x)\}\phi_i(x) + \Delta t Q(x,t_{n+1})\phi_i(x)\Big]d\Omega\\ &\quad + \Delta t\int_{\partial\Omega}\Big[\phi_i(x)\underline{K}(x)\{h(x) - b(x)\}\nabla h^{n+1,m}(x)\Big]\bullet\mathbf{n}dS\end{aligned}$$

where the last term denotes the Neumann boundary conditions. This set of equations can be expressed more compactly in matrix form as

$$\mathbf{A\delta h = B} \qquad (6.11)$$

where

$$\delta\mathbf{h} = [\delta h_1^{n,m}\ \delta h_2^{n,m}\ \dots\ \delta h_n^{n,m}]^T$$

is the vector of corrections that must be applied to the nodal values $h_i^{n,m}$ ($i = 1, 2, \ldots, n$) to obtain the next iterate $h_i^{n,m+1}$.

Before Equation (6.11) can be used in actual computations, the hydraulic conductivity and specific yield have to be approximated in one form or another. A method often used for this purpose is to assume that they are piecewise constant over an element. However, this may introduce unwanted discontinuities into the equations, with disastrous results. To avoid this, it was assumed that both $\underline{\mathbf{K}}$ and $\theta_c$ will be supplied as nodal values, so that they can be approximated continuously by the finite element basis functions.

The basic idea behind this Newton type approximation is quite simple. At the first time step, the initial condition is used as a guess for $h^{1,0}(x)$. The system of linear equations in Equation (6.11) is then computed and solved for $\delta\mathbf{h}$. This correction is applied to $h^{1,0}(x)$ in order to get the new iterate $h^{1,1}(x)$, which is then used to compute a new correction $\delta\mathbf{h}$. The procedure is repeated until the Chebyshev, or maximum, norm of $\delta\mathbf{h}$ is smaller than a prescribed tolerance $\varepsilon$, i.e.

$$\|\delta\mathbf{h}\|_\infty \equiv \max\{\delta h_i | i = 1, \ldots, n\} \leq \varepsilon$$

The $h^{1,m}(x)$ obtained after this final correction is applied, is assumed to represent the solution of Equation (6.4) at the time $t_1$. This solution is then used as the first approximation for $h^{2,0}(x)$. The process is repeated until the full period for which the solution of Equation (6.4) is required has been covered.

The algorithms discussed above, for the solution of the non-linear Boussinesq equation, have been implemented in the computer code GWUN, of which a more detailed description can be found in Appendix C.

### 6.3.3 Testing of the Program

The task to ensure that all approximations have been implemented correctly in the program, was not an easy one, since there is no known analytical solution for the Boussinesq equation. This difficulty was partially avoided by using the analytical solution for the two-dimensional steady state drainage problem, with replenishment by rainfall, discussed by Tzimopoalos *et al.* (1987). With homogeneous Dirichlet boundary conditions on all four of the sides of its domain of definition, $x \in [0,a]$ and $y \in [-b/2,\ b/2]$, this problem has the analytical solution

$$h^2 = \frac{R}{K}\left[x(a-x) - \frac{8a^2}{\pi^3}\sum_{n=1,3,5,\ldots}\frac{\cosh(n\pi y/a)\sin(n\pi x/a)}{n^3\cosh(n\pi b/2a)}\right]$$

In all other situations, use had to be made of convergence and stability tests and how accurately the computations satisfied the law of mass conservation.

The convergence of the algorithms introduced above, was studied by through the Tzimopoalos problem on a sequence of meshes with bilinear Lagrange piecewise polynomials as basis functions. The first mesh used, had 25 nodes (see Figure 6–3). The other meshes were all of the same shape, but their number of nodes extended to 81, 169, 289, 441 and 625, respectively. The absolute errors, observed at the positions of nodes 7, 12 and 13 in Figure 6–3, are presented in Table 6–1. As can be seen from this table, the numerical solution converges rather rapidly as the mesh is refined.

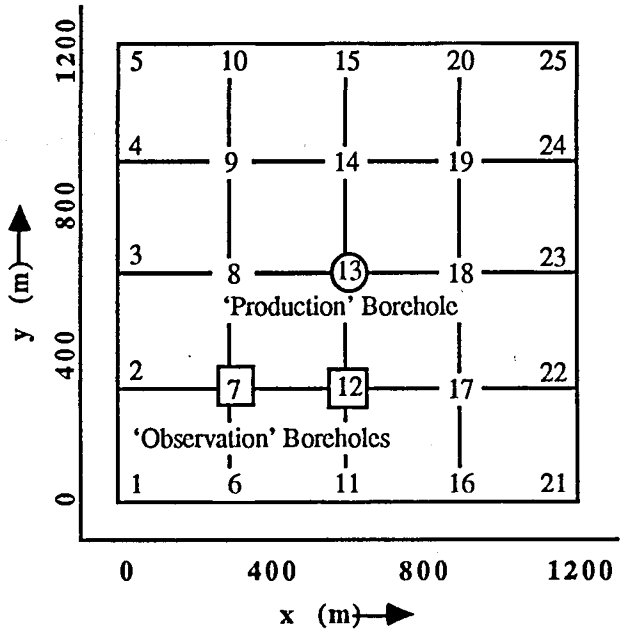

**Figure 6–3** The 25 node mesh used for the simulation of the phreatic model with the three fixed nodes used for comparison purposes

**Table 6–1** Absolute errors in the steady state solution for the phreatic aquifer as a function of the mesh coarseness

| Number of Nodes in the Mesh | Node Number and Associated Error | | |
|---|---|---|---|
| | 7 | 12 | 13 |
| 5 | $2,73.10^{-1}$ | $3,51.10^{-1}$ | $3,11.10^{-1}$ |
| 9 | $5,95.10^{-2}$ | $6,78.10^{-2}$ | $6,29.10^{-2}$ |
| 13 | $2,49.10^{-2}$ | $2,75.10^{-2}$ | $2,63.10^{-2}$ |
| 17 | $1,35.10^{-2}$ | $1,48.10^{-2}$ | $1,43.10^{-2}$ |
| 21 | $8,53.10^{-3}$ | $9,24.10^{-3}$ | $9,04.10^{-3}$ |
| 25 | $5,85.10^{-3}$ | $6,31.10^{-3}$ | $6,20.10^{-3}$ |

Based on the general theory of finite element approximations [see for example Botha and Pinder (1983)], one would expect the error in the finite element solution of Tzimopoalos' problem to converge as the square of the element size. A linear least squares analysis of the absolute error at the position of node 13 (see Figure 6–4) suggests that the rate of convergence is, in fact, slightly higher. These results can be considered as a good indication that the program is functioning correctly.

Since no analytical solution could be found in the available literature for the transient Boussinesq equation, another approach had to be used in order to test the efficiency of

Program GWUN for transient problems.

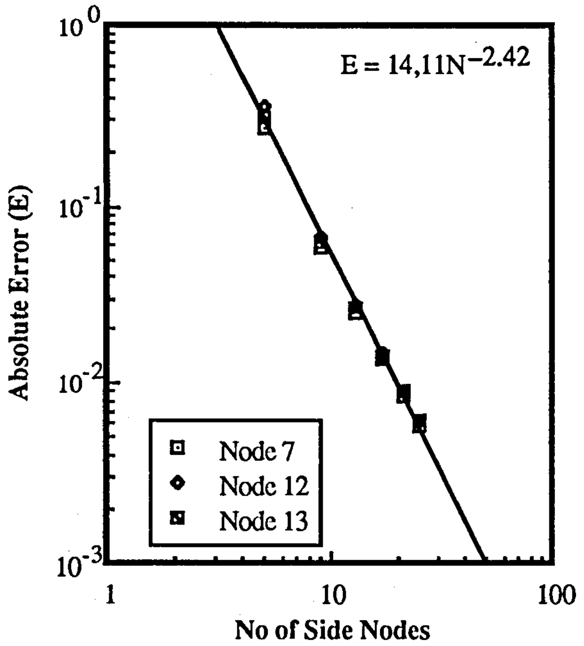

**Figure 6–4** Convergence of the absolute error in the finite element solution of Tzimopoalos' problem for nodes 7, 12 and 13 in Figure 6–3

As is known [Botha and Pinder (1983)], the solution of a parabolic differential equation tends to the solution of its elliptic counterpart, if all external conditions (boundary conditions, recharge and discharge rates and conceptual parameters) remain constant in time. In this situation, the transient solution of Equation (6.4) must approach that of the elliptic equation on its left-hand side, as time increases. The behaviour of Program GWUN for the transient Boussinesq equation, can thus be tested by solving Tzimopoalos' problem stepwise in time, rather than the one-step procedure used for the steady state analysis above.

To apply the previous procedure, Tzimopoalos' problem was solved on various meshes and time steps. Numerical experiments indicated that the solution obtained from the 625-node mesh with a time step of 30 minutes could be considered as sufficiently accurate to use as reference in subsequent calculations.

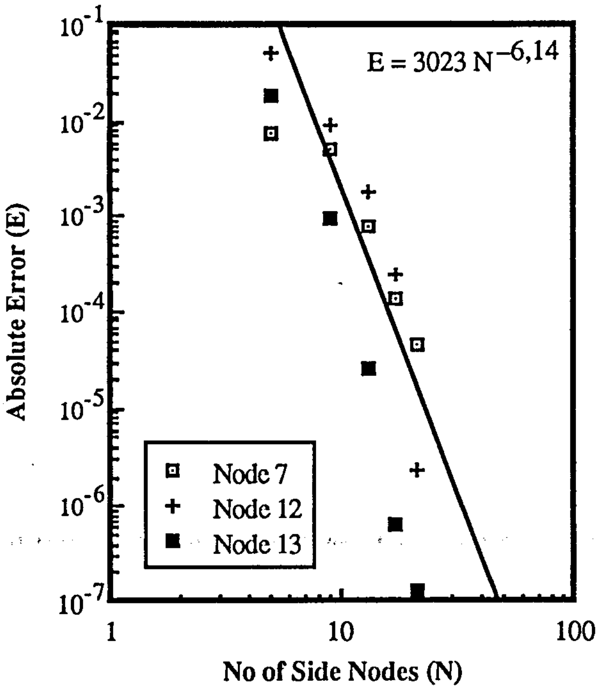

**Figure 6–5** Convergence of the transient solution for the phreatic aquifer as a function of the mesh coarseness (time step used = 2 h)

The convergence of the method in space was evaluated by comparing the solutions obtained with the same meshes used for the steady state solution and a time step of two hours, with the reference solution. The results, presented graphically in Figure 6–5, show that there is once again very rapid convergence as the finite element mesh is refined, although not as smoothly as with the steady-state solution. However, this may be partially due to the fact that the reference function is no longer a smooth analytical function, but a numerical solution which is not error free.

A rather unexpected behaviour of the results in Figure 6–5, is the high rate of convergence. Although this behaviour cannot be explained at present, the same behaviour has also been observed in other applications of the program.

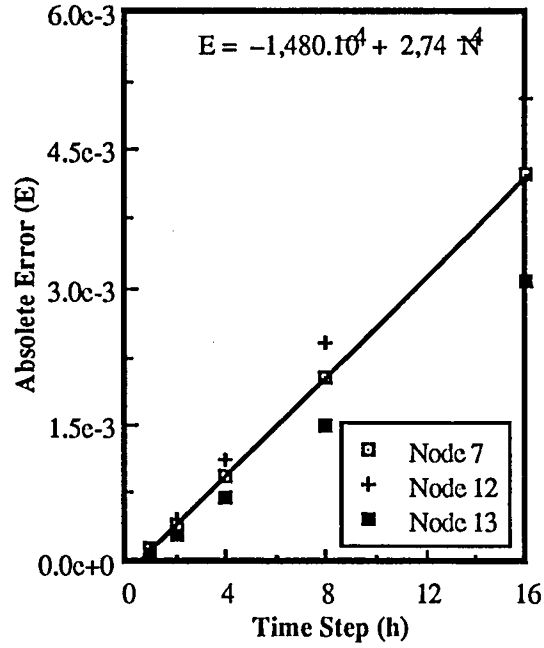

**Figure 6–6** Convergence of the transient solution for the phreatic aquifer as a function of the time step (625-node mesh)

The convergence of the transient solution in time was also evaluated by computing the solutions of the 625-node mesh with time steps of 1, 2, 4, 8 and 16 hours. As shown in Table 6–2 and Figure 6–6, the finite element solution converges linearly as the time step is decreased. However, this could be expected from the fact that the time derivative in Equation (6.7) was approximated by a backward finite difference approximation. The rate of convergence can be improved by using a higher order approximation, e.g. the Crank-Nicholson scheme [Botha and Pinder (1983)], but at the cost of a more complex computer code.

**Table 6–2** Convergence of the absolute error in the transient solution for the phreatic aquifer as a function of the time step for the 625-node mesh

| Time | Node Number and Associated Error | | |
|---|---|---|---|
| (h) | 7 | 12 | 13 |
| 1 | $1{,}35.10^{-4}$ | $1{,}61.10^{-4}$ | $9{,}88.10^{-5}$ |
| 2 | $4{,}05.10^{-4}$ | $4{,}83.10^{-4}$ | $2{,}97.10^{-4}$ |
| 4 | $9{,}42.10^{-4}$ | $1{,}13.10^{-3}$ | $6{,}93.10^{-4}$ |
| 8 | $2{,}02.10^{-3}$ | $2{,}41.10^{-3}$ | $1{,}49.10^{-3}$ |
| 16 | $4{,}24.10^{-3}$ | $5{,}07.10^{-3}$ | $3{,}09.10^{-3}$ |

As Figure 6–6 shows, the errors tend to diverge as the time step is increased. This behaviour is often encountered in the numerical solution of non-linear equations, such as Equation (6–4). Care should, therefore, be taken to avoid using too large time steps with this program. In fact, it is imperative that the modeller should conduct a number of numerical experiments, before deciding on what time step to use with his problem.

In conclusion, it can be said that the numerical behaviour of the program is excellent. It can thus be used with confidence in the modelling of phreatic aquifers.

## 6.4 APPLICATION OF THE PHREATIC MODEL TO THE ATLANTIS AQUIFER

### 6.4.1 Introduction

Müller and Botha (1986) recommended that the model they developed for the Atlantis aquifer, should be refined in future before being accepted as an aid in the management of the aquifer. Since this aquifer is basically a phreatic aquifer, the opportunity was seized not only to refine their model, but also to evaluate the efficiency of the computer program, developed during the present investigation, to actually model such an aquifer. Although every effort has been made to ensure that the numerical approximations are as accurate as possible, it must be kept in mind that this model, discussed below, is still based on a rather limited set of historical data. The model could thus be regarded as the second phase in the search for a reliable management model of the aquifer. However, it is believed that a true management model can be obtained, by simply updating the present model with data from observations in the next three to five years.

### 6.4.2 Review of the Data used

The volume of information available for the Atlantis aquifer has increased considerably since the original investigation of Müller and Botha (1986), because of the new boreholes drilled by the Department of Water Affairs for this investigation and the longer historical record of water levels for existing boreholes. This data, as well as the older data, are all available on the National Groundwater Data Base. Monthly rainfall values are available through the Computing Centre for Water Research (CCWR) in Pietermaritzburg.

The development of any groundwater model, whether it is based on the finite element or finite difference approximations of the conceptual equation, requires that the conceptual parameters, like $\theta_c$, $\underline{\mathbf{K}}$, $h_0$ and $b(\mathbf{x})$, be known at all the nodes of the mesh. Since these data are only known at a relatively small number of boreholes (in comparison with the number of nodes in the mesh), it was necessary to interpolate the values of the parameters to the nodes. As the method of kriging has already been shown to yield excellent results for stationary regionalized variables, like $\theta_c$ and $\underline{\mathbf{K}}$ [Van Tonder (1984)], the method was again used for these two parameters. However, as $h_0(\mathbf{x})$ and $b(\mathbf{x})$ are not stationary regionalized variables, another approach had to be used. In this case a preliminary version of an interpolation method based on Bayesian statistics, developed by the Department of

Mathematical Statistics in conjunction with the Institute [De Waal *et al.* (1988)], was applied with much more success.

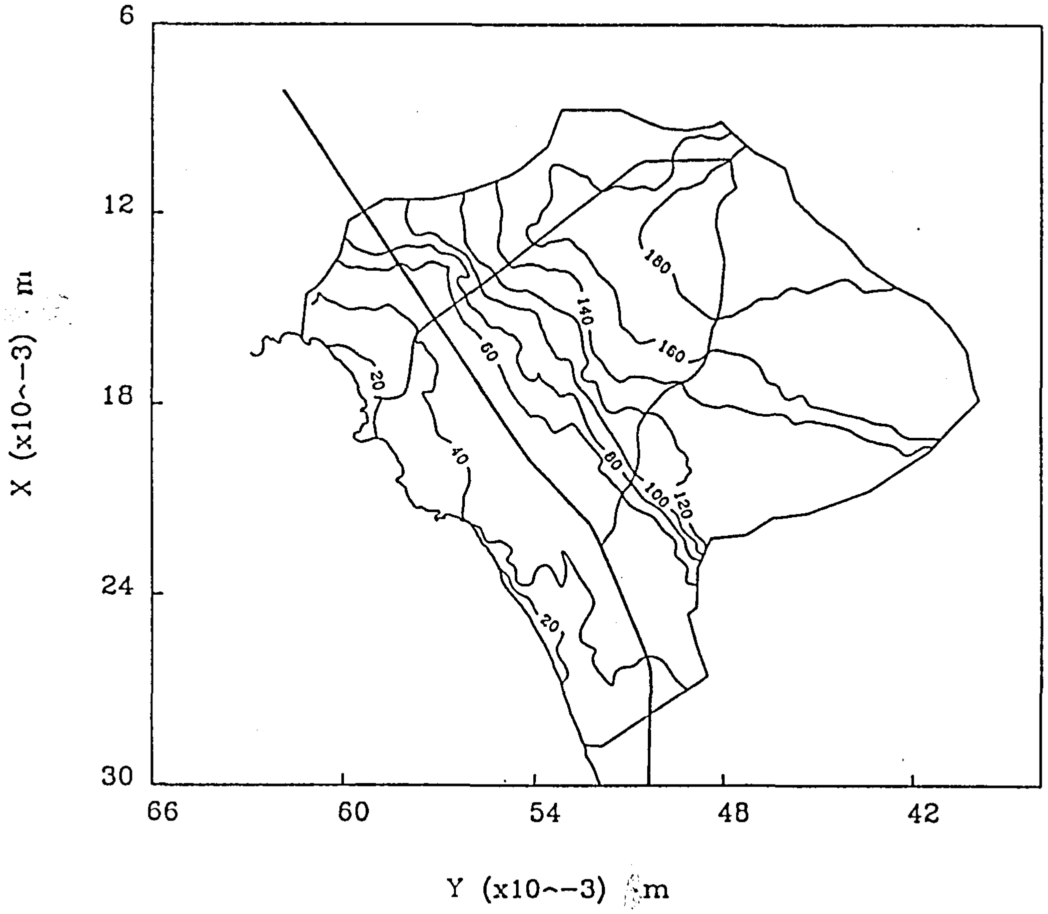

**Figure 6–7** Contours of the topography of the Atlantis aquifer, determined from the collar heights of boreholes, including those drilled during 1986 by the Department of Water Affairs

In order to obtain some feeling for the computer program and to relate its results to previous investigations, the present model was also restricted to the period January 1979 to January 1980, used by Müller and Botha (1986). Contours of these water-levels, the topography and bed-rock elevation of the area can be found in Figures 6–7 to 6–9.

### 6.4.3 Discussion

The original idea was to restrict the model to a smaller part of the aquifer, as proposed by Timmerman (1986). However, a few preliminary runs with the program indicated that, although the results are similar to those obtained by Botha and Müller (1986), the water levels on the inland boundary of Timmerman is not stationary. Because the solution of Equation (6.4) is largely determined by the prescribed boundary conditions, such a model can thus only be successful, if the variations in water levels on the Timmerman boundary are known *a priori*. Although these variations can be observed through a sufficient number of observation holes, such a model would not be very suitable for management purposes, as it cannot be used to simulate the future behaviour of the aquifer. The present model was, therefore, again based on the area used by Müller and Botha (1986).

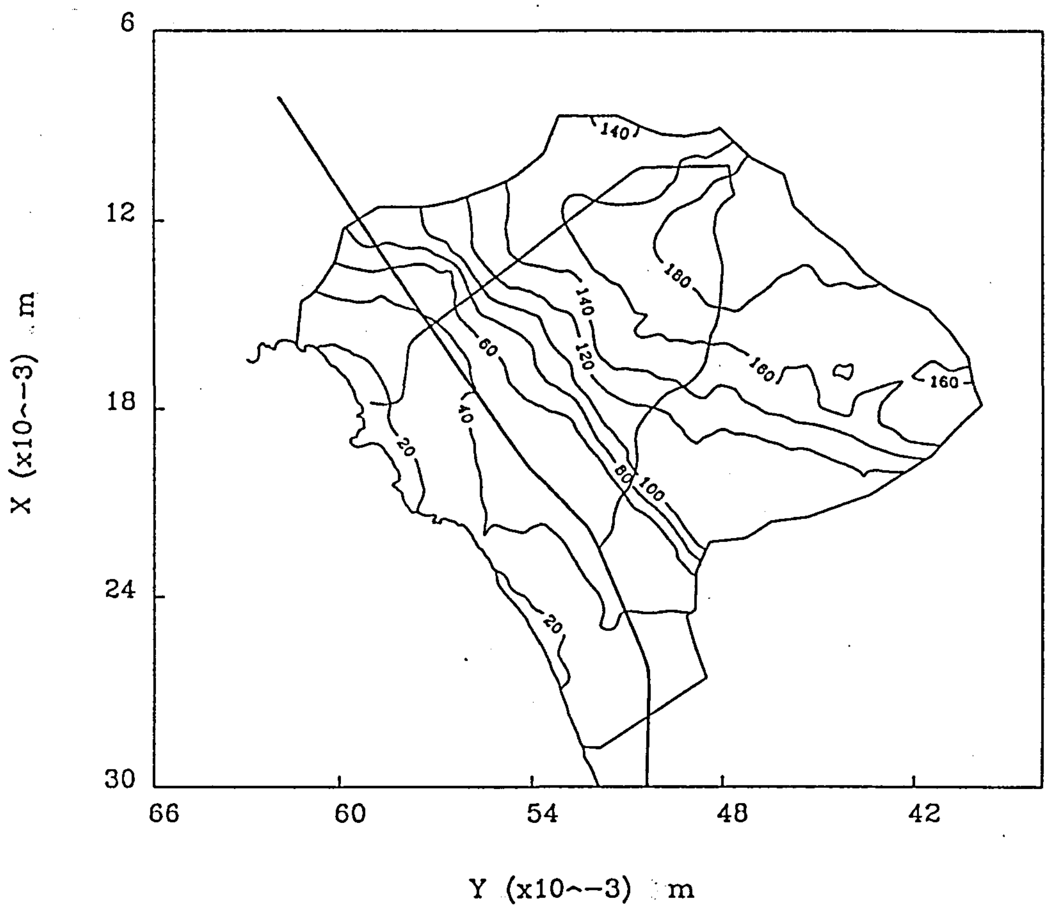

**Figure 6–8** Contours of the water levels in the Atlantis aquifer for January 1979, interpolated from the topography by the Bayes method

A major difficulty experienced by Müller and Botha with their 1986 model, was the steep gradients present between the 50 and 140 m contour lines (see Figure 6–7). The present mesh (see Figure 6–10) was consequently refined to 825 nodes and 768 elements, which is approximately double the number used by Müller and Botha.

The overall behaviour of the computer program in establishing the present model was quite satisfactory, except that it turned out to be very sensitive to small changes in the water levels and the base elevation. However, this could be expected, since Equation (6.4) is non-linear. Nevertheless, as shown by the contour maps of the observed and simulated water levels for January 1980, in Figures 6–11 and 6–12, the model is indeed able to simulate the observed water levels accurately.

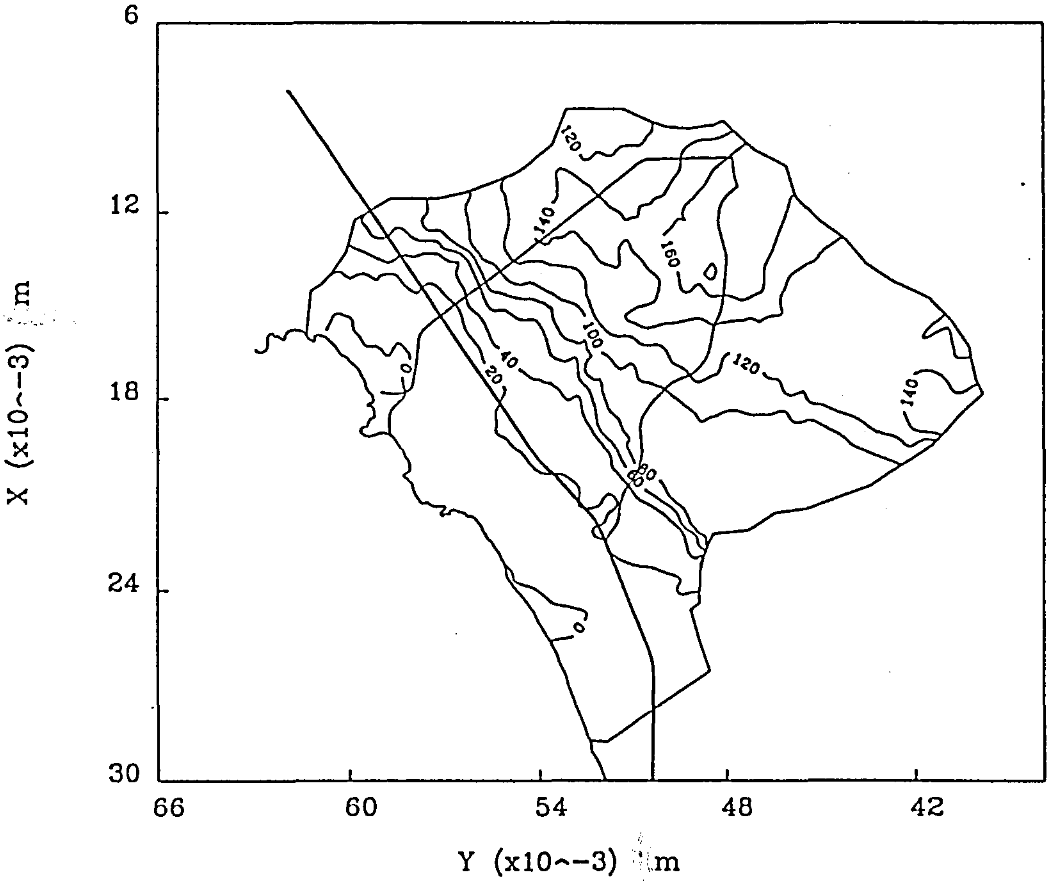

**Figure 6-9** Contours of the base elevation in the Atlantis aquifer, interpolated from the topography by Bayes method

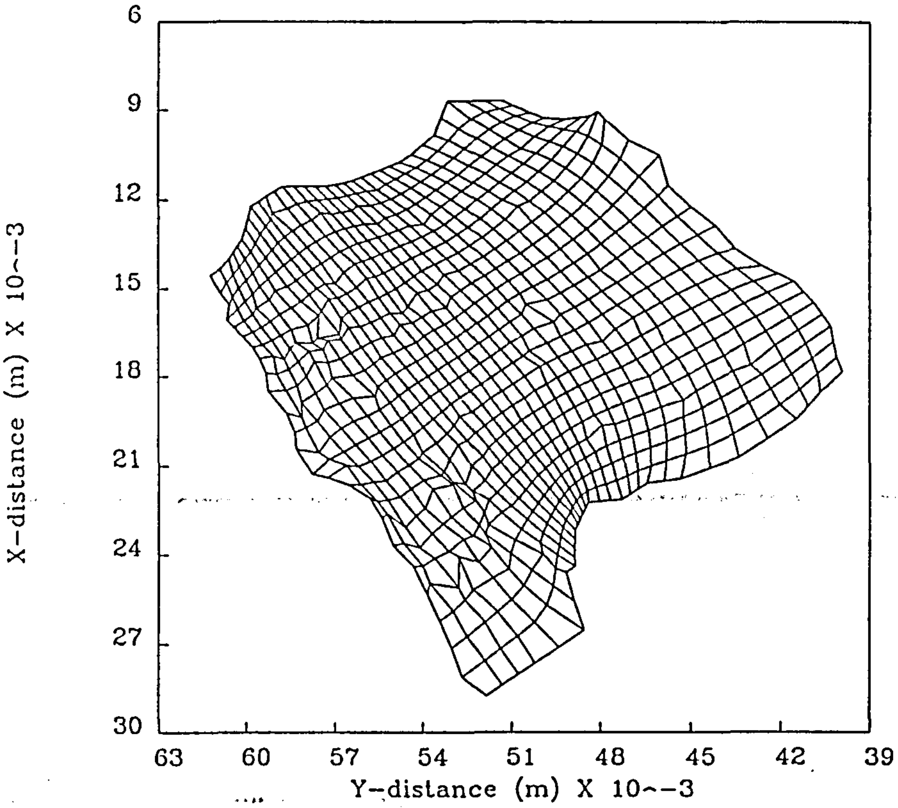

**Figure 6-10** The finite element mesh used in the present model for the Atlantis aquifer

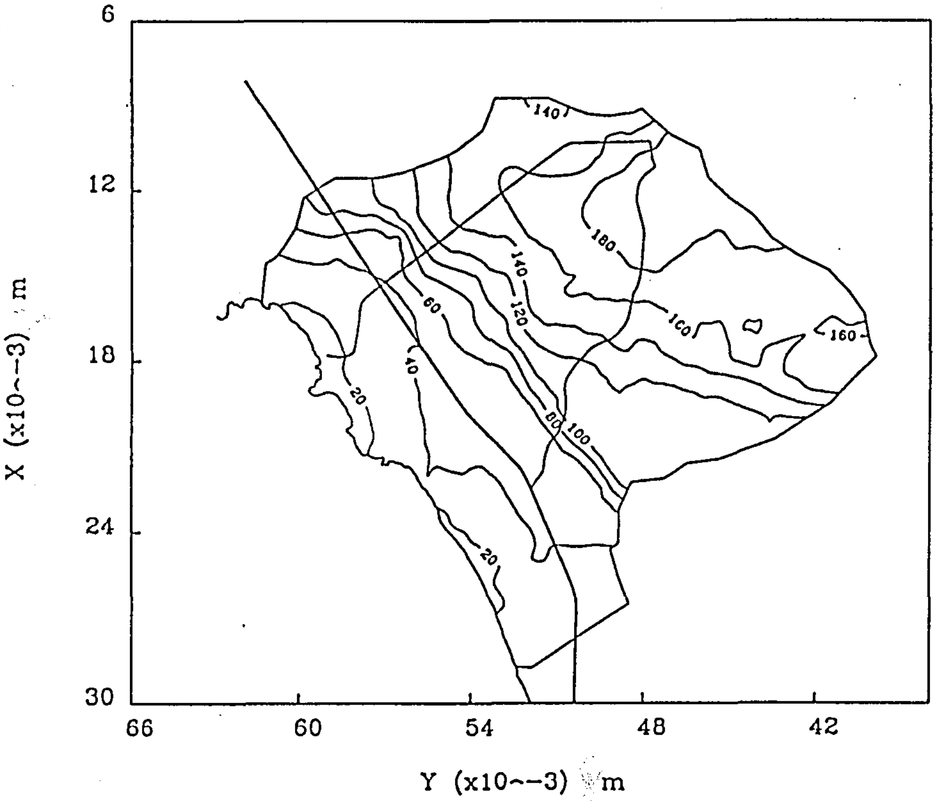

Figure 6-11 Contours of observed water levels in the Atlantis aquifer (January 1980)

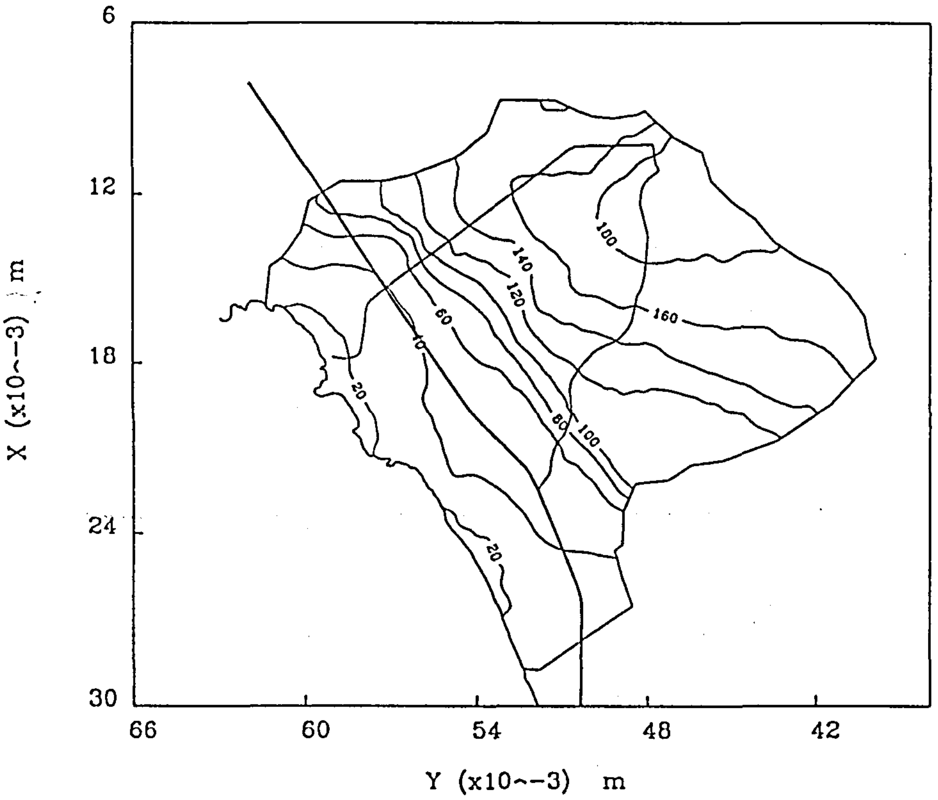

Figure 6-12 Contours of simulated water levels in the Atlantis aquifer (January 1980)

Many aquifers in South Africa, including a large number in the Karoo sediments, are water-table aquifers. The computer program developed in this investigation can thus be of considerable value, not only in evaluating any contamination of these aquifers, but also the water-bearing potential and the management of these aquifers.

# CHAPTER 7

# MODELLING UNSATURATED FLOW AND MASS TRANSPORT

## 7.1 GENERAL

As mentioned in Chapter 1, the computer programs available at the Institute for the simulation of mass transport, all suffered from an improper handling of the mass balance and numerical instabilities. The programs used for the present discussion were, therefore, developed from scratch under a grant from the FRD of the CSIR. These programs had been developed to handle the majority types of saturated/unsaturated flow and mass transport that may be encountered in practice. However, as they were only completed recently, they must be considered as experimental and cannot be made available to a larger audience, before more experience has been gained with their applications to actual problems.

Mass transport is conventionally modelled on either a global scale or a local scale. One of the major objectives envisaged in the original proposal to the WRC for the present project, was to develop a mass transport model for the pollution in the Atlantis aquifer as a whole. However, a more critical evaluation of the available data, showed that the pollution is presently limited to an area around the infiltration pan, which is too small to be observable in a large-scale model. The only alternative left, was thus to try and model the pollution around the pan on a local scale.

The modelling of unsaturated flow and mass transport, on a local scale, is best performed on a continuous basis and for specific purposes, for example, to trace the infiltration front and/or breakthrough curves during and after a rainfall event. Experience gained in the modelling of mass transport at Vaalputs, the National Radioactive Waste Repository, suggested that this can be done best if the moisture content and concentrations of dissolved material, in the unsaturated and saturated zones, are monitored continuously at hourly periods, from the onset to about 24 hours after the rainfall event. After that, the observation period can be steadily increased to a maximum of about one day, a week after the occurrence of the event. Unfortunately, the neutron moisture meter, used in the present investigation, had to be shared with the project on the recharge of small watersheds. It was thus not possible to obtain observations of this nature during the present investigation. The development of a pollution model for the Atlantis aquifer, even on a local scale, is thus not possible at the present moment in time. All that can be done, is to illustrate the behaviour of the computer programs that would have been used to develop such a model.

## 7.2 DATA REQUIREMENTS

### 7.2.1 General

One of the basic difficulties experienced with saturated/unsaturated flow and mass transport models, is the availability of suitable input data. These models, particularly an unsaturated flow model, are much more complex than any saturated flow model (see the discussion in Chapters 11 and 12). They, therefore, also require much more detailed observations than saturated flow models. Moreover, since the unsaturated flow equation is non-linear, the possibility exists that any small error in either the conceptual parameters or initial and boundary conditions can grow and finally swamp the true solution.

Apart from the conceptual parameters discussed in Chapter 11, a saturated/unsaturated mass transport also require the following additional information:

(a) Water levels in the saturated domain.
(b) Moisture distribution in the unsaturated/saturated zone.
(c) Distribution of the dissolved mass in both the saturated and unsaturated zones.
(d) Position and nature of suitable boundaries.

The Bellville Office of the Division of Water Technology of the CSIR was, by agreement with the Institute, responsible for the monitoring of pollution in the Atlantis aquifer. This work is fully described in Chapter 4.

### 7.2.2 Water Levels

The measurement of water levels is such a standard practice that this should not present any practical difficulties. However, if the aquifer is multi-layered or confined, it may be necessary to install a number of piezometers at different depths and positions within the aquifer. Moreover, as the data for Atlantis show, the response of the aquifer may be quite rapid. To capture the true reaction of water levels, it may be necessary to measure them at intervals of hours rather than weeks or months as is usual in saturated flow.

### 7.2.3 Moisture Distribution

There are a number of methods available for the determination of the soil moisture content in the unsaturated zone, of which the best known are probably gypsum blocks, tensiometers and the neutron moisture meter. Gypsum blocks and tensiometers have the advantage that they can be installed permanently and their readings monitored continuously. They suffer, however, from two serious disadvantages – a tendency to lose contact with the soil during a dry spell and dissolution of the blocks and porous cups. Nevertheless, they are the only methods available for measuring the moisture distribution below infiltration pans and waste disposal sites. Tensiometers have an additional advantage – they can be constructed to act at the same time as soil moisture samplers. When used in this way, tensiometers can provide valuable information on the distribution of the dissolved solids in both the saturated and unsaturated zones.

When it comes to spot readings of moisture contents, there is probably no better instrument than the neutron moisture meter. However, it suffers from three serious disadvantages. In the first place, neutrons are a form of radioactive radiation. The instrument has, therefore, to be adequately shielded if the operator is not to be over-exposed to radiation. The instrument, therefore, tends to be relatively heavy and not easily transportable. Secondly, the instrument operates discontinuously, with the result that its readings cannot be easily automated. However, its biggest disadvantage is probably the dependence of the readings on the density of the soil. To understand this behaviour, it will be necessary to briefly review the basic theory underlying the operation of a neutron moisture meter.

A neutron is a nuclear particle slightly heavier than a proton. In a collision between a neutron and proton, the neutron can transfer part of its energy (almost all in the case of a head-on collision) to the proton and moves at a slower speed. If its energy is reduced to below 0,25 MeV, the neutron is referred to as a thermal neutron. This phenomenon is customarily referred to as the *moderation of neutrons*. Therefore, if a source of neutrons is introduced at a constant rate into an environment containing hydrogen, the rate at which thermal neutrons is produced, will be proportional to the number of hydrogen atoms present per unit volume of the environment. In the case of soil, this relation can be expressed in terms of the neutron count rate, N, and volumetric soil moisture content, $\theta$, in the form

$$N = a\theta + b.$$

However, immediately after the introduction of the neutron moisture meter during the mid 1950's, it became clear that the relation is rather of the form

$$N = f(\theta,\rho_b) \tag{7.1}$$

where $\rho_b$ is the bulk density of the soil as defined in Equation (3.5). This behaviour can be briefly explained as follows [Botha (1963)].

The neutron is an electrical neutral particle and one of the building blocks of all atoms. When colliding with an atom, a neutron can, therefore, be absorbed instead of scattered. Such a neutron is lost and cannot contribute to the count rate. This implies that other elements in the soil may affect the count rate for thermal neutrons adversely. Soils, rich in elements with a high affinity for neutrons, will consequently show a much lower count rate than soils poor in these elements. Moreover, it is known [Botha (1963)] that elements, such as oxygen and carbon, are, in fact, far better moderators of neutrons than hydrogen. If it is kept in mind that the density of a soil is largely determined by its oxygen (the most abundant element in the earth's surface) and carbon content, then it is easy to see why the neutron count rate depends on the density of the soil.

By applying nuclear reactor theory, Vachaud *et al.* (1977) was able to show that the relation in Equation (7.1) is actually of the form

$$N = (\alpha\rho_b + \beta)\theta + \gamma\rho_b + \delta \tag{7.2}$$

where $\alpha$, $\beta$, $\gamma$ and $\delta$ are constants which depend on the scattering and absorption cross-sections of the moderator elements in question. Although these parameters could be determined in the laboratory, the equipment required for this purpose is beyond the means of even relatively well-equipped nuclear physics laboratories. However, since the bulk density is always available whenever $\theta$ is determined gravimetrically, these coefficients can also be determined from an ordinary drum calibration [Botha (1963)] by the method of linear least squares. This procedure was also used to establish a calibration curve for the neutron moisture meter used at Atlantis. The curve, which fitted the observed count rates (at depths $\geq$ 0,2 m) the best

$$N = (\alpha\rho_b + \beta)\theta + \gamma\rho_b + \delta$$

is presented graphically in Figure 7–1.

With the calibration curve of the neutron moisture meter established, the next question is how to apply it in the field. While it would be possible to determine the bulk density in the vicinity of a neutron tube for depths of up to say 1 m, it may require some rather extensive excavations for greater depths. As it is known [Botha (1963)] that the disturbance of the soil in the vicinity of a neutron observation hole can completely nullify the neutron meter reading, another approach has to be found.

Gamma rays, although of electromagnetic origin, are also produced by radioactive materials. In their passage through space, these rays tend to be attenuated and scattered by matter in their path at a rate proportional to the density of the attenuating matter *only*. Therefore, by counting the number of gamma rays scattered per unit of time in a given medium, the density of that medium can be determined. With this assumption, the relation between the wet density of the soil, $\rho_w$, and the gamma ray count rate, G, can be expressed mathematically as

$$G = a\rho_w + b. \tag{7.3}$$

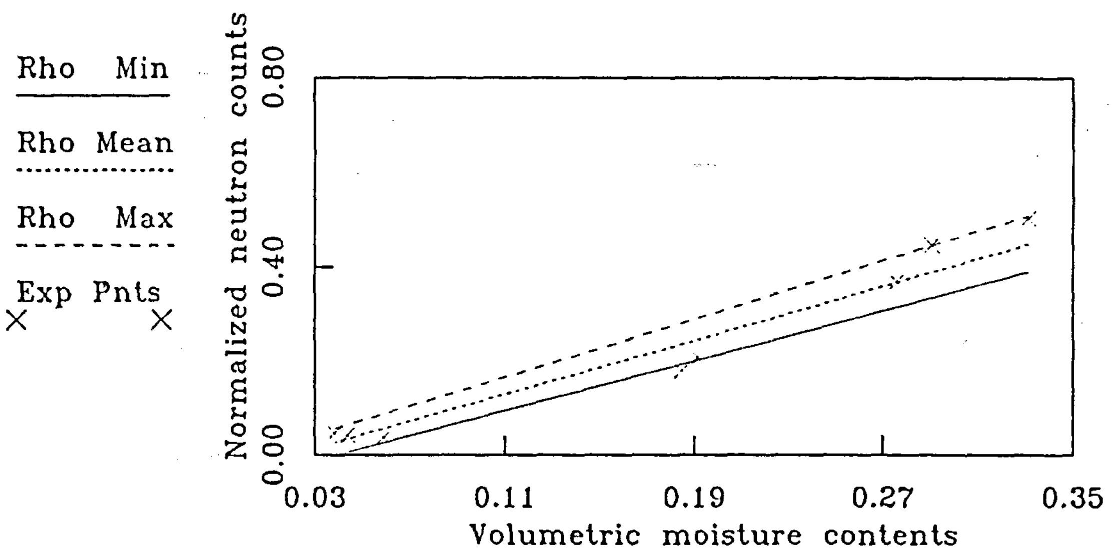

Figure 7–1 Graph of the calibration curve for the neutron moisture meter used at Atlantis (depths ≥ 0,2 m)

The coefficients a and b in Equation (7.3) can once again be determined by a drum calibration and the method of linear least squares [Botha (1986)]. A graph of the calibration curve for the gamma meter used at Atlantis, is shown in Figure 7–2.

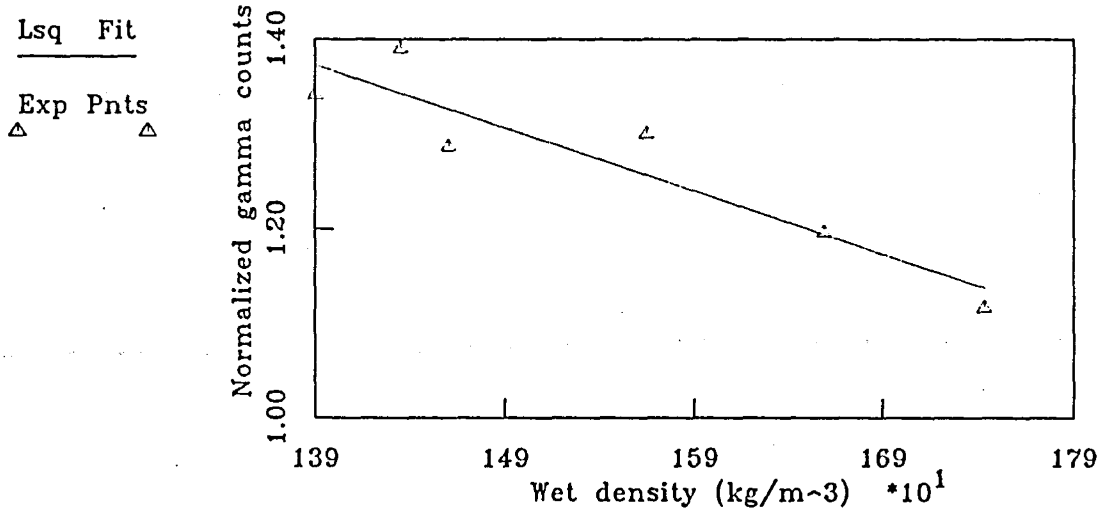

Figure 7–2 Graph of the calibration curve of the gamma ray density meter used at Atlantis (depth ≥ 0,2 m)

The determination of the dry density at a given depth in a neutron observation hole is straightforward, once the neutron and gamma ray meters have been calibrated. To see this, notice that the wet density of a soil is related to its bulk density and the density, $\rho$, of water through the equation (see Section 9.2.3)

$$\rho_w = \rho_b + \rho\theta$$

which yields, upon substitution into Equation (7.3), the equation

$$G = a(\rho_b + \rho\theta) + b. \tag{7.4}$$

Because the coefficients $\alpha$, $\beta$, $\gamma$, $\delta$, a and b are known, once the calibration curves have been established, Equations (7.2) and (7.4) can be used to solve for the two unknowns $\rho_b$ and $\theta$. Unfortunately, the two quantities occur as a product in Equation (7.2) and an iterative method, such as the Newton-Raphson method, has to be used to solve for them. However, unless there are clear indications to the contrary, the dry density has to be done only once for a given observation hole and depth. To illustrate this procedure, the dry densities determined for observation hole A9 at Atlantis are listed in Table 7–1.

**Table 7–1** Calibration of the neutron observation hole A9 at Pan 7 in Atlantis on 1987–08–06

| Depth (m) | Density (kg/m$^3$) | Moisture Contents (m$^3$/m$^3$) |
|---|---|---|
| 0,2 | 1 758,98 | 0,042 |
| 0,4 | 1 606,67 | 0,093 |
| 0.6 | 1 605,32 | 0,099 |
| 0,8 | 1 671,17 | 0,088 |
| 1,0 | 1 549,90 | 0,105 |
| 1,5 | 1 511,13 | 0,119 |
| 2,0 | 1 313,00 | 0,224 |

A rather surprising phenomenon, easily observed in Table 7–1, is the tendency of the densities to decrease with increase in depth. Although it is not possible to give an explanation for this behaviour without a more detailed investigation, the results are supported by the dry densities, gravimetrically determined from the samples used to establish the moisture retention curves in Chapter 9 and a similar behaviour observed at Vaalputs.

## 7.3 SATURATED/UNSATURATED FLOW

To illustrate the behaviour of unsaturated flow, a cross-section, running through the line of neutron observation holes A3, A4, A8, A9 and A10 (see Figure 7–3), was chosen. The topography of the cross-section, determined from the collar heights of nearby well points and boreholes, is shown in Figure 7–4. Since water levels and neutron moisture meter readings were never taken simultaneously, it was decided to use the soil moisture values and water levels, respectively observed on 1987-08-06 and 1987-08-13, as initial conditions for the program. Contours of the interpolated pressure head distribution, derived from these measurements, are presented graphically in Figure 7–5, across the cross-section of Figure 7–3, to a depth of approximately 10 m below the surface.

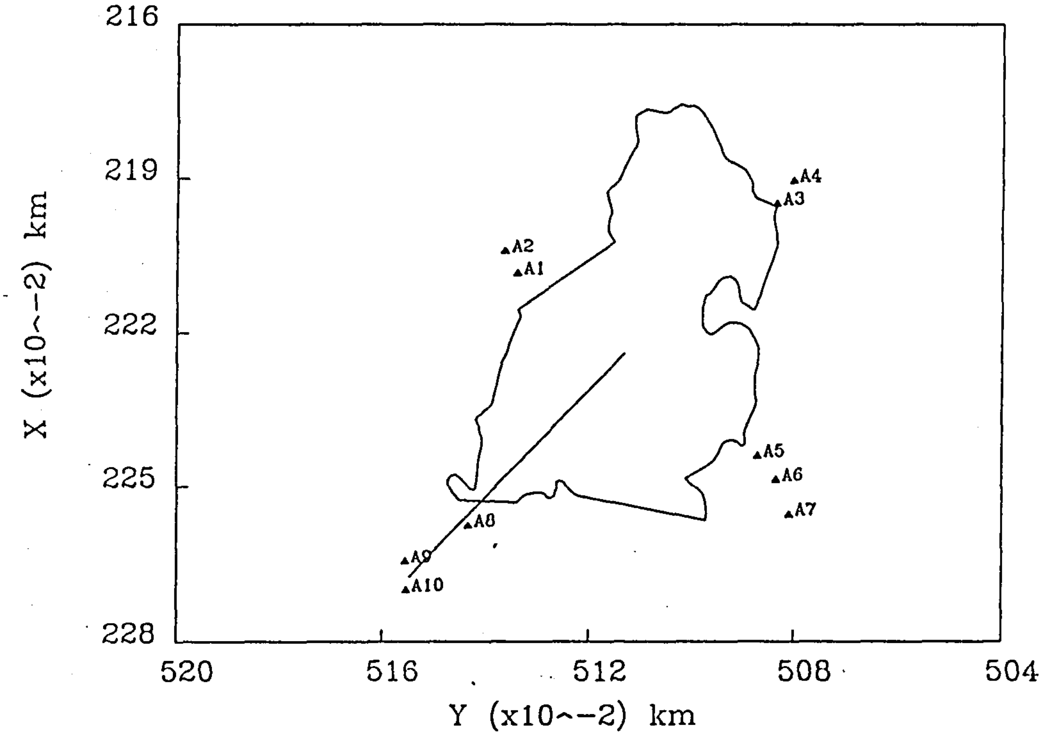

Figure 7–3 Location of the cross-section in the Atlantis aquifer used to illustrate the simulation of saturated/unsaturated flow

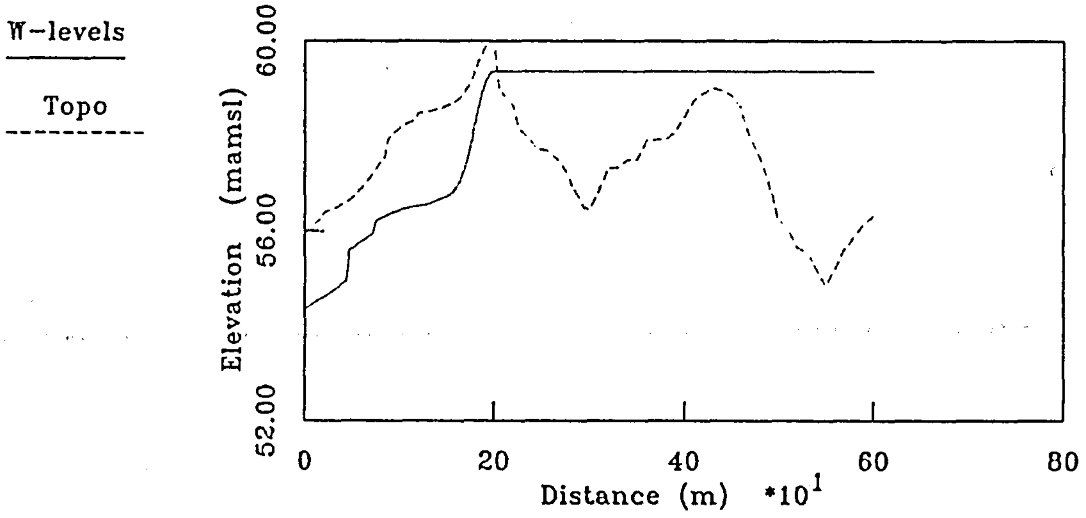

Figure 7–4 Interpolated topography of the land and Pan 7 along the cross-section in Figure 7–3

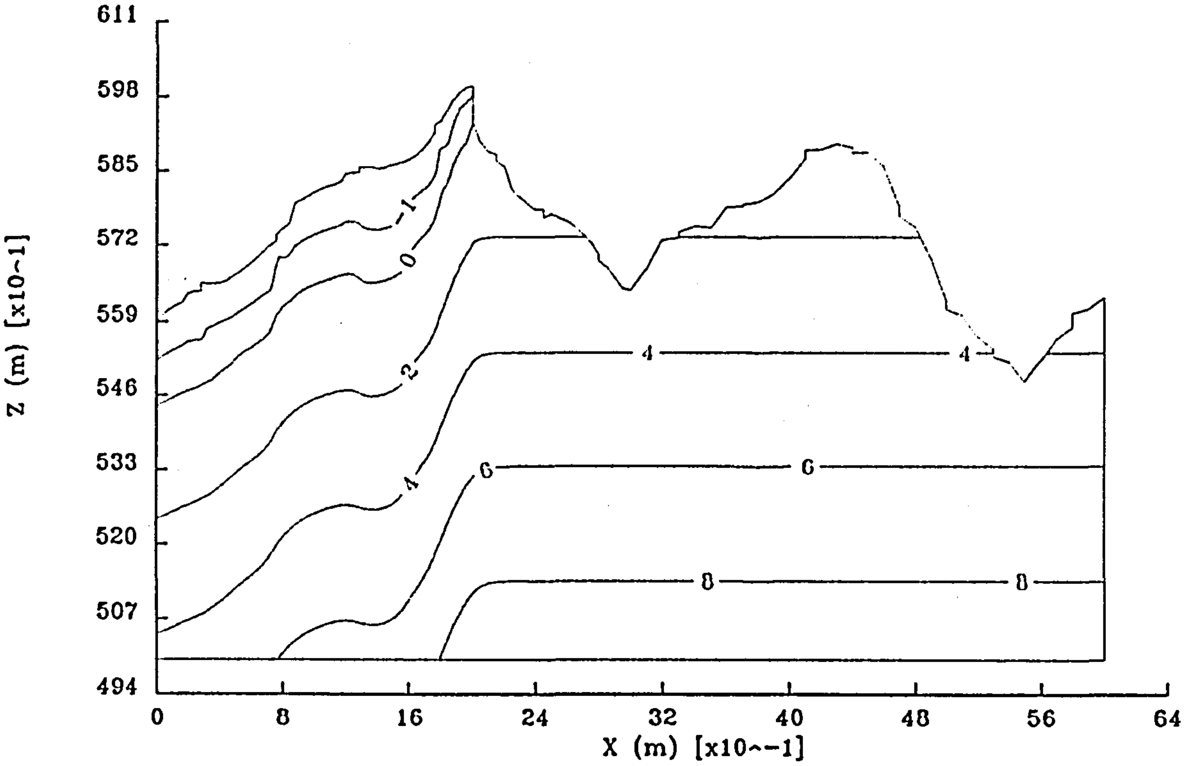

Figure 7–5 Contours of the interpolated pressure head distributions across the cross-section in Figure 7–3, up to a depth of approximately 10 m

The establishment of suitable boundary conditions, required by the program, was more difficult, because of the long intervals between observations of the moisture contents (see the discussion in Chapter 4). However, judging from the contours of the initial conditions in Figure 7–5, there is no flow across the right-hand boundary and very little across the left-hand boundary. In view of this, it was decided to use no-flow Neumann boundary conditions on the left, and right hand boundaries and Dirichlet conditions across the part of the pan itself. The fact that the piezometric levels in the deep boreholes and well points differ slightly from those in the shallow ones, see Section 2.4.1, suggests that there is a dividing layer between the Witzand and Springfontyn Members of the Bredasdorp Formation. Although this layer is propably not fully impermeable, it was nevertheless decided to use no-flow Neumann boundary conditions on the bottom side of the cross-section also. On the sloping part of the cross-section rainfall boundary conditions were used.

It is not possible to develop any model for infiltration from the pan with the available set of data. All that can be done at present, is to try and illustrate the behaviour of the computer program and the idiosyncrasies of unsaturated/saturtated flow through a numerical simulation. For this purpose use will be made of the situation where the water levels in the pan rose steadily from 59,36 to 59,42 mamsl, as observed over the period

1988-08-13 to 1988-08-19. To simulate this variation in water levels, it was necessary to use a time-dependent Dirichlet boundary condition across the pan. This was achieved by varying the prescribed heads at a constant rate of 0,01 m.d$^{-1}$. Contours of the simulated pressure head distribution for 1988-08-19 are shown in Figure 7–6.

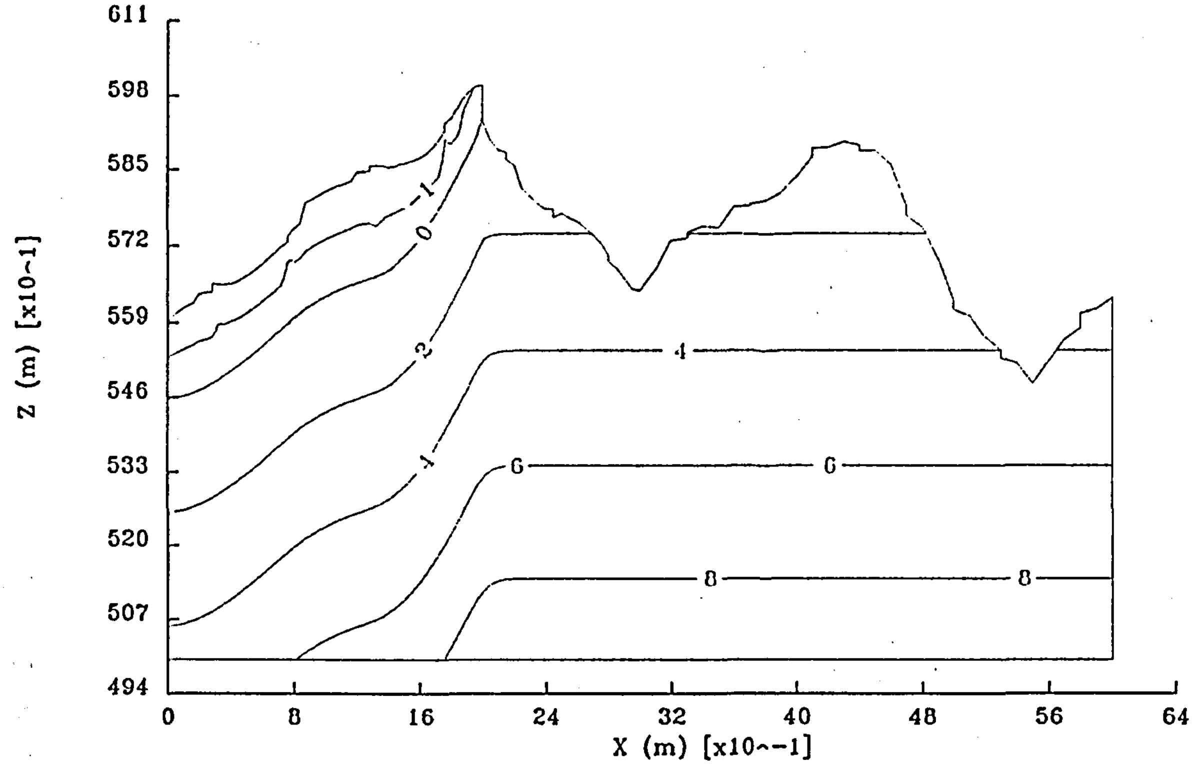

**Figure 7–6** Simulated pressure heads across the cross-section in Figure 7–3 after a period of six days with varying water levels in the pan

As could be expected, there is not very much variation in the pressure head distribution during such a short period of time. Nevertheless, as shown by a comparison of the contour lines in Figures 7–5 and 7–6, the pressure head did increase slightly across the cross-section. One particular noteworthy observation is the tendency to flatten the 'humps' in the initial pressure head distribution. However, this result should really be taken as a warning and not a vindication of the program.

A more detailed analysis revealed that the 'humps' present in the intial pressure levels of Figure 7–4, may not be real, but due to the inability of the interpolation algorithm used to derive them from the scanty available observations. The true behaviour of saturated-unsaturated flow can thus be completely masked by the use of inaccurate and insufficient initial conditions. The only way to ensure that a saturated/unsaturated model does indeed represent an actual flow sytem, is to observe the presure head distributions more carefully and frequently than is customary in satured flow.

## 7.4 SATURATED/UNSATURATED MASS TRANSPORT

The application of the mass transport program developed in conjunction with the saturated-unsaturated flow model to the Atlantis situation, is limited on two accounts. In the first place, as already noticed, the extent of the area, at present subjected to pollution in the aquifer, is too limited to be noticeable on a large-scale horizontal flow model, for example the phreatic flow model, discussed in Chapter 6. Secondly, the lack of accurate dispersivity values makes it difficult to interpret the results in a meaningful way. The following discussion of the program should thus be regarded as an illustration of its capabilities, rather than as a model for the pollution around the infiltration pan at Atlantis. For this purpose, use will be made of the potassium distribution observed by the DWT in and around the pan. The reason why potassium was chosen for this illustration is that it is known to be subject to ion exchange. It could thus be used to illustrate the ability of the program to simulate absorption-like phenomena through the Langmuir isotherm.

In the absence of any information on the distribution of adsorbed solids in the unsaturated domain, the initial conditions in this domain were set to zero. For the saturated domain, the initial conditions were interpolated from the potassium concentrations, observed by the DWT on 1987–08–13. In the absence of any information on the $K_d$-values for the sands at Atlantis, a value of 10 was selected from the available literature.

The observations on the potassium distribution, like all other chemical compounds, were limited to the deep and shallow boreholes and well points, with average depths of 10 and 20 m respectively. This presented somewhat of a problem, because the mass transport equation can only be solved accurately if a very fine mesh, with elements of the order of a few metres rather than kilometres, is used [Pinder and Huyakorn (1983)]. To circumvent this difficulty, suitable concentration values had to be interpolated from the observed concentrations. With the restrictions on the coarseness of the mesh and the limitations of the available computer resources, the finite element mesh was once again restricted to the cross-section used to simulate saturated/unsaturated flow. Only two sets of concentrations – those from the shallow observation points and those from the pan itself – could, therefore, be used in the interpolation. This lack of sufficient information on the concentration profile, with depth and across the pan, again caused the interpolated concentrations, shown by the contour map in Figure 7–7, to be suspect. Nevertheless, since the sole purpose of the present simulation is simply to illustrate the possibilities of the program, this should not cause too much difficulties.

To keep with the philosophy adopted in the simulation of the saturated/unsaturated flow, no-flow boundary conditions were again applied on the left, right and bottom sides of the domain, with the observed potassium concentration of 4,3 mg/L in the water of the pan as a Dirichlet boundary condition on its bottom. The rainfall boundary on the sloping surface could be incorporated as a third type or Cauchy boundary condition. However, since it is improbable that the rain would contain a significant amount of potassium, this boundary was changed to a Dirichlet boundary of zero potassium concentration.

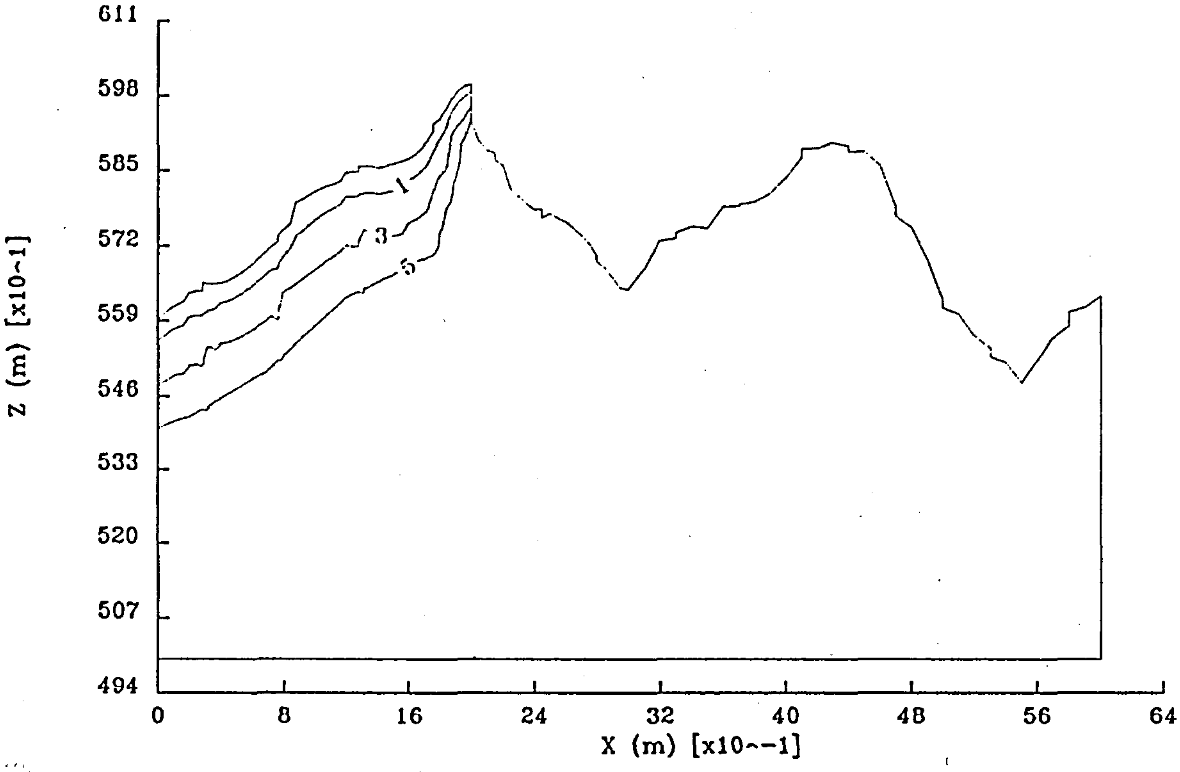

Figure 7–7 Distribution of potassium across the cross-section, used as initial condition for the simulation of mass transport

As shown by the conceptual equation [Equation (13.26)], a mass transport model needs to be supplied with the Darcy velocities of the fluid. A mass transport model can thus only be developed in conjunction with a flow model. The velocities, obtained for the six-day period, over which the water levels in Figure 7–6 were simulated, were consequently used to simulate the potassium distribution. The results for the six-day simulation period, are presented as a contour map in Figure 7–8.

The positions of the 1 and 3 mg/L contour lines in Figure 7–8, which are situated in the unsaturated zone, vary very little from their initial positions, but that of the 5 mg/L contour line, which more or less coincide with the boundary between the saturated and unsaturated zone, shifted considerably. This behaviour confirms the intuitive belief, that interactions between the solute and the soil matrix, should be stronger in the saturated than in the unsaturated zone.

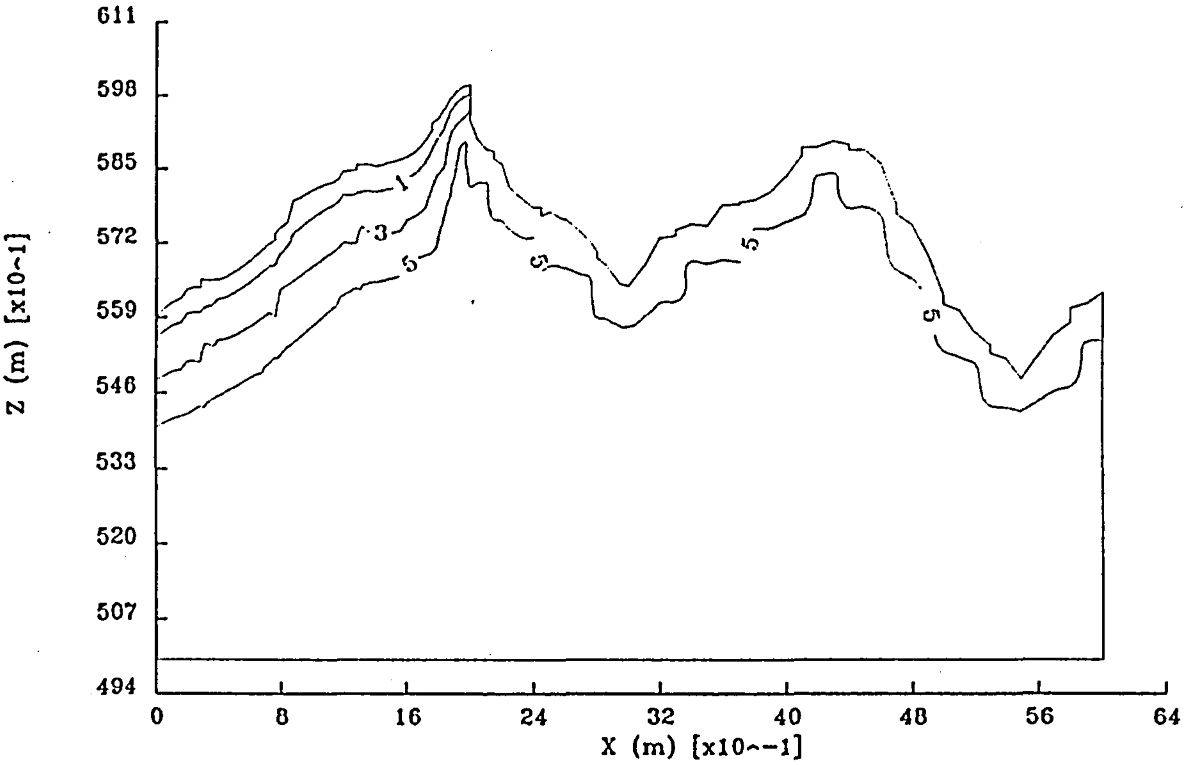

Figure 7–8 Potassium concentrations, simulated from the initial concentrations in Figure 7–7 and the flow velocities computed during the simulation of water levels in Figure 7–7, after a period of six days

At first sight, the rather jagged behaviour of the 5 mg/L contour line below the pan may seem strange. However, it must be kept in mind that the movement of the solute is mainly controlled by the seepage velocity of the water, which is determined by its Darcy velocity at a particular point in space and time (see Section 10.2.3), which varies considerably due to the irregularities in the pan floor.

Based on the previous results, one would expect a conservative tracer, i.e. a solute that does not interact with the soil matrix, to behave similarly. This assumption was tested by running the mass transport program again, but with the distribution coefficient set to zero. As can been seen from the contour map in Figure 7–9, this is not the case.

There are basically two ways to explain the observed behaviour of the concentrations. The most natural one is to assume that there is an error in the computer program. However, the program has been tested against various analytical solutions with excellent results. There is, however, another and more physical acceptable explanation. The assumption of a conservative tracer implies that the soil matrix does not contain potassium at any point in space and time. There is thus no possibility for the water infiltrating from the pan, with its lower concentration of potassium, to reach equilibrium with the soil matrix. The large seepage velocity of the infiltrating water thus simply 'washes' the potassium from the region immediate to the pan's boundary. Care should, therefore, be exercised when comparing observations of conservative tracers with that of non-conservative and particularly reactive tracers.

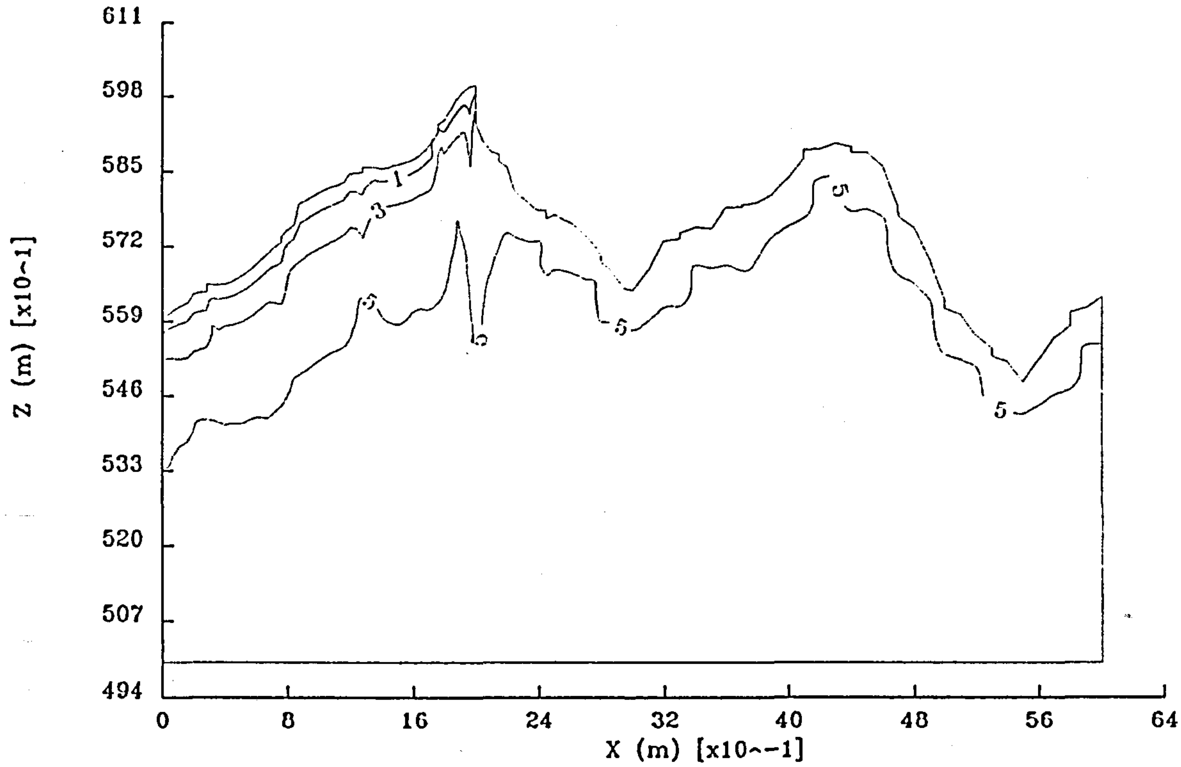

Figure 7–9 Potassium concentrations, simulated from the initial concentrations in Figure 7–7 and the flow velocities computed during the simulation of water levels in Figure 7–7, after a period of six days without adsorption

## 7.5 DISCUSSION

The previous discussion clearly demonstrates that the modelling of saturated/unsaturated mass transport is indeed feasible. However, to ensure that the model behaves in a physical realistic way, some of the errors, committed in the present investigation, should be avoided as far as possible in future investigations. For this reason, the more serious of these errors are detailed below.

**Underestimation of the reaction time.** The present investigation was planned mainly on experience gained in the initial phases of modelling the radioactive waste disposal site at Vaalputs. The model developed for that purpose (and the field data) suggested that the transport of dissolved solids in the unsaturated domain is a slow process. No provision was, therefore, made to cope with a situation where the water table can rise by more than a metre in a few days, as experienced in the present investigation. Observations should, therefore, be conducted at a frequency much higher than that used for saturated flow.

**Synchronized measurements of the relevant variables.** This was one of the most frustrating experiences encountered in the present investigation. It is of no use in developing a mass transport model to find that, while accurate data are available on the water levels in the saturated zone, there are no data on the soil moisture contents in the unsaturated zone and the concentrations for the *same period* of time. In hindsight, it would have been better if (with the exception of water levels) concentrated observations were taken during a few short strategic periods of time, rather than scattered measurements over a prolonged period of time, as was done here. The latter procedure can be followed between these time periods and after the model has been calibrated and verified.

**Supportive Measurements.** As the discussion in Part 2 tries to demonstrate, a successful conceptual model has to be based on measurements of the actual physical properties of the phenomenon to be modelled. There are just too many variations in natural phenomena, that have not been accounted for in present conceptual models, to discard any seemingly strange result of a model, on intuitive grounds alone. The behaviour of the concentrations in Figure 7–8 is a case in point. Whether these drastic changes in the concentration distribution are real or caused by the use of inappropriate initial and boundary conditions, can only be decided once sufficient information is available. Extreme care should, therefore, be exercised in planning a network of observation points to be used in conjunction with a model. Large-scale observations should, in particular, be supplemented with highly concentrated small-scale observations. For example, when trying to model the effect of pollution from an areal source, observations should not be limited to the surrounding area, but also include the domain immediately below the source.

The main direction of groundwater contamination is always from the soil surface downwards. One would, therefore, expect to find a sudden jump in concentration at some depth below the source, particularly in the case of young sources, such as the infiltration pan at Atlantis. Since this distribution of pollutants cannot be predicted *a priori*, they have to be measured at close distances along a few strategically placed vertical profiles at the observation sites.

**Use of models.** Many of the errors committed during the present investigation could have been avoided, if a preliminary model had been developed with the data available at that time. Unfortunately, this approach could not be followed in the present investigation, because of the absence of suitable computer programs. However, since these programs are now available, it is recommended that future models should be developed in *conjunction* with the field investigations and *not after* haphazardly planned observations have been started.

# PART 2

# PRINCIPLES OF MASS TRANSPORT IN POROUS MEDIA

# CHAPTER 8

# PHYSICAL PROPERTIES OF FLUIDS

## 8.1 GENERAL

Physical phenomena are, by definition, always connected with a single entity – *matter.* Matter itself consists basically of three basic building blocks: *protons*, *neutrons* and *electrons*. These particles are constantly subjected to two forces – *nuclear* and *electromagnetic* which bind them together in *atoms.* Atoms consist of a *nucleus,* which contains only protons and neutrons, surrounded by a cloud of electrons numerically equal to the number of protons in the nucleus. Atoms are consequently electrically neutral.

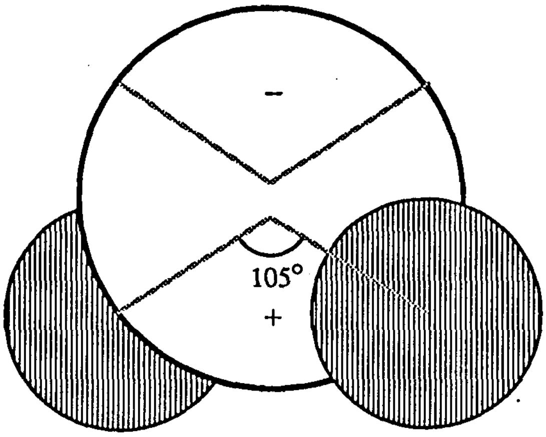

**Figure 8–1** Model of a water molecule consisting of one oxygen atom (white) and two hydrogen atoms (darkened)

The electrons surrounding the nucleus of an atom are not haphazardly distributed, but restricted to so-called *electron shells*. Every shell can contain a certain maximum number of electrons controlled by the Pauli exclusion principle. If an atom does not have enough electrons to fill its outer shell, it tends to combine with an electron(s) from another atom to form a *molecule*. Take for example, the water molecule. As the chemical formula for water ($H_2O$) signifies, this molecule consists of a bonding between two atoms of hydrogen and one of oxygen. The oxygen atom consists of a nucleus which contains eight protons and eight neutrons, surrounded by a cloud of eight electrons. Of these electrons, two are in an inner and six in an outer electron shell. The hydrogen atom, on the other hand, contains only one proton and one electron in the inner electron shell. As the outer electron shell in the oxygen is able to hold eight electrons, it can easily capture two hydrogen atoms to form the water molecule. The result of this is an asymmetrical arrangement of the hydrogen atoms in the water molecule, shown schematically in Figure 8–1. This distribution causes an excess positive charge on the hydrogen side and an excess negative charge on the oxygen side of the water molecule, thereby creating an *electric dipole*. Because of this dipole, a water molecule will tend to attract its neighbours, or other molecules with which it comes into contact. This *molecular* force is known as a *cohesive* force when acting between identical molecules, and an *adhesive* force when acting between different molecules.

An inherent property of all matter is its *temperature*, which can be related to the fact that, unless the matter is at absolute zero temperature (0°K on the Kelvin temperature scale), molecules and atoms are in a state of continuous motion and thus possess *kinetic energy.* This kinetic energy is responsible for the four *states* in which matter is observed in nature – *solids*, *fluids*, *gases* and *plasmas*.

By using an oversimplified interpretation, solids can be regarded as matter where the molecular forces are strong enough to ensure that the molecules remain in mean fixed positions relative to each other. If the temperature is increased, the molecules tend to move so far apart that the molecular forces cannot prevent a random drift in the mean distance between molecules and the solid changes into a fluid. With a further increase in temperature, the fluid is ultimately changed to a gas, where the mean distances between molecules are so large that the cohesive forces have no effect on the motion of the molecules. In fact, the molecules tend to drift away until they reach some restraining boundary. This phenomenon explains why gases fill the container in which they are placed, while liquids can exhibit a *free-surface*. Plasmas are a very esoteric form of gas and occur naturally only in stars, where the temperature is high enough to dislocate all atoms and even the electrons from the atom. Plasmas consist, therefore, only of the positively charged nuclei of atoms.

Since the molecules in fluids and gases are continuously in motion and surrounded by other molecules, collisions between them should occur quite frequently. According to Newton's laws of motion, these collisions must result in a change of momentum and thus the creation of a *force*. This force is observable as a *pressure* exerted by all fluids and gases, unless the temperature is 0°K.

## 8.2 THE FLUID CONTINUUM

The main idea behind the scientific investigation of a given physical phenomenon is man's ability to **order** and **predict** the future behaviour of the phenomenon. The two basic properties of matter, universally used for this purpose, are its *spatial position* and *mass*. Since fluids (and gases) have no form of their own, but only assumes the form of the vessel that contains them, these quantities are not very useful in this case and other measures have to be found.

A measure that is closely related to the mass of a fluid is its *density*. In Physics, the density of a material object is defined as the ratio between its mass and volume. In a fluid (or gas), this definition can, nevertheless, be ambiguous. Consider, for example, the determination of the density of a fluid. This can be achieved by simply relating a given volume of fluid, $\Delta V$, to its mass $\Delta m$. If the fluid is uniform, the ratio

$$r = \frac{\Delta m}{\Delta V}$$

will stay constant when $\Delta V$ is decreased continuously from a large value downwards. However, when $\Delta V$ reaches the dimensions of a molecule, the number of molecules and thus r will begin to fluctuate (see Figure 8–2). The volume $\Delta V_0$ used to determine the density of a fluid (or gas) must, therefore, be *much larger* than the molecular spacing in the fluid. If the fluid is to be regarded as a continuous distribution of matter, then $\Delta V_0$ must be a fixed quantity and very much smaller than the total volume of fluid. With this in mind, the density of a fluid can be defined as

$$\rho = \lim_{\Delta V \to \Delta V_0} \left[\frac{\Delta m}{\Delta V}\right] \equiv \frac{dm}{dV}. \tag{8.1}$$

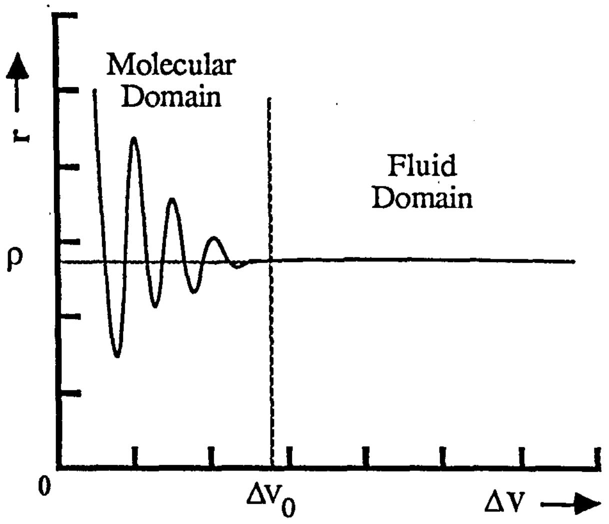

**Figure 8–2** Definition of a proper elementary fluid volume element $\Delta V_0$

Following Bear [1972], the quantity $\Delta V_0$ is customarily referred to as a *representative or proper elementary volume element.* However, these terms tend to be rather abstract and not very descriptive of the operation, at least from the physical point of view. To see this, take the example of a physicist who wants to determine the density of a fluid in the laboratory, but has only a small number of vessels available with which he can sample the fluid. As can be seen from Figure 8–2, he will always obtain the same result, provided that the volumes of the vessels are all larger than $\Delta V_0$. He may thus tend to regard any of these volumes as a representative or proper elementary volume element. But this is clearly not what is meant by the mathematical interpretation of the term. For this reason, the term *proper sample volume* will be used here and in what follows to describe the operation. However, it must be kept in mind that this concept is a mathematical artifact and does not have any physical meaning.

A similar situation exists in the case of fluid pressure. As defined above, pressure is caused by the collision between the molecules of a fluid or gas. Since a collision between particles occurs in a plane perpendicular to the line of motion, pressure is a surface phenomenon. A useful measure for pressure would thus be the force distribution over a surface area associated with the fluid. For this reason, pressure is defined mathematically through the equation

$$p = \lim_{\Delta A \to \Delta A_0} \left[\frac{\Delta F}{\Delta A}\right] \equiv \frac{dF}{dA}, \tag{8.2}$$

where

$$\Delta F \equiv \Delta \mathbf{F} \bullet \mathbf{n}$$

with **n** a unit vector normal to the area $\Delta A$. The pressure p is thus the resultant force acting normal to the *proper sample area* $\Delta A_0$ (similar to the proper volume element $\Delta V_0$ used in the definition of density).

The definition of pressure as the number of collisions of fluid particles (molecules or atoms) per unit area, implies that the pressure must increase (decrease) as the number of particles increases (decreases) per unit volume. The best known way to achieve this is to change either the volume or temperature (T) of the fluid. However, the number of particles per unit volume of fluid can also be altered by dissolving a solid in the fluid. For as is well-known, the ions of a dissolved solid tend to occupy the voids that exist normally between the particles of a fluid, without increasing the volume of the fluid noticeably. Since the density, $\rho_f$, of a fluid is clearly a function of the number of particles in the proper fluid element, any change in this number must be accompanied by a similar change in the density of the fluid. The density of a fluid is, therefore, not constant, but a function of both the temperature and pressure of the fluid, as well as the concentration (c) of any dissolved solids. The density of a fluid can thus be conveniently expressed in mathematical terms as

$$\rho_f = \rho_f(p,c,T) \tag{8.3}$$

Since the subsurface of the earth tends to be isothermal (except for the first few metres below the surface), the dependence of $\rho_f$ on the temperature is usually neglected in the study of subsurface flow phenomena, except for a few special situations. However, its dependence on the concentration and pressure is of considerable importance. In the case of temperature, this dependence is usually measured through the *isothermal compressibility*, or just compressibility, of the fluid

$$\beta = -\frac{1}{V} D_p V(p,c,T)|_{c,T} = \frac{1}{\rho_f} D_p \rho_f(p,c,T)|_{c,T} \tag{8.4}$$

where V is the volume of fluid. The minus sign in Equation (8.4) indicates that the volume decreases as the pressure increases and the symbol $|_{c,T}$ that both the temperature and concentration must be kept constant.

According to Newton's first law of motion, all material bodies tend to resist a change in their state of motion, unless acted on by a force. Thus, if a layer of fluid is set into *laminar motion* (motion in a straight line), the adjacent layers will tend to prevent this motion. This implies that there exists a force, the *shearing stress*, between the layers of a fluid as long as the relative motion persists.

Experimental measurements have shown that in a homogeneous fluid, the shearing stress is directly proportional to the rate of change of velocity perpendicular to the direction of flow, provided that the relative velocities are small and there is no heat exchange between the fluid and its surroundings. To illustrate this concept, consider the flow of a fluid between two parallel plates, shown in Figure 8–3. If $\tau_x$ denotes the shearing stress in the direction of flow and u(z) the velocity of flow in the xz-plane, the shearing stress can be expressed in the form

$$\tau_x \propto Du(z) = \mu Du(z). \qquad (8.5)$$

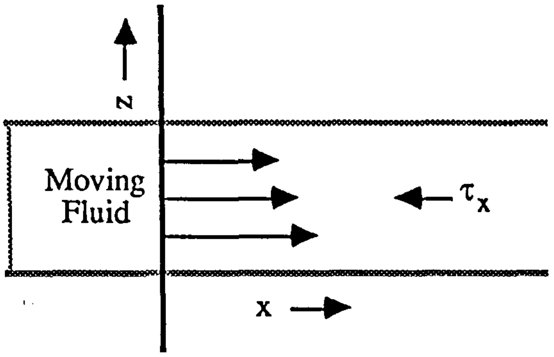

**Figure 8–3** Flow between two parallel plates used to illustrate the concept of viscosity

The parameter, $\mu$, introduced in Equation (8.5), is known as the absolute or *dynamic viscosity* of a fluid and is a constant for many fluids under the conditions stated above. Equation (8.5) was first suggested by Sir Isaac Newton. Fluids which satisfy it are, therefore, commonly referred to as *Newtonian fluids.*

## 8.3 THE FUNDAMENTAL LAW OF FLUID STATICS

The pressure in a fluid exists only because of the fluid. If the fluid is removed, pressure will vanish. A knowledge of the pressure at a particular point within a fluid, is thus of vital importance in the study of fluid motion.

Although there are a number of forces that can act on a fluid, the most important one in subsurface flow is the gravitational attraction of the earth on a fluid in equilibrium with its surroundings. To derive an expression for the pressure in this case, consider the elementary fluid volume, shown in Figure 8–4. Since the fluid is in equilibrium, the weight of the elementary fluid volume must be balanced by the difference of pressure across the volume. Using the definition of pressure in Equation (8.2) and the notation in

Figure 8–4, the pressure along the longitudinal axis of the fluid volume must satisfy the equation

$$p dA - (p + dp)dA - (\rho g \sin\theta)dAds = 0$$

or after division by dAds

$$\frac{dp}{ds} = -\rho g \sin\theta \tag{8.6}$$

Two very important pressure distributions that arise as limiting cases of Equation (8.6) are the horizontal distribution ($\theta = 0$)

$$\frac{dp}{ds}\Big|_{\theta=0} = \frac{dp}{dx} = 0 \tag{8.7}$$

and the vertical distribution ($\theta = \pi/2$)

$$\frac{dp}{ds}\Big|_{\theta=\pi/2} = \frac{dp}{dz} = -\rho g. \tag{8.8}$$

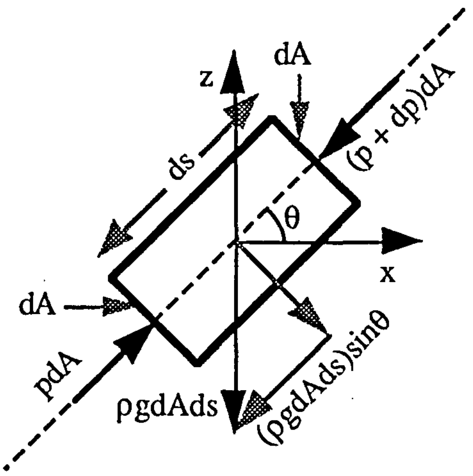

**Figure 8–4** Force diagram used in deriving the Fundamental Equation of Fluid Statics

Equation (8.7) is nothing else than a mathematical expression for the experimentally well-known fact that for a fluid in equilibrium with gravity, the pressure is constant everywhere over a horizontal plane within the fluid. Equation (8.8) indicates that in such a fluid there always exists a negative pressure gradient in the vertical direction. This is the *Fundamental Theorem of Fluid Statics.*

A question that frequently arises in subsurface flow is: given a pressure $p_0$ at a height $z_0$, what will the pressure, p, be at a height z? If ρ is a constant or a known function of both pressure and height, this question can be answered by a direct integration of Equation (8.8) to obtain

$$\int_{p_0}^{p} \frac{dp}{\rho g} = -\int_{z_0}^{z} dz = z_0 - z \tag{8.9}$$

The integral on the left-hand side of Equation (8.9) is often referred to as the *pressure head.*

In subsurface flow, it is sometimes more convenient to use the *piezometric head* (also known as Hubert's potential)

$$\phi = z + \int_{p_0}^{p} \frac{dp}{\rho g}, \tag{8.10}$$

instead of the elevation z to describe the pressure distribution in a fluid. This is particularly useful in the case of an incompressible fluid ($\beta = 0$), when Equation (8.10) simplifies to

$$\phi = z + \frac{p}{\rho g} \equiv z + h. \tag{8.11}$$

## 8.4 THE HAGEN-POISEUILLE LAW

An important application of Newton's law for viscous flow and the fundamental law of fluid statics arises in the case of *laminar flow*, i.e. where the fluid flows with a constant velocity parallel to the axis of a pipe. Consider, for example, the case of a circular pipe with constant radius R that slopes at an angle θ up to the right, as shown in Figure 8–5.

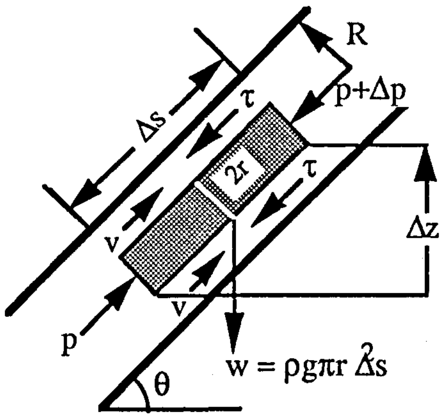

**Figure 8–5** Schematic representation of fluid flow through an inclined circular pipe

It follows from Newton's first law of motion that for a coaxial fluid cylinder of length Δs and radius r, shown in Figure 8–5, the fluid can only maintain its constant velocity if the forces acting on it are in equilibrium. This implies that the sum of the forces along the pipe axis must satisfy the equation

$$\Sigma F_s = 0$$

or, using the notation defined in Figure 8–5,

$$p\pi r^2 - (p + \Delta p)\pi r^2 - \tau_s 2\pi r \Delta s - \rho g \pi r^2 \Delta s \sin\theta = 0.$$

But, since $\Delta s \sin\theta = \Delta z$,

$$\tau_s = -\left[\frac{\Delta p}{\Delta s} + \rho g \frac{\Delta z}{\Delta s}\right]\frac{r}{2} \tag{8.12}$$

The shearing stress in a circular pipe thus varies linearly from zero at the pipe axis to a maximum value obtainable from Equation (8.12) with r = R. Notice that the pressure gradient and fluid weight combine in a manner dependent on their signs to force the fluid through the pipe, while the shearing stress always tends to retard the flow.

The linear variation of shearing stress in the pipe implies that the velocity should decrease steadily from the pipe axis towards the wall. To show that this is indeed the case, one only needs to replace $\tau_s$ in Equation (8.12) with its equivalent from Equation (8.5) to obtain

$$\mu Dv(r) = -\left[\frac{\Delta p}{\Delta s} + \rho g \frac{\Delta z}{\Delta s}\right]\frac{r}{2}$$

or on rearranging the terms

$$dv(r) = -\left[\frac{\Delta p}{\Delta s} + \rho g \frac{\Delta z}{\Delta s}\right]\frac{r}{2\mu}\,dr.$$

For an incompressible fluid, this equation can be directly integrated (assuming that $\mu$ is constant) to obtain

$$v(r) = -\left[\frac{\Delta p}{\Delta s} + \rho g \frac{\Delta z}{\Delta s}\right]\frac{r^2}{4\mu} + C.$$

The integration constant can be determined from the experimental fact that $v = 0$ at $r = R$ (the pipe wall). This yields

$$v(r) = \frac{1}{4\mu}\left[\frac{\Delta p}{\Delta s} + \rho g \frac{\Delta z}{\Delta s}\right](r^2 - R^2), \tag{8.13}$$

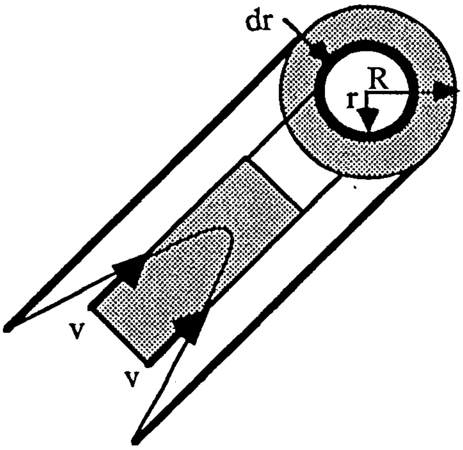

**Figure 8–6** The constant velocity distribution in a circular pipe with radius R

The velocity is thus distributed parabolically over the the radius of the pipe, as shown in Figure 8–6.

A quantity that plays an important role in fluid flow is the discharge rate, Q, defined as the volume of fluid flowing through a cross-section of the pipe per unit time. Referring to Figure 8–6, the discharge through a ring element of thickness dr is

$$dQ = v(r)dA = v(r)2\pi r dr,$$

or using the expression for the velocity in Equation (8.13)

$$dQ = \frac{\pi}{2\mu}\left[\frac{\Delta p}{\Delta s} + \rho g \frac{\Delta z}{\Delta s}\right](r^2 - R^2)r dr.$$

A direct integration of this equation from the axis of the pipe to its wall yields

$$Q = -\frac{\pi}{8\mu}\left[\frac{\Delta p}{\Delta s} + r g \frac{\Delta z}{\Delta s}\right]R^4. \tag{8.14}$$

The discharge rate for constant flow through a circular pipe is thus proportional to the fourth power of the radius of the pipe. This is the famous Hagen-Poiseuille law.

A comparison of Equation (8.14) with Equation (8.10) shows that the term in square brackets is nothing else than the quotient of the infinitesimal piezometric head $\Delta\phi$ and pipe length $\Delta s$. The discharge for constant flow can thus be expressed in differential form as

$$Q = -\frac{\pi\rho g}{8\mu} R^4 D\phi(s), \tag{8.15}$$

provided that the differential

$$D\phi(s) = \lim_{\Delta s \to 0} \frac{\Delta\phi}{\Delta s}$$

exists.

## 8.5 SURFACE TENSION

As noticed above, a fluid in a container can exhibit a horizontal free surface. It is a matter of common observation that this free surface has properties similar to those of an elastic membrane. (A clean dry needle can, for example, float on the surface of water). This behaviour can be explained as follows.

The molecules in a liquid must be very closely packed, for numerous experiments have shown that a liquid resists forces tending to compress it, even if these forces are enormously large. Since the molecules are so closely packed, the attracting forces between them must be very large. A molecule at the surface of a liquid is, however, not attracted equally in all directions, for there is no fluid above it (Figure 8–7). In consequence, these molecules tend to move towards the interior of the liquid, and as they occupy space, tend to diminish the surface area of the fluid. However, for a molecule to actually move towards the interior, it must overcome the forces caused by the molecules to its immediate left and right in the surface. The resultant force, which is responsible for the elastic behaviour of a liquid's surface, is universally known as *surface tension* and denoted by the symbol $\sigma$. Because surface tension is a force acting over an area, it is customarily measured as a force per unit length.

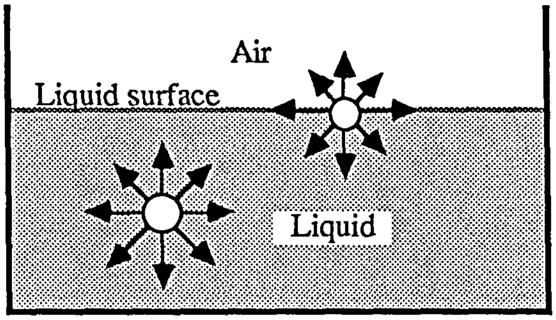

**Figure 8–7** The cohesive forces acting on a molecule inside and on the surface of a liquid open to air

To investigate the magnitude of the surface tension, consider the double-curved surface element with surface tension $\sigma$ and radii of curvature $r_1$ and $r_2$, subtending the angles $d\phi$ and $d\theta$, as shown in Figure 8–8. To remain in equilibrium, the external forces, $p_0$ and $p_i$, on this element must be balanced by the surface forces. Expressed mathematically, this means that

$$\sum F = 0$$

or, in terms of cartesian components (see Figure 8–8),

$$\sum F_x = \sigma r_1 d\phi \cos(d\theta/2) - \sigma r_1 d\phi \cos(d\theta/2) = 0$$

$$\sum F_y = \sigma r_2 d\theta \cos(d\phi/2) - \sigma r_2 d\theta \cos(d\phi/2) = 0$$

$$\sum F_z = (p_i - p_0)dA + 2\sigma r_1 d\phi \sin(d\theta/2) + 2\sigma r_2 d\theta \sin(d\phi/2) = 0$$

Since $\sin(\delta) \approx \delta$ for small values of $\delta$ and $dA = r_1 d\phi r_2 d\theta$, the previous equation can also be expressed in the form

$$(p_i - p_0)r_1 d\phi r_2 d\theta + 2\sigma r_1 d\phi(d\theta/2) + 2\sigma r_2 d\theta(d\phi/2) = 0,$$

which yields, on division by $r_1 d\phi r_2 d\theta$, the well-known Laplace equation

$$p_0 - p_i = \sigma(\frac{1}{r_2} + \frac{1}{r_1}) \qquad (8.16)$$

From the physical point of view, Equation (8.16) can be interpreted as saying that if the curvature across a fluid surface is positive, as in Figure 8–8, then the outward pressure is larger than the inward pressure and vice versa.

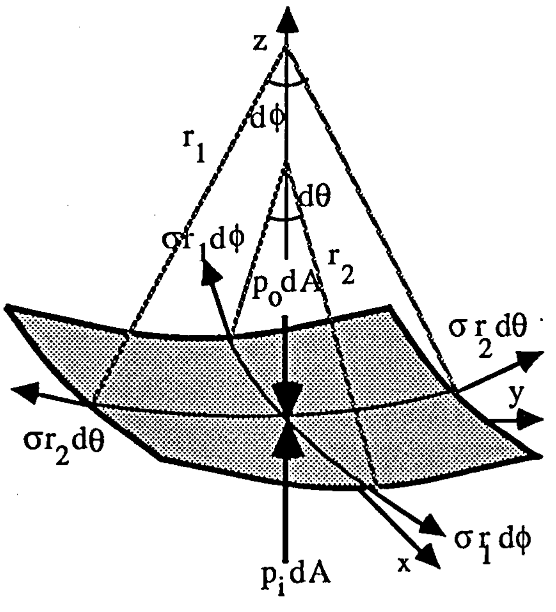

**Figure 8–8** Schematic representation of the pressure difference across a curved fluid surface.

The best known example of a curved interface is probably the interface between water and air. This, incidentally, explains why water rises in a capillary tube placed in a bowl of water. The pressure difference across a fluid surface is, for this reason, also known as the *capillary pressure* and denoted by

$$p_c = p_o - p_i \qquad (8.17)$$

It should be noticed that, in deriving Equation (8.16), no assumption was made as to what kind of external forces act on the surface element. Laplace's equation thus applies to all types of forces, *including* the very important gravitational force of the earth.

# CHAPTER 9

# PHYSICAL PROPERTIES OF A POROUS MEDIUM

## 9.1 GENERAL

When describing a porous medium, it would be desirable to have a measure available that could be used to characterize the geometric properties of the medium. Unfortunately, the pore system is such a complicated surface (see Figure 9–1) that its geometry cannot be defined by simple mathematical relations, as is the case with simple geometric objects such as spheres and rectangles. This difficulty is commonly avoided by characterizing the medium either as a mathematical continuum or a statistical ensemble of particles and pores. These two characterizations will now be described in more detail.

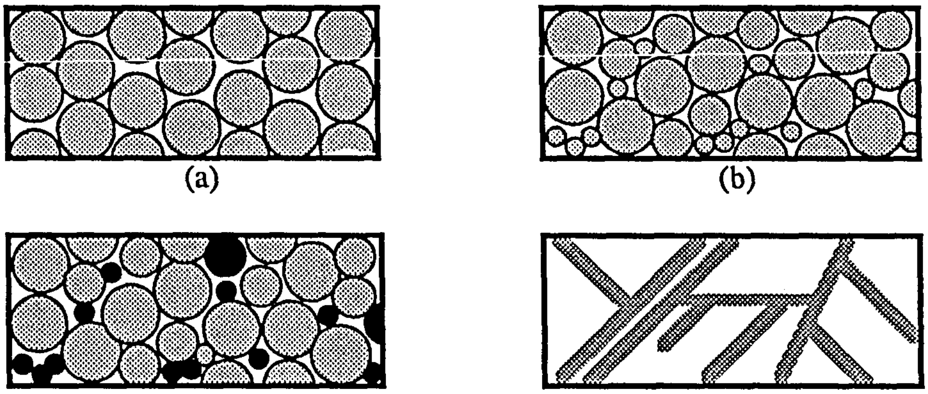

(a) (b)

(c) (d)

**Figure 9–1** Examples of pores found in geological formations. (a) A well-sorted sedimentary deposit. (b) A poorly sorted sedimentary deposit. (c) A well-sorted sedimentary deposit with deposition of mineral matter. (d) Rock rendered porous by fracturing.

## 9.2 THE POROUS CONTINUUM

### 9.2.1 Porosity

A porous medium can only store water, or any fluid for that matter, in the voids represented by the pores present within its *skeleton* or *matrix* of closely packed solid grains. Some geological formations, particularly volcanic material, occasionally contain pores that are isolated from adjacent pores. These pores cannot partake in the storage and interchange of fluids and are, therefore, of no importance in subsurface flow. In the discussion to follow, the term *pores* will be used exclusively to denote those pores which are *interconnected continuously by interstices to the flow domain.*

Because of its importance in storing fluids, the volume of pores is of prime importance in the study of fluid motion through a porous medium. Since the actual volume of pores varies considerably from one porous medium to another (see Figure 9–1), it is of the utmost importance to have a measure in order to compare different porous media.

To define a measure for the volume of pores uniquely, it must be remembered that the subsurface consists of at least three components – water, air and the solid matrix. With this in mind, consider the cross-section in Figure 4–2 through a piece of porous material with volume

$$\Delta V = \Delta V_w + \Delta V_s + \Delta V_a \tag{9.1}$$

where $\Delta V_w$, $\Delta V_s$, and $\Delta V_a$ denote the volume of water, solids and air respectively. A measure universally used for this purpose is the *porosity*, which can be intuitively defined as the ratio

$$\varepsilon \equiv \frac{\Delta V_w + \Delta V_a}{\Delta V} \tag{9.2}$$

between the volume of the porous medium and the volume of pores. However, as was the case with the fluid density, discussed in Section 3.2, this ratio may not be meaningful, unless the volume $\Delta V$ is specified in some manner. To arrive at an acceptable measure, consider the mathematical point P inside the subsurface as in Figure 9–2. Let $\Delta V_P$ be a volume element centred around P. In the case of materials from the earth's subsurface, the ratio

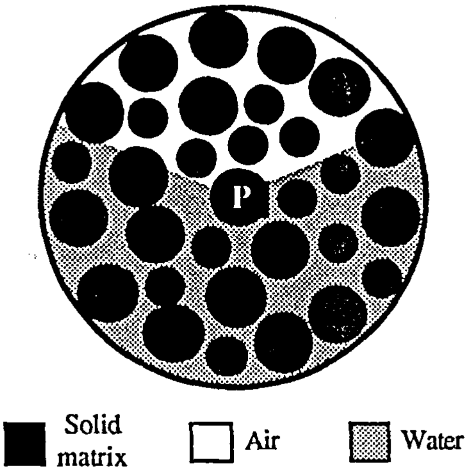

**Figure 9–2** Schematic diagram of a cross-section, showing the normal three phases of a geological formation in the earth's upper crust

$$\varepsilon_P = \frac{\Delta V_{Pw} + \Delta V_{Pa}}{\Delta V_P}$$

tends at first to either decrease or increase with decreasing $\Delta V_p$, until it reached a value $\Delta V_{max}$, after which it remains more or less constant up to a value $\Delta V_{min}$ (see Figure 9–3). This behaviour of $\varepsilon_P$ can be ascribed to the fact that the geological formations which form the earth's subsurface tend to be *heterogeneous*, i.e. contain a number of porous materials each with its own distribution of voids. It is only when $\Delta V_P$ reached a sufficiently small value ($\Delta V_{max}$) that the material becomes more or less *homogeneous* and $\varepsilon_P$ remains constant. If $\Delta V_P$ is decreased beyond $\Delta V_{min}$, $\varepsilon_P$ will begin to fluctuate violently until it finally assumes either the value of 0 or 1, depending on whether P lies within a pore or the solid matrix. To ensure that porosity is a meaningful and unique quantity, the proper sample volume to use in Equation (9.1) is thus the volume element $\Delta V_{min}$.

It follows from its definition in Equation (9.1), that the porosity of a geological formation will be influenced by a number of factors such as: its degree of compaction and cementation. As can be seen by comparing the porosities of sand- and siltstone with their uncemented counterparts (sand and silt) in Table 9–1, the influence of these factors is of considerable importance.

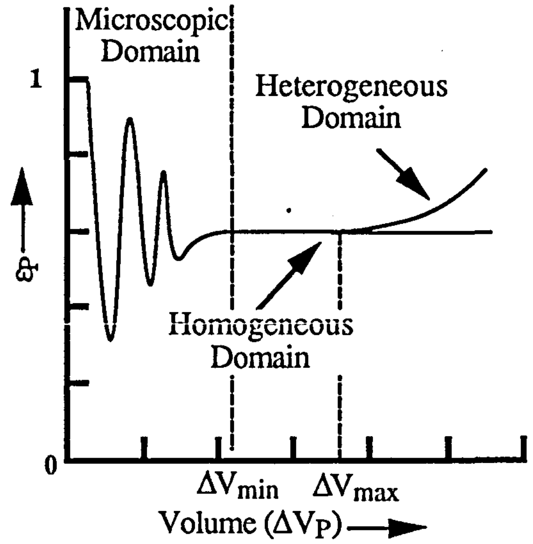

**Figure 9–3** Definition of the proper volume element and the porosity ε for a porous medium [after Bear (1979)]

Porosity, as defined in Equation (9.2), is related to a volume of a porous medium and thus also referred to as *volumetric* porosity. In a similar fashion, let

$$\Delta A(s) = \Delta A_s(s) + \Delta A_w(s) + \Delta A_a(s)$$

be a proper sample area within the proper sample volume ΔV along a line segment, s, perpendicular through the centre of ΔA(s), such that

$$\Delta V = \int_s \Delta A ds$$

Consider now the *directional areal porosity*, ε(s) defined by

$$\varepsilon(s) = \frac{\Delta A_v(s)}{\Delta A(s)} = \frac{\Delta A_w(s) + \Delta A_a(s)}{\Delta A(s)}$$

The total volume of pores in ΔV can then be expressed as

$$\Delta V_v = \int_s \Delta A_v \, ds \equiv \int_s \varepsilon_a \Delta A \, ds = \varepsilon \Delta V$$

Since ΔA is, by definition, always positive, the generalized mean value theorem of the integral calculus [Hardy (1955)] can be invoked to rewrite this equation in the form

$$\varepsilon\Delta V = \varepsilon(\zeta)\int_s \Delta A \; ds = \varepsilon(\zeta)\Delta V$$

where $\zeta$ is a point somewhere within s. Hence, it follows that

$$\varepsilon(\zeta) \equiv \varepsilon$$

Being a volumetric quantity $\varepsilon$, and thus $\varepsilon(\zeta)$, cannot depend on a specific direction within $\Delta V$. Every proper sample volume thus contains an *areal porosity* $\varepsilon_a \equiv \varepsilon(\zeta)$ which is numerically identical to its volumetric porosity $\varepsilon$.

**Table 9–1** Porosities of a number of materials frequently encountered in subsurface flow [after McWhorter and Sunada (1977)].

| Material | No of Analyses | Range | Mean Value |
|---|---|---|---|
| **Igneous Rocks** | | | |
| Weathered granite | 8 | 0,34 – 0,57 | 0,45 |
| Weathered gabro | 4 | 0,42 – 0,45 | 0,43 |
| Basalt | 94 | 0,03 – 0,35 | 0,17 |
| **Sedimentary materials** | | | |
| Sandstone | 65 | 0,14 – 0,49 | 0,34 |
| Siltstone | 7 | 0,21 – 0,41 | 0,35 |
| Sand (fine) | 243 | 0,26 – 0,53 | 0,43 |
| Sand (coarse) | 26 | 0,31 – 0,46 | 0,39 |
| Silt | 281 | 0,34 – 0,61 | 0,46 |
| Clay | 74 | 0,34 – 0,57 | 0,42 |
| Gravel (fine) | 38 | 0,25 – 0,38 | 0,34 |
| Gravel (coarse) | 15 | 0,24 – 0,36 | 0,28 |
| Limestone | 74 | 0,07 – 0,56 | 0,30 |
| **Metamorphic rocks** | | | |
| Schist | 18 | 0,04 – 0,49 | 0,38 |

### 9.2.2 Moisture Content

A measure closely related to the porosity of the subsurface matrix is the volume of fluid that it contains. This quantity is conventionally expressed by either one of two variables: the *moisture content,* defined (in terms of the proper sample volumes introduced above) by

$$\theta = \frac{\Delta V_w}{\Delta V} \tag{9.3}$$

and the *water saturation* defined by

$$S_w = \frac{\theta}{\varepsilon}. \tag{9.4}$$

A basic assumption in these definitions of $\theta$ and $S_w$ is that the moisture contents of a fully saturated porous medium, *the saturated moisture contents* $\theta_s$, equal the porosity of the medium. Hence, $\theta$ and $S_w$ must satisfy the inequalities

$$0 \leq \theta \leq \theta_s \equiv \varepsilon \quad \text{and} \quad 0 \leq S_w \leq 1.$$

### 9.2.3 Density

Another quantity that plays a particular important role in the flow of subsurface fluids is *density*. Because the subsurface does not consist of a single component (see Figure 9–2), density is a rather ambiguous term to use in the case of a porous medium. This ambiguity is usually circumvented by introducing not one, but three densities. These densities, defined in terms of the proper sample volumes in Equation (9.1) and their respective mass fractions

$$\Delta M = \Delta M_w + \Delta M_s + \Delta M_a$$

are:

$$\begin{aligned} &\text{(a) Density of solids} && \rho_s = \frac{\Delta M_s}{\Delta V_s} \\ &\text{(b) Dry bulk density} && \rho_b = \frac{\Delta M_s + \Delta M_a}{\Delta V} \qquad (9.5) \\ &\text{(c) Wet bulk density} && \rho_w = \frac{\Delta M}{\Delta V} \end{aligned}$$

These densities are, however, not independent from one another. Consider, for example, the case of

$$\rho_w = \frac{\Delta M_s + \Delta M_a}{\Delta V} + \frac{\Delta M_w}{\Delta V} = \rho_b + \rho \frac{\Delta V_w}{\Delta V} = \rho_b + \rho\,\theta$$

where

$$\rho = \frac{\Delta M_w}{\Delta V_w}$$

is the density of fluid. If it is assumed that $M_a$ is negligibly small, the dry density can be expressed through Equations (9.1) and (9.2) as

$$\rho_b = \frac{\Delta M_s + \Delta M_a}{V_s}(1 - \varepsilon) = \rho_s(1 - \varepsilon)$$

## 9.3 STATISTICAL DESCRIPTION OF POROUS MEDIA

### 9.3.1 Particle-size Distribution

Granular materials, such as soils and sands, are often described in terms of their particle-size distribution. However, this immediately raises the question of what is meant by particle size, as, except for a sphere or cube, the size of a particle cannot be uniquely defined by a single linear dimension. It should, therefore, not surprise one to learn that the two main methods used to determine particle-size distributions – sieve and hydrometer analysis – are both indirect methods. The sieve analysis is conventionally used for particles larger than 0,06 mm [Bear (1972)] and the hydrometer method for smaller particles.

A sieve analysis is performed by passing the material through a series of sieves with different standard square openings of specified size. The size of a particle determined in this way, thus only means that one has measured the largest dimension of the particle that will allow it to slip through the sieve. In the hydrometer method, the size of a particle is taken as the diameter of a sphere that settles in water at the same velocity as the particle.

Notwithstanding the fact that the sizes of particles determined from both a sieve or hydrometer analysis are only approximate descriptions of the true sizes of real particles, the results can be quite useful. Of particular importance in this connection is the *particle or grain-size distribution curve*, obtained by plotting the mass percentage of material that passes a given sieve (customarily denoted by the symbol $d_m$) as a function of the sieve. From such a graph, one can then determine various effective or average grain sizes, such as Hasen's *effective grain size*, $d_{10}$, and his effective grain-size coefficient

$$C_u = d_{60}/d_{10}.$$

Based on such a sieve analysis, a porous material composed entirely, or almost entirely, of grains that passes a single sieve, is referred to as a *uniform material*, while a material which requires a large number of sieves to classify its grains is known as a *well-graded* porous material.

### 9.3.2 Pore-size Distribution

The grain-size distribution function, introduced above, is obviously of no use in case of a consolidated porous medium. Consolidated porous materials are consequently characterized through their pore-size distribution. When describing the sizes of pores, it would be most desirable to be able to define a geometric quantity that would characterize the pore system of a given porous medium. Unfortunately, the pore system is such a complicated surface (see Figure 9–1) that it is difficult to describe it in terms of geometric quantities, such as its diameter or radius, which makes sense only if some further specifications are made. With this in mind, Scheidegger (1974) defined the *pore diameter* at any one point within the porous medium as *the diameter of the largest sphere which contains this point and remains wholly within the pore space.* In this way, a pore radius can be attached rigorously to any point in the pore space and, if desired, a *pore-size distribution* $\alpha(r)$ could be defined –

simply by determining what *fraction* of pore space has a pore radius between r and r+dr.

To account for all the pores in a porous medium, Scheidegger (1974) normalized the pore-size distribution function as

$$\int_0^{\infty} \alpha(r)dr = 1$$

as is usually done in the theory of mathematical statistics. A true porous material will, however, only contain pores with radii up to a maximum value ($r_{max}$ say), otherwise the flow may not be porous in nature. With this in mind, the pore-size distribution for a porous medium should really be normalized as

$$\int_0^{r_{max}} \alpha(r)dr = 1. \tag{9.6}$$

Although not physically fully correct, it is tempting to interpret an unsaturated porous medium as one where all pores with radii less than a given value, say r, are fully saturated. With this assumption, the moisture content of a porous medium can be expressed as

$$\theta(r) = \int_0^{r} \varepsilon\alpha(x)dx. \tag{9.7}$$

## 9.4 DISTRIBUTION OF FLUIDS IN A POROUS MEDIUM

Fluids can enter a porous medium only through the small pores between the solid grains of its matrix. According to the discussion in Section 9.2, some of the fluid will be adsorbed by the grains, while the rest will fill the pores as far as possible. The adhesive forces acting between the adsorbed layer of fluid, which are usually only a few molecular layers thick, and the solid matrix, are so strong that the adsorbed fluid can, for all practical purposes, be considered as immobile. This situation, illustrated in Figure 9–4, has important consequences for subsurface flow.

Depending on the type of material and fluid, the natural forces acting in unsaturated flow may not be able to drain the fluid from pores with radii smaller than say $r_{min}$. By following the same line of argument used in deriving Equation (9.7), the moisture contents of these pores, also known as the *irreducible* or *residual* moisture content, can be expressed as

$$\theta_r \equiv \theta(r_{min}) = \int_0^{r_{min}} \varepsilon\alpha(x)dx. \tag{9.8}$$

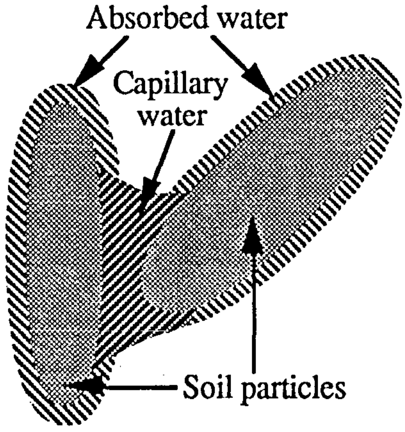

**Figure 9–4** Schematic diagram illustrating the distribution of water between the grains of a geological formation

It follows from the preceding discussion that not all the fluid adsorbed in a porous medium can be regained, unless the medium is subjected to what may be called extensive sources of external energy, for example heat. (This explains why not all the groundwater can be withdrawn from an aquifer). Moreover, since the ratio of surface area to volume of a particle is inversely proportional to its radius, the area exposed to pores will be larger in a fine-grained than a coarse-grained porous medium. A clayey formation with its fine-grained matrix can thus contain large volumes of water, but be unable to release it.

In an unsaturated (three phase) geological formation, the fluid not adsorbed to the porous medium will form curved menisci with the adsorbed water and soil grains. These isolated islands of water must thus obey Laplace's equation (8.16) for capillary pressure, hence the designation *capillary water* in Figure 9–4. If atmospheric pressure is taken to be the reference pressure and equated to zero, as is customarily, Laplace's equation reduces to

$$-p_w = \sigma\left[\frac{1}{r_2} + \frac{1}{r_1}\right]. \tag{9.9}$$

The pressure experienced by the capillary water is thus negative.

An important consequence of Equation (9.9) is that it will require less force to remove fluid from a pore with a large radius than from one with a small radius. In unsaturated flow, pores with a large radius will, therefore, drain before the pores with smaller radii.

The idea of a negative pressure may seem strange at first and soil scientists, therefore, introduced the positive quantity *capillary pressure*, defined by

$$\psi = -p_w, \tag{9.10}$$

to describe it. As discussed above, this pressure really derives from the interaction between capillary water, soil grains and adsorbed water. The term *matric pressure*, in use at present, is thus much more descriptive.

The introduction of a negative pressure has a tremendous advantage, as it allows one to describe the entire moisture profile in the field, in terms of a single continuous pressure extending from the saturated into the unsaturated region below and above the water table (see Figure 9–5). Nevertheless, there are situations where the term, matric pressure, as defined in Equation (9.10), may be used to advantage. One particular important example occurs in the definition of and calculations performed with the *moisture retention curve* described below.

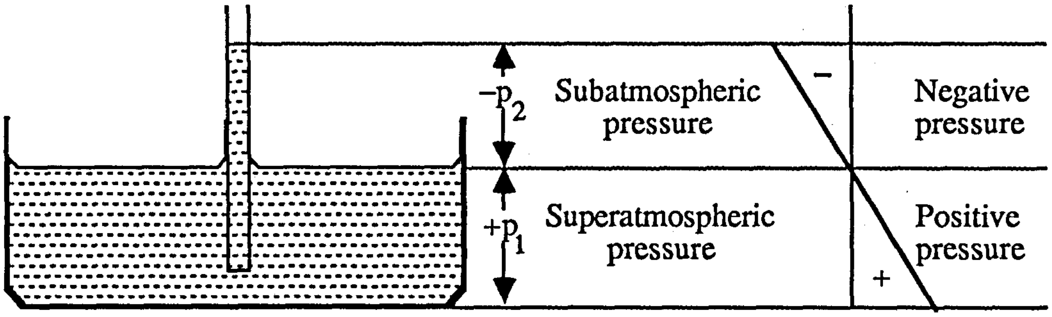

**Figure 9–5** The distribution of pressure below and above a free water surface

## 9.5 THE MOISTURE RETENTION CURVE

It has been observed experimentally that if capillary water is removed from an unsaturated porous medium, the curvature of the menisci formed by the remaining capillary water with the soil grains decreases (see Figure 9–4). However, Equation (9.9) requires that a decrease in radius must be accompanied by an increase in the matric pressure. The matric pressure is thus closely related to the volume of water contained by the geological formation. This relation, known as the *moisture retention (or characteristic) curve,* can be conveniently expressed mathematically in terms of the volumetric moisture content $\theta$, defined in Equation (9.3), as

$$\psi = \psi(\theta). \tag{9.11}$$

The most satisfactory way to determine an expression for the retention curve would be to derive it from basic physical principles. Because the structure of all porous media is so complex, this is unfortunately not possible. The only practical alternative is to determine it experimentally for the porous medium under investigation. While this is a relatively simple (but laborious) experimental exercise, that have been conducted for years by soil scientists, the interpretation and application of the moisture retention curve are not straightforward. For example, can one really apply the concept of a moisture retention curve to the many important dense geohydrological formations, such as fresh dolomites and dolerites, or to alluvial deposits with large boulders in it? Although some progress has been made in this direction [Bouwer and Rice (1984)], the question cannot be considered as fully answered.

Nevertheless, it will be assumed in the discussion to follow that a moisture retention curve can be determined, if not for all, then at least for the most important geological formations associated with subsurface flow.

The example of a moisture retention curve (shown in Figure 9–6) indicates that Equation (9.11) is not a simple, but a highly nonlinear relation of the moisture content. In more physical terms, $\psi(\theta)$ is said to a show a *hysteresis effect*. This means that the curve is at least double legged, with one leg valid during the drying cycle (desorption) and the other one during the wetting cycle (sorption). Moreover, since the surface of the earth is intermittently subjected to both drying and wetting cycles, the curve can change abruptly from the sorption to the desorption leg or *vice versa*. For example, a very dry soil may be wetted by rain which stops as soon as its moisture content reaches the point A in Figure 9–6. After that, desorption will set in, which, if allowed to proceed unchecked, will follow the path indicated by the line segment AB in Figure 9-6 and from there on the normal desorption leg. Care must, therefore, be exercised when using the retention curve in practical applications.

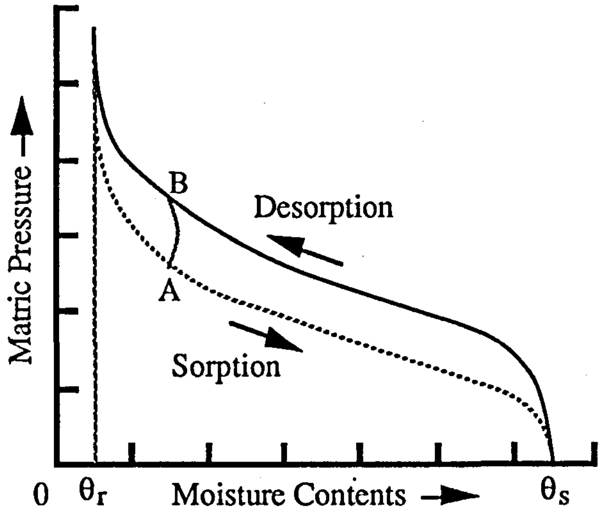

**Figure 9–6** Sorption and desorption branches of the moisture retention curve for a soil. The loop AB indicates a possible transition between the main branches.

It is interesting to note that the moisture retention curve generally does not approach infinity along the matric pressure axis as the moisture content decreases, but rather along an asymptote parallel to the matric pressure axis through a small positive value of $\theta$. This behaviour can be explained as follows.

As noted above, not all the fluid contained in a porous medium can be regained, unless the medium is supplied with external energy. The customary procedure to determine $\theta$ is to dry a sample of the porous medium in a constant temperature oven for a prescribed period of time. (In the case of soil, the sample is usually dried for a period of 24 h at 105°C). Since heat is freely available, it is possible that some water contained in the very small undrainable pores is also evaporated (see Section 9.4). The position of the asymptote in Figure 9–6 may, therefore, be equated with residual moisture content, defined in Equation (9.8). For this reason, it would be more appropriate to express the moisture retention curve, not in terms of the moisture content, but rather *the reduced moisture content,* defined by the equation

$$\Theta = \frac{\theta - \theta_r}{\theta_s - \theta_r}. \qquad (9.12)$$

Unfortunately, it is difficult, if not impossible, to determine $\theta_r$ directly from an experimental curve such as the one in Figure 9–6.

Viewed from a mathematical point of view, one should be able to represent the moisture retention curve by a smooth and continuous relation. However, since the curve can only be determined experimentally, its true behaviour is in practice only known at a finite number of points. There are two methods that can be used to obtain values at off-experimental points. The first and most obvious method is to use interpolation. Since the moisture retention curve is highly non-linear, this procedure, particularly linear interpolation, can only be successful in those cases where the experimental points are closely spaced and distributed over the full range of θ–values ($\theta_r \le \theta \le \theta_s$). Many scientists thus opt for the second alternative – the approximation of experimental values by an empirical equation. Although any suitable empirical expression would do, much can be gained if the expression is chosen judiciously. For example, the expression selected, should be able to represent the experimental results accurately and not require an exorbitant computational effort to evaluate.

The form of the moisture retention curve in Figure 9–6 very much resembles the sigmoidal shape of a cubic polynomial. Since a polynomial is easy to evaluate and able to match the experimental points exactly, this would seem to be an ideal choice. However, these properties may cause considerable difficulties for the prospective user of the fitted curves. One difficulty is that a polynomial approximation cannot be used to extrapolate data beyond the experimental points. Nevertheless, as has been shown by Case *et al* (1983) in their encyclopedic work on moisture retention curves, the approximation can be applied successfully, provided that interest is centred only on the domain *for which experimental data are available.* Another danger lies in the fact that it is easy to fit the data exactly with a polynomial. However, due to the inhomogeneity of natural soils, the data obtained from *in situ* or field samples are usually scattered considerably (see Figure 9–7). A smooth approximation, obtained for such data, may be aesthetically pleasing, but of no scientific value.

A scientific more correct approach would be to come up with a mathematical relation which resembles the moisture retention curve as closely as possible and fits this relation to the limited number of experimental data points, using for example a non-linear least squares or similar technique. Such a relation should not only yield a more unbiased representation of the moisture retention curve, but also a better approximation over the full range of moisture content values.

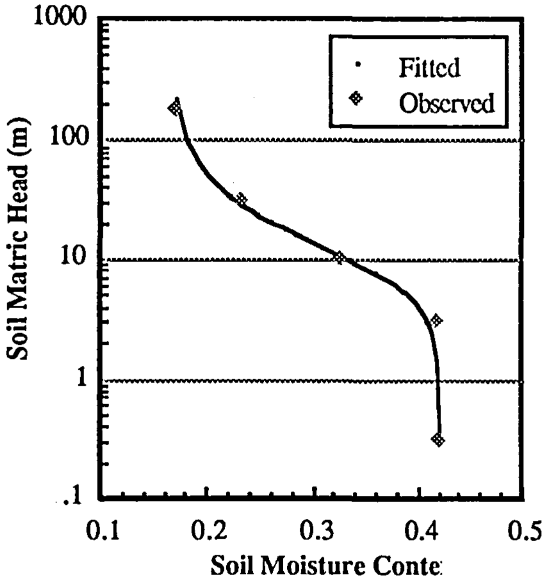

**Figure 9–7** Example of an experimentally observed soil moisture retention curve and the corresponding least squares fitted Van Genuchten approximation. [$\alpha = 0{,}110$; $n = 2{,}111$; $\theta_r = 0{,}164$ and $\theta_s = 0{,}380$]

Based on the analysis of a large set of experimental data, Brooks and Corey [1964, 1966] concluded that the retention curves for many soils can be fitted reasonably well with the analytical equation

$$\Theta = \left[\frac{\psi}{\psi_b}\right]^{-\lambda} \qquad (9.13)$$

where $\lambda$ and $\psi_b$, which they relate to the pore-size distribution and *bubbling pressure* (see also Bear [1972]), are characteristic constants of the soil that must be determined by the procedure used to fit the data. This relation is probably the one most widely used by soil scientists.

Another reason for using an approximation, such as Equation (9.13), is to be able to calculate the *moisture capacity*

$$C \equiv -D\theta(\psi), \qquad (9.14)$$

which plays an important role in soil moisture storage and its availability to plants. The relation used, should thus not only represent the moisture retention curve accurately, but also the moisture capacity. As can be seen from Figures 9–6 and 9–7, C → 0 as $\theta$ approach the saturated moisture content $\theta_s$. However, the value of C, calculated from Equation (9.14) for the retention curve defined by Equation (9.13), does not share this property. In fact, here

$$\lim_{\theta \to \theta_s} C = \lim_{\psi \to 0}\left[-(\theta_s - \theta_r)\left\{\frac{\lambda}{\psi_b}\right\}\left\{\frac{\psi_b}{\psi}\right\}^{\lambda + 1}\right] \to -\infty.$$

A moisture capacity, calculated from Equation (9.14), is thus discontinuous at the transition from unsaturated to saturated flow, which is highly unlikely [Van Genuchten and Nielsen (1985)].

To avoid discontinuities in the moisture capacity and also because Equation (9.13) does not represent the retention curve very accurately in the vicinity of $\theta_s$ [El-Kadi (1985)], the approximation in Equation (9.13) is often replaced by the approximation

$$\Theta = (1 - c\psi^{\kappa}).$$

over the range $\psi < \psi_b$. However, this does not materially affect the calculation of C, as the sole effect of this approximation is to shift the discontinuity in C from $\theta_s$ to $\theta_b$, the moisture equivalent of the bubbling pressure.

El-Kadi (1985) recently analysed a set of four of these empirical equations for the approximation of the moisture retention curve. His results can be summarized in saying that any one of them could be used to approximate an experimental moisture retention curve. There is, however, one equation [originally proposed by Van Genuchten (1980)] that deserves special attention. In this equation, the moisture retention curve is expressed as

$$\Theta = [1 + (\alpha\psi)^n]^{-m} \tag{9.15}$$

where $\alpha$, n and m are characteristic constants, which have to be determined for every soil type. In his original paper, Van Genuchten suggested that one should use the value $m = 1 - 1/n$. Later work by himself and Nielsen (1985), however, indicates that in certain cases it may be more advantageous to allow m to be independent of n. (See also the discussion in Section 10.5.3).

The main advantage of Equation (9.15) over Equation (9.13) is that it is $C^{\infty}$–continuous, if $n > 1$, and easy to evaluate. Although the majority of soils, analysed by Van Genuchten, did yield a value of $n > 1$, values of $n < 1$ were, nevertheless, observed in a few cases. However, as suggested by Van Genuchten and Nielsen (1985), these low values of n may be due to poorly defined or incomplete data sets. Assuming, therefore, that the identity $n > 1$, is valid for all natural soils, the moisture capacity can be expressed in terms of Equation (9.15) as

$$D\Theta(\psi) = \frac{D\theta(\psi)}{\theta_s - \theta_r} = -\frac{\alpha mn(\alpha\psi)^{n-1}}{[1 + (\alpha\psi)^n]^{m+1}},$$

with the result that

$$D\Theta(0) = 0.$$

The Van Genuchten approximation is thus able to represent the moisture capacity exactly at the transition from unsaturated to saturated flow.

From a practical point of view, the only disadvantage in using a non-linear equation, e.g. Equations (9.13) and (9.15), to approximate the moisture retention curve, is that the computations can be quite involved and that one has to use a computer and suitable software. Fortunately, there are a number of subroutines available (see for example the NAG Library manual) written specifically for this purpose. The two micro computer programs, RETC of Van Genuchten (1985) and RIEN of Botha (1988), have also been developed specifically for this purpose. However, the fitting procedure also has its advantages. As noticed above, it is difficult to determine the residual moisture content from the experimentally determined retention curve. Since $\theta_r$ can be considered as just another parameter, it (as well as the saturated moisture content for that matter) can be determined in the fitting procedure. An example of such a fitted curve based on the Van Genuchten approximation in Equation (9.15) , is shown in Figure 9–7.

## 9.6 COMPRESSIBILITY OF A POROUS MEDIUM

All matter are to some extent elastic or even plastic in nature and not rigid. The solid matrix of a porous medium will, therefore, also undergo a deformation when subjected to an external force. If it is assumed that the elasticity of the solids in the matrix of the medium is much less than that of the matrix itself, the deformation must be accompanied by a movement of the pore walls and thus a change in porosity. To describe this deformation in the subsurface of the earth, consider the situation depicted in Figure 9–8.

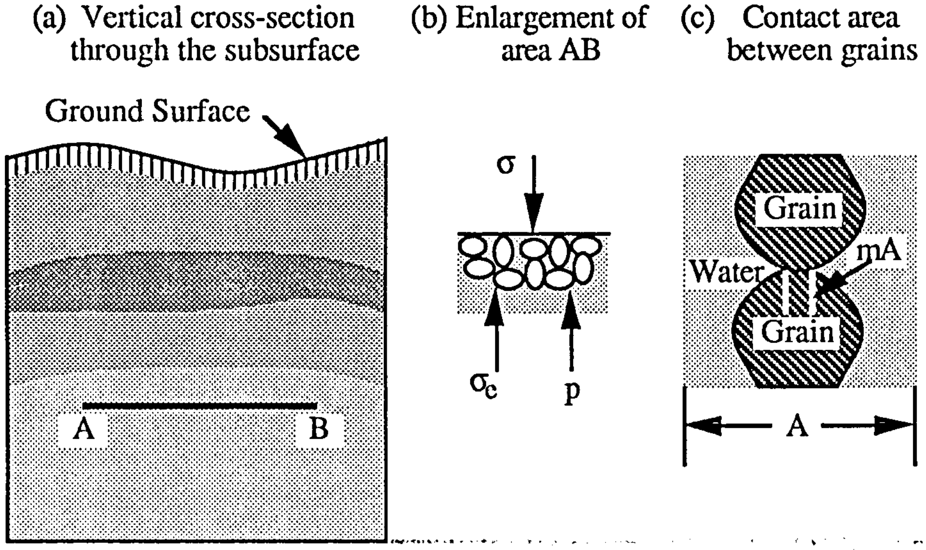

**Figure 9–8** Distribution of stresses and the pressure in the vertical direction of the earth's subsurface

Any horizontal plane, area A, passing through the medium, will intersect both solid and void spaces. Application of Newton's third law of motion [Terzaghi (1925, 1943, 1960)], shows that the total load of soil and any external forces (e.g. atmospheric pressure) applied above this surface, must be balanced by *interparticle stresses*, $\sigma_s$, created in the matrix and the pressure of a fluid, if present in the medium. If mA denotes the area of solid-solid contact, the forces across A must satisfy the equation

$$\sigma = p(1 - m) + m\sigma_s \tag{9.16}$$

where $\sigma$ is the total stress per unit area and p the fluid pressure. Although the actual value of m is small, $\sigma_s$ is very high. With this in mind, Equation (9.16) can also be expressed in terms of the *effective solid matrix stress* of Terzaghi, $\sigma_e = m\sigma_s$, as

$$\sigma = p + \sigma_e. \tag{9.17}$$

Although it is usual to take positive stresses as tensions, it was assumed in the derivation of Equations (9.16) and (9.17) that a positive p, $\sigma$, $\sigma_s$ or $\sigma_e$ means compression, i.e. the stress is directed *into* the surface upon which it acts.

The changes in porosity is obviously related to the effective stress, and through it to the total stress and pressure. The most frequent use of Equation (9.17) in subsurface flow arises where the total stress is kept constant, but the pressure is changed, for example, by pumping water from an aquifer. Hence, in this situation

$$d\sigma = 0 = dp + d\sigma_e, \quad \text{or} \quad dp = -d\sigma_e. \tag{9.18}$$

The elasticity of the solid matrix can be conveniently measured through its *coefficient of compressibility*, $\alpha$, defined by

$$\alpha = -\frac{1}{V_b} D_{\sigma_e} V_b, \tag{9.19}$$

where $V_b$ is the bulk volume of porous medium and the minus sign indicates that $V_b$ decreases as $\sigma_e$ increases. Since the volume of solids in $V_b$,

$$V_s = (1 - \varepsilon)V_b,$$

remains constant under the deformation, it follows from Equation (9.18) that

$$\alpha = -\frac{1}{V_b} D_{\sigma_e} V_b = -\left[\frac{1}{1 - \varepsilon}\right] D_{\sigma_e} \varepsilon = \left[\frac{1}{1 - \varepsilon}\right] D_p \varepsilon \tag{9.20}$$

The coefficient of compressibility for a porous material is thus related to a change in porosity caused by changes in the fluid pressure.

# CHAPTER 10

# DARCY'S LAW

## 10.1 GENERAL

The most basic quantity in fluid flow through a porous medium is, without any doubt, the volume of fluid that passes through the given medium. No wonder then that the French engineer, Henri Philibert Gaspard Darcy (1803–1858), selected precisely this quantity to measure in his pioneering investigation of the fountains of Dijon. The importance of this work will become clearer as the discussion proceeds.

## 10.2 DARCY FLOW

### 10.2.1 Darcy's Experiment

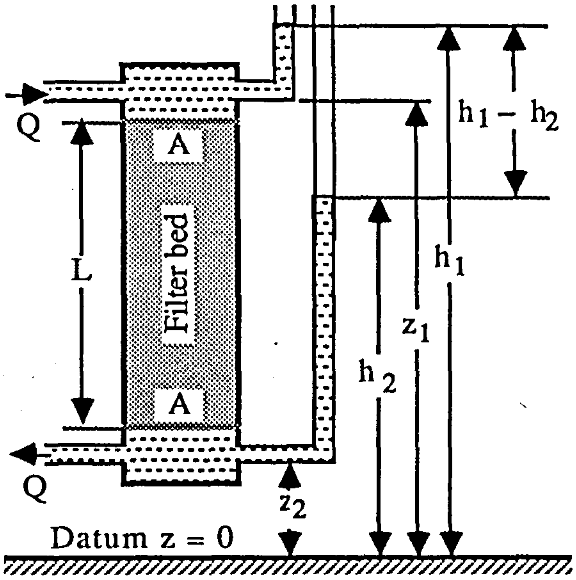

**Figure 10–1** Schematic illustration of Darcy's filtration experiment

Darcy's main interest was in the flow of water through vertical columns of homogeneous sand. A schematic illustration of the apparatus used by him is shown in Figure 10–1. Based on his experiments, Darcy concluded that the *rate of flow* (i.e. volume of water per unit time) through a vertical column, Q, is directly proportional to the cross-sectional area (A) of the column, the difference in water levels, $(h_1 - h_2)$, between the inlet and outlet and inversely proportional to the length, L, of the column. In mathematical terms, this yields the famous *Darcy's law*

$$Q \propto \frac{A(h_1 - h_2)}{L} = \frac{KA(h_1 - h_2)}{L} \tag{10.1}$$

where the proportionality constant, K, will be discussed in more detail below.

The quantities $h_1$ and $h_2$ in Equation (10.1) can be recognized as the piezometric head defined by Equation (8.10). This can be seen more clearly from Figure 10–2, which incidentally also shows that, since $p_2/\rho g < p_1/\rho g$, the flow of water is always from a *higher* to a *lower* piezometric head and *not* from a higher to a lower pressure. Darcy's law can thus also be expressed in terms of the piezometric head as

$$Q = -\frac{KA(\phi_2 - \phi_1)}{L}, \qquad (10.2)$$

where the minus sign indicates that the flow is in a direction opposite to that of increasing $\phi$. Since the piezometric head differs for a compressible and incompressible fluid [see Equations (3.10) and (3.11)], care must be exercised when using Darcy's law in this form.

As defined above, $\phi$ describes the sum of the pressure and potential energies of the fluid (in terms of head of water). The difference $(\phi_2 - \phi_1)$ may thus be interpreted as the energy loss, due to friction through the narrow tortuous paths of the porous medium.

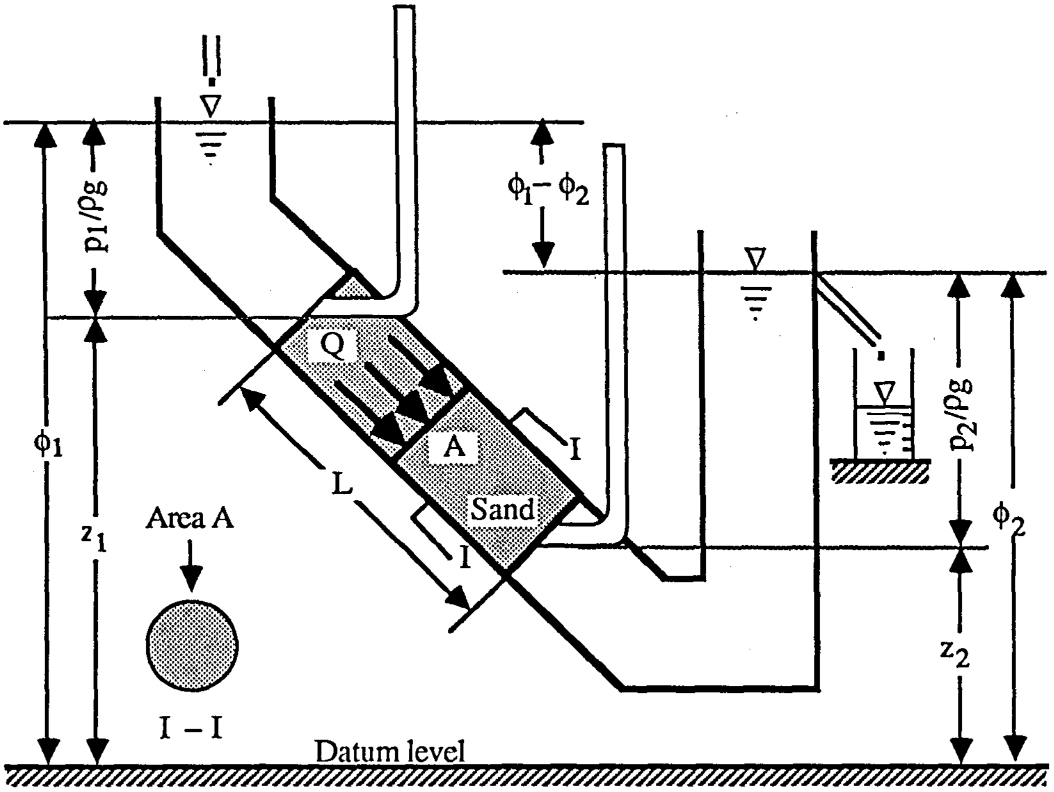

**Figure 10–2** Flow of water through a cylindrical porous body inclined to the vertical

### 10.2.2 Darcy Velocity

The flow defined by Equations (10.1) or (10.2) is the total flow through the area A. As this area may vary from one situation to the next, it would make sense to use a more objective quantity. Such a quantity is the specific discharge or Darcy *velocity* defined as the volume of water flowing per unit time through a unit cross-sectional area *normal* (perpendicular) to the flow. The Darcy velocity can be expressed, through Equation (10.2), as

$$q = -\frac{K(\phi_2 - \phi_1)}{L}. \tag{10.3}$$

As defined here, the term Darcy velocity is to be interpreted as a *flux* and not a velocity. The reason for the name Darcy velocity can probably be traced to the fact that its physical dimensions,

$$[q] = [L^3.L^{-2}.T^{-1}] \equiv [L.T^{-1}],$$

is that of a velocity. Nevertheless, the term is so entrenched in various branches of the literature on porous flow, that it will also be used here, but then only in the sense defined by Equation (10.3), or its generalization discussed below.

### 10.2.3 Seepage Velocity

As illustrated by the preceding discussion, the term velocity, when applied to fluid flow, can be quite misleading if not defined in a precise manner. Strictly speaking, the term velocity should really be applied only to the individual fluid molecules, where it can be defined as the time rate of change in the position of a particular molecule. However, when interest is centred not on a single molecule, but the fluid as a whole, this definition becomes meaningless. This difficulty is avoided in fluid mechanics by introducing a *control volume* with cross-section, A, perpendicular to the direction of flow (see Figure 10–3). The *flow velocity* is then defined as the volume of fluid which passes through A per unit time. If Q again represents the volume of fluid passing through A per unit time, the flow velocity is given by

$$v_f = \frac{Q}{A}. \tag{10.4}$$

Viewed from the physical point of view, the flow velocity can be regarded as the distance through which the cross-section C has moved per unit of time.

In the case of a porous medium, flow is restricted to that part of the medium which actually contains fluid. This implies that only a part of the area A, given by the product of A and the surface porosity of the medium ($A^*$ in Figure 10–3), will be active in transmitting the fluid. Since the surface porosity is numerically equal to the volumetric porosity (see Section 9.1), the flow or *seepage velocity* in a porous medium can be defined as

$$v = \frac{Q}{\varepsilon A},$$

or using Equations (10.3) and (10.4)

$$v = \frac{q}{\varepsilon}. \tag{10.5}$$

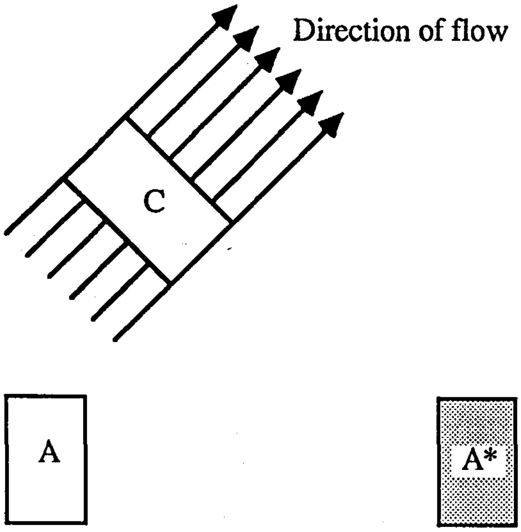

**Figure 10–3** Definition of a fluid control volume, C, and its cross-section, A, as well as the corresponding cross-section A* for a porous medium

The definition of seepage velocity in Equation (10.5) clearly applies only in the case where the porous medium is fully saturated, so that all the interstices are filled with the fluid. Flow in an unsaturated porous medium can be treated likewise by the introduction of a surface moisture content $\theta_a$. By using the same arguments as in Section 9.2.1, it can be shown that $\theta_a$ must be numerically equal to the volumetric moisture content $\theta$. However, since

$$\lim_{\theta \to \theta_S} \theta \equiv \varepsilon,$$

where $\theta_S$ is the saturated moisture content, the seepage velocity can, in general, be defined as

$$v = \frac{q}{\theta} = -\frac{K(\phi_2 - \phi_1)}{L\theta}. \qquad (10.6)$$

### 10.2.4 Validity of Darcy's Law

Darcy's law has been used above as if it is universally applicable, while in principle it should only be applied to situations similar to those for which it has been derived. Various attempts have consequently been made to establish the validity of this law [Scheidegger (1974), Bear (1979)]. One of the most recent of these experiments being that of Dybbs and Edwards (1984) who used laser anemometers and flow visualization techniques to study the flow through porous media, consisting of plexiglass beads and pyrex glass rods.

In these experiments, it is usual to compare two dimensionless numbers, one related to the piezometric head difference, $(\phi_2 - \phi_1)$ in Equation (10.2), and the other to either the Darcy or seepage velocities. Following Ergun (1952), Dybbs and Edwards (1984) used for this purpose a modified friction factor and Reynolds number, defined respectively by

$$\psi^* = \frac{\Delta p d(1-\varepsilon)}{L\varepsilon\rho v^2} \text{ and } Re^* = \frac{\rho v d\varepsilon}{\mu(1-\varepsilon)}$$

where

$\rho$ = the density of the fluid [M.L$^{-3}$]
$\mu$ = the dynamic viscosity of the fluid [M.L$^{-1}$.T$^{-1}$]
$\varepsilon$ = the porosity of the medium [M$^3$.M$^{-3}$]
$v$ = the seepage velocity defined by Equation (10.5) [L.T$^{-1}$]
$g$ = the acceleration of gravity [L.T$^{-2}$]
$\Delta p$ = $(\phi_2 - \phi_1)/\rho g$ [L]

and d and L are lengths characteristic of the pore diameter and distance travelled by a fluid molecule before colliding with the porous medium.

It is easy to show that for Darcy's law to be valid, $\psi^*$ must be related to $Re^*$ through an equation of the form

$$\psi^* = \frac{\text{const}}{Re^*}.$$

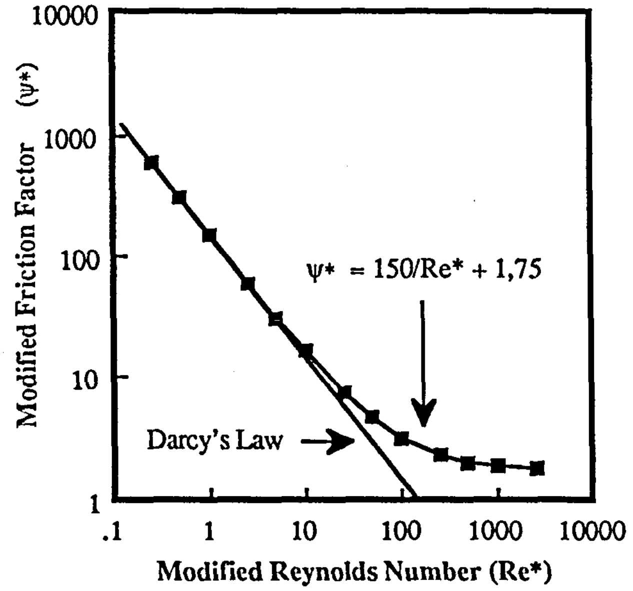

**Figure 10–4** Relation between the modified friction factor and Reynolds number reproduced from Dybbs and Edwards (1984)

As shown by the results of Dybbs and Edwards (1984), reproduced schematically in Figure 10–4, this is true over only part of the domain. In fact, they were able to distinguish four flow regimes in a porous medium. These are:

(a) **Darcy or creep flow,** where the flow is dominated by viscous forces and the velocity distribution is determined by the local geometry. This regime exists for flows with an $Re^* < 1$, but may extend to $1 \leq Re^* < 10$.

(b) **Inertial flow,** which persists from Darcy flow to an $Re^* \sim 150$. This flow is characterized by a steady growth in boundary layers that begin to appear near the solid boundaries of the pores at $Re^* = 1$.

(c) **Unsteady laminar flow,** observable as oscillations in the form of travelling waves, with distinct periods, amplitudes and growth rates, that appear in the pores themselves. At $Re^* \sim 250$ vortices begin to form which persist to $Re^* \sim 300$.

(d) **Chaotic flow,** which qualitatively resembles turbulent flow. This type of flow has been observed from Reynold's numbers of ~ 300 onwards.

As has been observed by [Bear (1979)], the last three types of porous flow only occur at conditions not usually observed under natural conditions. In the discussion to follow, these flows will consequently be neglected and the discussion restricted to flows that satisfy Darcy's law.

## 10.3 HYDRAULIC CONDUCTIVITY AND PERMEABILITY

The proportionality constant K, introduced in Equation (10.1), relates the volume of fluid passing through a given surface area with the difference in piezometric head. It may thus be considered as an indicator of how easy a fluid can flow through a porous material. For this reason, K is referred to as the *seepage conductivity* [Scheidegger (1974)] or more generally *hydraulic conductivity*. This characterization of fluid flow in a porous medium is not always satisfactory, as K depends on both the porous medium and fluid in combination. A more useful representation would be one where K can be factored into two, or more factors, which measure the influences of medium and fluid separately. As has been shown by Nutting (1930), this can be achieved by relating the hydraulic conductivity to a new parameter k, known as the *permeability* of a porous medium, through the equation

$$K = \frac{k\rho g}{\mu} \qquad (10.7)$$

where, as before,

| | | | |
|---|---|---|---|
| $\rho$ | = | the density of the fluid | $[M.L^{-3}]$ |
| $\mu$ | = | the dynamic viscosity of the fluid | $[M.L^{-1}.T^{-1}]$ |
| $g$ | = | the acceleration of gravity | $[L.T^{-2}]$ |

Since K has the dimensions $[L.T^{-1}]$ [see Equation (10.1)], k has the dimensions $[L^2]$. The two parameters thus differ in both the mathematical and physical sense and should *never* be used interchangeably.

The permeability has thus far been interpreted as an ordinary number or *scalar* quantity. This will only be true if the porous medium is either *homogeneous or uniform*, i.e. the material properties of the medium do not change from point to point, or *heterogeneous*, where the material properties are functions of the space coordinates. For a homogeneous medium, k will be a constant independent of the position in the medium and for a heterogeneous medium a function of position. However, there are many materials for which the material properties not only depend on the position within the medium, but also on the direction in which they are measured. Materials which behave in this way are said to be *anisotropic* in nature and their material properties have to be denoted by tensors.

Many of the geological formations present in the earth's subsurface, particularly those bearing fluids (e.g. sedimentary deposits), were formed by the flow of water and/or magma, which were driven by direction dominated forces. It is thus possible that in these formations the pore connections are directionally orientated, which means that the material may be more conducive to fluid flow in one direction than in the others. As noted above, k can be considered as a measure of the ease with which a fluid can flow through a porous medium. The permeability and hydraulic conductivities of such formations will, therefore, not be ordinary scalars but tensors. To account for their tensorial character, the permeability and hydraulic conductivity will, henceforth, be denoted in the tensorial notation as $\underline{k}$ and $\underline{K}$, respectively.

## 10.4 GENERALIZATION OF DARCY'S LAW

### 10.4.1 Saturated Flow

Darcy's law, given in Equation (10.3), has been derived for a fluid with constant density ρ that percolates through a saturated horizontal bed of finite thickness, L. In this form, the law is clearly very restrictive. A more satisfactory law should not only take care of the tensorial character of the hydraulic conductivity, but also of unsaturated flow. For the present, the discussion will, however, be restricted to saturated flow.

Assuming for the present that K is a scalar, the most natural way to generalize Darcy's law would be to cast it in differential form rather than the algebraic form of Equation (10.3). Unfortunately, there is no *a priori* way to achieve this. One possibility that presents itself is to change q into a three-dimensional vector q and replace the piezometric head difference by the head gradient to obtain the form

$$q = -K\nabla\phi = -\frac{k\rho g}{\mu}\nabla\phi. \qquad (10.8)$$

However, Darcy's experiment does not tell us what will happen if K (or k, ρ and μ) is a function of the spatial dimensions. In this case, the possibility exists that one should really include K under the gradient operator. Thus, Darcy's law may well be of the form

$$q = -\nabla(K\phi). \qquad (10.9)$$

It will never be possible to distinguish between these two forms of Darcy's law as long as experiments are performed with constant viscosity fluids and homogeneous porous media. Fortunately, such a critical real experiment needs not be performed, as a rather simple thought experiment will do [Scheidegger (1974)]. Consider for this purpose a porous medium subject to a constant piezometric head, but with a hydraulic conductivity that varies linearly across the medium. If Equation (10.9) is valid, there would be flow across the medium – a completely unthinkable situation. Equation (10.9) must, therefore, be wrong and Equation (10.8) correct.

With the differential form of Darcy's law established, it would seem natural that the tensorial character of the hydraulic conductivity can be taken into account by simply replacing the scalar K in Equation (10.8) by its equivalent tensor $\underline{K}$ to obtain the generalized Darcy law

$$q = -\underline{K}\nabla(\phi). \tag{10.10}$$

That this generalization of Darcy's law does indeed make sense can be demonstrated as follows.

It follows from the definition of the scalar product of two vectors that, if θ denotes the angle between the vectors q and J [$\equiv -\nabla(\phi)$], then (see Figure 10–5)

$$\cos\theta = \frac{q \bullet J}{qJ}. \tag{10.11}$$

For a scalar K, $q \bullet J = KJ \bullet J = KJ^2 = qJ$ and the two vectors are co-linear, while if K is a tensor with principal components $\{K_x, K_y, K_z\}$

$$\cos\theta = \frac{K_xJ_x^2 + K_yJ_y^2 + K_zJ_z^2}{qJ}. \tag{10.12}$$

If **n** is a unit vector in the direction of q, the projection of **J** on **n**, $J_n$, can be expressed, through Equation (10.10), as

$$J_n = n \bullet J = J\cos\theta = n \bullet \underline{K}^{-1}q = n \bullet \underline{K}^{-1}nq = K_n^{-1}q, \tag{10.13}$$

where $\underline{K}^{-1}$ is the inverse of $\underline{K}$ as defined in Section (2.4) and

$$K_n = \frac{1}{n \bullet \underline{K}^{-1}n},$$

is known as the *'directional hydraulic conductivity' in the direction of* q. If cosθ in Equation (10.13) is replaced by its explicit expression, given in Equation (10.12), the directional hydraulic conductivity can also be expressed as

$$K_n = \frac{q}{J_n} = \frac{q}{J\cos\theta} = \frac{q^2}{K_xJ_x^2 + K_yJ_y^2 + K_zJ_z^2}. \tag{10.14}$$

Let $\beta_1$, $\beta_2$, and $\beta_3$ now represent the angles between q and the three principal axes of $\underline{K}$ (see Figure 10–5). Then

$$q_x = K_x J_x = q\cos\beta_1, \quad q_y = K_y J_y = q\cos\beta_2, \quad q_z = K_z J_z = q\cos\beta_3,$$

which, when substituted in Equation (10.14), yields

$$\frac{1}{K_n} = \frac{\cos^2\beta_1}{K_x} + \frac{\cos^2\beta_2}{K_y} + \frac{\cos^2\beta_3}{K_z} \tag{10.15}$$

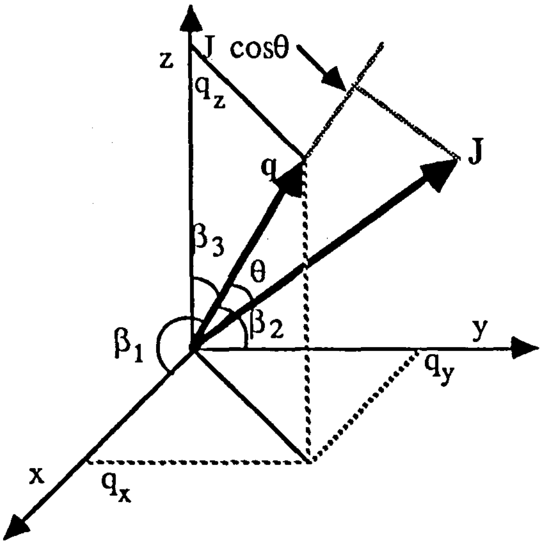

**Figure 10–5** Graphical illustration of the vectors q and J

Any vector **r**, co-linear with **q**, can always be expressed in terms of the unit vector **n**, introduced above as **r** = r**n**. Since ($\cos\beta_1$, $\cos\beta_2$, $\cos\beta_3$) are, by definition the components of

$$\mathbf{n} = \mathbf{i}x + \mathbf{j}y + \mathbf{k}z,$$

Equation (10.15) can also be written as

$$\frac{r^2}{K_n} = \frac{x^2}{K_x} + \frac{y^2}{K_y} + \frac{z^2}{K_z},$$

or if **r** is chosen as the vector with magnitude $(K_n)^{1/2}$,

$$1 = \frac{x^2}{K_x} + \frac{y^2}{K_y} + \frac{z^2}{K_z}.$$

The latter of these two equations is the canonical form of the equation for an ellipsoid in the x,y,z coordinate system. From this follows the very important result:

> If the directional hydraulic conductivity is measured for flow in all directions at a point in an anisotropic porous medium, the graph of its inverse square root as a function of the direction cosines of the normal vector n with respect to the principle axes of $\underline{K}$ is an ellipsoid. The axes of the ellipsoid is in the direction of the principal axes of $\underline{K}$; their length being equal to the square root of the principal hydraulic conductivities.

The simplest experiment to demonstrate the tensorial character of the permeability is to cut a cube (or sphere) from a geological formation and measure the directional permeability across all its faces. If the measured permeabilities are not the same across all the faces and also differ between cubes taken from the same rock, but at different orientations, there is a strong indication that the permeability is a tensor. That this is indeed the case has been confirmed by numerous experiments [Scheidegger (1974)].

The tensorial character of the permeability and hydraulic conductivity can perhaps be best visualized by drawing polar graphs, such as the one shown in Figure 10–6. If $K_n$, or (as in Figure 10–6) the corresponding *directional permeability* $k_n$ is used as the length dimension, the curve obtained more or less resembles that of the number 8, while a perfect ellipsoid (ellipse in two dimensions) is obtained, if $k_n^{-1/2}$ (or $K_n^{-1}$) is used as the unit of length.

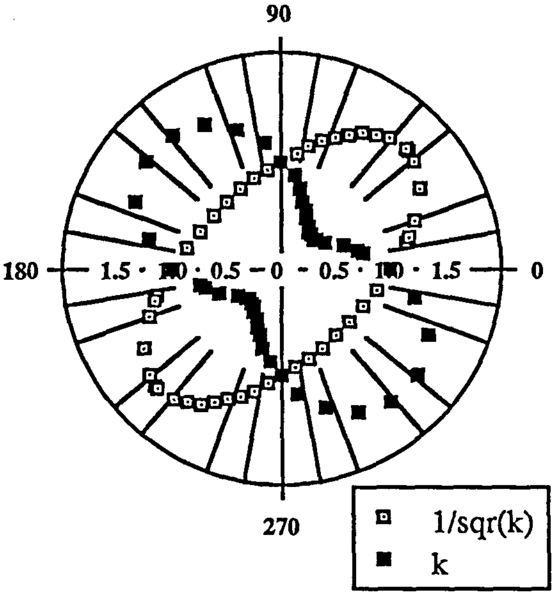

**Figure 10–6** Polar graph of the permeability as measured for a porous medium

### 10.4.2 Unsaturated Flow

As shown in Section 9.4, there is, from the mathematical point of view, no difference between the piezometric head distribution in saturated and unsaturated flow, provided that one is willing to accept that the pressure is negative in unsaturated flow. With this in mind, one would expect that Darcy's law will also be applicable in unsaturated flow. However, it must be kept in mind that in unsaturated flow, fluid will be drawn from zones where the capillary menisci are less curved to zones where they are more curved. In other words, fluid will flow from regions with small to regions with large suctions.

Unsaturated flow can only occur if the fluid molecules move in pores that remain filled at the given suctions and the fluid films that surround partially drained pores (Figure 10–4). The Darcy velocity for unsaturated flow should, therefore, be less than that of saturated flow and steadily decrease as the moisture content of the porous medium decreases. However, this implies that the unsaturated hydraulic conductivity, for a given porous material, should be smaller than its saturated hydraulic conductivity and, moreover, *that it should decrease as the moisture content decreases.* That this is indeed the case can be seen by considering two samples of the same porous material, one less saturated than the other, but subjected to the same absolute piezometric gradients. *The unsaturated hydraulic conductivity of a porous medium, therefore, depends on the moisture content or the piezometric head of the material.* Following Richards (1931), Darcy's law for unsaturated flow is thus conventionally expressed in the form

$$q = -K(\psi)\nabla\phi \qquad (10.16)$$

or, if the tensorial character of K is taken into account, as

$$q = -\underline{\mathbf{K}}(\psi)\nabla\phi. \qquad (10.17)$$

The fact that $\psi$ is a highly non-linear relation of the moisture contents (see Section 9.5), makes it sometimes difficult to distinguish between the tensorial and non-linear character of $\underline{\mathbf{K}}$. This is particularly true in subsurface unsaturated flow, which is dominated by the force of gravity, with the result that the principal direction of flow is vertically downwards. In practical applications of unsaturated flow, Darcy's law is, therefore, frequently limited to the use of Equation (10.16), or a diagonal representation of $\underline{\mathbf{K}}$.

## 10.5 SEMI-EMPIRICAL EXPRESSIONS FOR THE PERMEABILITY

### 10.5.1 General

Because of its importance in porous flow, numerous attempts have been made to derive expressions for the hydraulic conductivity, or more appropriately the permeability, from the general properties of a porous medium. In the following two sections, a few of these attempts will be reviewed. However, the reader is warned that, because of its implicit complex structure, idealizations of the porous medium have to be used in deriving them. None of these expressions are consequently universally applicable, unless verified experimentally. This applies in particular to the parameters appearing in these expressions, hence the designation semi-empirical expressions.

The simplest representation of a porous medium is through a bundle of parallel capillary tubes, all of the same uniform diameter r (see Figure 10–7). The majority expressions for the permeability available in the literature, are consequently based on some form of this idealized model.

The main advantage of the parallel capillary tube model is that one can use the Hagen-Poisseuille law, discussed in Section 9.4, to derive expressions for the volumetric rate and velocity of flow. For example, it follows from Equation 9.14 that the discharge rate through a single capillary tube is

$$Q = -\frac{\pi\rho g}{8\mu} r^4 D\phi(s), \qquad (10.18)$$

and the velocity of flow

$$v = -\frac{\rho g}{8\mu} r^2 D\phi(s). \tag{10.19}$$

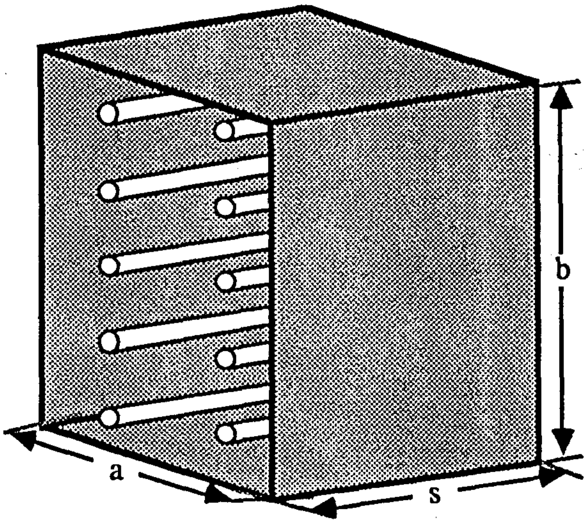

**Figure 10–7** The uniform capillary tube representation of a porous medium

A comparison of these equations with Darcy's law [see Equation (10.3)] suggests that the permeability for a real porous medium will depend on some measure of the pore radius. Keeping in mind that the flow can only take place through the tortuous paths of interconnected pores, this dependence is not unexpected. However, as will be shown below, the pore size is not the only factor contributing to the permeability.

### 10.5.2 Saturated Flow

The simplest expression for the saturated permeability follows directly from the representation of a porous medium by the bundle of capillary tubes in Figure 10–7. The Darcy velocity per unit cross-sectional area (normal to the flow direction), with N of these tubes, can be expressed through Equation (10.18) as

$$q \equiv \frac{Q}{ab} = -\frac{N\pi ab\rho g}{8\mu ab} r^4 D\phi(s) = -\frac{N\pi\rho g}{8\mu} r^4 D\phi(s). \tag{10.20}$$

The porosity of this medium is, by definition, of the form

$$\varepsilon = \frac{N\pi r^2 abs}{abs} = N\pi r^2, \tag{10.21}$$

On substituting this value into Equation (10.20) and comparing the result with Darcy's law [Equation (10.3)], the permeability of such a bundle of capillary tubes is seen to be given by

$$k = \frac{\varepsilon r^2}{8}. \tag{10.22}$$

Before Equation (10.22) can be used to compute k for a real porous medium, one must be able to relate the parameters that appear in it to the medium. Although $\varepsilon$ can be considered as well-defined for a porous medium, there is no obvious measure with which $r^2$ can be connected. Following Scheidegger (1953), this difficulty can be avoided by using a representation in which the capillary tubes are orientated in arbitrary directions with radii that vary continuously up to a maximum, $r_{max}$. If $\varepsilon$ denotes the porosity of this hypothetical medium (the volume of voids per unit volume of porous medium), a piece of the medium with unit cross-sectional area perpendicular to the x-axis in a cartesian coordinate system and length $\Delta s$ will, therefore, contain a volume

$$dV_v = \varepsilon\Delta s.$$

of voids, of which a certain fraction, $\beta$ (usually taken as 1/3), will be contributed by pores directed parallel to the x-axis. The volume of voids attributable to pores with radii between r and r+dr, which will contribute to the flow in the x-direction, can thus be expressed as

$$dV_v^r = \beta\varepsilon\Delta s\alpha(r)dr.$$

where $\alpha(r)$ is the fractional pore-size distribution function (see Section 4.3.2) and their frontal areal porosity as

$$\varepsilon_a(r) = \beta\varepsilon\alpha(r)dr. \tag{10.23}$$

By using the definition of seepage velocity in Equation (10.5), the Darcy velocity through this unit area of capillary tubes must be of the form

$$dq = \varepsilon_a(r)v(r) = \beta\varepsilon v(r)\alpha(r)dr.$$

where v(r) is the velocity through a single capillary tube with radius r in Equation (10.19). The total Darcy velocity through the unit cross-sectional area is thus

$$q = -D\phi(x)\frac{\varepsilon\beta\rho g}{8\mu}\int_{r_{min}}^{r_{max}} r^2\alpha(r)dr.$$

On comparing this equation with Darcy's law [Equation (10.3)] and taking the definition of permeability in Equation (10.7) into account, one obtains

$$k = \frac{\varepsilon\beta}{8}\int_{r_{min}}^{r_{max}} r^2\alpha(r)dr \equiv \frac{\varepsilon\beta}{8}<r^2>, \tag{10.24}$$

where

$$<r^2> = \int_{r_{min}}^{r_{max}} r^2\alpha(r)dr,$$

the mean square pore radius is now a well-defined quantity.

The expression for k in Equation (10.24) is still based on the straight capillary tube hypothesis. To account for the tortuous nature of a real porous medium, Scheidegger

(1974) introduced the concept of a tortuousity factor T and obtains

$$k = \frac{\varepsilon\beta}{8T^2}\langle r^2\rangle. \qquad (10.25)$$

As shown in Section 9.4, the flow of fluid in a porous medium is hampered by its interaction with the solid matrix. A good expression for the permeability should thus not only concentrate on the flow path [as was done in deriving Equations (10.22) – (10.25)], but also include a measure of the solid area exposed to the flow.

To derive such an expression, consider once again the bundle of capillary tubes in Figure 10–7. The total volume of solids, $V_s$, per unit cross-sectional area (perpendicular to the flow) in the porous medium can be expressed through Equations (9.1) and (9.2) in the form

$$V_s = V(1 - \varepsilon),$$

where V (= s) is the total volume in a unit cross-sectional area. Substitution of this expression into Equation (10.20) yields

$$q = -\frac{\rho g}{2\mu}\varepsilon\left[\frac{V_s\varepsilon}{A_s(1-\varepsilon)}\right]^2 D\phi(s)$$

where use was made of the expression for the porosity in Equation (10.21) and

$$A_s = 2N\pi rs$$

is the area of solids exposed to the flow. The permeability of the hypothetical porous medium can thus also be expressed as

$$k = \frac{\varepsilon}{2}\left[\frac{V_s\varepsilon}{A_s(1-\varepsilon)}\right]^2. \qquad (10.26)$$

It is interesting to note that the expression for the permeability in Equation (10.26), first suggested by Childs and Collis-George (1950), is of the same form as the well-known Fair-Hatch formula

$$k = \frac{1}{\beta}\left[\frac{\varepsilon^3}{(1-\varepsilon)^2}\right]\left[\frac{\alpha}{100}\sum_m \left\{\frac{P_m}{d_m}\right\}^2\right]^{-1} \qquad (10.27)$$

often used to determine the permeability for sands [Bear (1979)], where β is a packing factor (found experimentally to be about 5), α a sand shape factor (varying from 6,0 for spherical grains to 7,7 for angular ones), $P_m$ the percentage of sand held between adjacent sieves and $d_m$ the geometric mean diameter of adjacent sieves as obtained from a sieve analysis (see Section 9.3.1).

A fairly detailed analysis [Anonymous (1985)] has shown that Equation (10.27) is a quite useful approximation for the permeability of unconsolidated alluvial deposits. The possibility thus exists that Equation (10.26) may be useful for the approximation of permeabilities in hard-rock formations, where Equation (10.27) does not apply. However, such an application would require that the quantities $V_s$ and $A_s$ in Equation (10.26) be measured on a more regularly basis than is done at present. As pointed out by Hillel (1982), this may not be a bad practice, for these parameters are more descriptive of a porous medium than the 'structure parameters' (e.g. grain-size distribution and pore diameters) at present in use.

### 10.5.3 Unsaturated Flow

As shown in Section 9.4, the larger pores will drain more quickly than the smaller ones in unsaturated flow. This suggests that the pore geometry will play an import role in any expression for the unsaturated permeability. Fortunately, as will be shown below, it is not too difficult to incorporate this aspect into an hypothetical capillary tube porous medium. Consider, therefore, once again the arbitrary capillary tube representation used in deriving the expression in Equation (10.24) for the saturated permeability.

The area (per unit cross-sectional area) covered by tubes with radii between $r_i$ and $r_i$+dr, obtained from Equation (10.23), is

$$dA_i = \beta_i \varepsilon \alpha(r_i) dr,$$

A cut perpendicular to the x-direction through the tube representation will exhibit two faces with similar areas $dA_i$. If one now regards a column of porous material as the random juxtaposition of these two faces, there will be pores of radii $r_i$ connected to pores of radii $r_j$. If $dA_i$ is the area covered by pores with radii between $r_i$ and $r_i+dr_i$ and $dA_j$ the area covered by pores with radii between $r_j$ and $r_j+dr_j$, the law of probabilities implies that the area $dA_{ij}$ covered by pores with radii $r_i$ and *connected* to pores with radii $r_j$ must satisfy

$$dA_{ij} = dA_i dA_j = \beta_i \beta_j \varepsilon^2 \alpha(r_i) \alpha(r_j) dr_i dr_j. \qquad (10.28)$$

Therefore, if an expression can be found for the velocity of the fluid through this area, the procedure used in deriving Equation (10.24) can again be used to derive an expression for the unsaturated permeability.

Following Mualem (1976), consider the two capillary tubes, shown in Figure 10–8, with radii $r_1$ and $r_2$ and lengths $s_1$ and $s_2$ proportional to their radii, i.e.

$$\frac{s_1}{s_2} = \frac{r_1}{r_2}. \qquad (10.29)$$

The volume of fluid flowing per unit time through the two tubes can be obtained directly from Equation (10.23) and is

$$Q_1 = -\frac{\pi\rho g}{8\mu}\left[\frac{\phi_1}{s_1}\right]r_1^4 \text{ and } Q_2 = -\frac{\pi\rho g}{8\mu}\left[\frac{\phi_2}{s_2}\right]r_2^4, \qquad (10.30)$$

where, $\phi_i$ is the drop in piezometric pressure across the length $s_i$ of the i-th tube and $Q_1 \equiv Q_2 \equiv Q$, if mass is to be conserved.

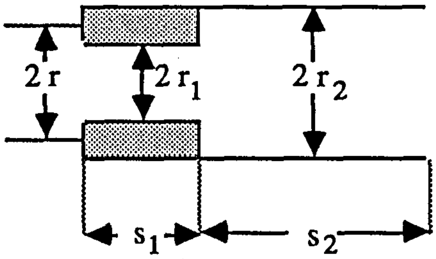

**Figure 10–8** A staggered capillary tube representation of a porous medium

It is interesting to compare the flow through these two tubes with that through an equivalent tube of radius r and length s, defined by the relation

$$Q = -\frac{\pi\rho g}{8\mu}\left[\frac{\phi}{s}\right]r^4$$

or, in its equivalent form,

$$r^4\phi = Cs$$

where $\phi = \phi_1 + \phi_2$, $s = s_1 + s_2$ and

$$C = \frac{8Q\mu}{\pi\rho g}.$$

If the $\phi_i$ $(i = 1, 2)$ in this equation is replaced with their equivalent values

$$\phi_i = \frac{Cs_i}{r_i^4} \quad (i = 1,\ 2),$$

from Equation (10.30), and the equivalency of volumes

$$r^2 s = r_1^2 s_1 + r_2^2 s_2,$$

as well as Equation (10.29) is used, one finds that

$$r^2 = r_1 r_2. \qquad (10.31)$$

Two capillary tubes which satisfy the identity in Equation (10.29), can thus always be replaced by an equivalent tube with radius r given by (10.31). This result shows that the velocity of flow through the equivalent tube

$$v_{12} = -\frac{\rho g}{8\mu} r_1 r_2 D\phi(x). \qquad (10.32)$$

obtained on substituting Equation (10.31) into Equation (10.19), can also be interpreted as the velocity through two tubes with radii $r_1$ and $r_2$ when connected as in Figure 10–8.

Since no special assumptions were made in deriving Equation (10.32), except for the relation between the length and radius of the tubes, the flow through the juxtaposed area element in Equation (10.28) can now be expressed as

$$dq_{ij} \equiv dA_{ij}v_{ij} = -\frac{\rho g}{8\mu}\beta_i\beta_j\varepsilon^2 D\phi(x) r_i r_j \alpha(r_i)\alpha(r_j)dr_i dr_j.$$

The assumption (see Section 4.3.2) that an unsaturated porous medium can be represented as a medium where all pores with radii $r_{min} < r$ are filled with fluid, allows one to express the rate of flow per unit cross-sectional area of $A_{ij}$ as

$$q(r) = -\frac{\rho g}{8\mu}\beta_i\beta_j\varepsilon^2 D\phi(x)\int_{r_{min}}^{r} r_i\alpha(r_i)dr_i \int_{r_{min}}^{r} r_j\alpha(r_j)dr_j$$

$$= -\frac{\rho g}{8\mu}(\beta\varepsilon)^2 D\phi(x)\left[\int_{r_{min}}^{r} r\alpha(r)dr\right]^2$$

where it was assumed that $\beta_i = \beta_j = \beta$. A comparison of this equation with Darcy's law, Equation (10.3), and Equation (10.7), shows that the unsaturated permeability must satisfy the equation

$$k(r) = -\frac{(\beta\varepsilon)^2}{8}\left[\int_{r_{min}}^{r} r\alpha(r)dr\right]^2 \tag{10.33}$$

It follows from the definition of $\varepsilon$ and $\alpha(r)$ in Chapter 9, that $\varepsilon\alpha(r)dr$ is the volume of voids occupied by pores with radii between r and r+dr per unit volume of porous material. Therefore, if all pores with radii between r and r+dr are filled with fluid, $\varepsilon\alpha(r)dr$ can be interpreted as the contribution of these pores to the moisture content of the medium, i.e.

$$\varepsilon\alpha(r)dr = d\theta.$$

Moreover, since the inner surface of a capillary tube can be considered as a curved surface with two radii of curvature, one with magnitude r and the other one infinite, the matric pressure in a capillary tube is of the form

$$\psi \equiv -p_c = \frac{\sigma}{r}$$

[see Equations (8.10) and (8.11)]. By using these expressions for $\psi$ and $\varepsilon\alpha(r)dr$, the unsaturated permeability in Equation (10.33) can be rewritten in the form

$$k(\theta) = \frac{(\beta\sigma)^2}{8}\left[\int_{\theta_r}^{\theta(r)} \frac{d\theta}{\psi}\right]^2 . \qquad (10.34)$$

where, $\theta_r$, is the residual moisture content defined by Equation (9.8). The quantity $\beta$, appearing in Equation (10.34), was introduced in Section 10.5.2 to account for the orientation of pores in the direction of flow. As not all pores contribute to the total flow in an unsaturated porous medium, it is natural to assume that $\beta = \beta(\theta)$. More specifically, it will be assumed that $\beta \propto (\theta - \theta_r)^\delta$, so that

$$k(\theta) = K_0(\theta - \theta_r)^\delta \left[\int_{\theta_r}^{\theta(r)} \frac{d\theta}{\psi}\right]^2 \qquad (10.35)$$

The importance of Equation (10.35) lies in the fact that it presents one with the possibility, at least in principle, to compute the unsaturated permeability from a knowledge of the moisture retention curve for a given porous medium. However, it contains two unknown constants, $K_0$, and $\delta$, that have to be determined first.

The determination of $K_0$ is quite straightforward. For, if Equation (10.35) is to be valid for all values of $\theta$, it must also be valid when $\theta \rightarrow \theta_s$, the saturated moisture contents. With this in mind, it is natural to introduce the *relative permeability*

$$k_r(\Theta) \equiv \frac{k(\Theta)}{k_s} = \Theta^\delta \frac{\left[\int_0^{\Theta} \frac{d\Theta}{\psi}\right]^2}{\left[\int_0^{\Theta} \frac{d\Theta}{\psi}\right]^2} \qquad (10.36)$$

where $\Theta$ is the reduced moisture content defined in Equation (9.12). The determination of $\delta$ is, on the other hand, not so simple. Detailed analyses of available soil moisture data by Mualem (1976) and Van Genuchten and Nielsen (1985), indicate that the value $\delta = 1/2$ is the most suitable choice for the soil types considered in their analyses. This value will consequently be adopted as a universal value applicable to all soils.

To illustrate the application of Equation (10.36), consider the Van Genuchten moisture retention curve, as defined in Equation (9.13). Solving this equation for $\psi = \psi(\Theta)$ and substituting the resulting expression into Equation (10.36) give

$$k_r(\Theta) = \sqrt{\Theta}\left[\frac{f(\Theta)}{f(1)}\right]^2$$

where,

$$f(\Theta) = \int_0^{\Theta} \left[\frac{x^{1/m}}{(1 - x^{1/m})}\right]^{1/n} dx$$

or, if the substitution $x = y^m$ is used,

$$f(\Theta) = m \int_0^{\Theta^{1/m}} [y^{m-1+1/n}(1 - y)^{-1/n}]dy.$$

The integral appearing in the previous equation is a particular form of the Incomplete Beta-function for which no closed solution is known in general. However, it is not difficult to show that closed form solutions do exist in case $\kappa = (m-1+1/n)$ is an integer. For the particular case $\kappa = 0$ (i.e., $m = 1 - 1/n$), one finds

$$f(\Theta) = 1 - (1 - \Theta^{1/m})^m$$

and because $f(1) = 1$,

$$k_r(\Theta) = \Theta^{1/2}[1 - (1 - \Theta^{1/m})^m]^2.$$

The determination of unsaturated hydraulic conductivity as a function of the pressure head, is one of the most difficult and time-consuming investigations in soil physics. The advantage of an expression, such as Equation (10.36), in any practical investigation of flow in the unsaturated zone, can thus not be emphasized enough.

# CHAPTER 11

# THE EQUATION OF FLUID MOTION

## 11.1 THE CONTINUITY EQUATION

Darcy's law relates the three basic quantities: discharge rate, $q(x,t)$, piezometric head gradient, $\nabla\phi(x,t)$ and hydraulic conductivity, $\underline{K}(x,t)$, to one another. Thus, if any two of these quantities are given at any moment in time, the third one can be calculated from Darcy's law. For example, if the hydraulic conductivity and discharge rate, $q(x_0,t)$ from a point source situated at $x_0$ in a porous medium are known, Darcy's law can be used to calculate $\nabla\phi(x_0,t)$ as a function of time. Although these quantities are important, the behaviour of $\phi(x,t)$ as a function of both x and t is of much more practical interest. What is thus needed, is an equation that describes the general motion of a fluid in a porous medium. How to derive such an equation is not immediately obvious, but since a fluid is just another form of matter (see Section 8.1), it must obey the universal law of mass conservation. It may thus be worthwhile first to derive a quantitative description of the law of mass conservation, better known as the *continuity equation for mass conservation.*

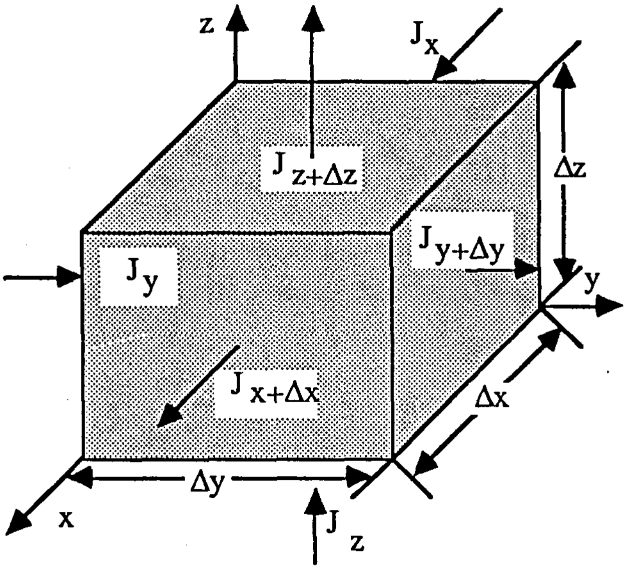

**Figure 11–1** Schematic representation of the mass fluxes across the sides of an elementary volume element in a porous medium

There are a number of methods that can be used to derive the continuity equation for mass conservation. However, it is more informative to derive the equation from elementary considerations. Consider, for this purpose an elementary volume element of a porous medium, fixed in space (see Figure 11–1). Fluid can enter and leave the element through any one of its sides, or sources and sinks that may be present. If the law of mass conservation is to be satisfied, any excess of fluid (arising from the possibility that more fluid flows into the element than leaving it) must obviously be stored in element.

A very convenient quantity to use in the description of fluid flow is the *mass flux,* defined as the mass that flow per unit area per unit time through a plane perpendicular to the direction of flow. Let

$$\mathbf{J}(x,t) = \mathbf{i}J_x(x,t) + \mathbf{j}J_y(x,t) + \mathbf{k}J_z(x,t)$$

denotes the total mass flux through the elementary volume element in Figure 11–1. During a short time interval $\Delta t$, a certain mass of fluid will enter the element through the face in the xz-plane at the origin, while another mass will leave it through the opposite face. Using the notation above and Taylor's theorem (see also Figure 11–1), the difference in mass entering and leaving the element can be expressed as

$$[(J_y - J_{y+\Delta y})\Delta x\Delta z]\Delta t = -D_yJ_y\Delta x\Delta y\Delta z\Delta t,$$

where terms in $(\Delta y)^2$ and higher have been dropped from the Taylor series expansion of $J_y$. Similar expressions obviously also hold for the x- and z-directions. The excess of mass inflow over outflow across the volume element is thus of the form

$$\Delta m = [-D_xJ_x - D_yJ_y - D_zJ_z]\Delta x\Delta y\Delta z\Delta t,$$

or if vector notation is used

$$\Delta m = -\nabla \bullet \mathbf{J}(x,t)\Delta x\Delta y\Delta z\Delta t. \qquad (11.1)$$

The formulation in Equation (11.1) only accounts for the flow of fluid across the volume element. In practical situations, fluid is often recharged to, or discharged from the medium. To account for this, let

$$\Delta Q(x,t) = f(x,t)\Delta x\Delta y\Delta z \qquad (11.2)$$

be the volume of fluid recharged to the volume element per unit of time. If $\rho$ denotes the density of the fluid, the mass recharged to the medium during the time $\Delta t$ can then be expressed as $\rho f(x,t)\Delta x\Delta y\Delta z$. On combining this expression with that in Equation (11.1), the total excess of mass inflow over outflow in the volume element, during the time interval $\Delta t$, is found to be

$$\Delta m = [-\nabla \bullet \mathbf{J}(x,t) + f(x,t)]\Delta x\Delta y\Delta z\Delta t. \qquad (11.3)$$

The quantity f(x,t), introduced in Equation (11.2), is known as the *strength* of the *source*. Implicit in this definition is the idea of a *point source*, i.e. a source with the dimensions of mathematical point. Although such a source cannot be realized physically, it is a very convenient idealization in the mathematical theory of fluid flow. With this in mind, the strength of a source can, in general, be defined by the equation

$$f(x,t) = \frac{\text{Volume of fluid entering a volume of porous material per unit time}}{\text{Volume of porous material}}$$

To account for either recharge or discharge, f(x,t) is taken as positive in the case of *sources* (recharge) and negative for *sinks* (discharge).

The fluid can obviously only obey the law of mass conservation if the excess fluid, given by Equation (11.3), is stored within the element. If $\theta$ denotes the moisture content of the medium at time t, the mass of fluid present in the element at that time can be expressed mathematically as $(\rho\theta)_t\Delta x\Delta y\Delta z$. The excess mass of fluid accrued in the element during the time $\Delta t$, is thus given by

$$[(\rho\theta)_{t+\Delta t} - (\rho\theta)_t]\Delta x\Delta y\Delta z = D_t(\rho\theta)|_t\Delta x\Delta y\Delta z,$$

after another application of Taylor's theorem. To satisfy the law of mass conservation, this excess of mass must equal that given in Equation (11.3). Hence,

$$D_t(\rho\theta)_t\Delta x\Delta y\Delta z\Delta t = -[\nabla\bullet J(x,t) + \rho f(x,t)]\Delta x\Delta y\Delta z\Delta t.$$

Since $\Delta t$ is finite and the elementary volume element arbitrary, this equation may be divided throughout by the product $\Delta P = \Delta x\Delta y\Delta z\Delta t$ ($\neq 0$) to obtain

$$D_t[\rho\theta(x,t)] = -\nabla\bullet J(x,t) + \rho f(x,t). \qquad (11.4)$$

This equation, better known as the *continuity equation*, is nothing else than a mathematical expression for the law of mass conservation.

Expressed in physical terms, Equation (11.4) says that the time rate of change in mass per unit volume of porous material must be accompanied by a spatial variation in the mass flux through the sides of the unit volume and the volume of fluid entering (or leaving) it from external sources or sinks. The continuity equation is thus also an abstract formulation of the motion of fluids through a given porous medium.

## 11.2 THE GENERAL EQUATION OF FLOW IN A POROUS MEDIUM

The continuity equation, as defined in Equation (11.4), contains the as yet unknown mass flux term J(x,t). Since Darcy's velocity (see Section 10.2) gives the volume of fluid that flows across a unit surface per unit time, it is tempting to define the mass flux as

$$J(x,t) \equiv \rho q(x,t) = -\rho\underline{K}(x,t)\nabla\phi(x,t). \qquad (11.5)$$

However, it must be remembered that Equation (11.4) was derived by assuming that the volume element remains *fixed* and the fluid moves *through* it. (In hydrodynamics, this is called the *Eulerian approach* to distinguish it from the *Lagragian approach*, where a fixed volume of fluid is followed as it moves through the porous medium.) But, Darcy's law, as derived in Section 10.2, really applies to a coordinate system *fixed with respect to the porous medium itself*, which means that it is valid *relative* to a coordinate system fixed to the porous medium. Equation (11.5) cannot, therefore, be considered as a suitable definition of the mass flux in Equation (11.4), *unless the porous medium is stationary.* Since a porous matrix is not rigid (see Section 9.6), the matrix may be deformed at any time. In other words, the matrix can be set in motion relative to the Eulerian coordinate system used in deriving Equation (11.4).

To account for any motion of the porous matrix relative to a fixed coordinate system, let $v_m(x,t)$ denotes the velocity of the porous matrix relative to the fixed coordinate system and $v_r(x,t)$ the velocity of the fluid relative to the porous medium respectively. The velocity of the fluid relative to the fixed coordinate system is then given by

$$v(x,t) = v_r(x,t) + v_m(x,t).$$

By following the same line of reasoning used in deriving Darcy's velocity, the mass flux relative to the fixed coordinate system can then be defined as

$$q(x,t) \equiv \theta\ v(x,t) = \theta v_r(x,t) + \theta v_m(x,t),$$

or, after applying Darcy's law

$$q(x,t) = -\underline{K}\nabla\phi(x,t) + \theta v_m(x,t). \qquad (11.6)$$

The most general equation governing the *simultaneous* motion of the fluid and porous medium is thus of the form

$$D_t[\rho\theta(x,t)] = \nabla\bullet[\rho\{\underline{K}\nabla\phi(x,t) - \theta v_m(x,t)\}] + \rho f(x,t). \qquad (11.7)$$

where use has been made of Equations (11.5) and (11.6) to replace the mass flux, J(x,t), in Equation (11.4).

Although there are phenomena in subsurface flow where the displacement of the porous medium is important (for example those related to land subsidence), many phenomena can be analysed in terms of a fixed medium. The discussion to follow will, therefore, be limited to the equation for non-deformable porous media

$$D_t[\rho\theta(x,t)] = \nabla\bullet[\rho\{\underline{K}\nabla\phi(x,t)\}] + \rho f(x,t). \qquad (11.8)$$

Equation (11.8) is a three-dimensional partial differential equation, which contains different dependent variables on its left- and right-hand sides. While such a formulation may be quite useful in the numerical solution of the equation [Allen (1985)], it hampers a theoretical investigation. Fortunately, the moisture retention curve [see Equation (9.11)] can be used to express either $\theta$ in terms of $\phi$ , or $\phi$ in terms of $\theta$, whichever representation one prefers. Because $\theta$ is defined in terms of the pore space (see Section 9.2.2), $\theta(x,t)$ is in general a discontinuous function of the space coordinates x. The piezometric head depends, on the other hand, only on the pressure distribution and elevation [see Equation (8.10)]. Since pressure is a fluid property and fluid a continuous distribution of matter, $\phi(x,t)$ must be a continuous function of space. From a theoretical point of view, it would thus be advantageous to base the discussion of fluid flow in a porous medium on the $\phi$-representation. As will be shown below, this choice has another advantage in that it allows one to derive a unified theory for flow in a porous medium.

By using the definition of the moisture saturation $S_w$ in Equation (9.4) and keeping in mind that the porosity is a function of the pressure (see Section 9.6), the left-hand side of Equation (11.8) can be rewritten as

$$\begin{aligned} D_t[\rho\varepsilon S_w(x,t)] &= S_w(x,t)D_p[\rho\varepsilon]D_tp(x,t) + \rho\varepsilon D_p[S_w(x,t)]D_tp(x,t) \\ &= [\varepsilon S_w(x,t)D_p(\rho) + \rho S_w(x,t)D_p(\varepsilon) + \rho\varepsilon D_p\{S_w(x,t)\}]D_tp(x,t). \end{aligned} \tag{11.9}$$

Substitution of the expressions for the compressibility coefficients of a fluid and porous matrix [see Equations (8.4) and (9.20)] into Equation (11.9) now yields

$$D_t[\rho\varepsilon S_w(x,t)] = \rho S_w(x,t)[\varepsilon\beta + (1-\varepsilon)\alpha]D_tp(x,t) + \rho\varepsilon D_p\{S_w(x,t)\}]D_tp(x,t).$$

If it is assumed that $\rho$ is only a function of the pressure (as is the case with fluids that do not contain large quantities of dissolved solids, see the discussion in Section 8.2), Equation (8.10) can be invoked to express the time derivative in this equation in the form

$$D_tp(x,t) = D_t\phi(x,t)D_\phi p(x,t) = \rho g D_t\phi(x,t).$$

With these assumptions, Equation (11.9) can be rewritten in the form

$$\begin{aligned} D_t[\rho\varepsilon S_w(x,t)] &= \rho^2 g S_w(x,t)[\varepsilon\beta + (1-\varepsilon)\alpha]D_t\phi(x,t) + \rho^2 g\varepsilon D_p\{S_w(x,t)\}]D_t\phi(x,t) \\ &= \rho[S_w\{\rho g(\varepsilon\beta + (1-\varepsilon)\alpha)\} + \varepsilon D_\phi\{S_w(x,t)\}]D_t\phi(x,t) \\ &= \rho[S_wS_0 + C(\phi)\}]D_t\phi(x,t), \end{aligned} \tag{11.10}$$

where,

$$S_0 = \rho g[\varepsilon\beta + (1-\varepsilon)\alpha] \tag{11.11}$$

is known as the *specific storativity* of the medium with respect to the piezometric head and

$$C(\phi) = \varepsilon D_\phi\{S_w(x,t)\} \tag{11.12}$$

just another expression for the moisture capacity, defined in Equation (10.14). Substitution of Equation (11.10) into Equation (11.8) yields

$$\rho[S_wS_0 + C(\phi)]D_t\phi(x,t) = \nabla\bullet[\rho\{\underline{\mathbf{K}}\nabla\phi(x,t)\}] + \rho f(x,t). \tag{11.13}$$

This is the most general equation governing the motion of a fluid in a non-deformable porous medium, with the piezometric head as dependent variable.

Assuming that the fluid density and gravitational acceleration are constant, Equation (11.10) shows that $S_0$ is a function of the compressibility coefficients, $\alpha$ and $\beta$, of the medium and fluid. Values of $\beta$ are well-known and tabulated in various texts on fluid mechanics and related publications [see e.g. Weast (1969), *Handbook of Physics and Chemistry*.]. The value of $\alpha$ depends, on the other hand, primarily upon the change in $\varepsilon$, created by a shift of the granules which forms the porous medium. Therefore, it is unreasonable to expect that $\alpha$ will remain constant from one porous medium to the next, particularly when applied to the inhomogeneous geological formations which form the earth's upper surface. However, since $\alpha(1 - \varepsilon)$ is always larger than or equal to zero, Equation (11.11) can be used to calculate a lower bound for $S_0$. By using the lower bounds on the porosities in Table 9–1 and the value of $\beta$ (= $4{,}74.10^{-10}$ $m^2.N{-}1$ at 20°C), lower bounds for $S_0$ have been calculated for the same materials and listed in Table 11–1.

**Table 11–1** Lower bounds for the specific storativity of the geological formations frequently encountered in groundwater ($\rho = 1\ 000$ kg.m$^{-3}$, $g = 9{,}80$ m.s$^{-2}$)

| Material | Lower Bound ($m^{-1}$) | Material | Lower Bound ($m^{-1}$) |
|---|---|---|---|
| Weathered Granite | $1{,}58.10^{-6}$ | Weathered Gabbro | $1{,}95.10^{-6}$ |
| Basalt | $1{,}39.10^{-7}$ | Sandstone | $6{,}50.10^{-7}$ |
| Siltstone | $9{,}75.10^{-7}$ | Sand (fine) | $1{,}21.10^{-6}$ |
| Sand (coarse) | $1{,}44.10^{-6}$ | Silt | $1{,}58.10^{-6}$ |
| Clay | $1{,}58.10^{-6}$ | Gravel (fine) | $1{,}16.10^{-6}$ |
| Gravel (coarse) | $1{,}11.10^{-6}$ | Limestone | $3{,}25.10^{-7}$ |
| Schist | $1{,}86.10^{-7}$ | | |

Before leaving this discussion of the general flow equation, it is interesting to note that the quantity $\rho\varepsilon$ is nothing else than the mass of fluid present in a unit volume of saturated porous medium. The derivative, $D_p[\rho\varepsilon]$, appearing in the second term on the right-hand side of Equation (11.9) and its equivalent expression, $\rho S_0$, in Equation (11.10), may thus be interpreted as the mass of fluid released from (added to) a unit volume of porous material per unit decline (rise) in pressure and piezometric head respectively. Since $\rho$ is the mass of fluid per unit volume of porous material, the specific storativity, $S_0$ may be interpreted as the volume of water released from (added to) a unit volume of porous material per unit decline (rise) in piezometric head. Therefore, if $\Delta V_w$ denotes the volume of water added to a porous medium with volume $\Delta V_b$,

$$S_0 = \frac{1}{\Delta V_b} \frac{\Delta V_w}{\Delta \phi} \qquad (11.14)$$

This expression not only gives an expression for $S_0$ in terms of the more regularly measured piezometric head, but it also shows that the dimension of is $[L^{-1}]$.

## 11.3 FLOW IN THE EARTH'S SUBSURFACE

### 11.3.1 General

Although fluid motion is a continuous process, the nature of the earth's upper subsurface is such that groundwater flow can be conveniently divided into *unsaturated flow*, present in the top layers of the earth's surface which are filled by water and air, and *saturated flow* in the deeper layers. Since the ability to transmit fluids varies considerably from one geological formation to the next, the situation frequently arises that a highly permeable formation is bounded from below and/or above by less permeable formations. A very important situation of this kind, is where two saturated formations are separated by a relatively thin, but less permeable formation (see Figure 11–2), often referred to as a *confining layer*.. If the hydraulic conductivity of the confining layer is small, but not zero, fluid may leak from the upper to the lower formation (or *vice versa*). Because of this, saturated groundwater flow is customarily further subdivided into *confined*, *semi-confined* and *unconfined flow*. However, as will be shown later, the nature of semi-confined flow does not differ physically from that of confined flow. In the discussion to follow, no distinction will, therefore, be made between confined and semi-confined flow, unless explicitly stated to the contrary.

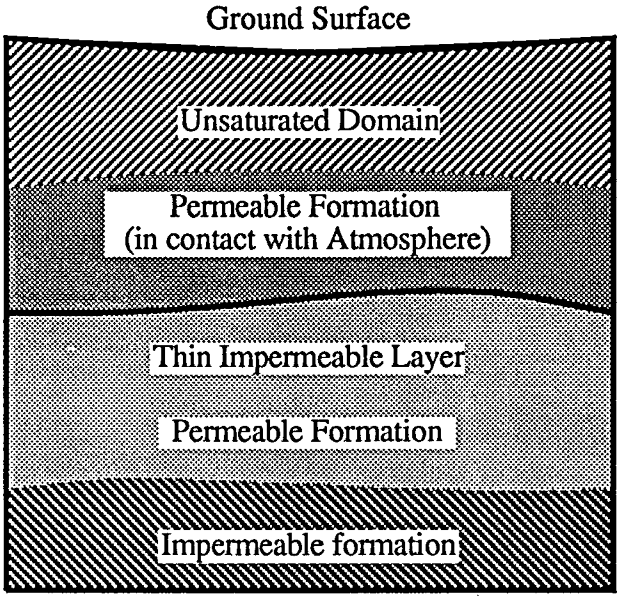

**Figure 11–2** Schematic representation of a vertical cross-section through the top geological formations of the earth's subsurface

### 11.3.2 Unsaturated Flow

An unsaturated porous medium can be characterized as one where the pressure acting on the fluid is negative (see Section 9.4). If not constrained, the fluid can, therefore, be easily displaced into partially or fully drained pores when subjected to an external pressure. In such situations, the fluid may be considered as incompressible and the term containing the compressibility coefficient, $\beta$, dropped from Equation (11.11). Because the fluid is free to move, it will have a minimum effect on the structure of the porous matrix. In the absence of external forces, applied directly to the porous matrix, the matrix compressibility $\alpha$, may also be neglected. With these assumptions, the term $S_0$ in Equation (11.13) can be dropped and unsaturated flow described by the equation

$$\rho[C(\phi)]D_t\phi(x,t) = \nabla\bullet[\rho\{\underline{K}\nabla\phi(x,t)\}] + \rho f(x,t), \qquad (11.15)$$

or if the fluid does not contain large quantities of dissolved solids, so that $\rho$ may be taken as constant,

$$C(\phi)D_t\phi(x,t) = \nabla\bullet[\underline{K}\nabla\phi(x,t)] + f(x,t). \qquad (11.16)$$

### 11.3.3 Unconfined Flow

The term, unconfined flow, is conventionally applied to the flow of fluid present in the saturated subsurface layer, which underlies the unsaturated top layers of the earth's surface (see Figure 11–2). If there is no confining layer between the water table and atmosphere, the fluid can move freely in and out of the unsaturated layers, whenever acted on by an external force. From the physical point of view, unconfined flow should thus also be described by Equations (11.15) or (11.16), which govern unsaturated flow. However, the real influence of the unsaturated component is usually restricted to the *capillary fringe* immediately above it. Because the thickness of the capillary fringe is usually very much smaller than that of the saturated zone, and the equations governing unsaturated flow are non-linear, unconfined flow is often regarded as being restricted to the saturated zone alone. With these assumptions, the equation governing unconfined flow simplifies to

$$\nabla\bullet[\underline{K}\nabla\phi(x,t)] + f(x,t) = 0, \qquad (11.17)$$

since $C(\phi) = 0$ in the saturated zone.

The fact that the governing equation of unconfined flow is the well-known Poisson equation, should not be construed as that it is a simple matter to obtain analytical solutions for this type of flow. On the contrary, the simplification of the governing equation has been achieved at a cost. Any fluid added to, or removed from, the saturated zone must obviously be accompanied by a shift in the position of the saturated-unsaturated interface. Although this may not seem to be a serious problem, it must be kept in mind that if Equation (11.17) is used to describe the flow, the boundary will only be known after the equation has been solved. However, a partial differential equation (particularly an elliptic equation) cannot be solved without a *complete* knowledge of the conditions on the boundary over which it is defined. Unconfined flow can thus only be described adequately by Equation (11.17), if defined as *a moving boundary problem.* This means that the position of the boundary and the solution of Equation (11.17) (on which it depends) must be determined at the same time, which is no mean mathematical exercise.

### 11.3.4 Confined Flow

The term confined flow is usually applied to the situation where the two layers that bound the highly permeable formation in Figure 11–2, are both impermeable. Fluid can, therefore, not enter or leave the formation vertically, with the result that the permeable formation itself and any fluid present in it, must bear the weight of the overlying formations and any other external pressures exerted on them. Both the fluid and porous matrix will thus be subjected to deformation. Keeping in mind that $C(\phi) \equiv 0$ and $S_w \equiv 1$ for saturated flow, Equation (11.16) yields

$$\rho S_0 D_t \phi(x,t) = \nabla \bullet [\rho\{\underline{K} \nabla \phi(x,t)\}] + \rho f(x,t). \qquad (11.18)$$

as the governing equation for confined flow, or using the same assumptions as in the derivation of Equation (11.17)

$$S_0 D_t \phi(x,t) = \nabla \bullet [\underline{K} \nabla \phi(x,t)] + f(x,t). \qquad (11.19)$$

By applying the same line of reasoning, used in the derivation of the continuity equation [Equation (11.4)], the left-hand side of either the preceding equations is seen to represent the ability of the porous medium to hold or release fluid. Based on this interpretation and the definition of $S_0$ in Equation (11.11), the existence of confined flow in the geological formations of the earth's subsurface is due to the fact that geological formations in the earth's subsurface, and the fluids they contain, are compressible.

## 11.4 REDUCTION OF DIMENSIONS

### 11.4.1 General

Equation (11.8) and all the other equations derived from it are general three-dimensional partial differential equations, for which no analytical solution is known, in general. The behaviour of the solutions of these equations can thus only be studied numerically, or if they are simplified to such an extent that analytical methods can be applied. Although a numerical solution can handle extremely complex situations [Hyakorn and Pinder (1983)], it lacks the generality of an analytical solution. For this reason and also because a numerical solution requires vast volumes of data and computer resources [Pinder and Gray (1976)], simplified versions of Equation (11.8) still, and in future will, play an important part in investigations of subsurface flow phenomena. It may thus be worthwhile to first have a look at the nature of these equations and the natural phenomena they describe, before discussing some of the methods that can be used to simplify them.

A natural phenomenon can be described as an event that occurs in the four-dimensional space-time continuum S = {x,t}, with properties that can be expressed quantitatively in terms of the space coordinates **x** and the time t. The equations used in describing natural phenomena must, consequently, also depend on one or more of the four physical dimensions. While there exist phenomena (the one-dimensional vibrating string is perhaps the best known example) that can be described by equations with less than the four basic dimensions, most equations [e.g. Equation (11.8)] are based on all four the physical dimensions.

As a cursory glance at any of the higher dimensional equations established thus far will show, an increase in the number of dimensions is generally accompanied by an increase in the complexity of the equation. With this in mind, a given equation can be simplified by one of two procedures: (a) dropping all terms whose influence is demonstrably much smaller than the rest [as was done, for example, in the derivation of Equations (11.16) and (11.18) from Equation (11.8)] and (b) reduce the dimensions of the equation. For the present, the discussion will be restricted to the latter procedure.

The dimensions of differential equations can be reduced either *physically or mathematically* [Botha (1988)]. The physical reduction can be used whenever a natural phenomena behave in such a way that most of its activity is restricted to less than the usual four dimensions. This approach may be applied whenever the phenomenon naturally requires less dimensions for its description (e.g. the vibrating string), or by restricting the dimensions artificially in a laboratory, as in Darcy's original experiment, for example. Because of its relation to the actual phenomenon, Botha (1988) refers to this approach (with its sound physical basis) as the *physical reduction of dimensions*. It should obviously be preferred as far as possible. However, there are many phenomena where the action in one, or more, dimensions is smaller, but not negligibly smaller than in the rest. If sufficient information is available, these phenomena should be investigated with equations based on all the physical dimensions. Situations of this nature are frequently encountered in subsurface flow, but the full dimensional equation cannot be used, because of a lack of sufficient resources to obtain the necessary information. In these situations, it makes sense to try and reduce the dimensions mathematically. This approach, which Botha (1988) refers to as the *mathematical reduction of dimensions*, will now be discussed in more detail.

### 11.4.2 Mathematical Reduction of Dimensions

The mathematical reduction of dimensions can be applied to any type of differential equation. To cover the more general types of problems to be discussed later on, the present discussion will, therefore, be based on the equation

$$D_t[\alpha(\mathbf{x},t)u(\mathbf{x},t)] = \nabla \bullet [\beta(\mathbf{x},t)\mathbf{J}(\mathbf{x},t)] + \gamma(\mathbf{x},t)f(\mathbf{x},t), \qquad (11.20)$$

where u(x,t) denotes the solution of the equation, J(x,t) and f(x,t) flux and forcing terms respectively and $\alpha(x,t)$, $\beta(x,t)$, $\gamma(x,t)$ parameter functions with the property

$$\alpha(x,t),\ \beta(x,t),\ \gamma(x,t)\ >\ 0. \qquad (11.21)$$

The basic tool in reducing the dimensions of a given differential equation is Leibnitz' rule for the differentiation of integrals [Bear (1979)]. Application of this rule to the differential equation, defined by Equation (11.20) yields

$$\begin{aligned}
&\int_{\xi_1}^{\xi_2} D_t[\alpha(x,t)u(x,t)]d\xi = \int_{\xi_1}^{\xi_2} \nabla\bullet[\beta(x,t)J(x,t)]d\xi + \int_{\xi_1}^{\xi_2}\gamma(x,t)f(x,t)d\xi \\
&= \nabla'\bullet \int_{\xi_1}^{\xi_2}[\beta(x,t)J(x,t)]d\xi + \int_{\xi_1}^{\xi_2}\gamma(x,t)f(x,t)d\xi + \beta(x',\xi_1,t)J(x',\xi_1,t)\bullet\nabla'\xi_1(x',t) \\
&\quad - \beta(x',\xi_2,t)J(x',\xi_2,t)\bullet\nabla\xi_2(x',t) - \beta(x',\xi_1,t)J_\xi(x',\xi_1,t) \\
&\quad + \beta(x',\xi_2,t)J_\xi(x',\xi_2,t). \qquad (11.22)
\end{aligned}$$

The left-hand side of Equation (11.2) can be expressed similarly as

$$\begin{aligned}
&\int_{\xi_1}^{\xi_2} D_t[\alpha(x,t)u(x,t)]d\xi = D_t \int_{\xi_1}^{\xi_2}[\alpha(x,t)u(x,t)]d\xi + \alpha(x',\xi_1,t)u(x',t)D_t\xi_1(x',t). \\
&\qquad - \alpha(x',\xi_2,t)u(x,t)D_t\xi_2(x',t), \qquad (11.23)
\end{aligned}$$

Since the boundary values ($\xi_1$, $\xi_2$) are functions of x' and t only, all terms on the right-hand side of Equations (11.22) and (11.23) are independent of $\xi$. The final dimensionally reduced equivalent of Equation (11.20) is thus given by

$$\begin{aligned}
&D_t \int_{\xi_1}^{\xi_2}[\alpha(x,t)u(x,t)]d\xi + \alpha(x',\xi_1,t)u(x',t)D_t\xi_1(x',t) - \alpha(x',\xi_2,t)u(x',t)D_t\xi_2(x',t) \\
&= \nabla'\bullet \int_{\xi_1}^{\xi_2}[\beta(x,t)J(x,t)]d\xi + \int_{\xi_1}^{\xi_2}\gamma(x,t)f(x,t)d\xi + \beta(x',\xi_1,t)J(x',\xi_1,t)\bullet\nabla'\xi_1(x',t) \\
&\quad - \beta(x',\xi_2,t)J(x',\xi_2,t)\bullet\nabla\xi_2(x',t) - \beta(x',\xi_1,t)J_\xi(x',\xi_1,t) \\
&\quad + \beta(x',\xi_2,t)J_\xi(x',\xi_2,t). \qquad (11.24)
\end{aligned}$$

The type of a differential equation is closely related to a particular physical process. For example, elliptic and parabolic equations arise from the laws of conservation of energy and mass, while hyperbolic equations are associated with energy dissipating processes. It is, therefore, of the utmost importance that the type of equation should be invariant under a reduction of dimensions.

A superficial comparison of Equations (11.24) and (11.20) would suggest that this is indeed the case. The various terms in Equation (11.20) have been replaced with integrals in Equation (11.24) and a number of boundary terms added, but the basic structure of the terms has not changed. However, this is not correct. The integrals in Equation (11.24) apply to the *complete* integrand and not to the various factors *alone*. For example, there is no *a priori* reason to believe that the integral

$$I(x',t) = \int_{\xi_1}^{\xi_2} [\beta(x,t)J(x,t)]d\xi, \qquad (11.25)$$

would fulfil the same role in Equation (11.24) as the term $\beta(x,t)J(x,t)$ in Equation (11.20). It is thus of the utmost importance that Equation (11.24) should be interpreted properly, before accepting it as a satisfactory two-dimensional representation for the three-dimensional Equation (11.20).

## 11.5 INTERPRETATION OF THE REDUCED EQUATION

### 11.5.1 The Expectation Value

An interpretation for the integrals in Equation (11.24) that has been applied almost universally in subsurface flow, is that of the *mean* or *expectation value* [Bear (1979), (1977)]. The main reason for this choice is that integration is an averaging operation, so that it is quite normal to try and interpret an integral as some average value over a given interval. Consider, for example, the function g(x), defined over the interval [a,b]. The expectation value of this function is conventionally defined as

$$E[g] \equiv \left[\frac{1}{b-a}\right]\int_a^b g(x)dx$$

The expectation value of a multivariable function $g(x',\xi,t)$ [$\equiv g(x,t)$] can likewise be defined along a line in the direction of $\xi$ as

$$E[g] \equiv [1/L(x',t)] \int_{\xi_1}^{\xi_2} g(x,t)d\xi = [1/L(x',t)][G(x',\xi_2,t) - G(x',\xi_1,t)]$$

provided that the indefinite integral

$$G(x',\xi,t) = \int g(x,t)d\xi,$$

exists and

$$L(x',t) = \int_{\xi_1}^{\xi_2} d\xi \equiv \xi_2(x',t) - \xi_1(x',t) \neq 0. \qquad (11.26)$$

The *expectation operator,* E[•], introduced above, has a very interesting property – it is *idempotent,* that is

$$E[E[g]] = E[g].$$

To see this, notice that as defined above, E[g] is independent of $\xi$. Hence

$$E[E[g]] = [1/L(x',t)] \int_{\xi_1}^{\xi_2} E[g]d\xi = E[g]. \qquad (11.27)$$

Equation (11.25) can thus be expressed in terms of its expectation value as

$$I(x',t) = L(x',t)E[I]. \qquad (11.28)$$

Although the interpretation of an integral as the product of its expectation value and interval length makes a lot of sense physically, it is not without its difficulties when applied to products of functions and thus dimensionally reduced equations. To see this, notice that as the expectation operator is a single number, one can always associate it with a *residual,* R[g], defined for the arbitrary function, g(x,t) as

$$g(x,t) \equiv E[g] + R[g,\xi].$$

The residual is thus a function of $\xi$, but its expectation value

$$E[R[g]] = E[g] - E[E[g]] \equiv 0, \qquad (11.29)$$

vanishes, as can be seen from Equation (11.27).

As noticed above, a dimensionally reduced representation can only be accepted, if it is *mathematically and physically* equivalent to the irreduced representation from which it was derived. This means, for example, that I(x',t) in Equation (11.28) must be equivalent to the first term on the right-hand side of Equation (11.20), that is

$$I(x',t) \sim I(x,t) \doteq \beta(x,t)J(x,t). \qquad (11.30)$$

When written out in full, Equation (11.28) assumes the form

$$I(x',t) = L(x',t)E[\beta J]. \qquad (11.31)$$

On comparing the last two representations, it is seen that $\beta(x,t)$ and $J(x,t)$ appear as two distinct factors in Equation (11.30), whereas Equation (11.31) contains the single factor $E[\beta\nabla u]$. The two equations are thus not identical from the mathematical point of view.

It is tempting to try and reconciliate the two representations by expanding E[βJ] in terms of the residual operators, R[β] and R[J], and then apply Equation (11.29). This yields

$$\begin{aligned} E[\beta J] &= E[\{E[\beta]+R[\beta]\}\{E[J]+R[J]\}] \\ &= E[\beta]E[J]+E[\,R[\beta].R[J]]. \end{aligned} \qquad (11.32)$$

Although E[β] and E[J] now appear as two separate factors, this representation is clearly not identical to I(x,t) in Equation (11.30), unless the unknown quantity, E[R[β].R[J]], in Equation (11.32), vanishes identically. However, this will only be the case if the parameter β(x,t) is a constant, or if one of β(x,t) and J(x,t) is independent of ξ, so that its residual vanishes. Products of functions in a higher dimensional model *cannot*, therefore, be considered as equivalent to their expectation values in a less dimensional model without further *simplifying* assumptions. The assumptions advocated in the literature for this purpose [see e.g. Bear (1979), (1977)] are, unfortunately, based more on *ad hoc* hypotheses rather than true physical or mathematical principles. For this reason, it may be worthwhile to try and establish another interpretation.

### 11.5.2 The Reduced Value Plane

The most satisfactory representation of I(x',t), equivalent to I(x,t), would be one in which the terms β(x,t) and J(x,t), appearing under the integral in Equation (11.25), separate naturally in the (x',t)–representation. The easiest way to achieve this, would be to find a method whereby one or both factors can be taken outside the integral sign.

If the function β(x,t) satisfies Equation (11.21), the generalized mean value theorem of the integral calculus [Hardy (1955)] can be invoked to rewrite Equation (11.25) in the form

$$I(x',t) = J(x',\chi,t)L(x',t)E[\beta], \qquad (11.33)$$

where L(x',t) is defined in Equation (11.26), E[β] the expectation value of β(x,t) and χ a fixed, but unknown parameter, which depends on E[β] and satisfies the inequality

$$\xi_1 < \chi < \xi_2.$$

However, since the present interest is centred on the product

$$P(x,t) = \beta(x,t)J(x,t),$$

it makes sense to consider P(x,t) as a single function of x and t multiplied by unity. Application of the generalized mean value theorem yields in this case

$$I(x',t) = \beta(x',\zeta,t)J(x',\zeta,t)L(x',t) \equiv B(x',\zeta,t)J(x',\zeta,t), \qquad (11.34)$$

where $\zeta$ is another parameter, which satisfies the inequality,

$$\xi_1 < \zeta < \xi_2$$

and depends on L(x',t) [Hardy (1955)] and

$$B(x',\zeta,t) = L(x',t)\beta(x',\zeta,t). \tag{11.35}$$

The functions $B(x',\zeta,t)$ and $J(x',\zeta,t)$ in Equation (11.34) may be interpreted mathematically, as two functions defined over a fixed, but unknown, plane

$$P_\zeta = \{x',\zeta,t\},$$

in the (x',t)-coordinates, *which pass through* the point $(x,\zeta,t)$. This plane (illustrated graphically in Figure 11–3) will in future be referred to as *the reduced value plane in the coordinates* (x',t), or simply as the reduced value plane.

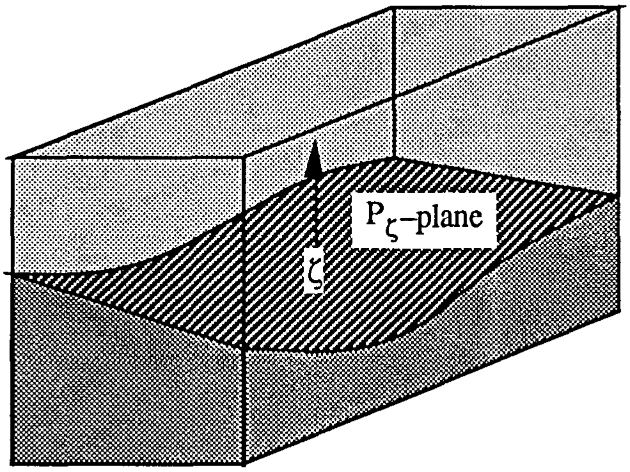

**Figure 11–3** Graphical illustration of the hypothetical $P_\zeta$–plane

It is important to note that the functions $B(x',\zeta,t)$ and $J(x',\zeta,t)$ in Equation (11.34) are related to the *same* points in (x',t)–space, as required of variables to replace $\beta(x,t)$ and $J(x,t)$ of Equation (11.20) in a less dimensional space. The plane $P_\zeta$ can, therefore, be regarded as the natural reference plane for a dimensionally reduced three-dimensional equation in two-dimensional space. Because it is difficult to derive a similar interpretation for $E[\beta]$ and $J(x',\zeta,t)$ in Equation (11.33), Equation (11.34) would seem to be a more natural two-dimensional representation of $I(x,t)$ than either Equations (11.28) and (11.31).

At this stage of the discussion, it should be noticed that Equations (11.32) – (11.34) are nothing more than relations between different mathematical variables. They will, therefore, only be useful in practice, *if the different variables can be related to observable physical quantities.*

### 11.5.3 Physical Interpretation of Reduced Variables

It is generally accepted in physics that the detail of a phenomenon can be investigated only, if the resolution of the instruments used, are comparable with the detail to be observed. For example, to obtain an image of a molecule, one has to use an electron and not optical microscope. The reason for this difference is not that the properties of a molecule suddenly change when viewed under two different kinds of microscopes, but rather in the fact that the wavelength of ordinary light is much longer than either the wavelength of an electron or the diameter of a molecule. Electrons can thus penetrate the electron clouds surrounding the atoms which constitute a molecule and produce an image of the molecules, while ordinary light cannot.

In subsurface flow many, if not all, routine observations are conducted with instruments whose resolution is rather restricted. Consider, for example, the observation of the piezometric pressure distribution, $\phi(x,t)$, in an aquifer. Because of the difficulties involved, measurements of this kind are usually restricted to observations of water levels in boreholes and piezometers [Kruseman and De Ridder (1970)]. The question that now arises is: how does one interpret these observations?

If the flow in the aquifer is truly horizontal, the piezometric pressure will be independent of the vertical direction. In this idealised situation, the piezometric pressures will be the same, no matter where they are measured in the aquifer. The depth to the piezometer opening used for this purpose is, therefore, immaterial. The observed water levels could thus be regarded as the experimental (or observational) equivalent of the mathematical problem of reducing dimensions.

Natural aquifers are, unfortunately, not horizontal, except over small distances. For this reason, it is customarily recommended that the length of the inlet to a piezometer should be kept to a minimum [Bear (1979)] and installed at a depth equal to the midpoint of the screen in the pumping well [Kruseman and De Ridder (1970)]. Inherent in this recommendation is the assumption that the observed water level is equal to the mean value of the piezometric pressure over the thickness of an aquifer. In other words, the observed water level is equal to the piezometric head midway between the top and bottom of the aquifer. However, the assumption is nothing more than a generalization of the situation that exists in the horizontal flowing aquifer discussed above. It is an assumption and not a physical fact. The reason for this assumption, quite common in groundwater studies, can be briefly explained as follows.

When viewed in terms of its three-dimensional physical context, the water level in a borehole, that *fully penetrates* an aquifer, can be taken as a quasi-stationary representation of the piezometric head at that point in the aquifer. Such a situation can, however, only exist, if the z-component of the Darcy velocity in the borehole is zero or negligibly small. Assuming (for the ease of notation) that the aquifer is isotropic, but inhomogeneous, this behaviour can be expressed mathematically as

$$q_z = -K(x,y,z)D_z\phi(x,y,z,t) = 0, \qquad (11.36)$$

or since $K(x,t)$ is a positive definite quantity, $D_z\phi(x,t) = 0$. Since the water pressure $p(x,t)$ in the borehole is independent of z, according to Pascal's law for a static fluid, Equation (8.10) can be integrated at once to obtain

$$\int_{z_0}^{z_1}\phi dz = (z_1 - z_0)\left[\frac{z_1 + z_0}{2} + I(p)\right] = LE_z[\phi], \qquad I(p) = \int_{p_0}^{p_1}\frac{dp}{\rho g}. \quad (11.37)$$

The expectation value of $\phi$ in the z-direction, $E_z[\phi]$, is thus mathematical equivalent to the piezometric pressure midway between the top and bottom of the aquifer. However, this does not imply that $E_z[\phi]$ is physically related to the observed water level. Moreover, as the integration of simple functions (such as $x^2$) will show, the expectation value of a function need not always coincide with the centre point of the interval over which it is integrated. Indeed, this is true *if and only if the function is a constant, symmetric, or anti-symmetric (with respect to the integration interval), or a linear function of the variable over which it is integrated*,as was the case with the piezometric head.

The difficulty experienced in associating $E_z[\phi]$ with the observed water level is not the only one experienced with the customary interpretation. Equation (11.37) was derived above by dividing Equation (11.36) throughout by $K(x,t)$. However, this makes it impossible to find an $E[K]$, or any other K-value, that can be uniquely associated with $E_z[\phi]$, on physical or mathematical grounds. *The expectation value interpretation of observed water levels must thus be regarded as an ad hoc assumption and not a physical fact.*

As shown by the discussion following Equation (11.32), it would, of course, be possible to associate a value of $E_z[K]$ with $E_z[\phi]$. However, such values would only be physical significant if it can be shown *a priori* that their residuals are zero or negligibly small insignificant. The only situation where this will always be true is when either one or both of $K(x,t)$ and $D_z\phi(x,t)$ is independent of z. Although this may be the case in ordinary flow problems, where $D_z\phi(x,t)$ is independent of z, there are numerous phenomena of practical importance (e.g. land subsidence and stratified contaminant transport) where $D_z\phi(x,t)$ is a function of z and the expectation value interpretation becomes questionable.

The question now arises what about the reduced plane interpretation? As observed above, the reduced plane $P_\zeta$ is not known in general. However, it is just as acceptable to equate the water level with the position of the reduced plane $P_\zeta$, as to equate it with the expectation value of the piezometric head, from the physical point of view. In fact, as the application of the generalized mean value theorem to Equation (11.36)

$$\int_{z_0}^{z_1} q_z dz = -(z_1 - z_0)K(x,y,\zeta)D_z\phi(x,y,\zeta,t) = g(x',t).$$

shows, there always exists a unique value of K(x,y,ζ) corresponding to φ(x,y,ζ,t). Moreover, since neither K(x',t) nor $D_z\phi(x',t)$ has to be determined from the integration of their three-dimensional equivalents, there is no reason to try and relate them to a specific point in the aquifer, should one (or both) of them be more complicated functions than the sets of functions mentioned above.

In summary, it can thus be said that the reduced plane interpretation of a reduced equation is often more acceptable on physical grounds than the expectation value interpretation. The only disadvantage of the interpretation is that the function to be reduced, should be measured simultaneously over the full length of the interval over which it is defined. In the case of groundwater levels, this means that all measurements should be conducted in *fully* and not partially penetrating boreholes as suggested by Kruseman and De Ridder (1970).

## 11.6 REDUCED BOUNDARY CONDITIONS

### 11.6.1 General

Equation (11.24) can be expressed more compactly in terms of the reduced plane interpretation as

$$\begin{aligned} D_t[A(x',t)u(x',t)L(x',t)] &+ \alpha(x',\xi_1,t)u(x',t)D_t\xi_1(x',t) - \alpha(x',\xi_2,t)u(x',t)D_t\xi_2(x',t) \\ &= \nabla'\bullet[B(x',t)J'(x',t)] + \Gamma(x',t)f(x',t) \\ &\quad + \beta(x',\xi_1,t)J'(x',t)\bullet\nabla'\xi_1(x',t) - \beta(x',\xi_2,t)J'(x',t)\bullet\nabla'\xi_2(x',t) \\ &\quad + \beta(x',\xi_1,t)J_\xi(x',\xi_1,t) - \beta(x',\xi_2,t)J_\xi(x',\xi_2,t), \qquad (11.38) \end{aligned}$$

where B(x,z,t) is given in Equation (11.35), and

$$A(x',t) \equiv \alpha(x',t)L(x',t) \text{ and } \Gamma(x',t) \equiv \gamma(x',t)L(x',t) \qquad (11.39)$$

are the equivalent expressions for α(x,t) and β(x',t) in the (x',t)-plane. To ease the notation, all explicit references to ζ have been dropped. In what follows, the prime symbols used thus far to distinguish between two- and three-dimensional variables, will also be dropped, unless there is a danger of confusion. This difference in notation should not be construed as that Equation (11.38), or any other equation derived from it, now applies to any plane. *All such equations are only valid in the plane* $P_\zeta$.

Equation (11.38) contains a number of terms, which depend on the end points, $[\xi_1, \xi_2]$, of the line segment used in the reduction of dimensions. These *reduced boundary* *conditions* should not be confused with the boundary conditions required for the solution of a differential equation. They are completely different and *refer to conditions on the boundaries of the reduced dimension.*

The reduced boundary conditions are clearly mathematical artifacts and have, therefore, to be determined *a priori* before Equation (11.38) can be applied in practice. However, to determine and incorporate them in the solution of Equation (11.38) are not easy tasks. Nevertheless, there are a few important exceptions which merit some discussion.

### 11.6.2 Time-independent Boundaries

Although there are situations where the boundaries, $\xi_1(x',t)$ and $\xi_2(x',t)$, of importance in subsurface flow, are functions of time, e.g. the problem of land subsidence, the nature of most phenomena is such that they may be considered as time-independent. In these situations, the boundary terms on the left-hand side of Equation (11.38) vanish, which leaves one with the terms, henceforth referred to as the *spatially reduced boundary conditions*, on the right-hand side to account for.

The gradients that appear in the spatially reduced boundary conditions could, in principle, be determined from the known (or assumed) positions of the boundary planes, but the flux terms are generally not known. However, the undulations present in the horizontal boundaries of the majority of geological formations are usually considerably smaller than their vertical thickness. These boundaries may thus be considered as horizontal planes. (Boundaries that have a non-negligible slope can be transformed to horizontal boundaries by a suitable rotation of coordinate axes.) The gradients of $\xi_1(x',t)$ and $\xi_2(x',t)$ thus vanish and Equation (11.38) reduces to

$$D_t[A(x',t)u(x',t)] = \nabla'\bullet[B(x',t)J'(x',t)] + G(x',t)f(x',t) + \beta(x',\xi_1,t)J_\xi(x',\xi_1,t) - \beta(x',\xi_2,t)J_\xi(x',\xi_2,t). \qquad (11.40)$$

Equation (11.40) is still not free of all the spatially reduced boundary conditions. However, there are a number of important practical phenomena where the fluid motion is more or less perpendicular to the vertical axis, with very little motion in the vertical, as for example, in confined flow (see Figure 11–2). Flows of this nature can be accounted for mathematically by assuming that

$$J_z(x',\xi_1,t) = J_z(x',\xi,t) = J_z(x',\xi_2,t) \equiv 0.$$

With this assumption, Equation (11.40) reduces to the well-known form of a two-dimensional partial differential equation

$$D_t[A(x,t)u(x,t)] = \nabla\bullet[B(x,t)J(x,t)] + G(x,t)f(x,t). \qquad (11.41)$$

Bear (1979) refers to this assumption as the *hydraulic approach.*

### 11.6.3 Artificially Induced Boundaries

Although very useful, there are nevertheless phenomena where the hydraulic approach cannot be applied successfully. Two examples from the field of groundwater flow are:

(a) the problem of sea-water intrusion, particularly in the study of the sea/fresh-water interface, and

(b) the problem of contaminant transport from the soil surface.

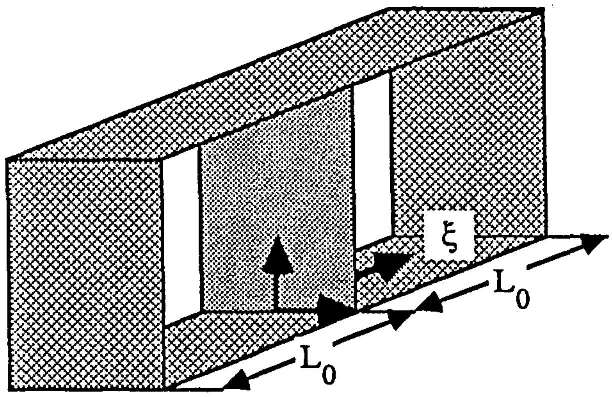

**Figure 11–4** An example of artificial boundaries in the three-dimensional space continuum

To fully understand these phenomena, would require a representation which takes all three space dimensions into account. However, the resources required for such an investigation are frequently not available. Fortunately, situations of this kind usually arise when interest is restricted to an area much smaller than that covered by the true physical boundaries. If this is true, the domain of interest can be bounded in the direction which is not of primary interest, by prescribing boundaries at fixed distances from a conveniently chosen origin, as illustrated in Figure 11–4. With this assumption the thickness of the integration interval is given by

$$L(x',t) = \xi_2 - \xi_1 = 2L_0.$$

Unfortunately, the dimension to be reduced may not necessarily coincide with the direction in which there is very little flow. The terms $\beta(x',\xi_1,t)J_\xi(x',\xi_1,t)$ and $\beta(x',\xi_2,t)J_\xi(x',\xi_2,t)$ cannot, therefore, be discarded as in the case where the hydraulic approach applies. However, as $L_0$ is, by definition, a non-negative constant, Equation (11.38) can be divided throughout by $2L_0$ to obtain

$$D_t[\alpha(x,t)u(x,t)] = \nabla\bullet[\beta(x,t)J(x,t)] + \gamma(x,t)f(x,t) + [1/2L_0][\beta(x,\xi_2,t)J(x,\xi_2,t) - \beta(x,\xi_1,t)J(x,\xi_1,t)].$$

If $L_0$ is now allowed to increase indefinitely, the offending boundary terms vanish and Equation (11.38) reduces to

$$D_t[\alpha(x,t)u(x,t)] = \nabla\bullet[\beta(x,t)J(x,t)] + \gamma(x,t)f(x,t). \qquad (11.42)$$

### 11.6.4 The Practical Application of Reduced Equations

The major difference between Equations (11.41) and (11.42) is that Equation (11.42) contains the original parameter functions, $\alpha(x,t)$, $\beta(x,t)$ and $\gamma(x,t)$, while Equation (11.41) contains the transformed parameter functions, A(x,t), B(x,t) and $\Gamma(x,t)$. Equation (11.42) is thus completely independent of L(x,t) (or even $L_0$). This must not be construed as that Equation (11.42) is to be preferred above Equation (11.41) in modelling exercises. On the contrary, as the preceding discussion clearly indicates, both equations have their own domain of validity and the one cannot be used in place of the other. *The choice of which equation to use*, must *be decided on by the type* of problem to be investigated. In this regard, it is interesting to note that while Equation (11.41) has a sound physical basis, Equation (11.42) is rather artificial, as it is difficult to visualize any naturally occurring phenomenon which covers all space in one of the three space dimensions.

Equation (11.38), or any equation based upon it, applies strictly *only to the reduced value plane* $P_\zeta$. As shown above, the position of this plane is not known in general, but some indication of its true position can be gained (at least for problems where Equation (11.41) applies) by observing point values of u(x',t) along different planes, $P^j$ (j = 1, ... ), over the full length of L(x,t). The plane, $P^m$ say, along which the observations compare best with the computed solution, may then be considered as an *observed reduced value plane* and equated with $P_\zeta$. However, if L(x,t) is too large for the experimental determination of $P^m$, one must be satisfied with the observed values, and regard these as defining an *observational plane*, $P_0$, which *need not coincide with* $P_\zeta$.

The procedure outlined above cannot be applied in the case of Equation (11.42) to establish a reduced value plane, but the comparison of observed and computed values along different planes may still provide useful information on the behaviour of the relevant phenomenon. Moreover, it must be kept in mind that the parameters of a differential equation can always be adjusted so as to ensure an acceptable match between the computed and observed values, which it is supposed to represent. The parameters obtained in this way, may not be a true representation of the actual physical parameters of the phenomenon being investigated, but at least will allow one to get an idea of its behaviour. If one can, therefore, show that the reduced equation defined on $P_0$, reproduces the observed data accurately over long periods of time, the equation may be taken as an accurate representation of the phenomenon under investigation over $P_0$.

Although any method can be used to adjust the parameters when fitting the reduced equation to observational data, much can be gained by using a method which not only provide information on the parameters, but also on their variability. A method of this nature is not only useful in the fitting procedure, but can also provide valuable information on the variability of the parameters and thus the position of the plane $P_0$. This suggests the use of one or other statistical method. One such method that has been applied with success in a number of fields relevant to subsurface flow, is the method of kriging [Van Tonder and Botha (1986)].

# CHAPTER 12

# TWO-DIMENSIONAL FLOW IN NON-DEFORMABLE POROUS MEDIA

## 12.1 INTRODUCTION

The partial differential equations, derived in Chapter 11, have one property in common – they implicitly contain information on what happens at a point (x,t) within the domain in which a certain physical phenomenon occurs. To obtain this information, requires that one must be able to solve the differential equation. However, this is not a simple exercise.

As is well-known, the solution of a differential equation is determined not only by the equation itself, but more importantly the boundary and/or initial conditions that must be specified independent of the differential equation. Furthermore, the conceptual parameters in these equations, such as the storativity and hydraulic conductivity, must be known *a priori* before a solution can be obtained. To satisfy these requirements in the case of subsurface flow, generally require detailed and expensive investigations over long periods of time. To circumvent these dificulties groundwater flow phenomena has in the past often been modelled by the simplest, but stil realistic conceptual models possible. However, to be sure that he is using the correct conceptual model for his specific problem, the modeller should have a good insight into his problem. For this reason the various two-dimensional conceptual models available for groundwater flow will be discussed here in greater detail.

For reasons that will become clear later, confined flow is the simplest type of flow from the mathematical point of view. The discussion to follow will, therefore, begin with confined flow, before proceeding to unconfined and saturated/unsaturated flow.

## 12.2 CONFINED FLOW

As shown in Section 11.3.3, confined flow is governed in three-dimensional space by the equation

$$S_0 D_t \phi(x,t) = \nabla \bullet [\underline{K} \nabla \phi(x,t)] + f(x,t). \qquad (11.19)$$

However, confined flow is, by its definition, restricted to the domain bounded by two impermeable geological formations and satisfies all the assumptions of the hydraulic approach. It is thus quite natural to restrict the study of confined flow to a horizontal plane and interpret the vertical integration interval, $L(x,\zeta,t)$, as the thickness of the formation at the point $(x,\zeta,t)$. Using this interpretation, the two-dimensional equivalent of

Equation (11.19) can be expressed as

$$SD_t\phi(x,t) = \nabla\bullet[\{\underset{\sim}{T}\nabla\phi(x,t)\}] + L(x,t)f(x,t). \tag{12.1}$$

where x now denotes the two horizontal space coordinates (x,y). The quantities

$$S(x,t) \equiv L(x,t)S_0(x,t), \text{ and } \underset{\sim}{T}(x,t) \equiv L(x,t)\underset{\sim}{K}(x,t), \tag{12.2}$$

introduced here, are in the literature better known as the *storage coefficient* and *transmissivity* tensor respectively. They are obviously the confined flow equivalents of the parameters A(x',t) and B(x',t) in Equations (11.35) and (11.37) and, therefore, known if L(x,t), $S_0(x,t)$, and $\underset{\sim}{K}(x,t)$ are known for the particular aquifer. Since $\underset{\sim}{K}(x,t)$ and $S_0(x,t)$ has dimensions $[L.T^{-1}]$ and $[L^{-1}]$ respectively, see the discussion in Sections 10.3 and 11.2, $\underset{\sim}{T}(x,t)$ and S(x,t) has the dimensions $[L^2.T^{-1}]$ and [1] respectively.

A confined aquifer can only exist if its thickness, $L(x,t) > 0$. Since $S_0(x,t)$, and $\underset{\sim}{K}(x,t)$ are, by definition, always positive quantities, the parameters S(x,t) and $\underset{\sim}{T}(x,t)$ can vary as functions of space and time, but *never* vanish in confined flow. In other words, S(x,t) and $\underset{\sim}{T}(x,t)$ are positive definite quantities.

The only term in Equation (12.1) that still needs some interpretation, is the forcing term, L(x,t)f(x,t). As this term represents discharge and/or recharge to the aquifer, its final form will depend on the form of the recharge (discharge). This usually occurs in either one of two forms: *areal* and *point* sources or sinks. As the name implies, areal sources are recharge (discharge) sources (sinks), which cover an appreciable area of the aquifer. The best known example of an areal source is probably precipitation. Point sources (sinks), on the other hand, are sources whose areal dimensions can be judged as infinitesimal in relation to the area of the aquifer. Artificially drilled boreholes and springs are perhaps the best known examples of point sources. These definitions can now be used to derive explicit expressions for the forcing term in Equation (12.1).

To arrive at an expression for the forcing term, it is necessary first to obtain an expression for the strength of a source, defined in Section 11.1. The intensity of precipitation is customarily expressed in units of $[L.T^{-1}]$. With this in mind, the intensity of an areal source can be conveniently expressed as R(x,t) and the volume of fluid recharged (discharged) per unit square area per unit of time as $V_a = R(x,t)$. Since the volume of a confined aquifer, per unit square area, equals the thickness, L(x,t), of the aquifer, the strength of an areal source is given by

$$f(x,t) = \frac{R(x,t)}{L(x,t)},$$

from which follows $L(x,t)f(x,t) = R(x,t)$. The forcing term for an areal source in a confined aquifer is thus numerically equal to the intensity of the source.

While the previous procedure could also be used to arrive at an expression for the forcing term of a point source, it is custom not to measure the intensity of the source, but rather its yield (recharge/discharge rate), Q(t), with units $[L^3.T^{-1}]$. The strength of a point source at the position $x_0 = (x_0,y_0)$, in a confined aquifer could, therefore, be defined as

$$f(x_0,t) = \frac{Q(x_0,t)}{\delta V}, \qquad (12.3)$$

where

$$\delta V = \int_{dV} L(x_0,t)dV = \int_{dV} L(x,t)dAdz = L(x_0,t)\delta A$$

with $\delta A$ and $\delta V$ the area and volume of porous material affected by the source, respectively. However, there is another alternative. Consider the Dirac delta function, customarily denoted by the symbol $\delta(x-x_0)$, defined by the relation

$$\int_{-\infty}^{\infty} f(x)\delta(x-x_0)dx = f(x_0). \qquad (12.4)$$

For it follows from Equation (12.3) and the usual rules of integration that, since $Q(x_0,t)$ is independent of the spatial coordinates x,

$$\int_{-\infty}^{\infty} \frac{Q(x_0,t)}{\delta A} dxdy = \int_{\delta A} \frac{Q(x_0,t)}{\delta A} dxdy = Q(x_0,t).$$

But, using Equation (12.4)

$$\int_{-\infty}^{\infty} Q(x,t)\delta(x-x_0)\delta(y-y_0)dxdy = Q(x_0,t).$$

Hence,

$$\frac{Q(x_0,t)}{\delta A} = Q(x,t)\delta(x-x_0)\delta(y-y_0).$$

The forcing term of a point source (sink) in a confined aquifer can thus be expressed, symbolically, in the form

$$L(x,t)f(x,t) = Q(x,t)\delta(x-x_0)\delta(y-y_0),$$

and the most general two-dimensional equation, describing flow in a confined aquifer, subjected to both areal and point sources, as

$$SD_t\phi(x,t) = \nabla\bullet[\{\underline{T}\nabla\phi(x,t)\}] + R(x,t) + Q(x,t)\delta(x-x_0)\delta(y-y_0). \qquad (12.5)$$

## 12.3 UNCONFINED FLOW

### 12.3.1 General

A two-dimensional equivalent of the equation governing unconfined flow, Equation (11.17), can be derived along similar lines as that used for confined flow above. To be more specific, let $\xi_1 = b(x')$ represent the elevation of the fixed, impervious bottom of the aquifer, $\xi_2 = h(x',t)$ the phreatic surface, and

$$J(x,t) = \underline{K}(x,t)\nabla\phi(x,t) \tag{12.6}$$

the negative Darcy velocity of the flow. By replacing the corresponding variables in Equation (11.36) with these values, the reduced equation governing flow in an unconfined aquifer is found to be

$$\begin{aligned} \nabla'\bullet[L(x',t)J(x',t)] + L(x',t)f(x',t) + J'(x,t)\bullet\nabla'b(x,t) - J'(x,t)\bullet\nabla'h(x,t) \\ - J_z(x',b,t) + J_z(x',h,t) = 0, \end{aligned} \tag{12.7}$$

where

$$L(x',t) = h(x',t) - b(x',t) \tag{12.8}$$

from Equations (11.26) and (11.34). The last four terms of Equation (12.7) represent the reduced boundary conditions which has to be related to the prevailing conditions on the boundary of the aquifer. However, before proceeding with this discussion, it is advantageous to look at a few basic properties of an unconfined aquifer first.

### 12.3.2 Distribution of Water in an Unconfined Aquifer

The distribution of water in an unconfined aquifer can be basically divided into three zones: The unsaturated zone which extends from the top of the soil surface to the capillary fringe, the capillary fringe itself and the saturated zone below the water table (see Figure 12–1). The precise positions of these zones will of course varies continuously as water is removed or added to the aquifer. However, if the supply or demand of water is kept constant for a sufficiently long period of time, the different zones will more or less remain fix in space and time, in other words the aquifer will be in a *steady state* condition.

As defined above, a steady state condition in an unconfined aquifer can be characterized as a situation where there is no vertical motion. By using Darcy's law [Equation (10.10)] this condition is equivalent to the requirement that

$$q_z = -\underline{K}(x,t)D_z\phi(x,t) = 0$$

or, since $\underline{K}(x,t)$ is a positive definite quantity,

$$\phi(x,t) = \text{constant}.$$

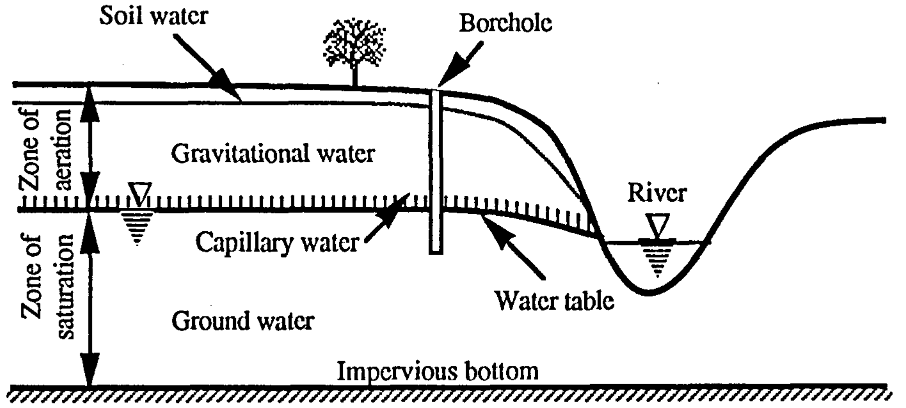

**Figure 12–1** Distribution of water in the subsurface of the earth

It follows from the preceding equation that the piezometric head distribution at a point z, above the water table, and that at a point $z_0$ on the water table must be equal. Hence, using Equation (8.11)

$$z_0 + h_0 = z_0 = z + h,$$

since $h_0 \equiv 0$ on the water table. It is now straightforward to see that, if $z_0$ is chosen as the origin of a coordinate system, the pressure head distribution above the water table must satisfy the equation

$$z = -h(z) = \psi(\theta).$$

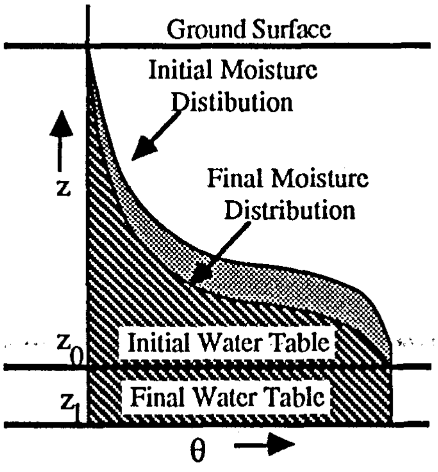

**Figure 12–2** Steady state distribution of water above in an unconfined aquifer before and after the water level was disturbed

The distribution of water in the unsaturated zone of an unconfined aquifer thus follows the moisture retention curve, defined in Equation (9.11), exactly.

An instantaneous decrease (or increase) in the water level of a unconfined aquifer in a steady state condition, will thus lead to a corresponding change of the water distribution in the unsaturated zone. Because the moisture retention curve is a rather complicated function of the moisture content of the soil, (see the discussion in

Section 9.5), it is difficult to describe the exact behaviour of the water distribution above the water table, until another steady state is reached, in which case the water distribution must again follow the moisture retention curve (see Figure 12–2).

The variation in the water table of an unconfined aquifer is customarily described in terms of two quantities, variously referred to as the *effective porosity* and *specific yield* [Bear (1972)]. To define these quantities more precisely, consider again the situation depicted in Figure 12–2. The total volume of water drained from a column of soil with unit cross-sectional area during such a change in the position of the water table is

$$W_d = \varepsilon(z_1 - z_0) - \int_{z_1}^{z_0} \theta(z)dz = [\varepsilon - \theta(\zeta)](z_1 - z_0) \qquad (z_0 < \zeta < z_1)$$

after applying the generalized mean value theorem of the integral calculus. The effective porosity of an unconfined aquifer is now defined as

$$\theta_e \equiv \frac{W_d}{(z_1 - z_0)} = \varepsilon - \theta_d, \tag{12.9}$$

with $\theta_d \equiv \theta(\zeta)$ the water contents retained by the aquifer, and the effective saturation as

$$S_e = \frac{\theta_e}{\varepsilon} = 1 - \frac{\theta_d}{\varepsilon} = 1 - S_d$$

The effective porosity of an unconfined aquifer can thus be taken as a measure of *the volume of water (per unit horizontal area) derived from storage in an unconfined aquifer when the water table level is lowered (heightened) a unit distance.* Following Bear (1972), the quantity $S_d$ will in future be referred to as the *retained moisture saturation of drainage.*

In deriving the expressions for $\theta_e$ and $S_e$ above, it was assumed that sufficient time has elapsed to establish a second steady state in the aquifer. This is equivalent to the assumption that water is *immediately released from storage during a change in the water table.* However, $\theta_e$ depends not only on the form of the moisture retention curve, but also the distance through which the water table changes. Moreover, $\theta_e$ will not be same for a rising as a falling water table, because of the hysteretic nature of the moisture retention curve (see Section 9.5). The effective porosity and retained moisture saturation are thus not well-defined quantities from the physical point of view. They should thus never be considered as characteristic parameters of a particular geological formation, or used as relational parameters (see Section 1.3) in a physically based conceptual model of a phreatic aquifer. They are at best convenient mathematical aids in the characterization of an unconfined aquifer. However, as will be shown below, they do play an important role in existing simplified conceptual models for a phreatic aquifer and will, therefore, continue to play an important part in the evaluation of phreatic aquifers, at least in the immediate future.

### 12.3.3 Two-dimensional Unconfined Flow Equation

The top boundary of a phreatic aquifer may be conveniently taken as a plane, F, where the piezometric head equals the elevation, measured from the same datum. In other words where

$$\phi(x',h,t) = h(x',t) = z.$$

The geometry of this plane, better known as the *phreatic surface*, can thus be described by an equation of the form

$$F(x,t) \equiv \phi(x,t) - z = h(x',t) - z = 0. \qquad (12.10)$$

This equation, incidentally, illustrates the interdependence of the solution and boundary of a phreatic aquifer, mentioned in Section 11.3.3, particularly the fact that the position of F may vary in both space and time, beautifully.

It follows from Equation (12.10), that the total (sometimes also referred to as the substantial) derivative of F(x,t) must satisfy the equation

$$\frac{DF}{Dt} \equiv \frac{\partial F}{\partial t} + \frac{\partial F}{\partial x}\frac{dx}{dt} + \frac{\partial F}{\partial y}\frac{dy}{dt} + \frac{\partial F}{\partial z}\frac{dz}{dt} = D_tF + v_F \bullet \nabla F = 0, \qquad (12.11)$$

The quantity $v_F$ introduced in this equation is obviously the velocity at which the phreatic surface F change its position. The velocity $v_F$ may thus be taken as the seepage velocity of the fluid particles on the phreatic surface (see Figure 12–3). The phreatic surface of an unconfined aquifer, is thus always accompanied by a Darcy type flux, which can be expressed, through Equations (10.5) and (12.9), in the form

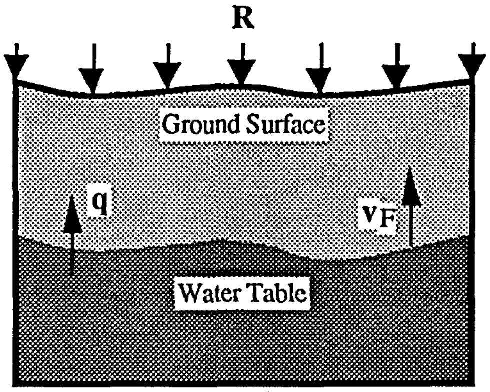

**Figure 12–3** Schematic representation of the velocity of and fluxes across the phreatic surface in an unconfined aquifer

$$q_F = \theta_c v_F.$$

To satisfy the law of mass conservation this flux must be balanced by the difference between the ever present Darcy flux q(x,t), directed from the saturated towards the unsaturated zone, and the rate, R(x,t), at which water may accrue across the phreatic surface from external sources or sinks (see Figure 12–3).

The most common factors affecting the accretion of water in an unconfined aquifer are: recharge by precipitation and evapotranspiration. By assuming that R(x,t) is positive when directed downwards, i.e.

$$R(x,t) = -kR(h,t)$$

the law of mass conservation will be satisfied if $v_F(x,t)$ satisfies the equation

$$[q(x,t) - R(x,t)]\bullet\mathbf{n} = \theta_e v_F(x,t)\bullet\mathbf{n} \qquad (12.12)$$

where **n** is a unit vector *normal* to the phreatic surface. Interpreted in more physical terms Equation (12.12) states that the velocity of the phreatic surface F depends on the velocities of the water on both sides of F.

Since the gradient of a function is always normal to the surface, the unit vector **n** in Equation (12.12) can also be expressed as

$$\mathbf{n} = \frac{\nabla F}{|\nabla F|}.$$

Substitution of this result into Equation (12.12) and keeping in mind that ∇F never vanishes for a normal surface, Equation (12.6) can be used to rewrite Equation (12.11) in the form

$$\theta_e D_t F(x,t) + [-J(x,t) - R(x,t)]\bullet\nabla F = 0.$$

By inserting the value of F(x,t) from Equation (12.10), one obtains

$$\theta_e D_t h(x,t) + [-J(x,t) - R(x,t)]\bullet\nabla[h(x',t) - z] = 0$$

or using the expression for R(x,t) above,

$$\theta_e D_t h(x,t) - R(h,t) = J(x',t)\bullet\nabla h(x',t) - J_z(x,h,t). \qquad (12.13)$$

where the '-symbol is again used to distinguish between the three-dimensional xyz-space and the two-dimensional xy-plane.

In the case of an unconfined aquifer bounded below by a fixed and impervious boundary, the two corresponding boundary terms in Equation (12.7) must vanish. By using this fact and replacing the expression $J'(x,t)\bullet\nabla'h(x,t) - J_z(x',h,t)$ with its equivalent on the right hand side of Equation (12.13) in Equation (12.7), now yields,

$$\theta_e D_t h(x',t) = \nabla'\bullet[L(x',t)J(x',t)] + L(x',t)f(x',t) + R(h,t), \qquad (12.14)$$

or if J(x',t) and L(x',t) are replaced by their explicit expressions in Equations (12.6) and (12.8) respectively,

$$\theta_e D_t h(x',t) = \nabla'\bullet[\{h(x',t) - b(x')\}\underline{K}(x',t)\nabla(x',t)] + [h(x',t) - b(x')]f(x',t)$$

$$+ R(h,t). \tag{12.15}$$

This is the basic two-dimensional equivalent of Equation (11.17), which governs the flow of groundwater in a saturated phreatic aquifer with an impervious bottom. Equation(12.15) is a generalization of the well-known *Boussinesq equation* [Bear (1979], to which it reduces if $b(x') \equiv 0$.

## 12.4 SATURATED/UNSATURATED FLOW

Saturated/unsaturated flow is governed by the general flow equation [Equation (11.8)], which reduces in the case of density-independent flow to

$$D_t\theta(x,t) = \nabla \bullet [\underline{K}(x,t)\nabla\phi(x,t)] + f(x,t). \tag{12.16}$$

Although it is mathematically possible to reduce the dimensions of this equation in the z-direction, it is not clear how one should interpret the resulting reduced piezometric head. The reduction in the dimensions of Equation (12.16) is thus usually restricted to one of the horizontal coordinates, taken here to be y. The correct reduced equation to use in this case is thus given by

$$D_t\theta(x,z,t) = \nabla \bullet [\underline{K}(x,z,t)\nabla\phi(x,z,t)] + f(x,z,t). \tag{12.17}$$

according to Equation (11.40).

# CHAPTER 13

# CONTAMINATION OF GROUNDWATER

## 13.1 GENERAL

Not all the waste produced on earth are necessarily dangerous, if released to the environment. For this reason, attention is mostly directed to what is known as *hazardous waste*, which, according to the USEPA (United States Protection Agency) [Princeton University Water Resources Program (1984)] is waste with any one of the following characteristics:

(1) *Ignitability* – waste that poses a fire hazard during routine management.

(2) *Corrosivity* – waste that requires special containers because of their ability to corrode standard materials, or segregation from other wastes because of their ability to dissolve toxic contaminants.

(3) *Reactivity* – waste that tends to react spontaneously, vigorously with air or water, be unstable to shock or heat, generate toxic gases, or explode during routine management.

(4) *Toxicity*– waste that may release toxicants in sufficient quantities to pose a substantial hazard to human health or the environment when improperly managed.

All of these characteristics produce *acute* effects likely to cause immediate damage, while the fourth also deals with substances that may create chronic effects, more likely to appear over prolonged periods of time.

As mentioned in Chapter 1, the primary mechanism for the transport of improperly discarded hazardous waste through the environment is via the movement of water through ground and surface waterways. To study this movement, requires that one must be able to measure the quantity of waste present at a particular point in space and time. The measure universally used for this is the *concentration* , expressed in terms of either a *mass fraction* or *mass volume.* This usage is somewhat unfortunate as the two measures, although related, are not physically equivalent. To see this, let $m_s$ be the mass of solid dissolved in a mass $m_f$ of fluid with v the volume occupied by the total mass

$$m = m_s + m_f.$$

The concentration can now be expressed quantitatively in terms of a mass fraction as

$$C = \frac{m_s}{m}, \tag{13.1}$$

and in terms of a volume fraction as

$$c = \frac{m_s}{v} . \tag{13.2}$$

Substitution of $m_s$ in Equation (13.2) by its equivalent expression from Equation (13.1), shows that

$$c = \frac{m}{v} C \equiv \rho C , \tag{13.3}$$

where $\rho$ is the density of the fluid and dissolved solid, often referred to as the *solute*. The concentration expressed as a volume fraction is thus $\rho$ times larger than the concentration expressed in terms of a mass fraction.

A rather important observation that follows directly from Equation (13.3), is that the density of the solute is not a constant, but a function of the concentration

$$\rho = \rho(c) = \rho(m_s) = \rho(C) \tag{13.4}$$

Experimental evidence suggests that this dependence is rather weak for a fairly large range of concentration values. When working with these low concentrations, or *watery* solutions, the density may thus be considered as independent of the concentration. It has, therefore, become a custom to use the volumetric concentration (c) as a measure for watery solutions and the mass concentration (C) for high concentration solutions.

With the measure for the quantity of solids dissolved in a fluid defined, it should not be too difficult to try and establish a suitable conceptual model for the motion of the fluid and dissolved solid. However, before proceeding with this, it may be advantageous first to look at the nature of the movement of dissolved solids through a porous medium.

Experimental evidence indicates that a dissolved solid in contact with the matrix of a porous medium, may (a) pass through the matrix with no apparent effect, (b) be absorbed partially (or fully) by the porous matrix and (c) reacts with other substances in the porous matrix and/or fluid. The dissolved solids encountered in porous flow are, for this reason, often classified as *conservative, non-conservative* and *reactive* tracers. This behaviour implies that the concentration of a dissolved solid, present in a porous medium at any point in space and time, not only depends on the flow pattern, but also the nature of the porous matrix and other solids that may be present in the solute.

The fraction of a dissolved solid that partakes in reactions with the porous matrix and/or solute, does not depend on concentration alone, but also on other factors, such as the temperature and acidity of the solution. Nevertheless, experience indicates that the fraction of dissolved solids partaking in a reaction, s, can be related mathematically to the concentration of the dissolved solid through a relation, or *isotherm* [Bear (1979)], defined by an equation of the form

$$s = f(C,t) = g(c,t).$$

The isotherms encountered in groundwater polution can be quite complex, especially in the case of reactive tracers. However, many tracers encountered in groundwater pollution are non-conservative tracers, whose adsorption properties can be described in terms of the simple *Freundlich* isotherm

$$s = K_d c = K_d^* C, \tag{13.5}$$

To discuss the Freundlich isotherm in more detail, let $m_a$ and $m_m$ denote the mass of absorbed solid and porous matrix respectively, and

$$m_b = m_a + m_m$$

the total mass of solids in a volume $v_b$ of porous material. The fraction of dissolved solids absorbed by the porous medium can then be expressed as

$$s = \frac{m_a}{m_b}. \tag{13.6}$$

On comparing Equations (13.6) and (13.5), it is easy to see that the *volumetric distribution coefficient*

$$K_d = \left[\frac{(m_a/m_b)}{(m_s/v)}\right], \tag{13.7}$$

and that the *mass distribution coefficient*

$$K_d^* = \left[\frac{(m_a/m_b)}{(m_s/m)}\right] \equiv \rho K_d. \tag{13.8}$$

When applying Equations (13.5) to (13.8) in practice, it should be noted that the mass distribution coefficient is dimensionless, while the volumetric coefficient has the dimensions $[L^{-3}.M]$. They should, therefore, never be used interchangeably.

## 13.2 THE HYDRODYNAMIC DISPERSION EQUATION

There are various ways that can be used to establish a conceptual model for the transport of dissolved solids through a porous medium [Bear (1972)]. However, the method that makes the most sense physically, is to consider a volume ($\Omega_0$) of partially saturated porous material, situated at a position $x_0$ in the fluid at the time $t = 0$. Since no material, especially porous materials, are rigid, the volume $\Omega_0$ will tend to deform to a new volume $\Omega = \Omega(x,t)$ at the time $t > 0$. To account for this, the present discussion will be based on the

Lagragian formulation for fluid motion.

By using the definitions introduced above, the total mass of dissolved solids contained in the volume $\Omega$, can be conveniently expressed in the form

$$M(x,t) = \int_{\Omega} (\theta c + \rho_b s) d\Omega. \tag{13.9}$$

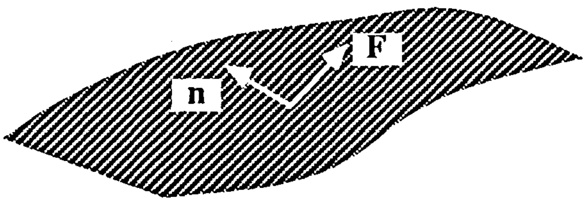

**Figure 13–1** Schematic representation of the flux, F, through the boundary of $\Omega$

where $\theta$ is the volumetric moisture content of the medium, defined in Equation (9.3), and

$$\rho_b = \frac{m_b}{v_b}$$

the bulk density of the fraction of adsorbed solids and the solid matrix. Since the fluid is in continuous motion, there will be a continuous loss of dissolved solids through the boundary $\partial\Omega$. If F is used to denote this flux of particles per unit area of the boundary, the total flux of dissolved solids, per unit of time, may be expressed as (see Figure 13–1)

$$M_F = \int_{\partial\Omega} \mathbf{n} \bullet \mathbf{F} dA$$

or, after applying Gauss' theorem,

$$M_F = \int_{\Omega} \nabla \bullet \mathbf{F} d\Omega \tag{13.10}$$

One form of waste that has received considerable attention during the last couple of years is radioactive waste. This type of waste differs from others in that its activity, hence its concentration, decreases naturally with time. If N(t) is used to denote the number of radioactive atoms present at a time t, this decay process can be described by the equation

$$DN(t) = -\lambda N(t), \tag{13.11}$$

where $\lambda$ is the decay constant. In the case of radioactive material, an additional quantity of material, which can be expressed through Equations (13.11) and (13.9), in the form

$$M_R = \lambda \int_{\Omega} (\theta c + \rho_b s) d\Omega \tag{13.12}$$

will thus be lost from $\Omega$ per unit of time. The total loss of mass from $\Omega$ per unit of time,

$$M_L = M_F + M_R \tag{13.13}$$

must, according to the law of mass conservation, be balanced by a corresponding decrease, $D_tM(t)$, in the mass present in $\Omega$. Hence

$$D_tM(x,t) + M_L = 0,$$

or

$$\frac{d}{dt}\left[\int_{\Omega} (\theta c + \rho_b s)d\Omega\right] + M_L = 0 \tag{13.14}$$

Because the discussion is based on the Lagrange formulation of fluid flow, $\Omega$ is a function of time. It is consequently not possible to simplify Equation (13.14) directly, by interchanging the derivative and integral appearing in it. However, the position x of $\Omega$ at time t is, according to classical mechanics, related to the position $x_0$ of $\Omega_0$ at time t = 0 through the equation

$$x = x(x_0,t),$$

However, the volume elements $d\Omega$ and $d\Omega_0$ are related to one another by the equation

$$\begin{aligned} d\Omega &= [i(J_x \bullet dx_0) \times j(J_y \bullet dx_0)] \bullet [k(J_z \bullet dx_0)] \\ &= J dx_0 dy_0 dz_0 = J d\Omega_0, \end{aligned} \tag{13.15}$$

where J is the Jacobian of the transformation between x and $x_0$. Substitution of this expression for $d\Omega$ in Equation (13.14) yields

$$\frac{d}{dt}\left[\int_{\Omega_0} (\theta c + \rho_b s)J d\Omega_0\right] + M_L = 0$$

Since $\Omega_0$ is a constant independent of time, the differentiation and integration can now be interchanged to obtain

$$\int_{\Omega} \left[\frac{d}{dt}(\theta c + \rho_b s)J + (\theta c + \rho_b s)\frac{dJ}{dt}\right]d\Omega_0 + M_L = 0 \tag{13.16}$$

It is not easy to interpret the result in Equation (13.16) directly. However, it follows from Equation (13.15) that

$$\frac{d}{dt}d\Omega = \frac{dJ}{dt}d\Omega_0.$$

Hence, as x is a function of the time,

$$\frac{1}{J}\frac{dJ}{dt} = \frac{d\Omega_0}{d\Omega}\frac{1}{d\Omega_0}\frac{d}{dt}d\Omega$$

$$= \frac{1}{dxdydz}\left[\frac{d}{dt}(dx)dydz + \frac{d}{dt}dx(dy)dz + \frac{d}{dt}dxdy(dz)\right]$$

$$= \frac{d}{dx}\frac{dx}{dt} + \frac{d}{dy}\frac{dy}{dt} + \frac{d}{dz}\frac{dz}{dt} \equiv \nabla \bullet \mathrm{v}. \qquad (13.17)$$

As the quantity $(\theta c + \rho_b s)$ is, in general, a function of both the spatial coordinates **x** and time t, a direct application of the chain rule for differentiation yields

$$\frac{d}{dt}(\theta c + \rho_b s) = D_t(\theta c + \rho_b s) + D_x(\theta c + \rho_b s)\frac{dx}{dt} + D_y(\theta c + \rho_b s)\frac{dy}{dt}$$
$$+ D_z(\theta c + \rho_b s)\frac{dz}{dt} = D_t(\theta c + \rho_b s) + \mathrm{v}\bullet\nabla(\theta c + \rho_b s)$$

Substitution of this equation and Equation (13.17) into Equation (13.16) now gives

$$-M_L = \int_{\Omega}\left[D_t(\theta c + \rho_b s) + \mathrm{v}\bullet\nabla(\theta c + \rho_b s) + (\theta c + \rho_b s)\nabla\bullet\mathrm{v}\right]Jd\Omega_0$$

$$= \int_{\Omega}\left[D_t(\theta c + \rho_b s) + \nabla\bullet\{\mathrm{v}(\theta c + \rho_b s)\}\right]d\Omega$$

By using this equation and Equations (13.10) and (13.12), Equation (13.13) can be rewritten in the form

$$\int_{\Omega}\left[D_t(\theta c + \rho_b s) + \nabla\bullet\{\mathrm{v}(\theta c + \rho_b s)\}\right]d\Omega = -\lambda\int_{\Omega}(\theta c + \rho_b s)d\Omega - \int_{\Omega}\nabla\bullet\mathbf{F}d\Omega$$

or

$$\int_{\Omega}\left[D_t(\theta c + \rho_b s) + \nabla\bullet\{\mathrm{v}(\theta c + \rho_b s)\} + \lambda(\theta c + \rho_b s) + \nabla\bullet\mathbf{F}\right]d\Omega = 0.$$

Since $d\Omega_0$ and thus $d\Omega$ is, by assumption, an arbitrary volume element,

$$D_t(\theta c + \rho_b s) + \nabla\bullet\{\mathrm{v}(\theta c + \rho_b s)\} = -\lambda(\theta c + \rho_b s) - \nabla\bullet\mathbf{F} \qquad (13.18)$$

is the differential equivalent of the mass balance in Equation (3.13).

Sources and sinks have been completely neglected in the derivation of Equation (13.18). However, this defect can be easily rectified by adding the flux $cf_0(\mathbf{x},t)$ from a source (sink) with strength $f_0(\mathbf{x},t)$ (see Section 11.1), to the right-hand side of Equation (13.18). This yields the famous hydrodynamic dispersion equation

$$D_t(\theta c + \rho_b s) + \nabla\bullet\{\mathrm{v}(\theta c + \rho_b s)\} = -\lambda(\theta c + \rho_b s) - \nabla\bullet\mathbf{F} + cf_0(\mathbf{x},t), \qquad (13.19)$$

which is at the moment considered to be the best conceptual model for mass transport in a porous medium.

## 13.3 THE DISPERSION COEFFICIENT

Very little is known at present about the physical mechanisms responsible for the existence of the mass flux F. However, it is reasonable to assume that F is related to the *microscopic fluid velocity*, i.e. the velocity of the fluid at a particular point in the medium. With this in mind, F can be conveniently expressed in the form

$$F = cq^*,$$

where $q^*$ is the generalized microscopic Darcy velocity, defined in Equation (11.6). Because of the nature of porous flow, $q^*$ is not a constant, but varies continuously from point to point in space and time. Because of the resolution of available instruments, most measurements of fluid velocity are not concerned with the microscopic Darcy velocity, but rather its mean value $\bar{q}^*$. The mass flux can, therefore, also be expressed in the form

$$F = c(q^* + q_0),$$

where $q_0$ is the deviation of $q^*$ from $\bar{q}^*$. The terms $c\bar{q}^*$ and $cq_0$ are often referred to as the *advective* and *dispersive* mass fluxes.

Experimental evidence suggests that the term $cq_0$ in the previous equation can be represented mathematically by an equation of the form

$$cq_0 = -\rho\theta\underline{D}\nabla C, \qquad (13.20)$$

where $\underline{D}$ is a symmetric second rank tensor, similar to the hydraulic conductivity tensor, customarily referred to as the *coefficient of mechanical dispersion* or *dispersion tensor.*

While numerous determinations of $\underline{D}$ have been conducted in the laboratory, very little is still known about its true behaviour in the field. What these experiments do indicate, is that $\underline{D}$ is strongly dependent on the mean velocity of the flow and generally greater in the direction of flow than perpendicular to it. Based on these considerations and a theoretical investigation, similar to that used in deriving expressions for the hydraulic conductivity, Bear (1972) suggests that the ij–th component of $\underline{D}$ is given by

$$\theta D_{ij} = \alpha_T\bar{q}^*\delta_{ij} + (\alpha_L - \alpha_T)\frac{q_i q_j}{\bar{q}^*}. \qquad (13.21)$$

It is well-known that a dissolved mass always tends to spread evenly through the solution, even if the fluid is at rest. This property, known as *molecular diffusion*, is usually represented mathematically by *Fick's law*

$$F_m = -D_m\nabla c,$$

where $D_m$ is the *molecular diffusion coefficient* of the dissolved mass in the free fluid. To account for the tortuous nature of a porous medium, Bear (1979) expressed the molecular diffusion in porous flow in the form

$$F_m = -D_m\underline{T}\nabla c = -\underline{D}_m\nabla c, \tag{13.22}$$

where $\underline{T}$ is the tortuosity tensor of the medium, and $\underline{D}_m$ the *molecular diffusion tensor.* The complete coefficient of hydrodynamic dispersion can thus be defined as

$$\underline{D}_h = \underline{D} + \underline{D}_m, \tag{13.23}$$

i.e. as the sum of the coefficient of mechanical dispersion in Equation (13.20) and the molecular diffusion tensor in Equation (13.22). Substitution of the Equations (13.20) to (13.23) into Equation (3.19), yields the more usual form of the hydrodynamic dispersion equation

$$D_t(\theta c + \rho_b s) + \nabla \bullet \{v(\theta c + \rho_b s)\} = -\nabla \bullet (c\bar{q}^* - \rho\theta\underline{D}_h\nabla C) - \lambda(\theta c + \rho_b s) + cf_o(x,t). \tag{13.24}$$

## 13.4 MASS CONSERVATION IN HYDRODYNAMIC DISPERSION

Equation (13.24) is obviously an expression for the mass conservation of the dissolved solids and fluid combined. However, each of these components must also satisfy the law of mass conservation separately. The possibility thus exists that Equation (13.24) may contain a number of redundant terms. In this connection, it is interesting to note that the terms containing the fluid fraction can also be written in the equivalent form

$$D_t(\theta c) + \nabla \bullet (v\theta c) = \rho\theta\{D_tC + v \bullet \nabla C\} + C\{D_t(\rho\theta) + \nabla \bullet (\rho\theta v)\}$$

where C is the mass fraction concentration defined in Equation (13.1). The second term on the right-hand side of this equation can be replaced by its equivalent expression from Equation (11.7) to obtain

$$D_t(\theta c) + \nabla \bullet (v\theta c) = \rho\theta\{D_tC + v \bullet \nabla C\} + C\{-\nabla \bullet \rho q + \rho f\} \tag{13.25}$$

where

$$q = -\underline{K}\nabla\phi$$

is the ordinary Darcy velocity.

The terms relating to the mass fraction s can be expressed along similar lines of reasoning as

$$D_t(\rho_b s) + \nabla \bullet \{v(\rho_b s)\} = s\{D_t\rho_b + \nabla \bullet \rho_b v\} + \rho_b\{D_t s + v \bullet \nabla s\}$$

The first term on the right-hand side of this equation expresses nothing else than the law of mass conservation for the mass fraction s and the porous matrix. Hence

$$D_t(\rho_b s) + \nabla\bullet\{v(\rho_b s)\} = \rho_b\{D_t s + v\bullet\nabla s\}. \qquad (13.26)$$

Substitution of Equations (13.25) and (13.26) into Equation (13.24), keeping in mind that

$$\nabla\bullet(c\overline{q}^*) = C\nabla\bullet(\rho q + \rho\theta v) + \rho(q + \theta v)\nabla\bullet C,$$

yields

$$[\rho\theta D_t C + \rho_b D_t s + \rho q\bullet\nabla C] + v\bullet[\rho\theta\nabla C + \rho_b\nabla s]$$
$$= \nabla\bullet(\rho\theta\underline{\underline{D}}_h\nabla C) + \rho C(f_o - f) - \lambda(\theta\rho C + \rho_b s) - C\nabla\bullet(\rho\theta v) - \rho\theta v\bullet\nabla C. \qquad (13.27)$$

This is the most general equation for the description of density-dependent mass transport in a consolidating porous medium.

Equation (13.27) is quite complex, with the result that it is seldom applied in practice. Fortunately, the media encountered in groundwater phenomena are often of such a nature that terms containing the matrix velocity, v, can be safely discarded. The resulting equation

$$\rho\theta D_t C + \rho_b D_t s + \rho q\bullet\nabla C = \nabla\bullet(\rho\theta\underline{\underline{D}}_h\nabla C) + \rho C(f_o - f) - \lambda(\theta\rho C + \rho_b s), \qquad (13.28)$$

without the term representing radioactive decay, is particularly useful in modelling density-dependent mass transport, as for example encountered in the phenomenon of sea-water intrusion. However, the equation can be simplified further, if one is only interested in the pollution of groundwater resources, where the density may be taken as independent of the concentration and, in fact, a constant. In such situations, Equation (13.28) can be expressed in its more usual form

$$\theta D_t c + \rho_b D_t s + q\bullet\nabla c = \nabla\bullet(\theta\underline{\underline{D}}_h\nabla c) + c(f_o - f) - \lambda(\theta c + \rho_b s), \qquad (13.29)$$

This is the equation that will be used in the present study.

# CHAPTER 14

# SUMMARY AND RECOMMENDATIONS

## 14.1 GENERAL

The most important result of the present investigation is that the principles of groundwater motion and contaminant transport in porous flow is now better understood than before. Future modellers should, therefore, have no difficulty to model other aquifers with the computer programs developed for this investigation, or similar programs, *provided that the experiences gained during this investigation is kept in mind.* It may, therefore, be useful to again summarize the major results and recommendations here, although they have already been discussed in the main body of the report.

There is no doubt that the success with which a conceptual model can be applied in modelling a given phenomenon, depends ultimately on the developer's ability to understand and interpret the physical basis of the conceptual model. This information is available in a few highly mathematical text books, e.g. Bear (1972, 1979), with little or no attention to the physics involved. Previous experience in teaching postgraduate courses on groundwater modelling, locally and overseas, has indicated that students have difficulty in using these texts to develop a model for their specific application. Part 2 of the present report is consequently devoted to a dicussion of the physics of groundwater motion, which hopefully is more understandable to present and future groundwater modellers. Some parts of this work are new and the rest a new interpretation of accepted results.

## 14.2 VIROLOGICAL STUDIES

Enteric viruses were demonstrated in the inflow water to both Pans 6 and 7 at Atlantis. The viruses isolated, were human in origin and all potentially pathogenic to man. However, no viruses were recovered from borehole water below the injection pans. Survival studies in water indicated an extinction interval of more than 36 weeks for the viruses at ambient room temperature. Several studies were, therefore, initiated in an effort to determine the fate of the viruses.

Several laboratory column models, using both distilled (rain) and storm water, were developed to try and simulate conditions in the aquifer. Unfortunately, these models were less sensitive to adsorption/elusion studies than was visualized. In fact, no adsorption could be detected, using these models.

An additional study was introduced to provide information for determining migration patterns. These kinetic adsorption experiments were extremely sensitive and showed that adsorption to the Atlantis sand differed with virus strain and with pH. The linear relationships observed in the adsorption of viruses to the sand, not only validate the experimental data, but could simplify the modelling of virus migration in the aquifer considerably.

The variability in adsorption of viruses is noted elsewhere in the international literature and can be ascribed to minor alterations in the protein coat of a virus, which affects its charge density. Viruses of the same family, or even of the same species, may differ in this characteristic. Integration of this information into a mathematical model, would thus seem to be the only feasible alternative to determine a safety factor, as far as virus migration in the aquifer is concerned.

## 14.3 GROUNDWATER QUALITY

### 14.3.1 General

The new well points, installed in the aquifer, have filled important voids in the monitoring network, which existed before the investigation. Gaps still exist with regard to the monitoring of natural groundwater on the eastern side of the basin, as well as in the deeper deposits and in the region of the production well field, due to difficulties experienced in installing suitable sampling points with conventional drilling techniques. Since it is of the utmost importance to have sufficient observation points to monitor the spreading of contaminants, it may be worthwhile to search for better and more cost-efficient techniques, to install monitoring points and sample aquifer material, than the drilling and pumping techniques used in this investigation.

### 14.3.2 In the Atlantis Aquifer

The water-level data indicate that the main flow direction of the water, from the infiltration pan, is in a south-southwesterly direction. However, it is possible that if the water level in the pan rises sufficiently high, the aquifer can even be replenished in an easterly direction. Unfortunately, surface flow, especially on the southern side of the basin, complicates the interpretation.

An analysis of the chemical composition of the groundwater in the vicinity of the recharge pan indicated that there is considerable hydrochemical stratification in the aquifer, with the replenished water restricted mainly to the upper layers. However, specific constituents seem to be subjected to divergent processes which need further study, particularly in the region of the production well field.

The groundwater quality in the vicinity of the recharge pan started to improve in 1987, as a result of the suspension of recharge of maturation pond effluent in November 1986, and the good winter rainfall in 1987.

## 14.4 Parameter Identification

The most difficult part in the development of a model for the chemical pollution of groundwater, is to derive suitable boundary and initial conditions and the conceptual parameters required by the model. The conceptual parameters in present conceptual models for groundwater pollution include:

(a) Hydraulic conductivity and specific storativity of a confined aquifer (transmissivity and storage coefficient for a two-dimensional representation).
(b) Hydraulic conductivity and porosity of an unconfined aquifer (hydraulic conductivity, saturated thickness and effective porosity for a two-dimensional representation).
(c) Soil moisture retention curves and saturated hydraulic conductivities for the soils in the unsaturated zone.
(d) Dispersivities for mass transport.

The importance of these parameters in developing an accurate model for a given aquifer, should never be underestimated. For, as demonstrated by this investigation, the accuracy with which the behaviour of a pollutant can be predicted, depends critically on the accuracy with which these parameters are known.

The Atlantis aquifer is, apart from the more obvious chemical pollution, also subjected to sea-water intrusion. This possibility was investigated through a series of cross-borehole packer tests. These investigations indicated not only that sea-water intrusion into the aquifer is a real possibilty, but also that cross-borehole packer tests may be superior to ordinary pumping tests for the evaluation of the conceptual parameters in Karoo type aquifers.

A major disappointment experienced during the investigation, was the failure to determine dispersivities for the Atlantis aquifer, notwithstanding numerous attempts. This failure, which can be ascribed to the divergent processes observed in the transport of dissolved solids in the aquifer, is rather unfortunate. For it meant that one of the objectives of the study, the development of a mass transport model for the aquifer, had to be abandoned.

## 14.5 Horizontal Flow Models

Computer programs for saturated flow were in the past developed with the assumption that the boundaries of aquifers can be considered as impermeable. This is certainly not true for many of the South African aquifers. A new computer program was, therefore, developed for confined and semi-confined aquifers with general boundary conditions. Extensive numerical tests were conducted to verify the mathematical and numerical correctness of the program. However, its application under actual field conditions, has to wait until suitable field data are available.

Unconfined or phreatic flow has in the past often been modelled with computer programs based on the conceptual model for confined flow [Pinder (1973)]. In order to evaluate the correctness of this appraoch, a completely new program, using the Boussinesq equation as the basic conceptual model, was developed. This program was used to develop a preliminary model for groundwater flow in the Atlantis aquifer with excellent results.

## 14.6 Modelling Unsaturated Flow and Mass Transport

An earlier, but similar investigation as the one reported on here, showed that the computer programs available at the Institute for modelling saturated/unsaturated flow, used numerical approximations that tend to be unstable or do not satisfy the law of mass conservation. New computer programs had, therefore, to be developed for that particular investigation. These programs have been discussed elsewhere [Botha (1986, 1990)], but are available to interested parties.

A rather unexpected result obtained from the investigation of mass transport around the infiltration pan at Atlantis, are the large differences observed in the transport of conservative and non-conservative tracers. These differences, which can be ascribed to the influence of the Darcy velocity on the transport of dissolved solids, should be taken as a warning not to try and derive various properties of mass transport by comparing the behaviour of different types of tracers with one another.

## 14.7 GENERAL RECOMMENDATIONS

### 14.7.1 The Atlantis Aquifer

Although the present investigation has shown that the Atlantis aquifer is not seriously polluted at present, the fact remains that it is situated in an industrial area and could, therefore, easily be contaminated by accidental spills and/or wrong management decisions. Two areas that would definitely require more attention, if the pollution of the aquifer is to be avoided, are: (a) the determination of more precise dispersivity values and (b) a more detailed investigation of sea-water intrusion, particularly in the Silwerstroom area.

### 14.7.2 Surface Pollution Sources and Waste Disposal Sites

The experience gained in this investigation of the Atlantis aquifer, suggested that the following precautions should be taken in investigating surface pollution sources and waste disposal sites:

(a) Observations should be conducted at a frequency higher than is usual for saturated flow.

(b) Observations on the different variables, such as water levels, concentrations and soil moisture contents should be limited to strategical periods of time, such as rainfall and flood events, and carried out simultaneously, rather than scattered over long periods of time. The latter procedure can be followed between these strategic periods of time.

(c) Observations should not be limited to the immediate surrounding area of a surface pollution source, but extended to areas immediately below the source.

(d) Piezometric water levels in the aquifer, containing a surface pollution source, should be measured over as large an area as possible. However, observations on the other variables could be limited to detailed studies in profile at a few strategically placed observation sites.

(e) The highly non-linear nature of unsaturated flow and mass transport makes it impossible to predict the spread of pollution from a surface source situated in the unsaturated zone of the earth's surface *a priori*, even by someone with considerable practical experience. This ignorance can be avoided, if the observations on a waste disposal site, as prescribed by law or otherwise, are supplemented with a saturated/unsaturated flow and mass transport model. In view of this, it is recommended that suitable models should be developed for all existing and future major waste disposal sites, if such a model does not exist already, along the lines suggested above.

# APPENDIX A

## UNIVERSITY OF CAPE TOWN
## DEPARTMENT OF MEDICAL MICROBIOLOGY

Table A–1 Observed concentrations of Viruses in Water from Atlantis

| | |
|---|---|
| **Sample:** Borehole G30966 – Infiltration Pond Atlantis | **Code:** A1/87 |
| **Date:** 9 March 1987 | **Date of Report:** 5 June 1987 |
| **Date of Receipt:** 10 March 1987 | |
| **Tissue Culture** | No virus isolated |
| **Microscopic Examination** | No virus detected |
| **Test for Rotavirus** | Rotalex negative |
| **Bacteriology** | < 2 coliphages/100 ml<br>< 2 faecal coliforms/100 ml |
| SPC | < 2,0/100 ml |
| **Remarks** | |

| | |
|---|---|
| **Sample:** Borehole G33110 (shallow) – Infiltration Pond Atlantis | **Code:** A2/87 |
| **Date:** 10 March 1987 | **Date of Report:** 8 June 1987 |
| **Date of Receipt:** 11 March 1987 | |
| **Tissue Culture** | No virus isolated |
| **Microscopic Examination** | No virus detected |
| **Test for Rotavirus** | Rotalex negative |
| **Bacteriology** | < 2 coliphages/100 ml<br>= 1,0x10$^{3}$ faecal coliforms/100 ml |
| SPC | = 2,0x10$^{6}$/100 ml |
| **Remarks** | |

| | |
|---|---|
| **Sample:** Borehole G33135 – Infiltration Pond Atlantis | **Code:** A3/87 |
| **Date:** 17 March 1987 | **Date of Report:** 8 June 1987 |
| **Date of Receipt:** 18 March 1987 | |
| **Tissue Culture** | No virus isolated |
| **Microscopic Examination** | No virus detected |
| **Test for Rotavirus** | Rotalex negative |
| **Bacteriology** | < 2 coliphages/100 ml<br>= 1,0x10$^{2}$ faecal coliforms/100 ml |
| SPC | = 9,0x10$^{3}$/100 ml |
| **Remarks** | |

| | |
|---|---|
| **Sample:** Borehole G33109 (deep) – Infiltration Pond Atlantis | **Code:** A4/87 |
| **Date:** 23 March 1987 | **Date of Report:** 8 June 1987 |
| **Date of Receipt:** 24 March 1987 | |
| **Tissue Culture** | No virus isolated |
| **Microscopic Examination** | No virus detected |
| **Test for Rotavirus** | Rotalex negative |
| **Bacteriology** | < 2 coliphages/100 ml<br>< 2 faecal coliforms/100 ml |
| SPC | $= 2{,}5 \times 10^3$/100 ml |
| **Remarks** | |

| | |
|---|---|
| **Sample:** Borehole G33134 – Infiltration Pond Atlantis | **Code:** A5/87 |
| **Date:** 30 March 1987 | **Date of Report:** 8 June 1987 |
| **Date of Receipt:** 31 March 1987 | |
| **Tissue Culture** | No virus isolated |
| **Microscopic Examination** | No virus detected |
| **Test for Rotavirus** | Rotalex negative |
| **Bacteriology** | < 2 coliphages/100 ml<br>< 2 faecal coliforms/100 ml |
| SPC | $> 5{,}0 \times 10^6$/100 ml |
| **Remarks** | |

| | |
|---|---|
| **Sample:** Borehole G33110 – Infiltration Pond Atlantis | **Code:** A6/87 |
| **Date:** 8 April 1987 | **Date of Report:** ......... |
| **Date of Receipt:** 9 April 1987 | |
| **Tissue Culture** | No virus isolated |
| **Microscopic Examination** | No virus detected |
| **Test for Rotavirus** | Rotalex negative |
| **Bacteriology** | < 2 faecal coliforms/100 ml |
| SPC | $> 2{,}0 \times 10^5$/100 ml |
| **Remarks** | Sample taken after rain |

| | |
|---|---|
| **Sample:** Borehole 33135 – Infiltration Pond Atlantis | **Code:** A7/87 |
| **Date:** | **Date of Report:** 30 September 1987 |
| **Date of Receipt:** | |
| **Tissue Culture** | No virus isolated from 10 L of water |
| **Microscopic Examination** | No virus detected |
| **Test for Rotavirus** | Rotalex negative |
| **Bacteriology** | < 2 coliphages/100 ml |
| | < 2 faecal coliforms/100 ml |
| SPC | = 3,0x10$^{5}$/100 ml |
| **Remarks** | |

| | |
|---|---|
| **Sample:** Atlantis Pan 7 Inlet | **Code:** A8/87 |
| **Date:** 27 April 1987 | **Date of Report:** 30 September 1987 |
| **Date of Receipt:** 28 April 1987 | |
| **Tissue Culture** | ±20 Coxsackie B1 virus/litre<br>±20 Reovirus III/litre isolated |
| **Microscopic Examination** | Enterovirus and Reovirus detected |
| **Test for Rotavirus** | Rotalex negative |
| **Bacteriology** | = 8,0x10$^{2}$ coliphages/100 ml |
| | = 80,0 faecal coliforms/100 ml |
| SPC | = 4,0x10$^{6}$/100 ml |
| **Remarks** | Coxsackie B viruses are pathogenic to man. They may cause Bornholm disease, myocarditis, meningitis and bronchitis and pneumonia in children.<br>Reoviruses are ubiquitous and could be from humans or animals |

| | |
|---|---|
| **Sample:** Atlantis Pan 7 Inlet | **Code:** A9/87 |
| **Date:** 5 May 1987 | **Date of Report:** 30 September 1987 |
| **Date of Receipt:** 5 May 1987 | |
| **Tissue Culture** | ±20 Coxsackie B6 virus/litre<br>100 Reovirus III/litre isolated |
| **Microscopic Examination** | Enterovirus and Reovirus detected |
| **Test for Rotavirus** | Rotalex negative |
| **Bacteriology** | = 1,3x10$^{4}$ coliphages/100 ml |
| | = 100,0 faecal coliforms/100 ml |
| SPC | = 2,0x10$^{6}$/100 ml |
| **Remarks** | Coxsackie B viruses are pathogenic to man. They may cause Bornholm disease, myocarditis, meningitis and bronchitis and pneumonia in children.<br>Reoviruses are ubiquitous and could be from humans or animals |

| | |
|---|---|
| **Sample:** Atlantis Pan 7 Inlet | **Code:** A10/87 |
| **Date:** 11 May 1987 | **Date of Report:** 30 September 1987 |
| **Date of Receipt:** 12 May 1987 | |
| **Tissue Culture** | ±10 Coxsackie B4 virus/litre |
| **Microscopic Examination** | Enterovirus detected |
| **Test for Rotavirus** | Rotalex negative |
| **Bacteriology** | = 200,0 coliphages/100 ml<br>= 60,0 faecal coliforms/100 ml<br>SPC = $2{,}5\text{x}10^5$/100 ml |
| **Remarks** | Coxsackie B viruses are pathogenic to man. They may cause Bornholm disease, myocarditis, meningitis and bronchitis and pneumonia in children.<br>Reoviruses are ubiquitous and could be from humans or animals |

| | |
|---|---|
| **Sample:** Storm water to Pond 6 Atlantis | **Code:** A1/88 |
| **Date:** 23 August 1988 | **Date of Report:** 23 September 1988 |
| **Date of Receipt:** 23 August 1988 | |
| **Tissue Culture** | Enterovirus – like CPE detected |
| **Microscopic Examination** | Picornavirus and Reovirus detected |
| **Test for Rotavirus** | Rotalex negative |
| **Bacteriology** | = 13,0 coliphages/100 ml<br>< 2 faecal coliforms/100 ml |
| **Remarks** | |

| | |
|---|---|
| **Sample:** Borehole G33443 | **Code:** A2/88 |
| **Date:** 24 August 1988 | **Date of Report:** 23 September 1988 |
| **Date of Receipt:** 25 August 1988 | |
| **Tissue Culture** | No viruses isolated |
| **Microscopic Examination** | No virus detected |
| **Test for Rotavirus** | Rotalex negative |
| **Bacteriology** | < 2 coliphages/100 ml<br>< 2 faecal coliforms/100 ml |
| **Remarks** | |

# APPENDIX B

## Computation of the Three-dimensional Hydraulic Conductivity Tensor using the Cross-borehole Packer Method

Since the computational aspects associated with the computation of the hydraulic conductivity tensor $\underline{K}$ and storage coefficient $S_0$ from cross-borehole packer tests, are independent of the depth, the present discussion will be restricted to the results for the test at 42 m in the Malmesbury Formation, which underlies the Atlantis Aquifer.

The first step in applying the method is to choose a global coordinate system $(x^1,x^2,x^3)$ to which the measurements can be referred. In this investigation, the global coordinate system was chosen as the right-handed Cartesian equivalent of the left-handed Lo-system in Figure 5–1, with the z-direction vertically upward. This coordinate is shown schematically in Figure B–1.

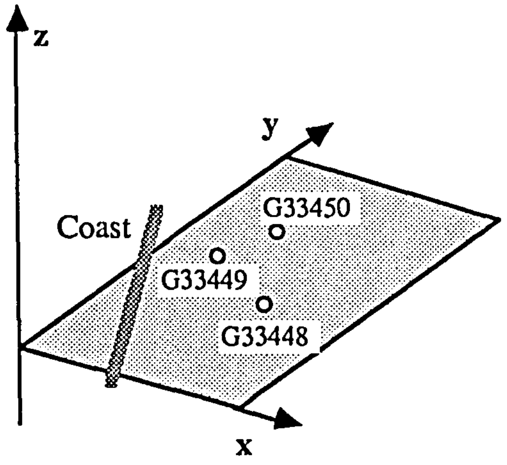

**Figure B–1** The position of the three test boreholes, G33448, G33449 and G33450, relative to one another and the global (x,y,z)–coordinate system (not according to scale)

As discussed in Chapter 5, it is advantageous to combine the boreholes in groups of two, when conducting the actual field observations associated with cross-borehole tests. The three groups of boreholes, used in the present investigation, and the associated coordinates of the individual boreholes are summarized in Table B–1.

**Table B–1** The group combinations of the three test boreholes, together with the coordinates of each borehole

| Group 1 | Group 2 | Group 3 | (x,y)–Coordinates | |
|---|---|---|---|---|
| G33448 | G33449 | G33448 | G33448 | (–57523,240; –20522,200) |
| G33449 | G33450 | G33450 | G33449 | (–57530,185; –20521,555) |
| | | | G33450 | (–57526,695; –20519,900) |

The combination of tests used for calculating $\underline{K}$ at the depth of 42 m, is presented graphically in Figure B–2. The arrows in this figure represent the position vector r defined in Equation (5.8) and Figure 5–3. The complete set of pressure variations (in m of water) as a function of time, is given in Table B–2.

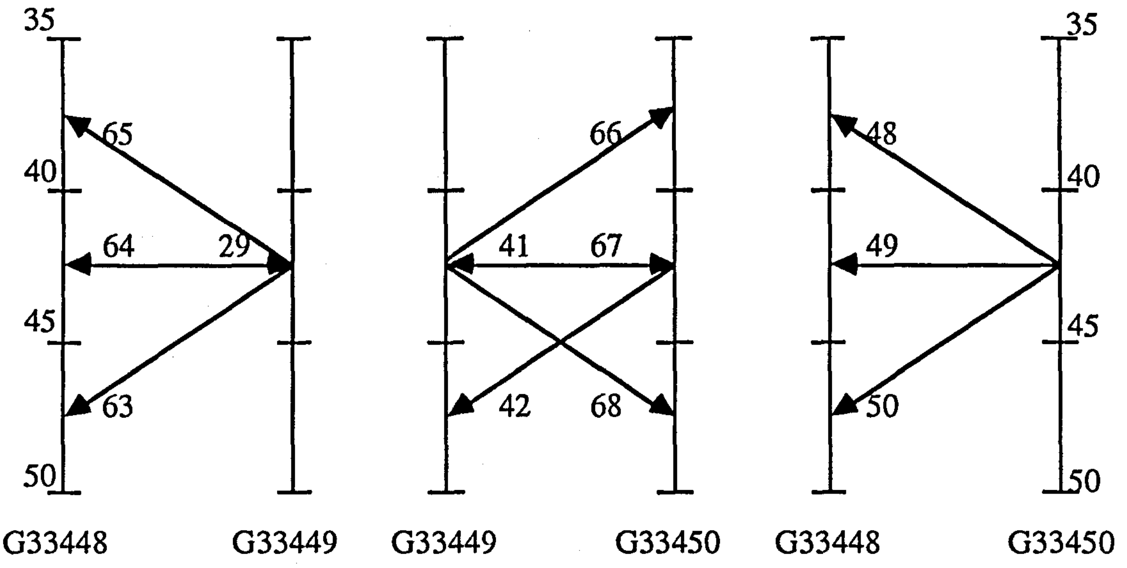

**Figure B–2** Combination of the tests used in the computation of the hydraulic conductivity tensor and specific storage at the depth of 42 m. The arrows indicate the direction of a specific test

**Table B–2** Pressure increases in the observation boreholes as a function of time for all tests used to obtain <u>K</u> and $S_0$ at a depth of 42 m

| Time | Test number | | | | | | | | | | | |
|---|---|---|---|---|---|---|---|---|---|---|---|---|
| (s) | 29 | 41 | 42 | 48 | 49 | 50 | 63 | 64 | 65 | 66 | 67 | 68 |
| 0 | 1,341 | 1,411 | 0,894 | 0,905 | 1,011 | 0,858 | 0,862 | 0,886 | 0,980 | 0,988 | 0,956 | 0,839 |
| 60 | 1,423 | 1,447 | 0,894 | 1,294 | 1,764 | 1,235 | 0,917 | 0,949 | 1,011 | 1,011 | 1,003 | 0,878 |
| 120 | 1,482 | 1,482 | 0,976 | 1,341 | 2,388 | 1,341 | 0,964 | 0,988 | 1,050 | 1,043 | 1,027 | 0,901 |
| 180 | 1,505 | 1,505 | 1,129 | 1,376 | 2,435 | 1,376 | 0,988 | 0,996 | 1,074 | 1,058 | 1,050 | 0,925 |
| 240 | 1,505 | 1,505 | 1,211 | 1,388 | 2,458 | 1,399 | 1,003 | 1,003 | 1,090 | 1,082 | 1,058 | 0,941 |
| 300 | 1,517 | 1,505 | 1,223 | 1,399 | 2,482 | 1,411 | 1,003 | 1,019 | 1,098 | 1,090 | 1,074 | 0,956 |
| 360 | 1,505 | 1,505 | 1,247 | 1,411 | 2,482 | 1,423 | 1,011 | 1,019 | 1,105 | 1,090 | 1,082 | 0,964 |
| 420 | 1,482 | 1,541 | 1,258 | 1,411 | 2,482 | 1,423 | 1,003 | 1,011 | 1,113 | 1,098 | 1,090 | 0,972 |
| 480 | 1,505 | 1,541 | 1,247 | 1,411 | 2,482 | 1,447 | 1,019 | 1,011 | 1,129 | 1,113 | 1,098 | 0,988 |
| 540 | 1,482 | 1,541 | 1,247 | 1,423 | 2,505 | 1,458 | 1,027 | 1,043 | 1,121 | 1,113 | 1,098 | 0,996 |
| 600 | 1,494 | 1,529 | 1,247 | 1,435 | 2,541 | 1,470 | 1,043 | 1,043 | 1,121 | 1,113 | 1,105 | 0,996 |
| 660 | 1,494 | 1,529 | 1,247 | 1,435 | 2,529 | 1,458 | 1,027 | 1,050 | 1,121 | 1,121 | 1,113 | 1,003 |
| 720 | 1,505 | 1,541 | 1,270 | 1,447 | 2,517 | 1,470 | 1,019 | 1,050 | 1,121 | 1,121 | 1,113 | 1,011 |
| 780 | 1,505 | 1,541 | 1,258 | 1,435 | 2,517 | 1,470 | 1,011 | 1,043 | 1,129 | 1,121 | 1,121 | 1,011 |
| 840 | 1,517 | 1,541 | 1,270 | 1,435 | 2,517 | 1,470 | 1,027 | 1,035 | 1,121 | 1,129 | 1,121 | 1,019 |
| 900 | 1,505 | 1,529 | 1,270 | 1,435 | 2,505 | 1,470 | 1,035 | 1,043 | 1,137 | 1,137 | 1,129 | 1,019 |
| 960 | 1,505 | 1,541 | 1,247 | 1,423 | 2,517 | 1,482 | 1,043 | 1,050 | 1,145 | 1,145 | 1,137 | 1,027 |
| 1020 | 1,505 | 1,541 | 1,270 | 1,423 | – | – | 1,043 | 1,050 | 1,145 | 1,152 | 1,137 | 1,027 |
| 1080 | 1,505 | 1,541 | 1,258 | 1,423 | – | – | 1,027 | 1,050 | 1,152 | 1,145 | 1,145 | 1,035 |
| 1140 | 1,517 | 1,541 | 1,247 | 1,423 | – | – | – | 1,058 | 1,152 | 1,145 | 1,152 | 1,043 |
| 1200 | 1,517 | 1,541 | 1,258 | 1,423 | – | – | – | 1,043 | 1,176 | 1,152 | 1,160 | 1,050 |
| 1260 | 1,517 | 1,529 | 1,270 | 1,423 | – | – | – | 1,050 | 1,176 | 1,152 | – | 1,050 |
| 1320 | 1,517 | 1,541 | 1,282 | 1,423 | – | – | – | 1,050 | 1,168 | 1,152 | – | 1,050 |
| 1380 | 1,517 | 1,541 | 1,282 | – | – | – | – | – | 1,168 | – | – | 1,058 |
| 1440 | 1,517 | 1,541 | 1,294 | – | – | – | – | – | 1,176 | – | – | – |
| 1500 | 1,529 | – | 1,270 | – | – | – | – | – | – | – | – | – |

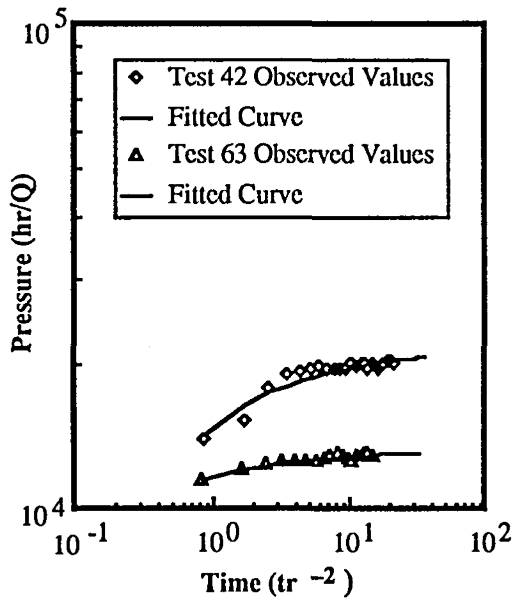

**Figure B–3** Graphical representation of the observed normalized pressures and associated fitted curves, for the tests conducted at 42 and 63 m

The relation between pressure variations in the observation borehole and time is given by Equation (5.10), with $K_d(n)/D$ and $S_0/K_d(n)$ the unknown parameters. These parameters can be determined by either a graphical method [Hsieh, *et al.* (1983)], or the curve fitting method, described in Chapter 5. The results obtained with the latter method are displayed grahically in Figure B–3, for two of the tests conducted at Atlantis; one at a depth of 42 m and the other at a depth of 63 m.

**Table B–3** Components of the position vectors **r** used in obtaining $\underline{\mathbf{K}}$ and $S_0$ at a depth of 42 m, with the values of $K_d(\mathbf{n})/D$ and $S_0/D$, obtained from the curve fitting procedure

| Test | Coordinates of r | | | Magnitudes of | |
|---|---|---|---|---|---|
| Number | $x_i^1$ | $x_i^2$ | $x_i^3$ | $K_d(n_i)/D$ | $S_0/D$ |
| 29 | –6,945 | 0,645 | –5,028 | $2{,}3757.10^{11}$ | $2{,}0558.10^{09}$ |
| 41 | –3,525 | –5,610 | 0,036 | $4{,}6109.10^{10}$ | $1{,}1643.10^{09}$ |
| 42 | –3,525 | –5,610 | –4,964 | $7{,}9602.10^{10}$ | $3{,}3566.10^{10}$ |
| 48 | 3,420 | –6,255 | 5,064 | $4{,}3552.10^{10}$ | $1{,}5332.10^{09}$ |
| 49 | 3,420 | –6,255 | 0,064 | $1{,}0787.10^{11}$ | $3{,}5049.10^{10}$ |
| 50 | 3,420 | –6,255 | –4,936 | $4{,}9559.10^{10}$ | $5{,}3551.10^{09}$ |
| 63 | 6,945 | –0,645 | –4,972 | $2{,}8386.10^{10}$ | $1{,}4811.10^{09}$ |
| 64 | 6,945 | –0,645 | 0,028 | $2{,}0249.10^{10}$ | $1{,}2624.10^{09}$ |
| 65 | 6,945 | –0,645 | 5,028 | $3{,}9620.10^{10}$ | $3{,}0049.10^{09}$ |
| 66 | 3,525 | 5,610 | 4,964 | $3{,}7242.10^{10}$ | $2{,}7949.10^{09}$ |
| 67 | 3,525 | 5,610 | –0,036 | $2{,}4265.10^{10}$ | $3{,}1801.10^{09}$ |
| 68 | 3,525 | 5,610 | –5,036 | $3{,}2886.10^{10}$ | $4{,}8407.10^{09}$ |

The next step in obtaining $\underline{\mathbf{K}}$ is to substitute $x_i$, $r_i$ and $K_d(n_i)/D$ for each test (see Table B–3) into Equation (5.7). When solved, this set of linear equations yields the adjoint of $\underline{\mathbf{K}}$, the matrix A. However, as mentioned in Chapter 5, there are a number of conditions that must be satisfied, to ensure that this system of linear equations does not become ill-conditioned. Because of the large number of observations available, the resulting set of equations was solved with a multiple regression method. The components of the matrix A, obtained in this way, are shown in Table B–4.

**Table B–4** Components of the coefficient matrix in Equation (5.7) for the test at 42 m depth

| $(x_i^1)^2$ | $(x_i^2)^2$ | $(x_i^3)^2$ | $2x_i^1x_i^3$ | $2x_i^2x_i^3$ | $2x_i^1x_i^2$ | $\frac{R_i^2D}{K_d(n_i)}$ |
|---|---|---|---|---|---|---|
| 48,23 | $4,160.10^{-1}$ | $2,528.10^{+1}$ | $6,984.10^{+1}$ | $6,486.10^{+0}$ | $-8,959.10^{+0}$ | $3,112.10^{-10}$ |
| 12,43 | $3,147.10^{+1}$ | $1,296.10^{-3}$ | $-2,538.10^{-1}$ | $-4,039.10^{-1}$ | $3,955.10^{+1}$ | $9,520.10^{-10}$ |
| 12,43 | $3,147.10^{+1}$ | $2,464.10^{+1}$ | $3,499.10^{+1}$ | $5,569.10^{+1}$ | $3,955.10^{+1}$ | $8,610.10^{-10}$ |
| 11,69 | $3,913.10^{+1}$ | $2,564.10^{+1}$ | $3,464.10^{+1}$ | $6,335.10^{+1}$ | $-4,278.10^{+1}$ | $1,756.10^{-09}$ |
| 11,69 | $3,913.10^{+1}$ | $4,096.10^{-3}$ | $4,378.10^{-1}$ | $-8,006.10^{-1}$ | $-4,278.10^{+1}$ | $4,712.10^{-10}$ |
| 11,69 | $3,913.10^{+1}$ | $2,436.10^{+1}$ | $-3,376.10^{+1}$ | $6,175.10^{+1}$ | $-4,278.10^{+1}$ | $1,517.10^{-09}$ |
| 48,23 | $4,160.10^{-1}$ | $2,472.10^{+1}$ | $-6,906.10^{+1}$ | $6,414.10^{+0}$ | $-8,959.10^{+0}$ | $2,585.10^{-09}$ |
| 48,23 | $4,160.10^{-1}$ | $7,840.10^{-4}$ | $3,889.10^{-1}$ | $-3,612.10^{-2}$ | $-8,959.10^{+0}$ | $2,403.10^{-09}$ |
| 48,23 | $4,160.10^{-1}$ | $2,528.10^{+1}$ | $6,984.10^{+1}$ | $6,486.10^{+0}$ | $-8,959.10^{+0}$ | $1,866.10^{-09}$ |
| 12,43 | $3,147.10^{+1}$ | $2,464.10^{+1}$ | $3,499.10^{+1}$ | $5,569.10^{+1}$ | $3,955.10^{+1}$ | $1,840.10^{-09}$ |
| 12,43 | $3,147.10^{+1}$ | $1,296.10^{-3}$ | $-2,538.10^{-1}$ | $-4,039.10^{-1}$ | $3,955.10^{+1}$ | $1,809.10^{-09}$ |
| 12,43 | $3,147.10^{+1}$ | $2,536.10^{+1}$ | $-3,550.10^{+1}$ | $5,650.10^{+1}$ | $3,955.10^{+1}$ | $2,106.10^{-09}$ |

Once A has been determined, its determinant D, which is the same as the determinant of $\underline{K}$ see (5.3), can be computed from

$$D = (A_{11}A_{22}A_{33} + 2A_{12}A_{23}A_{13} - A_{11}A_{23}^2 - A_{22}A_{13}^2 - A_{33}A_{12}^2)^{1/2} \quad (B.1)$$

and the components of the hydraulic conductivity tensor $\underline{K}$ from the inverse of Equation (5.4)

$$K_{11} = \frac{A_{22}A_{33} - A_{23}^2}{D} \qquad K_{22} = \frac{A_{11}A_{33} - A_{13}^2}{D} \qquad K_{33} = \frac{A_{11}A_{22} - A_{12}^2}{D}$$

$$K_{12} = \frac{A_{13}A_{23} - A_{12}A_{33}}{D} \qquad K_{23} = \frac{A_{12}A_{13} - A_{23}A_{11}}{D} \qquad K_{13} = \frac{A_{12}A_{23} - A_{13}A_{22}}{D} \quad (B.2)$$

The hydraulic conductivity tensor, obtained from the data in Table B–4 and Equation B.2, is given by

$$\underline{K} = \begin{pmatrix} K_{xx} & K_{xy} & K_{xz} \\ K_{yx} & K_{yy} & K_{yz} \\ K_{zx} & K_{zy} & K_{zz} \end{pmatrix} = \begin{pmatrix} 3,0922 & -0,5433 & 2,2977 \\ -0,5433 & 4,1093 & 0,6911 \\ 2,2977 & 0,6911 & 9,0722 \end{pmatrix} x10^{-6} \quad (B.3)$$

It is not easy to visualize $\underline{K}$ in this form. The magnitudes of the principle axes, with their direction cosines, were consequently calculated and given in Tables 5–3 and 5–4, together with those for the other two depths at which observations were made. Mathematically, this means that one has to calculate the eigenvalues and eigenvectors of the matrix in Equation (B.3). A particular advantage of the three mutually orthogonal principle axes, is that they allow one to express the hydraulic conductivity tensor in diagonal form as

$$\underline{K} = \begin{pmatrix} K_{xx} & 0 & 0 \\ 0 & K_{yy} & 0 \\ 0 & & K_{zz} \end{pmatrix} = \begin{pmatrix} 2{,}04 & 0 & 0 \\ 0 & 4{,}34 & 0 \\ 0 & 0 & 9{,}89 \end{pmatrix} x10^{-6} \quad (B.4)$$

These three principle components of the hydraulic conductivity tensor and their components in the global coordinate system, are represented graphically in Figure 5–8.

With the determinant D known, the values of the specific storativity, $S_0$, can be computed for each test from the $S_0/D$ values obtained from the curve fitting. The averages of $S_0$, for the three observation depths used in the present investigation, can be found in Table 5–2.

# APPENDIX C

# DISCUSSION OF THE TWO-DIMENSIONAL FLOW PROGRAMS

## C.1 Introduction

Two computer programs were developed by the Institute for Groundwater Studies to model the two-dimensional motion of saturated groundwater. The first one, GCON, is for confined aquifers and the second, GWUN, for unconfined or phreatic aquifers. The two programs were developed as 'twins' in the sense that their numerical and algorithmic details are very similar and that their input and output formats are almost identical.

The aim of this appendix is to give the user a better understanding of what he is doing, rather than a detailed description of either the physics of groundwater flow or the finite element method. A detailed account of the physics of groundwater flow can be found in Part 2 of this report, while readers interested in a more detailed discussion of the finite element method are referred to Botha and Pinder (1983) and Pinder and Gray (1977).

## C.2 Isoparametric Finite Elements

Many programs for the modelling of groundwater resources are based on triangular finite elements. However, because of their potential to approximate irregular boundaries and the solution of the differential equation more accurately than a triangular element, isoparametric quadrilateral elements were used in this program. Botha and Bakkes (1982) have shown that not much can be gained by using elements of order greater than one when point sources or sinks are present in the aquifer. Nevertheless, higher order elements can increase the accuracy of the solution considerably, if these sources are absent. To allow the modeller greater flexibility of choice, all Lagrange and Serendip elements, up to the order two, were included in the present program.

The basic idea behind the quadrilateral finite element is quite simple. Let $\phi_i(\xi,\eta)$ be one of the interpolation polynomials, defined in Table C–1, where $(\xi,\eta)$ is in the local rectangular coordinate system, shown in Figure C–1. Let $N_e$ denotes the number of nodes in the local rectangular element of Figure C–1 and $\delta_{ij}$ the Kronecker delta defined as:

$$\delta_{ij} = \begin{cases} 1 & i = j \\ 0 & i \neq j \end{cases} .$$

Since $\phi_i(\xi,\eta)$ is an interpolation polynomial, $\phi_i(\xi_j,\eta_j) \equiv \delta_{ij}$. Any set of coordinates in the global coordinate system (x,y), like $\{(x_i,y_i) \mid i = 1, 4)\}$ in Figure C–1, can then be expanded in terms of the isoparametric transformation [Botha and Pinder (1983)]

$$x = \sum_{i=1}^{N_c} x_i \, \phi_i(\xi,\eta) \quad y = \sum_{i=1}^{N_c} y_i \, \phi_i(\xi,\eta). \tag{C.1}$$

**Table C–1** Explicit expressions for two-dimensional Lagrange and Serendip basis functions in local coordinates

| | Lagrange | Serendip |
|---|---|---|
| **Linear** | $\frac{1}{4}(1+\xi\xi_i)(1+\eta\eta_j)$ | $\frac{1}{4}(1+\xi\xi_i)(1+\eta\eta_j)\times$ |
| **Quadratic** | | |
| Corner nodes | $\frac{1}{4}\xi\xi_i(1+\xi\xi_i)\eta\eta_j(1+\eta\eta_j)$ | $\frac{1}{4}(1+\xi\xi_i)(1+\eta\eta_j)\times$<br>$(\xi\xi_i+\eta\eta_j-1)$ |
| Side nodes $(0,\eta_j)$ | $\frac{1}{2}(1-\xi^2)\eta\eta_j(1+\eta\eta_j)$ | $\frac{1}{2}(1-\xi^2)(1+\eta\eta_j)$ |
| Side nodes $(\xi_i,0)$ | $\frac{1}{2}\xi\xi_i(1+\xi\xi_i)(1-\eta^2)$ | $\frac{1}{2}(1+\xi\xi_i)(1-\eta^2)$ |
| Interior node | $(1-\xi^2)(1-\eta^2)$ | – |
| **Cubic** | | |
| Corner nodes | $\frac{1}{256}(9\xi^2-1)(\xi_i\xi+1)\times$<br>$(9\eta^2-1)(\eta_j\eta+1)$ | $\frac{1}{32}(1+\xi\xi_i)(1+\eta\eta_j)\times$<br>$[9(\xi^2+\eta^2)-10]$ |
| Side nodes<br>$(\xi_i=\pm\frac{1}{3},\eta_j)$ | $\frac{9}{256}(1-\xi^2)(1+3\xi\xi_i)\times$<br>$(9\eta^2-1)(\eta_j\eta+1)$ | $\frac{9}{32}(1-\xi^2)(1+9\xi\xi_i)\times$<br>$(1+\eta\eta_j)$ |
| $(\xi_i,\eta_j=\pm\frac{1}{3})$ | $\frac{9}{256}(9\xi^2-1)(\xi_i\xi+1)\times$<br>$(1-\eta^2)(1+3\eta\eta_j)$ | $\frac{9}{32}(1-\eta^2)(1+\xi\xi_i)\times$<br>$(1+9\eta\eta_j)$ |
| Interior nodes<br>$(\xi_i=\pm\frac{1}{3},\eta_j=\pm\frac{1}{3})$ | $\frac{81}{256}(1-\xi^2)(1-\eta^2)\times$<br>$(1+3\xi\xi_i)(1+3\eta\eta_j)$ | – |

$\xi_i = \eta_j = \pm 1$ [Botha and Pinder (1983)]

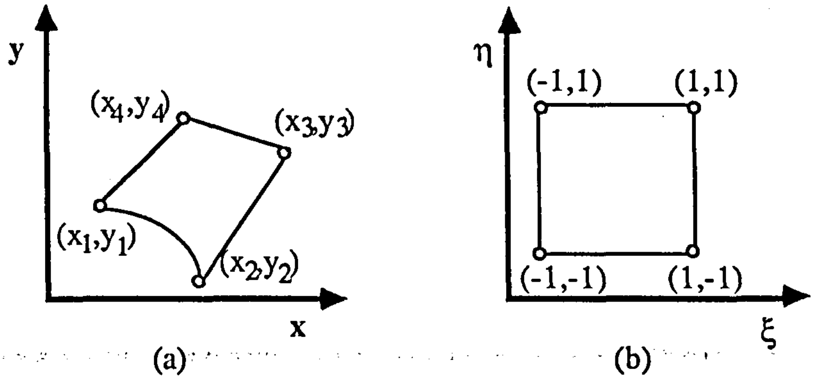

**Figure C-1** Schematic representation of (a) a global and (b) a local rectangular element [Botha and Pinder (1983)]

The transformation, defined in Equation (C.1), is not limited to coordinate values alone, but can also be used to transform derivatives and integrals from global to local coordinates. To achieve this, it is necessary that the Jacobian of the transformation

$$\mathbf{J} = \begin{pmatrix} \dfrac{\partial x}{\partial \xi} & \dfrac{\partial y}{\partial \xi} \\ \dfrac{\partial x}{\partial \eta} & \dfrac{\partial y}{\partial \eta} \end{pmatrix},$$

which results when the chain rule of differentiation is applied to a composite function (such as $f(x,y) = f[x(\xi,\eta), y(\xi,\eta)]$), does not vanish for all values of $(\xi,\eta)$.

## C.3 Application to the Confined Flow Equation

An appropriate approximation for the confined flow equation [Equation (6.1)], can be derived in exactly the same way as used for the phreatic flow in equation in Section 6.3.2. The only real difference is that the resulting time discretized approximation

$$S(x)[h^{n+1}(x) - h^{n}(x)] = \Delta t \; [\nabla \bullet \mathbf{T}(x) \nabla h^{n+1}(x) + Q(x,t_{n+1})]$$

is a linear elliptic partial differential equation. The system of N equations arrived at, after application of the Galerkin finite element method,

$$\int_{\Omega} [\Delta t \mathbf{T}(x) \nabla h^{n+1}(x) \nabla \phi_i(x) + S(x) h^{n+1}(x) \phi_i(x)] d\Omega$$

$$= \int_{\Omega} [S(x) h^{n}(x) \phi_i(x) + \Delta t Q(x,t_{n+1}) \phi_i(x)] d\Omega + \int_{\partial\Omega} n \bullet [\mathbf{T}(x) h(x)] \phi_i(x) dS,$$

where the last term denotes the Neumann boundary conditions, is consequently also linear and need not be solved iteratively.

## C.4 Initial and Boundary Conditions, Source and Sinks

Initial and boundary conditions are, without a doubt, the most important information required in the modelling of subsurface flow phenomena. Initial conditions are generally straightforward to apply, in the sense that any set of suitable water levels can be used for this purpose, but boundary conditions are a little bit more involved.

The boundary conditions encountered in subsurface flow can be either time-dependent, time-independent, homogeneous or non-homogeneous Dirichlet and Neumann conditions, or a combination thereof. In groundwater flow, Dirichlet conditions are encountered where the aquifer is bounded by another body of water (e.g. rivers and lakes), while Neumann conditions are encountered where there is a prescribed flux across a boundary (e.g. an impermeable boundary or a leaky dyke).

A major difficulty experienced with the programs for the simulation of groundwater motion, available at the Institute, was their inability to handle the more complex boundary conditions. Specific attention was, therefore, paid in developing the programs GCON and GWUN to ensure that they can both handle all kinds of boundaries encountered in groundwater flow phenomena. This was achieved by increasing the complexity of the programs somewhat, in the sense that the boundary conditions are read by separate subroutines. In its present form, the program must be supplied with time-dependent boundary conditions at every time step and node (where they apply) in the simulation. However, they can also be generated internally, by defining a new set of subroutines to read them.

To use Dirichlet boundary conditions, the user must specify the total number of Dirichlet boundary nodes, as well as the number of time-dependent Dirichlet boundaries (NDN and NDT) in input Record 3. The user should, however, exercise some care when specifying the actual Dirichlet heads in input record 18, as the program assumes that the first NDT of these values is associated with time-dependent values. The parameter NDT should thus be set to zero if there are no time-dependent Dirichlet nodes, otherwise the program will try to update them from time to time.

Homogeneous Neumann, or zero-flux, boundary conditions are ignored by both programs, as is done in all finite element programs. Non-homogeneous fluxes must, on the other hand, be specified nodewise for each element side where they are applicable. The program then computes the total flux into or out of the element by integrating the flux over the length of the element's side. However, this should not present any difficulties, *provided* that the user remembers that *all* Neumann fluxes *directed into the aquifer* are *positive* and *all* Neumann fluxes *directed out of the aquifer* are *negative, irrespective of the coordinate directions*. Time-dependent Neumann fluxes are handled in a similarly way as their Dirichlet counterparts.

Provision has also been made in the program for time-dependent recharge and discharge to the aquifer, as either areal sources (e.g. rainfall) or point sources (boreholes and springs). To use this facility, the user must supply either the intensity (dimensions $[L.T^{-1}]$) for areal, or the yield (dimensions $[L^3.T^{-1}]$), for point sources or sinks, in profiles. In the case of rainfall, a number of profiles can be specified over the region, with a specific profile assigned to each node. The profiles need not cover the whole simulation period, but there should be no unspecified intervals in a time profile. The beginning and end of the first interval, in each profile, must be specified, but for the rest only the end must be specified. For example, if the simulation period is 10 days and water withdrawn at a rate of 100 ($m^3/d$) from day three, then at a rate of 150 ($m^3/d$) from day four to six and again at the rate of 100 ($m^3/d$) on day seven, the profile should be of the one shown in Table C–3.

**Table C–2** Example of a point source profile

| Time (h) | Pumping Rate ($m^3/d$) |
|---|---|
| 25 | 100 |
| 36 | 100 |
| 144 | 150 |
| 168 | 100 |

## C.5 Darcy Velocities

As can be seen from the discussion in Chapter 13, the Darcy velocity must always be known as a function of space and time in the modelling of contaminant transport in groundwater. These velocities can be derived from Darcy's law

$$q(x,t) = -\underline{T}\nabla h(x,t),$$

where $\underline{T} = \underline{K}(h - b)$ for a phreatic aquifer, and a direct differentiation of the approximate solution for the flow equation. However, when using the Galerkin finite element method with the Lagrange or Serendip basis functions in Table C–1, the velocities are discontinuous at element boundaries.

This difficulty was avoided in the present programs by applying the Galerkin method, in the form

$$q(x) \approx \sum_{i=1}^{n} q_i \, \phi_i(x) \quad \text{and} \quad h(x) \approx \sum_{i=1}^{n} h_i \, \phi_i(x),$$

directly to Darcy's law, to obtain the set of N linear equations (irrespective of whether the aquifer is confined or phreatic)

$$\int_{\Omega} q(x)\phi_i(x)d\Omega = -\int_{\Omega} \underline{T}\nabla h(x)\phi_i(x)d\Omega, \quad (i = 1, 2, \ldots, N)$$

as soon as the flow equation has been solved. Although originally introduced only for the purpose of modelling contaminant transport, the Darcy velocities proved to be extremely helpful in the calibration of flow models.

## C.6 Data Input

As remarked already, the input formats for data are almost identical for the two programs. The only records that need extra consideration, are those associated with the hydraulic parameters – transmissivity and storativity for a confined aquifer and hydraulic conductivity and specific yield for a phreatic aquifer – while the bottom elevation has also to be specified in the latter case. These differences apply, in particular, to the records numbered 7, 8, 11, 12, 17 and 18, below. To avoid a rather lengthy repetition of format descriptors, records that apply only to GCON are marked with ‘$^{(\#)}$’ and records that apply only to GWUN with ‘$^{(\dagger)}$’. Some records marked ‘$^{(\#\dagger)}$’ apply to both programs. The order of the input records to both programs is fixed and must be adhered to. Free formats are used throughout the programs, except for the first two records. Data for optional conditions, like boundary conditions, recharge and discharge rates need only be specified when used. The different input records are described in more detail below.

**Table C–3** Definition of the variables used in the program

| Variable | Physical Meaning |
|---|---|
| AER$^{\dagger}$, | Absolute error for terminating the iteration |
| ASI (I,J,M) | Areal source profiles [J = j-th entry in profile I, M = 1 time that source starts to operate, M = 2 intensity of the discharge (-) or recharge (+) rate] |
| BOT (I)$^{\dagger}$ | Base elevation of node I |
| DPS (I,J,M) | Point source profiles [J = j-th entry in profile I, M = 1 time that source starts to operate and M = 2 the discharge (–) or recharge (+) rate] |
| DT | Time step increment [A value of not more than 2 hours is recommended] |
| DTM | Maximum value of time increment |
| HCX (I)$^{\dagger}$ | Hydraulic conductivity of node I in the X-direction |
| HCY (I)$^{\dagger}$ | Hydraulic conductivity of node I in the Y-direction |
| HEAD | Problem identification name |
| IAS (I,J) | Node numbers and number of incidences associated with areal source I. [J = 1 node number and J = 2 number of incidences of the areal source] |
| IBE (I,J) | Nodal and element incidences of boundary element I. [J = 1 Number of element with which boundary side is associated, J = 2, ..., KPP+1 node numbers along the element side in a counter-clockwise direction] |
| IDB | Number of time step where time-dependant Dirichlet boundary conditions start |
| IDE | Number of time step where time-dependant Dirichlet boundary conditions stop |
| IDN(I) | Node number where Dirichlet conditions apply. |
| IE (L,N) | Finite element incidences [L = element numbers and N = 1, NEN element node numbers in a counter-clockwise direction] |
| INE (I,J) | Element and node numbers where Neumann conditions apply. [J = 1 element number and J = 2, ..., KPP+1) node numbers along the element side in a counter-clockwise direction] |
| IPRO | Number of rainfall profiles |
| IPS (I,J) | Node number and incidences of point source I. [J = 1 refers to node number and J = 2 to number of incidences] |
| IRE (I,J) | Element and profile number of rainfall elements. [I = element number, J = rainfall profile number] |
| KBW | Estimate of half-bandwidth of the coefficient matrix |
| KDB | Kind of Dirichlet boundary conditions. [KDB = 1 Time-independent, 2 Time-dependent] |
| KNB | Kind of Neumann boundary conditions. [KNB = 1 Time-independent, 2 Time-dependent] |
| KOW | Kind of output wanted [1 = Flow and mass balance parameters, 2 = 1 plus pressure head, 3 = 2 plus Darcy velocity components] |
| KPP | Number of knots in the polynomial used as basis function [2, 3 or 4] |
| LAS | Intensity of the distributed areal sources or sinks [see LHC for options] |
| LDS | Unit in which ALL distances will be supplied [1 = mm, 2 = cm, 3 = m, 4 = km] |
| LHC$^{\dagger}$ | Unit of the hydraulic conductivity [1 = mm/s, 2 = mm/min, 3 = mm/h, 4 = mm/d, 5 = cm/s, 6 = cm/min, 7 = cm/h, 8 = cm/d, 9 = m/s, 10 = m/min, 11 = m/h, 12 = m/d] |
| LHT$^{\#}$ | Unit of the transmissivity [1 = mm$^2$/s, 2 = mm$^2$/min, 3 = mm$^2$/h, 4 = mm$^2$/d, 5 = cm$^2$/s, 6 = cm$^2$/min, 7 = cm$^2$/h, 8 = cm$^2$/d, 9 = m$^2$/s, 10 = m$^2$/min, 11 = m$^2$/h, 12 = m$^2$/d] |
| LNF | Unit of prescribed Neumann fluxes [see LHC for options] |

**Table C-3** (continued)

| | |
|---|---|
| LPI | Line print initial and boundary conditions [LPI = 0 No output required] |
| LPR[†] | Line print residual in the iteration procedure [0 = Print nothing, 1 = print summary to screen and file GWUN.ITR, 2 = 1 plus non-conforming node numbers to file] |
| LPS | Discharge/recharge unit of point sources or sinks. [1 = l/s, 2 = l/min, 3 = l/h, 4 = l/d, 5 = m$^3$/s, 6 = m$^3$/min, 7 = m$^3$/h, 8 = m$^3$/d] |
| LPT | Line print solutions after every LPT time steps [LPT = 0 No output required] |
| LRI | Unit of prescribed rain intensity [see LHC for options] |
| LSD | Store solution on disk in file GWUN.STR every LSD time steps [LSD = 0 Solution not stored] |
| LTS | Unit in which ALL times will be supplied [1 = s, 2 = min, 3 = h, 4 = d, 5 = year (365,25 d)] |
| LTW | Unit in which ALL times must be printed [see LTS for options] |
| MIT[†] | Maximum number of iterations allowed in a time step |
| NAI | Number of areal source incidences in a profile |
| NAS | Number of areal sources or sinks |
| NBE | Number of element sides on boundaries |
| NDN | Number of nodes with Dirichlet type boundary conditions |
| NDP | General index specifier |
| NDT | Number of time-dependent Dirichlet boundaries |
| NE | Number of elements |
| NEN | Number of nodes in an element |
| NH | Highest node number with a prescribed value VAR |
| NI | Increment of node numbers from NL to NH |
| NL | Lowest node number with prescribed value VAR |
| NN | Number of nodes |
| NNE | Number of element sides where a Neumann type boundary condition apply |
| NNN | Number of nodes with a Neumann boundary condition |
| NPI | Max number of point source incidences in a profile |
| NPS | Number of point sources or sinks |
| NRE | Number of elements subjected to rainfall |
| NRI | Number of rainfall incidences in a profile |
| NRP | Number of rainfall profiles |
| NTI | Number of time intervals to be used in the simulation |
| OMEG[†] | Successive relaxation factor for phreatic aquifer [$1.5 \leq$ OMEG $< 5$, Steady-state, OMEG = 1.0 Transient] |
| PDH(I) | Read the time-dependent DB node at every time step, NDT at a time |
| PLN (I) | Initial piezometer level of node I |
| PNF (I,J) | Prescribed Neumann fluxes at the nodes INE (I,J) [J = 2, ..., KPP+1)] |
| PT | Type of piecewise continuous polynomial used as basis function [L = Lagrange, S = Serendip] |
| RFP (K,L,M) | Rainfall incidences [L = l-th entry in profile K, M = 1 time that the rain ends and M = 2 intensity of the rainfall] |
| SPY (I)[†] | Specific yield of node I |
| STY (I)[#] | Storage coefficient of node I |
| TB | Time at which simulation must start |
| TE | Time at which simulation must end |
| TM, | Time step multiplier. [DT (n + 1) = (TM + 1) * DT (n); a value of not more than 0,25 is recommended] |
| TX (I)[#] | Transmissivity of node I in the X-direction |
| TY (I)[#] | Transmissivity of node I in the Y-direction |
| VAR | Value of a prescribed variable (piezometric levels, Dirichlet boundary conditions, bottom elevations, etc.) |
| VARX | Value of hydraulic conductivity in the X-direction |
| VARY | Value of hydraulic conductivity in the Y-direction |
| X (N) | X-coordinate of node N |
| Y (N) | Y-coordinate of node N |

## Table C-4 Definition of the input records required by the programs

| Record No | Description of Record | Variable(s) |
|---|---|---|
| 1 | Program heading (Format 2(A76) | HEAD |
| 2 | Properties of interpolation polynomial used (Format 4X, A1, I5) | PT, KPP |
| 3 | Nodal information | NN, NE, NEN, NDN, NDT, NBE, NNE, NNN, NRE, NPS, NAS, KBW |
| 4 | Rainfall and point source profiles | NRP, NRI, NPI, NAI |
| 5 | Units of simulation parameters | LDS, LTS, LTW, LHC, LNF, LRI, LPS, LAS |
| 6 | Output control parameters | LPI, LPT, LPR†, KOW, LSD |
| 7 | Iteration parameters(†) | MIT, AER, OMEG |
| 8 | Number of time intervals1) | NTI |
| 9 | Time parameters | DT, TM, DTM, TB, TE |
| 10 | Number of hydraulic conductivity [GWUN] or transmissivity [GCON] values | NDP |
| 11 | Hydraulic conductivity or transmissivity values(#†) (different values or groups) | [I, HCX(I), HCY(I)] or [NL, VARX, VARY, NH, NI] |
| 12 | Number of specific yield [GWUN] or storage coefficient [GCON] values(#†) | NDP |
| 13 | Specific yield or storage coefficient (different values or groups) | [I,SPY(I)], or [NL, VAR, NH, NI] |
| 14 | Coordinates of the finite element nodes | N, X(N), Y(N) (N = 1, NN) |
| 15 | Element incidences | IE (L,N) (L = 1, NE; N = 1, NEN) |
| 16 | Number of base elevation values(†) | NDP |
| 17 | Base elevation(†) (different values or groups) | [I, BOT(I)] or [NL,VAR,NH,NI] |
| 18 | Number of different initial piezometric levels | NDP |
| 19 | Initial piezometer levels (different nodes or groups) | [I, PLN(I)] or [NL, VAR, NH, NI] |
| 20 | Boundary element information | IBE (I,J) |
| 21 | Kind of Dirichlet boundary conditions to use | KDB |
| 22 | Number of different Dirichlet boundary sets | NDP |
| 23 | Values of Dirichlet boundaries2) (different nodes or groups) | [IDN(I), DBV(I)] or [NL, VAR, NH, NI] |
| 24 | Kind of Neumann boundary conditions to use | KNB |
| 25 | Incidences and fluxes of Neumann conditions | INE (I,J), PNF (I,J) |
| 26 | Number of rainfall profiles | NDP |
| 27 | Rainfall profile numbers (different profiles or groups of profiles) | [IRE(I,J)] or [NL, IPRO, NH, NI] |
| 28 | Effective rainfall percentage | PER, |
| 29 | Rainfall profiles | RFP (K,L,M) |
| 30 | Identifier and strength of external point sources and sinks | IPS(I,J), DPS(I,J,M) |
| 31 | Identifier and strength of external areal sources and sinks | IAS (I,2), ASI(I,J,M) |
| 32 | Time steps where time-dependent Dirichlet boundaries apply | IBB, IBS |
| 33 | Piezometric heads of the time-dependent Dirichlet nodes | IDN(I), PDH(I) |
| 34 | Fluxes of the time-dependent Neumann boundaries | PNF(I,J) |

1) For a steady state problem, NTI = 0 and Record 9 must be skipped

2) Time-dependent Dirichlet boundary nodes must be placed at the top of the vector

## C.7 Program dimensions and Hardware specifications

The computer programs were developed for IBM personal, or compatible computers, with at least 640 KB of RAM and a hard disk of at least 20 MB. This assumption, which can be easily overruled on 80286/386 based machines and an appropriate Fortran compiler, places some restrictions on the dimensions that can be handled with these programs. To give the potential user some idea of what type of problems can be handled, the maximum dimensions for a basic machine are detailed in Table C–5.

**Table C–5** Program dimensions allowed for the computer programs GCON and GWUN on a basic IBM personal computer with 640 KB of RAM and a hard disk of 20 MB

| Property | Maximum Value |
|---|---|
| Number of nodes | 825 |
| Number of elements | 768 |
| Number of elemental nodes | 16 |
| Coefficient matrix band width | 33 |
| Number of Dirichlet nodes | 112 |
| Number of Neumann elements | 112 |
| Number of rainfall elements | 768 |
| Number of rainfall profiles | 20 |
| Number of rainfall incidences | 52 |
| Number of point sources | 80 |
| Number of point source incidences | 30 |
| Number of areal sources | 5 |
| Number of areal source incidences | 30 |
| Number of boundary elements | 112 |

## C.8 Typical examples

The programs, described above, were tested extensively on a wide range of problems that consisted of different grids, boundary values and hydraulic parameters. To illustrate the application of the programs, consider the phreatic aquifer with an area of 1 200 x 1 200 $m^2$, a bottom elevation of 0 m and initial water level of 10 m (see Figure C–2). The hydraulic conductivity and specific yield were kept constant across the

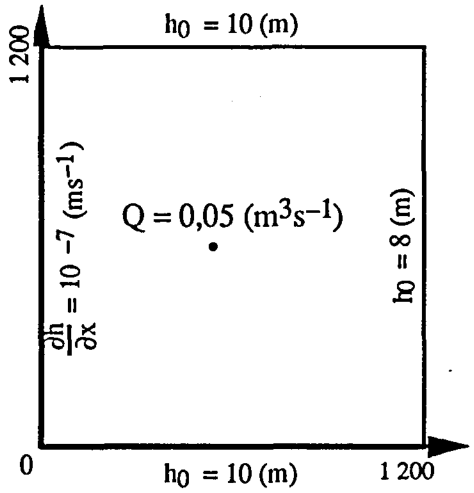

**Figure C-2** A graphical representation of the example model aquifer with $K_{xx} = K_{yy} = 10^3$ m/s and $\theta_c = 10^{-2}$. A well was placed near the centre of the aquifer and pumped at a rate of 0,05 $m^3/s$. Dirichlet boundary conditions were applied on the three sides

$$h(x,0) = h(1200,y) = 10 \text{ m} \quad \text{and} \quad h(x,1200) = 8 \text{ m}$$

and a Neumann condition

$$\frac{\partial h(0,y)}{\partial x} = 10^{-7} \text{ m/s}$$

on the last side.

This finite element mesh,used in this simulation (see Figure C–3) consisted of 169 nodes and 144 elements.

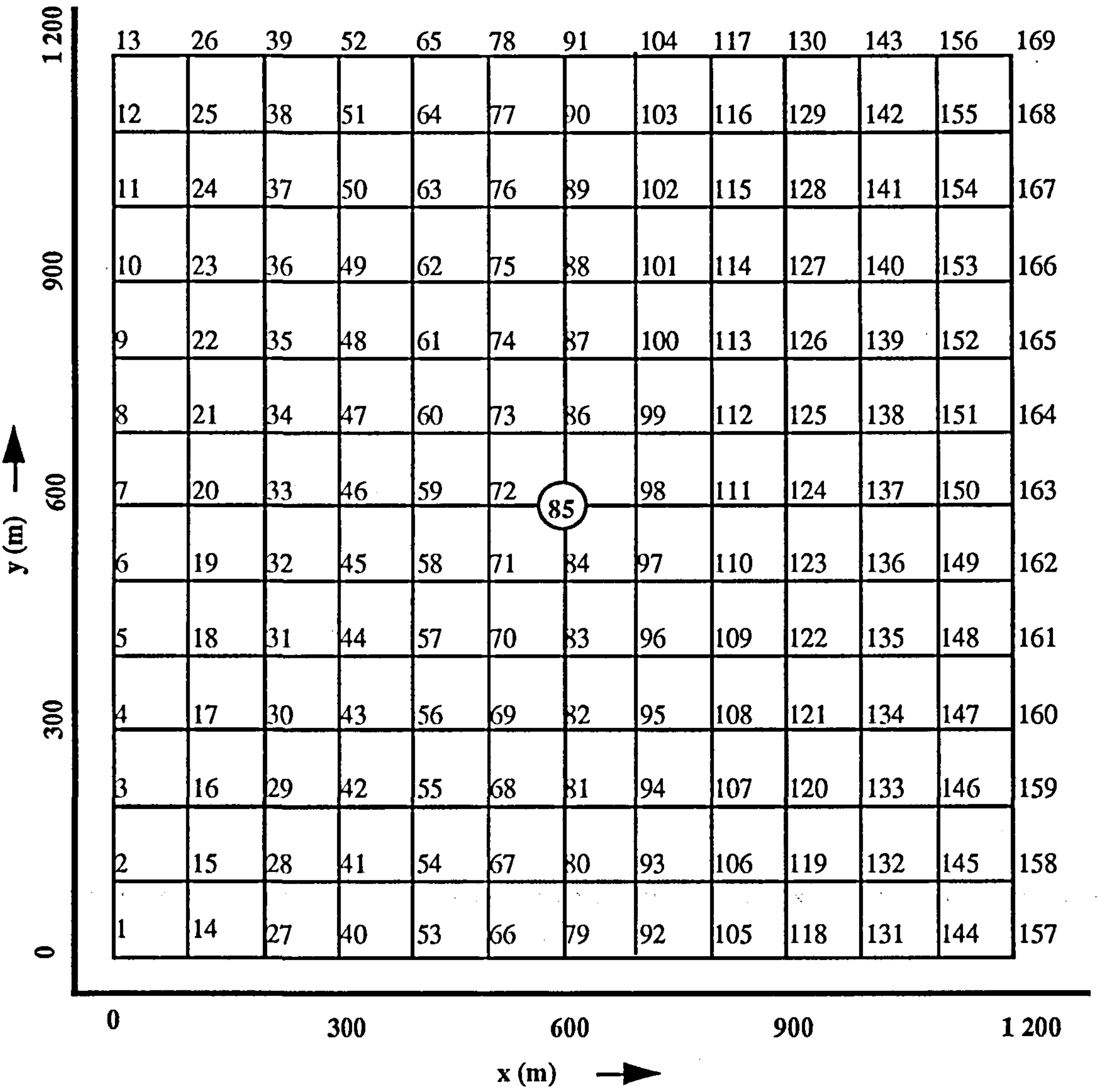

**Figure C–3** The finite element mesh that is used in the illustrative example. The well was placed at node 85

The program GWUN was used to simulate the water levels for a period of 60 h with an initial time step of 2 h. The data required for the simulation is given below in Table C–6. (The input for Program GCON is almost identical).

**Table C–6** An example data set for Program GWUN

| Record | Variable(s) |
|---|---|
| 1 | Example data set for the PROGRAM GWUN. The square mesh used for the aquifer has 169 nodes and 144 elements. |
| 2 | L 2 |
| 3 | 169 144 4 37 0 48 10 169 144 1 0 15 |
| 4 | 1 3 2 0 |
| 5 | 3 3 3 9 9 4 5 4 |
| 6 | 1 1 1 3 1 |
| 7 | 300 1.0E–12 1.0E0 |
| 8 | 10 |
| 9 | 2.0E0 0.25E0 10.0E0 0.0E0 6.0E1 |
| 10 | 1 |
| 11 | 1 1.0E–3 1.0E–3 169 1 |
| 12 | 1 |
| 13 | 1 1.0E–2 169 1 |
| 14 | 1 0.0000000E+00 0.0000000E+00 |
| | 2 0.0000000E+00 1.0000000E+02 |
| | 3 0.0000000E+00 2.0000000E+02 |
| | 4 0.0000000E+00 3.0000000E+02 |
| | 5 0.0000000E+00 4.0000000E+02 |
| | 6 0.0000000E+00 5.0000000E+02 |
| | 7 0.0000000E+00 6.0000000E+02 |
| | 8 0.0000000E+00 7.0000000E+02 |
| | 9 0.0000000E+00 8.0000000E+02 |
| | 10 0.0000000E+00 9.0000000E+02 |
| | 11 0.0000000E+00 1.0000000E+03 |
| | 12 0.0000000E+00 1.1000000E+03 |
| | 13 0.0000000E+00 1.2000000E+03 |
| | 14 1.0000000E+02 0.0000000E+00 |
| | 15 1.0000010E+02 1.0000090E+02 |
| | 16 1.0000010E+02 2.0000010E+02 |
| | 17 1.0000010E+02 3.0000020E+02 |
| | 18 1.0000010E+02 4.0000020E+02 |
| | 19 1.0000010E+02 5.0000020E+02 |
| | 20 1.0000010E+02 6.0000020E+02 |
| | 21 1.0000010E+02 7.0000010E+02 |
| | 22 1.0000010E+02 8.0000020E+02 |
| | 23 1.0000010E+02 9.0000020E+02 |
| | 24 1.0000010E+02 1.0000000E+03 |
| | 25 1.0000000E+02 1.1000000E+03 |
| | 26 1.0000000E+02 1.2000000E+03 |
| | 27 2.0000000E+02 0.0000000E+00 |
| | 28 2.0000010E+02 1.0000010E+02 |
| | 29 2.0000020E+02 2.0000020E+02 |
| | 30 2.0000020E+02 3.0000030E+02 |
| | 31 2.0000030E+02 4.0000030E+02 |
| | 32 2.0000030E+02 5.0000030E+02 |
| | 33 2.0000030E+02 6.0000040E+02 |
| | 34 2.0000030E+02 7.0000030E+02 |
| | 35 2.0000020E+02 8.0000040E+02 |
| | 36 2.0000020E+02 9.0000030E+02 |
| | 37 2.0000010E+02 1.0000000E+03 |
| | 38 2.0000010E+02 1.1000000E+03 |

**Table C-6** (Continued)

| Record | Variable(s) | | |
|---|---|---|---|
| | 39 | 2.0000000E+02 | 1.2000000E+03 |
| | 40 | 3.0000000E+02 | 0.0000000E+00 |
| | 41 | 3.0000020E+02 | 1.0000010E+02 |
| | 42 | 3.0000020E+02 | 2.0000020E+02 |
| | 43 | 3.0000040E+02 | 3.0000040E+02 |
| | 44 | 3.0000040E+02 | 4.0000040E+02 |
| | 45 | 3.0000040E+02 | 5.0000050E+02 |
| | 46 | 3.0000040E+02 | 6.0000050E+02 |
| | 47 | 3.0000040E+02 | 7.0000050E+02 |
| | 48 | 3.0000030E+02 | 8.0000040E+02 |
| | 49 | 3.0000030E+02 | 9.0000040E+02 |
| | 50 | 3.0000020E+02 | 1.0000000E+03 |
| | 51 | 3.0000010E+02 | 1.1000000E+03 |
| | 52 | 3.0000000E+02 | 1.2000000E+03 |
| | 53 | 4.0000000E+02 | 0.0000000E+00 |
| | 54 | 4.0000020E+02 | 1.0000010E+02 |
| | 55 | 4.0000040E+02 | 2.0000030E+02 |
| | 56 | 4.0000040E+02 | 3.0000040E+02 |
| | 57 | 4.0000050E+02 | 4.0000050E+02 |
| | 58 | 4.0000050E+02 | 5.0000050E+02 |
| | 59 | 4.0000050E+02 | 6.0000050E+02 |
| | 60 | 4.0000050E+02 | 7.0000050E+02 |
| | 61 | 4.0000050E+02 | 8.0000060E+02 |
| | 62 | 4.0000030E+02 | 9.0000050E+02 |
| | 63 | 4.0000030E+02 | 1.0000000E+03 |
| | 64 | 4.0000020E+02 | 1.1000000E+03 |
| | 65 | 4.0000000E+02 | 1.2000000E+03 |
| | 66 | 5.0000000E+02 | 0.0000000E+00 |
| | 67 | 5.0000020E+02 | 1.0000010E+02 |
| | 68 | 5.0000040E+02 | 2.0000030E+02 |
| | 69 | 5.0000050E+02 | 3.0000040E+02 |
| | 70 | 5.0000050E+02 | 4.0000050E+02 |
| | 71 | 5.0000050E+02 | 5.0000050E+02 |
| | 72 | 5.0000060E+02 | 6.0000060E+02 |
| | 73 | 5.0000060E+02 | 7.0000070E+02 |
| | 74 | 5.0000050E+02 | 8.0000050E+02 |
| | 75 | 5.0000050E+02 | 9.0000050E+02 |
| | 76 | 5.0000030E+02 | 1.0000000E+03 |
| | 77 | 5.0000020E+02 | 1.1000000E+03 |
| | 78 | 5.0000000E+02 | 1.2000000E+03 |
| | 79 | 6.0000000E+02 | 0.0000000E+00 |
| | 80 | 6.0000020E+02 | 1.0000010E+02 |
| | 81 | 6.0000040E+02 | 2.0000030E+02 |
| | 82 | 6.0000060E+02 | 3.0000040E+02 |
| | 83 | 6.0000050E+02 | 4.0000050E+02 |
| | 84 | 6.0000050E+02 | 5.0000050E+02 |
| | 85 | 6.0000070E+02 | 6.0000060E+02 |
| | 86 | 6.0000070E+02 | 7.0000070E+02 |
| | 87 | 6.0000060E+02 | 8.0000060E+02 |
| | 88 | 6.0000050E+02 | 9.0000060E+02 |
| | 89 | 6.0000040E+02 | 1.0000000E+03 |
| | 90 | 6.0000020E+02 | 1.1000000E+03 |
| | 91 | 6.0000000E+02 | 1.2000000E+03 |
| | 92 | 7.0000000E+02 | 0.0000000E+00 |
| | 93 | 7.0000020E+02 | 1.0000010E+02 |
| | 94 | 7.0000050E+02 | 2.0000030E+02 |
| | 95 | 7.0000050E+02 | 3.0000030E+02 |
| | 96 | 7.0000060E+02 | 4.0000040E+02 |

## Table C–6 (Continued)

| Record | Variable(s) | |
|---|---|---|
| 97 | 7.0000060E+02 | 5.0000050E+02 |
| 98 | 7.0000070E+02 | 6.0000070E+02 |
| 99 | 7.0000060E+02 | 7.0000070E+02 |
| 100 | 7.0000070E+02 | 8.0000070E+02 |
| 101 | 7.0000060E+02 | 9.0000070E+02 |
| 102 | 7.0000040E+02 | 1.0000000E+03 |
| 103 | 7.0000020E+02 | 1.1000000E+03 |
| 104 | 7.0000000E+02 | 1.2000000E+03 |
| 105 | 8.0000000E+02 | 0.0000000E+00 |
| 106 | 8.0000020E+02 | 1.0000010E+02 |
| 107 | 8.0000050E+02 | 2.0000020E+02 |
| 108 | 8.0000060E+02 | 3.0000030E+02 |
| 109 | 8.0000060E+02 | 4.0000040E+02 |
| 110 | 8.0000060E+02 | 5.0000050E+02 |
| 111 | 8.0000060E+02 | 6.0000060E+02 |
| 112 | 8.0000050E+02 | 7.0000060E+02 |
| 113 | 8.0000060E+02 | 8.0000060E+02 |
| 114 | 8.0000050E+02 | 9.0000060E+02 |
| 115 | 8.0000040E+02 | 1.0000000E+03 |
| 116 | 8.0000020E+02 | 1.1000000E+03 |
| 117 | 8.0000000E+02 | 1.2000000E+03 |
| 118 | 9.0000000E+02 | 0.0000000E+00 |
| 119 | 9.0000020E+02 | 1.0000010E+02 |
| 120 | 9.0000040E+02 | 2.0000020E+02 |
| 121 | 9.0000050E+02 | 3.0000030E+02 |
| 122 | 9.0000060E+02 | 4.0000040E+02 |
| 123 | 9.0000050E+02 | 5.0000040E+02 |
| 124 | 9.0000050E+02 | 6.0000050E+02 |
| 125 | 9.0000050E+02 | 7.0000050E+02 |
| 126 | 9.0000050E+02 | 8.0000050E+02 |
| 127 | 9.0000050E+02 | 9.0000050E+02 |
| 128 | 9.0000040E+02 | 1.0000000E+03 |
| 129 | 9.0000020E+02 | 1.1000000E+03 |
| 130 | 9.0000000E+02 | 1.2000000E+03 |
| 131 | 1.0000000E+03 | 0.0000000E+00 |
| 132 | 1.0000000E+03 | 1.0000010E+02 |
| 133 | 1.0000000E+03 | 2.0000010E+02 |
| 134 | 1.0000000E+03 | 3.0000020E+02 |
| 135 | 1.0000000E+03 | 4.0000030E+02 |
| 136 | 1.0000000E+03 | 5.0000040E+02 |
| 137 | 1.0000000E+03 | 6.0000040E+02 |
| 138 | 1.0000000E+03 | 7.0000040E+02 |
| 139 | 1.0000010E+03 | 8.0000040E+02 |
| 140 | 1.0000000E+03 | 9.0000040E+02 |
| 141 | 1.0000000E+03 | 1.0000000E+03 |
| 142 | 1.0000000E+03 | 1.1000000E+03 |
| 143 | 1.0000000E+03 | 1.2000000E+03 |
| 144 | 1.1000000E+03 | 0.0000000E+00 |
| 145 | 1.1000000E+03 | 1.0000000E+02 |
| 146 | 1.1000000E+03 | 2.0000010E+02 |
| 147 | 1.1000000E+03 | 3.0000010E+02 |
| 148 | 1.1000000E+03 | 4.0000020E+02 |
| 149 | 1.1000000E+03 | 5.0000020E+02 |
| 150 | 1.1000000E+03 | 6.0000020E+02 |
| 151 | 1.1000000E+03 | 7.0000020E+02 |
| 152 | 1.1000000E+03 | 8.0000020E+02 |
| 153 | 1.1000000E+03 | 9.0000020E+02 |
| 154 | 1.1000000E+03 | 1.0000000E+03 |

Table C-6 (Continued)

| Record | Variable(s) | | | | |
|---|---|---|---|---|---|
| | 155 | 1.1000000E+03 | 1.1000000E+03 | | |
| | 156 | 1.1000000E+03 | 1.2000000E+03 | | |
| | 157 | 1.2000000E+03 | 0.0000000E+00 | | |
| | 158 | 1.2000000E+03 | 1.0000000E+02 | | |
| | 159 | 1.2000000E+03 | 2.0000000E+02 | | |
| | 160 | 1.2000000E+03 | 3.0000000E+02 | | |
| | 161 | 1.2000000E+03 | 4.0000000E+02 | | |
| | 162 | 1.2000000E+03 | 5.0000000E+02 | | |
| | 163 | 1.2000000E+03 | 6.0000000E+02 | | |
| | 164 | 1.2000000E+03 | 7.0000000E+02 | | |
| | 165 | 1.2000000E+03 | 8.0000000E+02 | | |
| | 166 | 1.2000000E+03 | 9.0000000E+02 | | |
| | 167 | 1.2000000E+03 | 1.0000000E+03 | | |
| | 168 | 1.2000000E+03 | 1.1000000E+03 | | |
| | 169 | 1.2000000E+03 | 1.2000000E+03 | | |
| 15 | 1 | 1 | 14 | 15 | 2 |
| | 2 | 2 | 15 | 16 | 3 |
| | 3 | 3 | 16 | 17 | 4 |
| | 4 | 4 | 17 | 18 | 5 |
| | 5 | 5 | 18 | 19 | 6 |
| | 6 | 6 | 19 | 20 | 7 |
| | 7 | 7 | 20 | 21 | 8 |
| | 8 | 8 | 21 | 22 | 9 |
| | 9 | 9 | 22 | 23 | 10 |
| | 10 | 10 | 23 | 24 | 11 |
| | 11 | 11 | 24 | 25 | 12 |
| | 12 | 12 | 25 | 26 | 13 |
| | 13 | 14 | 27 | 28 | 15 |
| | 14 | 15 | 28 | 29 | 16 |
| | 15 | 16 | 29 | 30 | 17 |
| | 16 | 17 | 30 | 31 | 18 |
| | 17 | 18 | 31 | 32 | 19 |
| | 18 | 19 | 32 | 33 | 20 |
| | 19 | 20 | 33 | 34 | 21 |
| | 20 | 21 | 34 | 35 | 22 |
| | 21 | 22 | 35 | 36 | 23 |
| | 22 | 23 | 36 | 37 | 24 |
| | 23 | 24 | 37 | 38 | 25 |
| | 24 | 25 | 38 | 39 | 26 |
| | 25 | 27 | 40 | 41 | 28 |
| | 26 | 28 | 41 | 42 | 29 |
| | 27 | 29 | 42 | 43 | 30 |
| | 28 | 30 | 43 | 44 | 31 |
| | 29 | 31 | 44 | 45 | 32 |
| | 30 | 32 | 45 | 46 | 33 |
| | 31 | 33 | 46 | 47 | 34 |
| | 32 | 34 | 47 | 48 | 35 |
| | 33 | 35 | 48 | 49 | 36 |
| | 34 | 36 | 49 | 50 | 37 |
| | 35 | 37 | 50 | 51 | 38 |
| | 36 | 38 | 51 | 52 | 39 |
| | 37 | 40 | 53 | 54 | 41 |
| | 38 | 41 | 54 | 55 | 42 |
| | 39 | 42 | 55 | 56 | 43 |
| | 40 | 43 | 56 | 57 | 44 |
| | 41 | 44 | 57 | 58 | 45 |
| | 42 | 45 | 58 | 59 | 46 |
| | 43 | 46 | 59 | 60 | 47 |

**Table C–6** (Continued)

| Record | Variable(s) | | | | |
|---|---|---|---|---|---|
| | 44 | 47 | 60 | 61 | 48 |
| | 45 | 48 | 61 | 62 | 49 |
| | 46 | 49 | 62 | 63 | 50 |
| | 47 | 50 | 63 | 64 | 51 |
| | 48 | 51 | 64 | 65 | 52 |
| | 49 | 53 | 66 | 67 | 54 |
| | 50 | 54 | 67 | 68 | 55 |
| | 51 | 55 | 68 | 69 | 56 |
| | 52 | 56 | 69 | 70 | 57 |
| | 53 | 57 | 70 | 71 | 58 |
| | 54 | 58 | 71 | 72 | 59 |
| | 55 | 59 | 72 | 73 | 60 |
| | 56 | 60 | 73 | 74 | 61 |
| | 57 | 61 | 74 | 75 | 62 |
| | 58 | 62 | 75 | 76 | 63 |
| | 59 | 63 | 76 | 77 | 64 |
| | 60 | 64 | 77 | 78 | 65 |
| | 61 | 66 | 79 | 80 | 67 |
| | 62 | 67 | 80 | 81 | 68 |
| | 63 | 68 | 81 | 82 | 69 |
| | 64 | 69 | 82 | 83 | 70 |
| | 65 | 70 | 83 | 84 | 71 |
| | 66 | 71 | 84 | 85 | 72 |
| | 67 | 72 | 85 | 86 | 73 |
| | 68 | 73 | 86 | 87 | 74 |
| | 69 | 74 | 87 | 88 | 75 |
| | 70 | 75 | 88 | 89 | 76 |
| | 71 | 76 | 89 | 90 | 77 |
| | 72 | 77 | 90 | 91 | 78 |
| | 73 | 79 | 92 | 93 | 80 |
| | 74 | 80 | 93 | 94 | 81 |
| | 75 | 81 | 94 | 95 | 82 |
| | 76 | 82 | 95 | 96 | 83 |
| | 77 | 83 | 96 | 97 | 84 |
| | 78 | 84 | 97 | 98 | 85 |
| | 79 | 85 | 98 | 99 | 86 |
| | 80 | 86 | 99 | 100 | 87 |
| | 81 | 87 | 100 | 101 | 88 |
| | 82 | 88 | 101 | 102 | 89 |
| | 83 | 89 | 102 | 103 | 90 |
| | 84 | 90 | 103 | 104 | 91 |
| | 85 | 92 | 105 | 106 | 93 |
| | 86 | 93 | 106 | 107 | 94 |
| | 87 | 94 | 107 | 108 | 95 |
| | 88 | 95 | 108 | 109 | 96 |
| | 89 | 96 | 109 | 110 | 97 |
| | 90 | 97 | 110 | 111 | 98 |
| | 91 | 98 | 111 | 112 | 99 |
| | 92 | 99 | 112 | 113 | 100 |
| | 93 | 100 | 113 | 114 | 101 |
| | 94 | 101 | 114 | 115 | 102 |
| | 95 | 102 | 115 | 116 | 103 |
| | 96 | 103 | 116 | 117 | 104 |
| | 97 | 105 | 118 | 119 | 106 |
| | 98 | 106 | 119 | 120 | 107 |
| | 99 | 107 | 120 | 121 | 108 |
| | 100 | 108 | 121 | 122 | 109 |
| | 101 | 109 | 122 | 123 | 110 |

Table C-6 (Continued)

| Record | Variable(s) | | | | |
|---|---|---|---|---|---|
| | 102 | 110 | 123 | 124 | 111 |
| | 103 | 111 | 124 | 125 | 112 |
| | 104 | 112 | 125 | 126 | 113 |
| | 105 | 113 | 126 | 127 | 114 |
| | 106 | 114 | 127 | 128 | 115 |
| | 107 | 115 | 128 | 129 | 116 |
| | 108 | 116 | 129 | 130 | 117 |
| | 109 | 118 | 131 | 132 | 119 |
| | 110 | 119 | 132 | 133 | 120 |
| | 111 | 120 | 133 | 134 | 121 |
| | 112 | 121 | 134 | 135 | 122 |
| | 113 | 122 | 135 | 136 | 123 |
| | 114 | 123 | 136 | 137 | 124 |
| | 115 | 124 | 137 | 138 | 125 |
| | 116 | 125 | 138 | 139 | 126 |
| | 117 | 126 | 139 | 140 | 127 |
| | 118 | 127 | 140 | 141 | 128 |
| | 119 | 128 | 141 | 142 | 129 |
| | 120 | 129 | 142 | 143 | 130 |
| | 121 | 131 | 144 | 145 | 132 |
| | 122 | 132 | 145 | 146 | 133 |
| | 123 | 133 | 146 | 147 | 134 |
| | 124 | 134 | 147 | 148 | 135 |
| | 125 | 135 | 148 | 149 | 136 |
| | 126 | 136 | 149 | 150 | 137 |
| | 127 | 137 | 150 | 151 | 138 |
| | 128 | 138 | 151 | 152 | 139 |
| | 129 | 139 | 152 | 153 | 140 |
| | 130 | 140 | 153 | 154 | 141 |
| | 131 | 141 | 154 | 155 | 142 |
| | 132 | 142 | 155 | 156 | 143 |
| | 133 | 144 | 157 | 158 | 145 |
| | 134 | 145 | 158 | 159 | 146 |
| | 135 | 146 | 159 | 160 | 147 |
| | 136 | 147 | 160 | 161 | 148 |
| | 137 | 148 | 161 | 162 | 149 |
| | 138 | 149 | 162 | 163 | 150 |
| | 139 | 150 | 163 | 164 | 151 |
| | 140 | 151 | 164 | 165 | 152 |
| | 141 | 152 | 165 | 166 | 153 |
| | 142 | 153 | 166 | 167 | 154 |
| | 143 | 154 | 167 | 168 | 155 |
| | 144 | 155 | 168 | 169 | 156 |
| 16 | 1 | | | | |
| 17 | 1 | 0.0E0 | 169 | 1 | |
| 18 | 1 | | | | |
| 19 | 1 | 10.0E0 | 169 | 1 | |
| 20 | 144 | 155 | 168 | 169 | 156 |
| | 1 | 1 | 14 | | |
| | 1 | 2 | 1 | | |
| | 2 | 3 | 2 | | |
| | 3 | 4 | 3 | | |
| | 4 | 5 | 4 | | |
| | 5 | 6 | 5 | | |
| | 6 | 7 | 6 | | |
| | 7 | 8 | 7 | | |
| | 8 | 9 | 8 | | |
| | 9 | 10 | 9 | | |

**Table C-6** (Continued)

| Record | Variable(s) |
|---|---|
| | 10 11 10 |
| | 11 12 11 |
| | 12 26 13 |
| | 12 13 12 |
| | 13 14 27 |
| | 24 39 26 |
| | 25 27 40 |
| | 36 52 39 |
| | 37 40 53 |
| | 48 65 52 |
| | 49 53 66 |
| | 60 78 65 |
| | 61 66 79 |
| | 72 91 78 |
| | 73 79 92 |
| | 84 104 91 |
| | 85 92 105 |
| | 96 117 104 |
| | 97 105 118 |
| | 108 130 117 |
| | 109 118 131 |
| | 120 143 130 |
| | 121 131 144 |
| | 132 156 143 |
| | 133 144 157 |
| | 133 157 158 |
| | 134 158 159 |
| | 135 159 160 |
| | 136 160 161 |
| | 137 161 162 |
| | 138 162 163 |
| | 139 163 164 |
| | 140 164 165 |
| | 141 165 166 |
| | 142 166 167 |
| | 143 167 168 |
| | 144 168 169 |
| | 144 169 156 |
| 21 | 1 |
| 22 | 3 |
| 23 | 1 1.0E1 144 13 |
| | 157 8.0E0 169 1 |
| | 13 1.0E1 156 13 |
| 24 | 1 |
| 25 | 2 3 2 |
| | 1.0E-7 1.0E-7 |
| | 3 4 3 |
| | 1.0E-7 1.0E-7 |
| | 4 5 4 |
| | 1.0E-7 1.0E-7 |
| | 5 6 5 |
| | 1.0E-7 1.0E-7 |
| | 6 7 6 |
| | 1.0E-7 1.0E-7 |
| | 7 8 7 |
| | 1.0E-7 1.0E-7 |
| | 8 9 8 |
| | 1.0E-7 1.0E-7 |

Table C–6 (Continued)

| Record | Variable(s) |
|---|---|
| | 9 10 9 |
| | 1.0E–7 1.0E–7 |
| | 10 11 10 |
| | 1.0E–7 1.0E–7 |
| | 11 12 11 |
| | 1.0E–7 1.0E–7 |
| 26 | 1 |
| | 1 1 144 1 |
| 27 | 2.0E–1 |
| | 0.0E0 3.0E0 |
| | 1.8E1 1.0E0 |
| | 6.0E1 1.0E0 |
| 28 | 85 2 |
| | 0.0E0 –5.0E–2 |
| | 6.0E1 –5.0E–2 |

The output from both programs is printed every LPT time steps (specified by the user in the input record 6 of Table C–5) and consists basically of three tables : (1) time and iteration parameters, (2) flow and mass balances, (3) the piezometric head values in the order node number, piezometric head at the LPT-th time step and the difference between this piezometric head and the initial piezometric head and (4) average Darcy velocities over the depth of the aquifer.

The output tables from both the programs can be printed either to the screen or a printer. A similar set of data is also stored on disk for reference purposes, unless LSD is set equal to 0 in input record 6 of Table C–5.

Graphs of the simulated water levels, along the two cross-sections at y = 100 m and y = 600 m in Figure C–3, during the last time step, are presented graphically in Figure C–4. The depth averaged Darcy velocities across the hypothetical aquifer, again after 60 hours of simulation, are presented graphically in Figure C–5.

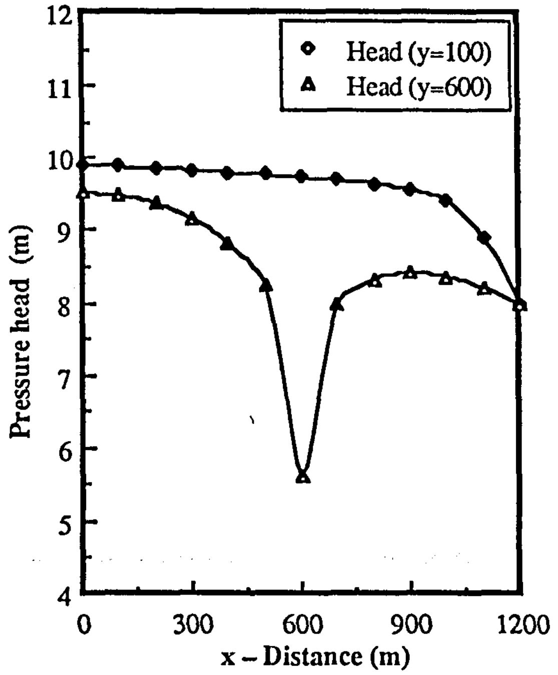

**Figure C–4** Water levels across two cross-sections of the aquifer at y = 100 and 600 m after 60 h of simulation with the phreatic model

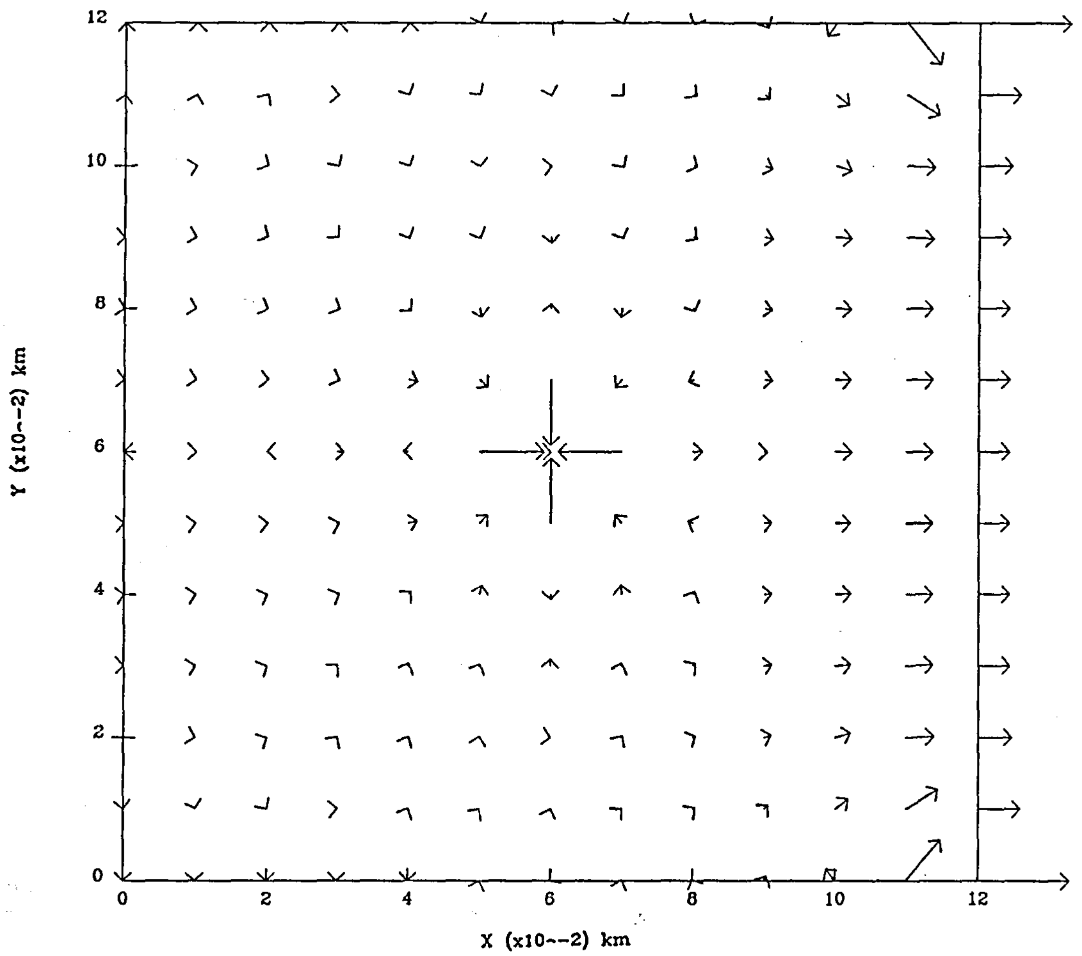

**Figure C–5** Graphical representation of the Darcy velocities after 60 h of simulation across the hypothetical aquifer used in the simulation.

# REFERENCES

Abriola L.M. and Pinder G.F. A multiphase approach to the modelling of porous media contamination by organic compounds. 1. Equation development. *Wat. Resour. Res.*, **21**, 11 – 18 (1985a)

Abriola L.M. and Pinder G.F. A multiphase approach to the modelling of porous media contamination by organic compounds. 2. Numerical simulation. *Wat. Resour. Res.*, **21**, 19 – 26 (1985b)

Allen M.B. Numerical Modelling of Multiphase flow in porous media. *Advances in Water Resources*, **8** : 162–187 (1985)

Anonymous *Alluvial Bed Recharge Project. Steering Committee Progress Report No. 2*, Department of Water Affairs, Geohydrology Division, Windhoek. (1985)

Bear J. *Dynamics of fluids in porous media.* American Elsevier Publishing Company, Inc., New York (1972)

Bear J. *Hydraulics of Groundwater*, McGraw-Hill series in Water Resources and Environmental Engineering. New York, N.Y. (1979)

Bear J. On the Aquifer's Integrated Balance Equations. *Advances in Water Resources*, **1**(1) : 15–23. (1977)

Botha J.F. *Grondvog en hitte-oordrag in gronde.* Unpublished M.Sc. Thesis, Department of Physics, University of Stellenbosch, Stellenbosch. (1963)

Botha J F. *A revised model for the National Waste Disposal Site at Vaalputs.* Institute for Ground-water Studies, University of the Orange Free State, Bloemfontein. (1986)

Botha J.F. Modelling contaminant transport using site specific data from Vaalputs. In *Radwaste '86, Conference on the treatment and containment of radioactive waste and its disposal in arid environments.* Cape Town. (1986)

Botha J.F. *Nonlinear Least Squares Analysis of Geohydrological Data*, Unpublished manuscript, Institute for Ground-water Studies, University of the Orange Free State, Bloemfontein. (1988)

Botha J.F. Interpretation of Two-dimensional Models in Geohydrology. Unpublished Report, Institute for Ground-water Studies, University of the Orange Free State, Bloemfontein (1988)

Botha J.F. Transport of Radioactive waste from the Disposal Site at Vaalputs. Institute for Ground-water Studies, University of the Orange Free State, Bloemfontein. (1990)

Botha J.F. and Bakkes G.N. The Galerkin finite element method and the groundwater flow equation: 1. Convergence of the method. *Adv. Water Resources*, **5** : 121–125 (1982)

Botha J.F. and Pinder G.F. *Fundamental concepts in the numerical solution of differential equations*. John Wiley and Sons, Inc., New York (1983)

Bouwer H. and Rice R.C. Hydraulic Properties of Stony Vadose Zones. Ground Water **22**: 696-705 (1984)

Brooks R.H. and Corey A.T. *Hydraulic properties of porous media.* Colorado State University, Hydrology Papers No. 3, Fort Collins, Colorado. (1964)

Brooks R.H. and Corey A.T. Properties of porous media affecting fluid flow. *Proc. Am. Soc. Civ. Engrs,* **92**(IR2), 61-87 (1966)

Case C., Kautsky M., Kearl P., Goldfarb R., Leatham S. and Metcalf L. *Unsaturated Flow Properties Data Catalogue,* Volume 1, Water Resources Center, Desert Research Institute, University of Nevada System. (1983)

Childs E.C. and Collis-George N. The Permeability of Porous Media. *Proc. Roy. Soc.* Ser A **201**: 392–405 (1950)

De Waal D.J., Botha J.F. and G.J. Van Tonder G.J. *Kriging: Bayesian estimation as an alternative.* Technical Report **144**. Department of Mathematical Statistics, University of the Orange Free State, Bloemfontein (1988)

Dybbs A. and Edwards R.V. A New Look at Porous Media Fluid Mechanics – Darcy to Turbulent. In: *Fundamentals of Transport Phenomena in Porous Media,* J. Bear and M. Yavus Carapcioglu (Eds), Marthinus Nijhoff Publishers, Dordrecht. (1984)

El-Kadi Aly I. On Estimating the Hydraulic Properties of Soil, Part 1. Comparison between Forms to estimate the Soil Water Characteristic Function. *Adv. Water Resources,* **8**: 136–147 (1985)

Ergun S. Fluid Flow through Packed Columns. *Chem. Eng. Prog.* **48**: 89–94 (1952)

Garrels R.M. and Christ C.L. *Solutions, minerals and equilibria.* Harper & Row, New York, 450 p (1965)

Hardy G.H. *A Course of Pure Mathematics.* Cambridge University Press, Cambridge (1955)

Hem J.D. Study and interpretation of the chemical characteristics of natural water. *U.S. Geol. Surv. Wat. Supply Pap.,* **1473**, 2nd Ed., Washington, 363 p (1970)

Hillel D. *Introduction to Soil Physics*, Academic Press, Inc., New York, New York. (1982)

Hsieh P.A. *et al* *Pressure testing of fractured rocks – a methodology employing three-dimensional cross-hole tests.* Topical Report, University of Arizona, Tucson (1983)

Huyakorn P.S. and Pinder G.F. *Computational methods in subsurface flow.* Academic Press Inc., New York, N.Y. (1983)

Kinniburgh D.G. General purpose adsorption isotherms. *Environ. Sci. Technol.*, **20**, 895 – 904 , (1986)

Krauskopf K.B. *Introduction to geochemistry.* McGraw-Hill, New York, 721 p (1967)

Kruseman G.P. and De Ridder N.A. *Analysis and evaluation of pumping test data.* Bulletin 11, International Institute for Land Reclamation and Improvement, Wageningen. (1970)

Mathess G. *Die Beschaffenheit des Grundwassers.* Gebrüder Borntraeger, Berlin, 324 p (1973)

McWhorter D.B. and Sunada D.K. *Ground-water Hydrology and Hydraulics*, Water Resources Publications, P.O. Box 303, Fort Collins, Colorado. (1977)

Meyer S.L. *Data Analysis for Scientists and Engineers.* John Wiley and Sons, New York, N.Y. (1975)

Meyer B.R., Bain C.A.R., De Jesus A.S.M. and Stephenson D. Radiotracer evaluation of groundwater dispersion in a multi-layered aquifer. *J. Hydrol.*, **50**, 259 – 271 (1981)

Molz F.J. and Widdowson M.A. Internal inconsistencies in dispersion-dominated models that incorporate chemical and microbial kinetics. *Wat. Resour. Res.*, **24**, 615 – 619 (1988)

Morel-Seytoux H.J. and Vauclin M. Superiority of two-phase formulation for infiltration. In *Advances in Infiltration*, Proceedings of the National Conference on Advances in Infiltration, Chicago (1983)

Mualem Y. A New Model for Predicting the Hydraulic Conductivity of Unsaturated Porous Media. *Water Resources Research* **12**: 513–522 (1976)

Müller J.L. and Botha J.F. *A preliminary investigation of modelling the Atlantis aquifer.* Bulletin **15**, Institute for Ground-water Studies, University of the Orange Free State, Bloemfontein (1986)

Nutting P.G. Physical Analysis of Oil Sands. *Bull. Amer. Ass. Petr. Geol.* **14**: 1337–1349 (1930)

Piet G.J. and Zoeteman B.C.J. Organic water quality changes during sand band and dune filtration of surface waters in The Netherlands. *J. Am. Wat. Wks. Ass.*, **72**, 400–404 (1980)

Pinder G.F. *Galerkin finite element models for aquifer simulation.* Rep. Water Resources Program, Princeton University, Princeton (1974)

Pinder G.F. and Gray W.G. *Finite Element Simulation in Surface and Sub-surface Hydrology.* Academic Press, New York, N.Y. (1976)

Princeton Water Resources Program *Groundwater contamination from hazardous wastes.* Prentice-Hall, Inc., Englewood Cliffs, New Jersey (1984)

Richards L.A. Capillary Conduction of Liquids in Porous mediums. *Physics* **1**: 318–333 (1931)

Rogers J. First report on the Cenozoic sediments between Cape Town and Elandsbay. *Open file Report 1980 - 0249,* Geological Survey, Pretoria, 64 p (1980)

Ronen D., Magaritz M, and Levy I. An *in situ* multi-level sampler for preventative monitoring and study of hydrochemical profiles in aquifers. *Ground Water Monitoring Rev.,* 7 (4), 69 – 74 (1987b)

Ronen D., Magaritz M., Gvirtzman H. and Garner W. Microscale chemical heterogeneity in groundwater. *J. Hydrol.,* **92**, 173 – 178 (1987a)

Roy W.R. and Griffin R.A. Mobility of organic solvents in water-saturated soil materials. *Environ. Geol. Wat. Sci.,* 7, 241 – 247 (1985)

Sauty J.P. An analysis of hydrodispersive transfers in aquifers. *Water Resour. Research.* **16**: 145–158. (1980)

Scheidegger A.E. *The Physics of Flow through Porous Media* (3rd Ed.). University of Toronto press, Toronto. (1974)

Scheidegger A.E. Theoretical Models of Porous Matter. *Producer's Monthly,* **17**(10): 17–23 (1953)

Scott P.S., Farquhar F.J. and Kouwen N. Hysteretic effects on net infiltration. In *Advances in Infiltration,* Proceedings of the National Conference on Advances in Infiltration, Chicago (1983)

Terzaghi K. *Erdbaummechanik auf bodenphysikalischer Grundlage,* Deuticke, Leipzig. (1925)

Terzaghi K. *From Theory to Practice in Soil Mechanics,* John Wiley and Sons, New York, N.Y. (1960)

Terzaghi K. *Theoretical Soil Mechanics,* John Wiley and Sons, New York, N.Y. (1943)

Timmerman K.M.G. Letter to the Institute for Ground-water Studies, Reference number BG4/8/G/4 (1986)

Tredoux G. and Tworek W. Artificial recharge of an unconfined aquifer at Atlantis, South Africa. In Proc. Intl. Conf. on Groundwater Technology. National Water Well Association, Worthington, Ohio. (1984)

Tredoux G. The role of artificial recharge in groundwater management at Atlantis. *IWPC Biennial Conf.*, Port Elizabeth, 18 p (1987)

Tzimopoalos C. and Sakellariou-Makrantonaki M. Water table drawdown for two dimensional drainage. *Adv. Water Resources*, **10** : 159–163 (1987)

Vachaud G., Royer J.M. and Cooper J.D. Comparison of methods of calibration of a neutron probe by gravimetry or neutron capture model. *J. of Hydrology*, **34**: 343–356 (1977)

Van der Merwe A.J. Eksplorasie, ontginning en evaluering van grondwater van die sandafsetting in die Atlantisgebied vir watervoorsiening aan die Atlantisontwikkelingsgebied. Unpublished M.Sc. thesis, University of the Orange Free State, Bloemfontein. (1983)

Van Genuchten M. Th. and Nielsen D.R. On Describing and Predicting the Hydraulic Properties of Unsaturated Soils. *Annales Geophysicae*, 3: 615–628 (1985)

Van Genuchten M. Th. A Closed-form Equation for predicting the Hydraulic Conductivity of Unsaturated Soils. *Soil Sci. Soc. Am. J.*, **44**: 892–898 (1980)

Van Rensburg H.J. *'n Ondersoek na die benutting van grondwater in die Grootfonteinkompartement (Wes-Transvaal).* Unpublished M.Sc. thesis, University of the Orange Free State, Bloemfontein (1984)

Van Tonder G.J. *Die toepassing van kriging in Geohidrologie.* Bulletin 12, Institute for Ground-water Studies, University of the Orange Free State, Bloemfontein (1984)

Van Tonder G.J. and Botha J.F. *Die Toepassing van Kriging in Geohidrologie.* Bulletin **15**, Institute for Ground-water Studies, University of the Orange Free State, Bloemfontein (1986)

Van Tonder G.J. and Cocho V.E. Aquamod: 'n twee-dimensionale Galerkin eindige element simulasieprogram vir mikrorekenaars vir die voorspelling van versadigde grondwatervloei en besoedeling. *Water SA*, **13** : 175–180 (1984)]

Verwey J.P. *'n Praktiese handleiding vir die Kruisboorgatmetode.* Unpublished manual, Institute for Ground-water Studies, University of the Orange Free State, Bloemfontein. (1987)

Walton C.W. *Groundwater resource evaluation.* McGraw-Hill Book Company, Inc., New York (1970)

Weast R.C. (Ed) *Handbook of Physics and Chemistry.* The Chemical Rubber Company, Cleveland, Ohio (1969), or any later edition.

Zoeteman B.C., Harmsen K., Linders J.B., Morra D.F. and Sloof W. Persistent organic pollutants in river water and ground water of the Netherlands. *Chemosphere,* **9,** 231 – 249 (1980)